Atomic Scale Processing Focus Topic
Room A214 - Session AP+2D+EM+PS+TF-MoM

Area Selective Deposition and Selective-Area Patterning

Moderators: Satoshi Hamaguchi, Osaka University, Japan, Eric A. Joseph, IBM T.J. Watson Research Center

8:40am **AP+2D+EM+PS+TF-MoM2 Surface Pre-functionalization of SiN_x and SiO_2 to Enhance Selectivity in Plasma–Assisted Atomic Layer Etching***, **Ryan Gasvoda**, Colorado School of Mines; Z. Zhang, S. Wang, E.A. Hudson,* Lam Research Corporation*; S. Agarwal,* Colorado School of Mines

To manufacture semiconductor devices in the current sub-7-nm node, stringent processing windows are placed on all aspects in manufacturing including plasma-etching. In recent years, atomic layer etching (ALE) has emerged as a patterning technique that can provide high etch fidelity, directionality, layer–by–layer removal, and selectivity to meet the tight processing windows. Plasma–assisted ALE of SiO_2 and SiN_x is of particular interest since Si-based dielectrics are commonly used throughout the entire fabrication process. Typically, these materials are etched in a cyclic ALE process consisting of two sequential half–cycles: fluorocarbon (CF_x) deposition from a fluorocarbon plasma followed by an Ar plasma activation step. Etch selectivity can be achieved through careful manipulation of the plasma and processing parameters. To further increase overall etch selectivity, we have proposed a methodology that selectively pre–functionalizes the SiO_2 or SiN_x surface with hydrocarbons prior to ALE. Recently, we showed that an etch blocking graphitic hydrofluorocarbon film will readily accumulate on a pre–functionalized SiO_2 surface.

In this study, we used *in situ* attenuated total reflection Fourier transform infrared (ATR–FTIR) spectroscopy and *in situ* 4–wavelength ellipsometry to monitor the surface reactions, film composition, and net film thickness during the entire ALE process. We show that aldehydes can be used to functionalize SiN_x with extremely high selectivity to SiO_2 surfaces. During ALE on bare SiN_x, a thick graphitic fluorocarbon film accumulates on the surface and can stop all etching after cycle 5. This is attributed to inefficient removal of both the C and N from the surface. To enhance removal and prevent graphitic carbon accumulation, we graft a branched hydrocarbon aldehyde to the SiN_x surface. This branched hydrocarbon provides an abundance of $–CH_3$ groups which allows for greater C and N removal possibly via HCN formation, thus lowering overall graphitic carbon formation. This retardation of the graphitic hydrofluorocarbon film formation leads to both an overall increase in the etch per cycle and the number of ALE cycles that can be run before an etch stop is observed.

9:00am **AP+2D+EM+PS+TF-MoM3 Area-selective Atmospheric-pressure Spatial ALD of SiO_2 using Interleaved Back-etch steps Yielding Selectivity > 10 nm***, A. Mameli,* Holst Centre / TNO, The Netherlands*; F. Roozeboom,* ***Paul Poodt****,* Holst Centre / TNO, The Netherlands, Netherlands

Area-selective atomic layer deposition (AS-ALD) has great potential in reducing cost by maskless device manufacturing of patterned layers. Still, in this new *bottom-up* approach the selectivities currently obtained for film growth on patterned growth areas vs. that on the non-growth areas are often very limited. Also the substrate throughput values for conventional low-pressure ALD is too low for industrial acceptance.(1,2) In this work we present a process for AS-ALD of SiO_2 using intermittent plasma etch-back steps to increase the selectivity above 10 nm film thickness.(3) In addition, the deposition process itself is performed in a spatial ALD reactor at atmospheric pressure which allows for achieving high throughput.(4)

AS-ALD of SiO_2 on a substrate with pre-patterned SiO_2 and ZnO areas was demonstrated using a highly chemo-selective inhibitor that chemisorbs preferentially on the non-growth area (ZnO) while allowing the deposition of SiO_2 on the growth area (SiO_2). In order to maximize the process selectivity, a blanket fluorocarbon plasma etch-back step was interleaved after every 110 ALD cycles. This way, selective SiO_2 deposition up to ~ 30 nm film thickness was demonstrated. Furthermore, X-ray Photoelectron Spectroscopy was carried out to verify the selectivity of the process: no Si was detected (detection limit 0.3 at. %) on the non-growth area, demonstrating the high selectivity of the process.

The process presented here combines selective inhibitor chemisorption, plasma-based spatial ALD with high deposition rates and plasma etch-back steps to correct for selectivity loss. This approach is compatible with *roll-to-roll* and *sheet-to-sheet* concepts and can therefore enable high-throughput AS-ALD on large-area and flexible substrates.

[1] A. Mameli, *et al.*, *ACS Nano*, **11**, 9303 (2017).

[2] F.S.M. Hashemi, *et al.*, *ACS Nano*, **9**, 8710 (2015).

[3] R. Vallat, *et al*., *J. Vac Sc. Technol. A*, **35**, 01B104 (2017).

[4] P. Poodt, *et al*., *Adv. Mater.*, **22**, 3564 (2010).

9:20am **AP+2D+EM+PS+TF-MoM4 Mechanisms of Precursor Blocking during Area-selective Atomic Layer Deposition using Inhibitors in ABC-type Cycles***, M.J.M. Merkx,* Eindhoven University of Technology, The Netherlands*; D.M. Hausmann,* Lam Research Corporation*; W.M.M. Kessels,* Eindhoven University of Technology, The Netherlands, Netherlands*; T.E. Sandoval,* Universidad Técnica Federico Santa María, Chile*;* ***Adrie Mackus***[1]*,* Eindhoven University of Technology, The Netherlands, Nederland

The development of new processes for area-selective atomic layer deposition (ALD) is currently motivated by the need for self-aligned fabrication schemes in semiconductor processing. For example, area-selective ALD processes for dielectric-on-dielectric deposition are being considered for fully self-aligned via (FSAV) fabrication schemes in advanced interconnect technology.

Instead of solely relying on surface functionalization prior to ALD, an novel strategy to area-selective ALD involves the dosing of inhibitor molecules during every cycle in an ABC-type recipe.[1,2] By using small molecules that can be dosed in vapor-phase as inhibitor, this approach is compatible with industrial process flows. Moreover, the reapplication of the inhibitor molecules during every cycle allows for the use of a plasma as the co-reactant, which broadens the range of materials that can be deposited selectively. In contrast to conventional approaches to area-selective ALD based on self-assembled monolayers (SAMs), very little is known about how small inhibitor molecules can block the ALD growth.

In this contribution, insight into the mechanisms of precursor blocking by inhibitor molecules as obtained from in-situ Fourier transform infrared spectroscopy (FTIR) and density functional theory (DFT) calculations will be discussed. Area-selective ALD of SiO_2 using acetylacetone (Hacac) as inhibitor will be described as a model system, illustrating various mechanisms that can contribute to the loss of selectivity. It was found that at saturation, Hacac adsorbs through a mixture of chelate and monodentate bonding configurations. Hacac in monodentate configuration is displaced from the surface when exposed to bis(diethylamino)silane precursor molecules, which limits the selectivity. Strategies for improving the selectivity based on the understanding from these studies will be discussed.

[1] A. Mameli, M.J.M. Merkx, B. Karasulu, F. Roozeboom, W.M.M. Kessels, and A.J.M. Mackus, ACS Nano **11**, 9303 (2017).

[2] A.J.M. Mackus, M.J.M. Merkx, and W.M.M. Kessels, Chem. Mater. **31**, 2 (2019).

9:40am **AP+2D+EM+PS+TF-MoM5 Area-Selective Deposition of TiO_2 using Isothermal Integrated Atomic Layer Deposition and Atomic Layer Etching in a Single Reaction Chamber***,* ***Gregory Parsons****, S.K. Song, H. Saare,* North Carolina State University **INVITED**

Several new approaches are emerging where chemical etching is being coupled with atomic layer deposition to achieve area-selective deposition of dielectrics and metals. During ALD, selectivity is generally lost when undesired nuclei form on the targeted non-growth surface. These undesired nuclei can sometimes be removed by periodic etching, improving the overall selectivity. However, it is not known to what extent these coupled deposition/etching sequences can proceed while maintaining good selectivity. As desirable deposition and etching reactions proceed, other changes in the process can occur to enhance unwanted nucleation and/or impede desired etching, thereby limiting the net selectivity. Recent experiments in our lab have used in-situ probes to explore coupled thermal ALD and ALE super-cycles, performed sequentially under isothermal conditions in a single reaction chamber, to achieve area selective deposition of TiO_2 on SiO_2 with hydrogen-terminated silicon (100) as the desired non-growth surface. We find that as ALD/ALE super-cycles proceed, small changes occur in the ALD and ALE reactions, particularly during the transition from ALD to ALE, or from ALE to ALD. Also, modeling studies allow us to quantitatively analyze the ASD results and compare our findings to other known approaches. These insights will be helpful to understand opportunities and challenges in advanced atomic scale reactions and process implementation.

---

[1] **Paul Holloway Award Winner**

10:40am **AP+2D+EM+PS+TF-MoM8 Area-Selective Atomic Layer Deposition of Metal Oxides on an Inhibitor-Functionalized SiO_2 Surface*,* *Wanxing Xu,*** Colorado School of Mines*; P.C. Lemaire, K. Sharma, D.M. Hausmann,* Lam Research Corporation*; S. Agarwal,* Colorado School of Mines

The continued downscaling of modern semiconductor devices together with the incorporation of 3D architectures places new constrains on conventional lithography techniques. To enable further advances in patterning process, new techniques will be required for next-generation devices to overcome the challenges of limiting the growth of desired materials in a specific area. One method to address these issues is area-selective atomic layer deposition (ALD), which provides the opportunity to build defined patterns from the bottom-up at the atomic-level accuracy. In this study, we will focus on area-selective ALD of metal oxides including ZrO_2 and Al_2O_3 with a metal as the growth surface and inhibitor-functionalized SiO_2 as the non-growth surface. To inhibit ALD, the SiO_2 surfaces were functionalized with aminosilane inhibitors through the vapor phase or with a solution-based method. The functionalized SiO_2 surfaces were characterized by transmission Fourier transform infrared (FTIR) spectroscopy, ellipsometry, and water contact angle measurements. Metal oxides including ZrO_2 and Al_2O_3 were deposited by ALD using metal precursors and H_2O over a temperature range of 150-250 °C. *In situ* attenuated total reflection FTIR spectroscopy was utilized to identify the surface reactions sites and absorbed surface species during ALD. In addition, the corresponding film growth was measured using *in situ* four-wavelength ellipsometry.

Using *in situ* optical diagnostics, we show the mechanism for the breakdown in selectivity during area-selective ALD on a SiO_2 surface that is functionalized with aminosilanes. The infrared spectra show that aminosilane inhibitors react with almost all of the surface –SiOH groups forming Si–O–Si–R bonds on the surface (see Figure 1). After repeated exposure of the functionalized SiO_2 surface to TEMAZ and ZTB, these precursors react with Si–O–Si bonds without surface –SiOH groups (see Figure 2). Although small growth in the first few ALD cycles is not detected by *in situ* ellipsometry, growth inhibition breaks down after an increased number of ALD cycles. These results suggest that it is an additional requirement to suppress other reactions with a higher activation energy barrier during ALD expect removing main surface reactive sites through surface functionalization. To further impede growth of metal oxides on functionalized SiO_2 surface, a two-step functionalization method was developed to passivate the SiO_2 surface while providing additional steric blocking for the underlying substrates. Comparative studies were carried out to evaluate the effect of different functionalization methods on suppressing the nucleation during ALD.

11:00am **AP+2D+EM+PS+TF-MoM9 Area-selective Deposition Achieved in a Continuous Process using Competitive Adsorption*,* *Taewon Suh*****,** *Y. Yang, K.U. Lao, R.A. DiStasio, Jr., J.R. Engstrom,* Cornell University

A significant challenge for single-nm fabrication technologies is the development of area selective deposition (ASD) processes, particularly for device structures with exposed metallic and dielectric surfaces on patterned, often three dimensional, substrates. A number of techniques have been proposed and examined for ASD processes, particularly with respect to ALD, and these include the use of "permanent" blocking layers in the form of SAMs, and repetitive deposition/etch cycles. Some success has been reported with these techniques, but they possess potential drawbacks. An ideal ASD process should be fast, preferably vapor phase, and leave no residue on the non-growth surface. One technique that can possibly provide this is the use of competitive adsorption to induce area selective deposition, where a co-adsorbate is chosen that will bind much more strongly to one surface vs. another. A significant challenge concerning this approach is avoiding direct reactions between the co-adsorbate and the thin film precursor in the case of ALD, and also the co-reactant in the case of CVD. We are coupling quantum mechanical calculations of co-adsorbate/thin-film precursor/substrate interactions with experiments using our coupled micro-reactor/UHV surface analysis system. We have examined the effect of a class of unsaturated hydrocarbons as co-adsorbates on the CVD growth of ZrO_2 thin films using a Zr amido-coordination complex as the thin film precursor and O_2 as the co-reactant. The substrates were SiO_2 and Cu, and we examined the effects of both temperature, T_s = 120-240 °C, and the partial pressure of the co-adsorbate hydrocarbon. DFT calculations predict that the binding energies of these hydrocarbons are at least a factor of two larger on Cu vs. those on SiO_2. For CVD growth of ZrO_2 thin films as thick as 22 nm (growth rates of ~ 1 nm-s^{-1}), we find that the co-introduction of the hydrocarbon results in linear growth with time on a SiO_2 substrate, with no apparent incubation time, while essentially no growth is observed on Cu. *In situ*, post-deposition analysis with XPS reveals ZrO_2 thin films on SiO_2, and only adventitious carbon and less than a monolayer of Zr on the Cu surface. Consistent with a model based on competitive adsorption, we find that selectivity is eventually lost at sufficiently high substrate temperatures or sufficiently low partial pressures of the hydrocarbon co-adsorbate. Finally, we will report on the CVD growth on patterned Cu/SiO_2 substrates where we observe deposition only on those areas covered by SiO_2. We will conclude with a discussion of the promise and challenges of this approach for ASD concerning both ALD and CVD processes.

11:20am **AP+2D+EM+PS+TF-MoM10 Surface Chemistry during Plasma-Assisted ALE: What Can We Learn from ALD?*,* *Sumit Agarwal,*** Colorado School of Mines **INVITED**

Due to ever decreasing device dimensions and the introduction of 3D device architectures, it is challenging to operate within a narrow processing window using conventional plasma etching. One method to address the demands of the next-generation of devices is atomic layer etching (ALE) which provides high fidelity, selectivity, and directionality, and layer-by-layer removal. Plasma-assisted ALE has been extensively studied for a variety of materials, including Al_2O_3, HfO_2, Si, and Si–based dielectrics. Plasma-assisted ALE of SiO_2 or SiN_x typically uses two sequential steps in a cyclic fashion: CF_x deposition from a C_4F_8/Ar plasma followed by an Ar plasma activation step. However, the surface chemistry during plasma ALE is not well understood. In this study, we used *in situ* attenuated total reflection Fourier transform infrared (ATR–FTIR) spectroscopy and *in situ* four-wavelength ellipsometry during ALE to monitor the surface reactions, film composition, as well as the net film thickness. Similar to area-selective atomic layer deposition, we show that surface functionalization prior to ALE can be used to alter the etch per cycle. Using this methodology, I will discuss how selective functionalization of SiO_2 or SiN_x can be used to alter the selectivity during plasma-assisted ALE.

Thin Films Division
Room A122-123 - Session TF+EM+MI+MN+OX+PS-MoM

Functional Thin Films: Ferroelectric, Multiferroics, and Magnetic Materials

Moderators: Christophe Vallee, LTM, Univ. Grenoble Alpes, CEA-LETI, France, Jessica Kachian, Intel Corporation

8:20am **TF+EM+MI+MN+OX+PS-MoM1 A Room-Temperature Magnetoelectric Multiferroic made by Thin Film Alchemy***, D.G. Schlom,* ***Megan Holtz****,* Cornell University **INVITED**

Materials that couple strong ferroelectric and ferromagnetic order hold tremendous promise for next-generation memory devices. Meticulous engineering has produced novel ferroelectric and multiferroic materials, although known single-phase multiferroics remain limited by antiferromagnetic or weak ferromagnetic alignments, by a lack of coupling between the order parameters, or by having properties that emerge only well below room temperature. Here we construct single-phase multiferroic materials in which ferroelectricity and strong magnetic ordering are coupled near room temperature. Starting with hexagonal $LuFeO_3$—a geometric ferroelectric with planar rumpling—we introduce individual monolayers of ferrimagnetic $LuFe_2O_4$ within the $LuFeO_3$ matrix, that is, $(LuFeO_3)_m/(LuFe_2O_4)_1$ superlattices. The rumpling of the $LuFeO_3$ drives the ferrimagnetic $LuFe_2O_4$ into a ferroelectric state, reducing the $LuFe_2O_4$ spin frustration. This increases the magnetic transition temperature to 281K for m=9. Moreover, the ferroelectric order couples to the ferrimagnetism, enabling direct electric-field control of magnetism at 200 kelvin. Further, charged ferroelectric domain walls align at $LuFe_2O_4$ layers, resulting in charge transfer which increases the magnetic moment. We are currently pursuing higher temperature multiferroics by incorporating cubic spinels with high magnetic ordering temperatures, such as $CoFe_2O_4$, into the $LuFeO_3$ matrix. Our results demonstrate a design methodology for creating higher-temperature magnetoelectric multiferroics through epitaxial engineering.

9:00am **TF+EM+MI+MN+OX+PS-MoM3 Magnetic Losses in FeGa/NiFe/Al_2O_3 Laminates for Strain-Mediated Multiferroic Micro-Antenna Applications***, **Kevin Fitzell**, A. Acosta, C.R. Rementer, D.J. Schneider, Z. Yao,* University of California, Los Angeles*; C. Dong,* Northeastern University*; M.E. Jamer, D. Gopman, J. Borchers, B. Kirby,* National Institute of Standards and Technology (NIST)*; N. Sun,* Northeastern University*; Y. Wang, G.P. Carman, J.P. Chang,* University of California, Los Angeles

The ability to reduce the size of antennae would enable a revolution in wearable and implantable electronic devices. Multiferroic antennae, composed of individual ferromagnetic and piezoelectric phases, could reduce antenna size by up to five orders of magnitude through the efficient coupling of magnetization and electric polarization via strain. This strategy requires a material with strong magnetoelastic coupling and acceptable magnetic losses at high frequency.

Galfenol ($Fe_{84}Ga_{16}$ or FeGa) is a promising candidate material due to its large magnetostriction (200 με), large piezomagnetic coefficient (5 ppm/Oe), and high stiffness (60 GPa), but it is highly lossy in the GHz regime. On the other hand, Permalloy ($Ni_{81}Fe_{19}$ or NiFe) is a soft magnetic material that has very low loss in the GHz regime, with a ferromagnetic resonance (FMR) linewidth of 10 Oe, but almost no magnetostriction. In this work, nanoscale laminates containing alternating layers of FeGa and NiFe were fabricated via DC magnetron sputtering to combine the complementary properties of the two magnetic phases, resulting in a composite material with a small coercive field, narrow FMR linewidth, and high permeability (Rementer et al., 2017). Optical magnetostriction measurements confirmed that these laminates retain the large saturation magnetostriction of FeGa (200 με) while enhancing the piezomagnetic coefficient (7 ppm/Oe), allowing for optimal piezomagnetic actuation at substantially reduced magnetic bias fields. Furthermore, multiferroic composites incorporating these magnetic laminates were studied via polarized neutron reflectometry, demonstrating uniform rotation of the individual layers' magnetization with an applied electric field across distances much larger than the exchange length of either material.

Due to the metallic nature of these FeGa/NiFe multilayer composites, however, resulting devices would be inefficient due to the generation of eddy currents at high frequency. To mitigate these losses, ultrathin layers of Al_2O_3 were incorporated into the multilayer materials to reduce the conductivity and mitigate the generation of eddy currents. The effect of Al_2O_3 thickness, FeGa:NiFe volume ratio, and multilayer architecture on the soft magnetic properties was also studied, resulting in a 50% reduction in the FMR linewidth. Optimized magnetic laminates were shown to exhibit a small coercive field (<20 Oe), narrow ferromagnetic resonance linewidth (<50 Oe), and high relative permeability (>500) while maintaining excellent magnetoelastic coupling, showing great promise for the use of FeGa/NiFe/Al_2O_3 laminates in strain-mediated micro-scale communications systems.

9:20am **TF+EM+MI+MN+OX+PS-MoM4 Multiferroic Gd-substituted HfO_2Thin Films***, **John Hayden**, F. Scurti, J. Schwartz, J.-P. Maria,* Pennsylvania State University

Modern ferroelectric technologies utilize perovskite structured materials, which have limited Si compatibility and modest bandgaps requiring thick films to reduce leakage current, hindering their implementation in realizable thin film devices. HfO_2 has been extensively researched as a gate dielectric thin film with excellent Si processing compatibility and has recently been found to exhibit ferroelectricity induced by a combination of impurity substitution, mechanical confinement by capping, intergranular surface area, and film thickness effects. This work investigates the microstructural characteristics, the ferroelectric response, and the potential for concomitant magnetic properties in sputtered Gd:HfO_2 thin films.

Gd-substituted HfO_2 thin films are a promising candidate as a multiferroic material, due to the presence of the magnetically active Gd^{3+} ion. Though substituting with Gd is known to induce ferroelectricity in HfO_2, the magnetic properties of Gd:HfO_2 have yet to be studied in depth. In this study, Gd:HfO_2 films are fabricated on TaN substrates by radio frequency sputtering of a composite Gd metal and HfO_2 oxide target in a mixed Ar and O_2 atmosphere. Grazing incidence x-ray diffraction is used to evaluate the suppression of the paraelectric monoclinic phase and stabilization of the ferroelectric orthorhombic phase. Electrical polarization measurements are used to study the room temperature spontaneous polarization in TaN/Gd:HfO_2/TaN metal-insulator-metal capacitors. Surface morphology of the films is characterized using atomic force microscopy, while magnetic properties are measured by variable temperature magnetometry. Initial magnetometry shows that Gd-substituted HfO_2 exhibits remnant magnetization at room temperature.

The scalability and simplicity of Gd:HfO_2, if it exhibits magnetoelectric coupling, make it an attractive model system for future developments in thin film multiferroics, having potential impacts for spintronics and other magnetoelectronic devices.

9:40am **TF+EM+MI+MN+OX+PS-MoM5 Epitaxial Growth of Antiferromagnetic NiO Films by Off-axis Sputtering for Spintronic Devices***, A. Churikova, G.S.D. Beach,* Massachusetts Institute of Technology*; **Larry Scipioni**, A. Shepard, J. Greer, T. Newhouse-Illige,* PVD Products, Inc.

High-quality epitaxial growth of antiferromagnetic thin films is essential for future spintronic devices, as it allows small antiferromagnetic domain sizes and efficient electrical manipulation of domain walls via reading and writing currents. Antiferromagnetic materials are candidates for ultrafast operation due to THz antiferromagnetic spin dynamics, high packing densities due to the absence of stray magnetic fields, and stability due to insensitivity to external magnetic fields [1,2]. Meanwhile, the long spin diffusion lengths [3] and theoretically predicted superfluid transport of spin currents [4] in antiferromagnetic insulators are crucial for low-power device operation. The electrical control of magnetic spin textures has been thus far realized in epitaxially grown NiO on MgO substrates [5] and ferrimagnetic maghemite (γ−Fe2O3) and magnetite (Fe3O4) thin films [6].

We report the preparation of antiferromagnetic NiO thin films with (111) orientation on *c*-plane sapphire (1000) substrates by off-axis RF magnetron sputtering from a NiO target. The off-axis angle was 45°, and the sputtering pressure was 5 mTorr. Samples were grown with thicknesses ranging from 5 – 50 nm, and with growth temperatures from room temperature to 600°C, to determine optimum conditions. Structural characterization by x-ray diffraction demonstrates a high degree of epitaxy across a range of deposition temperatures and thicknesses. The deposition temperature and thickness dependence of epitaxial quality is investigated, with a characterization of the strain state, mosaicity, and crystallographic relationship between substrate and film. Evidence for antiferromagnetic order forming domains in NiO is provided via magnetic characterization of the films. Our results are essential for the optimization of the fabrication of high quality epitaxial antiferromagnetic films for practical spintronics devices.

[1] J. Železný, P. Wadley, K. Olejník, A. Hoffmann, and H. Ohno, Nat. Phys. 14, 220 (2018)

[2] V. Baltz, A. Manchon, M. Tsoi, T. Moriyama, T. Ono, and Y. Tserkovnyak, Rev. Mod. Phys. 90, 015005 (2018).

[3] R. Lebrun, A. Ross, S. A. Bender, A. Qaiumzadeh, L. Baldrati, J. Cramer, A. Brataas, R. A. Duine, and M. Kläui, Nature 561, 222 (2018).

[4] S. Takei, B. I. Halperin, A. Yacoby, and Y. Tserkovnyak, Phys. Rev. B 90, 094408 (2014).

[5] T. Moriyama, K. Oda, T. Ono, Sci. Rep. 8, 14167 (2018).

[6] L. Baldrati, A. Ross, T. Niizeki, C. Schneider, R. Ramos, J. Cramer, O. Gomonay, M. Filianina, T. Savchenko, D. Heinze, A. Kleibert, E. Saitoh, J. Sinova, and M. Kläui, Phys. Rev. B 98, 024422 (2018).

10:00am **TF+EM+MI+MN+OX+PS-MoM6 Structural and Magnetic Properties of CoPd Alloys for Non-Volatile Memory Applications***, S. Gupta, J.B. Abugri, B.D. Clark,* University of Alabama*; P. Komninou,* Aristotle University of Thessaloniki*; **Sujan Budhathoki**, A.J. Hauser, P.B. Visscher,* University of Alabama

A study of perpendicular magnetic anisotropy (PMA) CoPd alloys is presented as a simple means of pinning MgO-based perpendicular magnetic tunnel junctions (pMTJs) for spin transfer torque magnetic tunnel junction (STT-MRAM) applications. A compositional study of the Co_xPd_{100-x} alloys at 50 nm thickness showed that the maximum coercivity and anisotropy was found for $Co_{25}Pd_{75}$. Perpendicular magnetic tunnel junction stacks were deposited using different compositions of CoPd. Current-in-plane tunneling measurements indicated that the TMR values roughly correlated with the coercivity and anisotropy of the single layers. A thickness study indicated that the alloy was fully perpendicular for thicknesses as low as 20 nm. Various seed layers were employed to optimize the coercivity of the $Co_{25}Pd_{75}$ layer. Magnetometry, X-ray diffraction (XRD), scanning electron microscopy (SEM) and high resolution transmission electron microscopy studies were carried out to relate the magnetic and structural properties of these layers. These studies showed

that the highest coercivity $Co_{25}Pd_{75}$ was achieved on a seed layer of Ta/Pd which helped to crystallize the CoPd layer in an fcc (111) orientation.

10:40am **TF+EM+MI+MN+OX+PS-MoM8 Size Effects of the Electromechanical Response in Ferroic Thin Films: Phase Transitions to the Rescue***, **Nazanin Bassiri-Gharb**,* Georgia Institute of Technology **INVITED**

Silicon-integrated ferroelectric thin films have been leveraged over the last two decades for fabrication of high performance piezoelectric microelectromechanical systems (MEMS) devices. Ceramic $Pb(Zr_xTi_{1-x})O_3$(PZT) thin films have been often the material of choice, due to their large electromechanical response, especially at morphotropic phase boundary compositions (MPB at x ~0.52), where co-existence of multiple crystallographic distortions can enhance extrinsic electromechanical contributions. However, ferroelectric thin films suffer from extrinsic size effects that lead to deteriorated piezoelectric properties in thin and ultra-thin films. Here we report on different strategies for processing of thin films with enhanced piezoelectric response with respect to traditionally processed PZT thin films.

Specifically, we will discuss preparation of superlattice-like polycrystalline PZT thin films through chemical solution depositions, polycrystalline relaxor-ferroelectric thin films (PMN-PT), and finally alternative non-ferroelectric compositions, where the electric field-induced phase transitions can result in substantial enhancement in thinner films, even where traditional

11:20am **TF+EM+MI+MN+OX+PS-MoM10 Ferroelectrics Meet Ionics in the Land of van der Waals***, S. Neumayer,* Center for Nanophase Materials Sciences, Oak Ridge National Laboratory*; J. Brehm,* Vanderbilt University*; M.A. McGuire,* Oak Ridge National Laboratory*; M.A. Susner,* Air Force Research Laboratory*; E. Eliseev,* National Academy of Sciences of Ukraine*; S. Jesse, S.V. Kalinin,* Center for Nanophase Materials Sciences, Oak Ridge National Laboratory*; A.N. Morozovska,* National Academy of Sciences of Ukraine*; S. Pantelides,* Vanderbilt University*; N. Balke, **Petro Maksymovych**,* Center for Nanophase Materials Sciences, Oak Ridge National Laboratory

Van der Waals crystals of metal thiophosphates can be thought of as derivatives of transition metal dichalcogenides where 1/3 of metal atoms is replaced with diphosphorous, thereby stabilizing the remaining 2/3 of metal ions in low oxidation states.1 Consequently, thiophosphates enable ultrathin magnetic, ferroelectric and Mott insulating materials, in q2D materials while also providing new opportunities for multifunctional interfaces .

Of particular interest is $CuInP_2S_6$, where ferroelectricity emerges out of ionically conducting state .2,3 In this work, we discuss unusual and perhaps anomalous properties observed in $CuInP_2S_6$ in both states.

$CuInP_2S_6$ exhibits giant negative electrostriction (Q_{33} = -3.2 m^4/C^2), which leads to large piezoelectric coefficients despite small polarization values and increase of Tc with applied pressure. It's the only material other than polymer PVDF for which such behavior is experimentally confirmed. Density functional theory reveals that the reason for negative electrostriction is a slight movement of Cu ions into the van der Waals gap due to anharmonicity of the potential well.4 Moreover, under high compressive strain, Cu starts to form interlayer bonds with sulfur across the van der Waals gap, leading to an additional phase of high polarization. Consequently, the potential distribution exhibits 4 instead of the usual two minima - a quadruple well, that is precisely tunable by strain. In the paraelectric state above ~70°C, Cu ion mobility drastically increases. Intriguingly, Cu can be reversibly extracted out of the lattice without visible damage. Finally, the selenide sibling $CuInP_2Se_6$, exhibits a lower transition temperature and propensity toward antiferroelectric ordering under the effect of depolarizing fields. In this material, we have for the first time observed piezoelectric response confined to domain walls (opposite to ferroelectrics), fulfilling the long-standing predictions for polar antiferroelectric domain walls and providing a new model system for emergent properties of topological defects in ferroic order parameter fields.

Research sponsored by Division of Materials Science and Engineering, Basic Energy Sciences, US Department of Energy. Microscopy was conducted at the Center for Nanophase Materials Sciences, which is a DOE Office of Science User Facility.

1Susner et al, Adv. Mater. 29,1602852 (2018)

2Neumayer et al, Phys. Rev. Materials **3**, 024401 (2019)

3Balke et al, ACS Appl. Mater. Interfaces 10, 27188 (2018)

4Brehm et al, in review

11:40am **TF+EM+MI+MN+OX+PS-MoM11 Adsorption-controlled Epitaxial Growth of the Hyperferroelectric Candidate LiZnSb on GaSb (111)***, D. Du, P. Strohbeen,* University of Wisconsin - Madison*; H. Paik,* Cornell University*; C. Zhang, P. Voyles, **Jason Kawasaki**,* University of Wisconsin - Madison

A major challenge for ferroelectric devices is the depolarizing field, which competes with and often destroys long-range polar order in the limit of ultrathin films. Recent theoretical predictions suggest a new class of materials, termed hyperferroelectics [1], should be immune to the depolarizing field and enable ferroelectric devices down to the monolayer limit. Here we demonstrate the epitaxial growth of hexagonal LiZnSb, one of the hyperferroelectric candidate materials, on GaSb (111) substrates. Due to the high volatility of all three atomic species, we find that stoichiometric films can be grown in a thermodynamically adsorption-controlled window, using an excess zinc flux. Outstanding challenges remain in controlling the point defects of LiZnSb and in controlling polytypism. While the films primarily grow in a hexagonal "stuffed wurtzite" phase (space group *$P6_3mc$*), which is has the desired polar structure, there exists a competing cubic "stuffed zincblende" polymorph that is nonopolar (*F-43m*). We will discuss our strategy towards controlling defects and polytypism in LiZnSb, which is based in large part on the wurtzite – zincblende polytypism observed in InAs. We will also present preliminary electrical measurements on phase pure ferroelectric capacitor structures.

This work was supported by the Army Research office (W911NF-17-1-0254) and the National Science Foundation (DMR-1752797).

[1] K. F. Garrity, K. M. Rabe, and D. Vanderbilt, Phys. Rev. Lett. **112**, 127601(2014).

Thin Films Division
Room A124-125 - Session TF-MoM
Thin Films for Electrochemistry and Energy Storage

Moderators: Parag Banerjee, University of Central Florida, Jason Avila, U.S. Naval Research Laboratory

8:20am **TF-MoM1 Enabling Energy Dense Lithium Batteries Using Thin Film Technology***, **Wyatt Tenhaeff**,* University of Rochester **INVITED**

As new materials and electrochemical cell compositions are developed to meet the ever-increasing demand for high capacity, long-life lithium batteries, thin film deposition technology provides critical capabilities for engineering key interfaces within these batteries. This presentation will present our efforts to address challenges in lithium metal and silicon anodes. Thin films are integrated as ultrathin solid electrolytes in Li metal batteries and as protective coatings on Si anodes to limit undesirable side reactions.

Key requirements for electrolytes in solid-state lithium metal batteries are a large electrochemical stability window and low area-specific resistance (ASR). Solid electrolytes must also possess robust mechanical properties to accommodate large-scale production and integration into conventional lithium battery cell designs. To realize these properties, 50 nm-thick films of lithium phosphate oxynitride (Lipon) were deposited onto microporous polymer separators (Celgard) using RF magnetron sputtering. These separators provide a low ASR due to the thin, dense Lipon film; the total resistance of the separator was determined to be 40 Ω cm^2 in alkyl carbonate electrolytes, which is much lower than traditional ceramic electrolytes membranes, such as those fabricated from Garnet and NASICON-class of solid electrolytes. Furthermore, these composite separators inhibit chemical cross-diffusion and reaction between anode and cathode in both Li-S and Li-$LiMn_2O_4$ cells.

Silicon is also an intriguing next-generation anode offering charge capacities comparable to lithium metal, yet significant challenges arise from the >300% volume expansion of Si during lithiation. To address continual electrochemical reduction of lithium ion battery electrolyte on Si anodes, nanoscale, conformal polymer films were synthesized as artificial solid electrolyte interface (SEI) layers. Initiated chemical vapor deposition (iCVD) was employed to deposit poly(1,3,5,7-tetravinyl-1,3,5,7-tetramethylcyclotetrasiloxane) (pV4D4) onto silicon thin film electrodes. 25 nm-thick pV4D4 films on Si electrodes improved initial coulombic efficiency by 12.9% and capacity retention over 100 cycles by 64.9% relative to

untreated electrodes. PV4D4 coatings also improved rate capabilities, enabling higher lithiation capacity at all current densities. Post-cycling FTIR and XPS showed that pV4D4 inhibited electrolyte reduction and altered the SEI composition, with LiF formation being favored. This work will guide further development of polymeric artificial SEIs to mitigate electrolyte reduction and enhance capacity retention in Si electrodes.

9:00am **TF-MoM3 Molecular Layer Deposition of Organic Li-containing Thin Film for Li Ion Solid-state Batteries***, **Haotian Wang**,* University of Maryland, College Park

High performance 3D solid-state Li ion batteries require uniform and conformal coating of solid electrolytes with high mechanical compliance, to enable the usage of high energy density anodes, such as Si, and maintain a good electrode-electrolyte contact during cycling. Molecular layer deposition (MLD) is a vapor phase deposition technique that deposits thin films in a layer by layer manner. The incorporation of organic moieties into the resulting MLD thin films potentially provides enhanced mechanical flexibility while retaining the high uniformity and conformality, making this technique promising for applications in the next generation 3D solid state batteries.

In this work, we are presenting a fundamental study of organic Li-containing thin film by MLD. A comprehensive understanding of the organic-inorganic reaction and growth mechanism was obtained based on a model chemistry with Li tertbutoxide (LiO^tBu) and propanediol (PPD). The ALD-like growth temperature window, linear growth and the self-limiting behavior were observed by employing in-situ ellipsometry during deposition. Chemical structure of the film grown by LiO^tBu and PPD was characterized by X-ray photoelectron spectroscopy (XPS) and simulated by ab-initio calculation. Based on both the experimental characterization and theoretical calculation, a hybrid inorganic-organic Li-containing material, Li propane oxide, with well-defined stoichiometry ($Li_{1.6}C_3H_6O_{2.2}$) was successfully synthesized via MLD.

Additionally, nucleation delay during film growth was observed, indicating an island growth and crystal formation. Single crystal nucleus with cubic crystal structure at early growth stage was observed by transmission electron microscopy (TEM), while at later growth stage, nucleus coalesced and formed polycrystalline thin film with high surface roughness. To reduce the surface roughness and enhance the applicability of the MLD film in high aspect ratio geometries, we applied nitrogen plasma to the Li propane oxide MLD process. The nitrogen plasma modified MLD process showed no nucleation delay and was later used as seeding for Li propane oxide growth. A significant attenuation of surface roughness of Li propane oxide MLD films grown on this seeding layer was observed. The understanding of the inorganic-organic reaction and the development of the seeding layers for the Li-containing thin film will benefit directly to the flexible and three-dimensional solid state battery research.

9:20am **TF-MoM4 Organic/Inorganic Solid Electrolytes and Electrode Coatings for 3D Lithium-ion Microbatteries***, **Ryan Sheil**[1], J. Lau,* University of California, Los Angeles*; K. Jungjohann,* Sandia National Laboratories*; J. Yoo,* Los Alamos National Laboratory*; B. Dunn, J.P. Chang,* University of California, Los Angeles

Lithium-ion batteries have been an enabling factor in the success of consumer electronics and have the potential to offer energy storage solutions for microelectromechanical systems (MEMS), such as sensors for IoT and biomedical applications. Three-dimensional battery architectures allow for an effective decoupling of the areal energy and power density resulting in improved areal footprint utilization required of these small devices. In 3D battery designs, the short distances between the anode and cathode improve the transport properties allowing for high areal power densities and the high aspect-ratio nature of the electrodes promotes high areal energy densities. One requirement in the utilization of 3D based electrodes is the incorporation of a solid electrolyte that can be coated pinhole free and conformally on high aspect ratio structures. The solid electrolyte material must be ionically conductive, electronically insulating, and be flexible to withstand the volume expansion and contraction of the electrode during charge and discharge.

The self-limiting nature of atomic layer deposition allows for precise thickness control across high aspect ratio structures. ALD $Li_xAl_ySi_zO$ was synthesized utilizing lithium tert-butoxide (LTB), trimethyl aluminum (TMA), and tris(tert-butoxy) silanol (TTBS). ALD $Li_xAl_ySi_zO$ was integrated with high aspect ratio SiGe nanowires for in-situ TEM characterization, where the chemical, structural, and morphological changes of the electrode/electrolyte system were characterized in-situ during lithiation and delithiation. An ALD $Li_xAl_ySi_zO$-coated $Si_{0.4}Ge_{0.6}$ nanowire demonstrates lithiation and delithiation with an intact solid state electrolyte layer with ~39% radial expansion observed upon lithiation. To further improve the mechanical properties for integration on high capacity/large volume expansion anodes, an MLD process was explored to synthesize lithium alkoxide and aluminum alkoxide utilizing trimethyl aluminum and lithium tert-butoxide coupled with glycerol. Incorporation of the MLD, ALD, and MLD/ALD coatings were integrated with Si and Co_3O_4 elecrodes, where improvements to cycling stability and coulombic efficiency were observed. $Li_xAl_ySi_zO$ coated Co_3O_4 thin films exhibited improved coulombic efficiency (99.5% (coated), 90.5% (uncoated) and capacity retention (2458 mAh/cm^3 (coated), 2038 mAh/cm^3 (uncoated)) after 100 cycles at 2C.

9:40am **TF-MoM5 Structural Rearrangement in $Li_xV_2O_5$ Thin Films, a Cathode Material for All-solid-state Batteries***, **Angelique Jarry**,* University of Maryland, College Park*; N. Pronin, M. Walker,* The Ohio State University*; J. Ballard,* University of Maryland*; D. Stewart,* University of Maryland, College Park*; L.J. Brillson,* The Ohio State University*; G.W. Rubloff,* University of Maryland, College Park

The requirements to enable all-solid-state batteries (SSBs) are extremely stringent and necessitate control of the chemistry and interfaces over a wide structural length and long-time scales. Investigations using multi-probe approaches have confirmed that surface composition, defects, structure, and morphology of the electrodes/electrolyte themselves has a strong impact on interfacial processes. Therefore, to understand how to overcome the barriers related to the implementation of SSBs, it is necessary to start with pure, well-defined models systems such as cathode thin films. V_2O_5 is of particular interest due to the large interlayer spacing of its metastable varieties that allows a topochemical de-intercalation of various cation ($M_xV_2O_5$ withM = Li, Na, Mg). However this cation de-insertion leads to structural distortion/surface reconstruction that impedes the cathode performance. A detailed understanding of these degradation mechanisms is needed to identify the appropriate remedies.

In this work, V_2O_5 thin films of ~500 nm were produced by atomic layer deposition (ALD) on sputtered gold on silicon substrate. The films were subsequently electrochemically lithiated in liquid electrolytes by galvanostatic cycling i.e, $Li_xV_2O_5$ with $x < 2$. We investigated the effects of lithiation on the structural characteristics and surface morphology of $Li_xV_2O_5$ thin films as a function of depth through multiple methods. Change in the crystallinity and local atomic structure were probed with Raman spectroscopy (RS), X-ray photoelectron spectroscopy (XPS), optical/scanning electron microscopy and, atomic force microscopy (AFM). We demonstrated that partial lithiation of V_2O_5 results in reduction of the vanadium that is accompanied by a progressive surface hydroxylation and amorphization of the films. At high lithium content, significant non reversible structural rearrangements associated with the destabilization of the V-O framework are observed. The correlation between the lithium content, structural stability, electrode's surface activity and electrochemical performance will be presented and discussed.

Acknowledgement

This work was supported by the Nanostructures for Electrical Energy Storage (NEES), an Energy Frontier Research Center funded by the U.S. Department of Energy, Office of Science and by the NSF grant DMR-18-00130.

10:00am **TF-MoM6 Atomic Layer Deposition and Performance of Sodium and Potassium Electrolytes for Conformal Solid State Batteries***, **Blake Nuwayhid**, A. Jarry, G.W. Rubloff, K. Gregorczyk,* University of Maryland, College Park

Solid-state batteries (SSBs) provide significant advantages over conventional liquid electrolyte based batteries, such as their non-flammable nature and improved chemical stability. Specifically, thin film SSBs possess the ability to provide high power densities due to a shorter transport pathway and are compatible with semiconductor device manufacturing. The fabrication of 3D thin film SSBs through conformal deposition processes is extremely promising due to the dramatic enhancement in both energy and power densities compared to planar cells. Our group recently demonstrated the fabrication of the first fully conformal 3D Li-based thin film SSBs, in which all battery components were deposited by Atomic Layer Deposition (ALD).[1] This was made possible through the development of a new lithium phosphazene (Li_2PO_2N) solid electrolyte. Sodium and potassium ion batteries are interesting as well for SSB applications due to the lower cost and higher abundance of the alkali metals compared to lithium. However, few such efforts have been put into

[1] **TFD James Harper Award Finalist**

solid state systems, and none in 3D thin film SSBs. In this presentation, we will discuss the development of conformal sodium phosphorous oxynitride (NaPON) and potassium phosphate (KPO) ion-conductors, and their potential in 3D thin film SSBs. Similar to our previously published LiPON ALD process[2], NaPON and KPO processes use the thermal reaction of sodium tert-butoxide or potassium tert-butoxide, with diethyl phosphoramidate. The growth behavior of NaPON and KPO were very similar, exhibiting a linearly increasing growth rate of 0.1-1.0 Å/cycle at 250-400 °C, but no temperature window was observed. An ultra-high vacuum chamber coupled the ALD reactor to a X-ray Photoelectron Spectrometer, allowing for sensitive film characterization as a function of temperature. Characterization was also complemented by Raman and IR spectroscopy to reveal differences in the phosphorus oxynitride bonding networks. The structure of NaPON resembled that of LiPON, containing similar atomic ratios (P/N = 1) and 2 nitrogen species (=N– and >N–), whereas KPO films contained only 1% nitrogen and a considerable amount of carbon incorporation. We will also highlight the electrochemical behavior of the films in planar solid-state cells and 3D systems in high aspect ratio substrates.

1. Pearse, A.; Schmitt, T.; Sahadeo, E.; Stewart, D. M.; Kozen, A.; Gerasopoulos, K.; Talin, A. A.; Lee, S. B.; Rubloff, G. W.; Gregorczyk, K. E. *ACS Nano* **2018,***12*, 4286-4294.

2. Pearse, A.; Schmitt, T. E.; Fuller, E. J.; El-Gabaly, F.; Lin, C. F.; Gerasopoulos, K.; Kozen, A. C.; Talin, A. A.; Rubloff, G.; Gregorczyk, K. E. *Chemistry of Materials* **2017,***29*, 3740-3753.

10:40am **TF-MoM8 ALD as Tool for Bottom-up Synthesis of Catalyst Powders***, F. Rosowski, **Daniel Loeffler**,* BASF Se, Germany **INVITED**

Atomic Layer Deposition is mainly applied in microelectronics as a thin film deposition technique. In academic research, ALD is also applied for synthesis of battery materials and catalysts. The main challenge for ALD in these research fields is the morphology of the substrate materials, usually small particles with high specific surface areas, e.g. up to 1000 m^2/g for zeolites. Catalytic reactors can hold packed beds of several cubic meters of catalyst. The high specific surface areas and the amounts in which such catalysts are needed require safe and efficient ways of dosing ALD precursors without bypass and waste. And while mass and heat transport limitations play only a minor role in the case of flat substrates, these phenomena need to be considered when coating large amounts of powder.

At BasCat, ALD is used in several projects to synthesize and modify catalysts. Some research is done along well-established lines of work in the field of supported metal catalysts, e.g. modifying supported metal catalysts with metal oxide layers, but the focus lies on catalysts used for selective oxidation reactions, typically consisting of mixed metal oxides or phosphates. Catalysts are usually prepared in two batch sizes. For establishing suitable ALD process conditions, a sample size of about 1 cm^3 is used. In a second step, catalyst amounts of 10–25 cm^3 are prepared. It is important that process conditions established on the small scale are easily transferrable to the large scale.

For this purpose, a new and unique test facility was installed at BasCat equipped with a thermogravimetric balance as analytical small scale ALD reactor and a second reactor for catalyst synthesis on a large scale via ALD.[1] Based on our first ALD results, a fixed bed was chosen as reactor geometry for the analytical reactor and the synthesis reactor.

In order to check the feasibility of our new in situ method and the ALD performance of our fixed bed reactor, first studies covered the deposition of alumina on a typical catalyst support, a silica with high surface area (Davisil 636). It was shown that the fixed bed geometry is suitable for ALD, that the substrate is homogeneously covered, and that scaling-up from 1 cm^3 to 10 cm^3 is possible.[2]

The combination of analytical reactor and synthesis reactor was then successfully used for modifying supported metal catalysts with layers of alumina, alucone, and zinc oxide. Other works included the deposition of rhenium on silver and phosphorus on vanadia.[3]

[1] Strempel et al., *Rev. Sci. Instrum.*, 074102. 2017

[2] Strempel et al., F.,*Nanomaterials*, 365. 2018

[3] Strempelet al., *J. Vac. Sci. Technol. A Vacuum, Surfaces, Film.*, 01A135. 2016

11:20am **TF-MoM10 Strategies for the Stabilization of Metal Anodes for Li and Na Metal Batteries***, **Yang Zhao**[1], X. Sun,* University of Western Ontario, Canada

Li-metal batteries (LMBs) and Na-metal batteries (NMBs) are considered as the promising candidates to replace the conventional Li-ion batteries due to their high theoretical energy density. Li metal and Na metal are the ultimate choices as anodes to achieve their high energy density due to the high specific capacity, low electrochemical potential and lightweight [1]. However, as alkali metals, both Li and Na metal anodes suffer from serious challenges including 1) dendrite formations and short circuits; 2) Low Coulombic efficiency (CE) and poor cycling performance; and 3) Infinite volume changes. This presentation mainly focuses on the design of multiple strategies for the stabilization of Li and Na metal anode for LMBs and NMBs.

Solid electrolyte interphase (SEI) layer is one of the key factors for the Li and Na deposition behaviors [2]. We developed different approaches to fabricate the artificial SEI with significantly improved electrochemical performances. Firstly, we have demonstrated different ultra-thin protective layers for Li and Na metal anodes by atomic layer deposition (ALD) and molecular layer deposition (MLD) techniques, including Al_2O_3, alucone, and polyurea, et al [3]. More recently, we designed a dual-protective layer for Li metal anode with precisely controlled thicknesses, compositions and mechanical properties [4]. Secondly, we developed the in-situ solution-based methods to fabricate the Li_3PS_4 and Na_3PS_4 as protective layers for both Li and Na metal anodes with enhanced performances and reduced dendrite growth [5].

To address another challenge of volume change, 3D conductive interlayers and hosts have been designed for Li and Na metal anodes. Carbon paper (CP) and modified CP with carbon nanotubes have been used as host/interlayer with excellent electrochemical performance under high current density and high capacity [6].

In conclusion, we developed the different approaches, including protective layers fabricated by ALD/MLD and solution methods, interlayers, and 3D skeleton design, for Li and Na metal anodes with enhanced electrochemical performances and reduced dendrite growth. Meanwhile, the ideas have been also applied to solve the practical issues for testing Li and Na metal batteries.

[1] ***Energy & Environmental Science***, 2018, 11, 2673

[2] ***Joule***, 2018, 2, 2583

[3] ***ACS Energy Letters***, 2018, 3, 899; ***Small Methods***, 2018, 2, 1700417; ***Advanced Materials***, 2017, 29, 1606663; ***Nano Letters***, 2017, 17, 5653; ***Advanced Materials***, 2019, 31, 201806541

[4] ***Matter***, 2019, in press

[5] ***Journal of Materials Chemistry A***, 2019, 7, 4119

[6] ***Nano Energy***, 2018, 43, 368; ***Energy Storage Materials***, 2018, 15, 415; ***Small***, 2018, 14, 1703717

11:40am **TF-MoM11 Competition Between Incorporation and Desorption of Nitrogen in Plasma-Enhanced Atomic Layer Deposition of Cobalt and Cobalt Nitride Catalysts***, **Gerben van Straaten**,* Eindhoven University of Technology, The Netherlands, Netherlands*; H.O.A. Fredriksson,* Syngaschem BV, Netherlands*; R. Deckers,* Eindhoven University of Technology, Netherlands*; M.F.J. Vos,* Eindhoven University of Technology, The Netherlands, Netherlands*; K.-J. Weststrate,* Syngaschem BV, Netherlands*; W.M.M. Kessels,* Eindhoven University of Technology, The Netherlands, Netherlands*; M. Creatore,* Eindhoven University of Technology, Netherlands

Cobalt catalysts have various applications in the chemical industry. Most prominently, metallic Co is used in the production of synthetic fuels via the Fischer-Tropsch process, while cobalt nitrides (with the general formula CoN_x) are being explored as noble-metal free electro-catalysts for the oxygen evolution reaction. Atomic Layer Deposition (ALD) of Co and CoN_x thin films and nanoparticles can be achieved using a variety of Co precursors with NH_3- plasma[1]. Moreover, the precursors $Co(CO)_8$ and $CoCp_2$ can yield either metallic Co or CoN_x, depending on temperature[2]. We will demonstrate here that this is due to the metastable nature of CoN_x.

We have found that film deposition below 350°C onto thermally grown SiO_2 using $CoCp_2$ and an inductively coupled NH_3 plasma yielded Co_2N, while deposition at higher temperatures resulted in Co with traces of N. To gain insight into the incorporation of N into the films, Spectroscopic

[1] **Late-Abstract Energy Transition Symposium Theme Award**

Ellipsometry (SE) and X-ray photoelectron spectroscopy (XPS) were performed on 20 nm Co films exposed to NH_3 plasma. These measurements revealed that at 150°C, 30 min of plasma exposure resulted into the formation of a 5 nm thick N-enriched diffusion layer at the film surface. However, the nitridation process is temperature-dependent: at 350°C and above, no N incorporation into the bulk of the layer was observed. The origin of this temperature dependence was analyzed using Temperature-Programmed Desorption (TPD), which showed that N could be released from the low temperature plasma-treated layers in two stages. Around 270°C, N desorbed from the surface, but no loss of N from the bulk of the Co layer was observed. Subsequently, starting at 350°C, complete effusion of bulk N took place, allowing the film to relax back to its original thickness.

These results show that at low temperatures N is incorporated into the growing film from the NH_3 plasma, leading to the formation of homogeneous CoN_x films, but at elevated temperatures, N desorption outpaces incorporation and metallic Co is formed instead. Thus, it is possible to deposit Co and CoN_x catalysts with controlled stoichiometry by balancing N incorporation and desorption. Preliminary measurements show that Co nanoparticles and thin films deposited in this way are capable of catalyzing the methanation reaction; further characterization of their activity is currently ongoing.

[1] M. F. J. Vos, G. van Straaten, W. M. M. Kessels, and A. J. M. Mackus, *J. Phys. Chem. C*, p. acs.jpcc.8b06342, Sep. 2018.

[2] H.-B.-R. Lee and H. Kim, *Electrochem. Solid-State Lett.*, vol. 9, no. 11, p. G323, Nov. 2006.

2D Materials
Room A226 - Session 2D+AP+EM+MI+MN+NS+PS+TF-MoA

Nanostructures including Heterostructures and Patterning of 2D Materials

Moderator: Deep Jariwala, University of Pennsylvania

1:40pm **2D+AP+EM+MI+MN+NS+PS+TF-MoA1 Tailoring and Patterning 2D Material Interfaces Through Chemical Functionalization***, **Arend van der Zande**,* University of Illinois at Urbana-Champaign **INVITED**

Two-dimensional materials are all surface, so any change in the surface chemistry affects the entire material. This offers a challenge and an opportunity to engineering the material properties and new device behavior. There are many strategies to altering the chemical structure of 2D materials, yet one of the most successful is the chemical functionalization with low energy plasmas such as hydrogen and fluorine. Functionalization enables phase changes within materials to dramatically alter their properties, can be applied post synthesis and device fabrication, and is compatible with lithography for spatial patterning. Most studies of chemical functionalization focus on single functionalization of single 2D materials, yet there are many opportunities when applying the principles of chemical functionalization to spatially engineer the properties though in plane interfaces or out of plane in heterostructures.

First, we will examine selective etching with XeF_2 to pattern heterostructures using graphene etch stops. These techniques are self-limiting, yet scalable, and enable the patterning of 2D heterostructures into 3D multilayer circuitry. Moreover, devices like encapsulated graphene transistors fabricated with these techniques have exceptionally low contact resistances and mobilities which approach theoretical limits.

Second we will present a new strategy for tailoring the stoichiometry of functionalized graphene compounds through the systematic control of the ratio between adatoms. We demonstrate new ternary HFG compounds and reversible switching of material stoichiometry via the sequential exposure of graphene to low energy H plasma and XeF_2 gas. By patterning regions of different functionalization on a single chip, we perform direct comparisons and show spatially controlled tuning of the relative surface properties such as wettability, friction, electronic conductivity and molecular adhesion. Taken together, these studies show that chemical functionalization offers new atomically precise nanofabrication and materials engineering techniques for scalable engineering of circuitry along all three dimensions.

2:20pm **2D+AP+EM+MI+MN+NS+PS+TF-MoA3 Dual-Route Hydrogenation of the Graphene/Ni Interface***, **Rosanna Larciprete**,* CNR-Institute for Complex Systems, Roma, Italy*; D. Lizzit,* Elettra - Sincrotrone Trieste, Trieste, Italy*; M.I. Trioni,* CNR-Institute of Molecular Science and Technologies, Milano, Italy*; P. Lacovig, L. Bignardi, S. Lizzit,* Elettra - Sincrotrone Trieste, Trieste, Italy*; R. Martinazzo,* Università degli Studi di Milano, Milano, Italy

Although the high surface-to-weight ratio would make graphene (Gr) one of the most promising material for hydrogen accumulation, up to now only moderate gravimetric density values of 1-2% have been obtained at room temperature (RT). The ultimate H coverage is limited by the competition between the adsorption and desorption/abstraction processes and by the elastic energy that accumulates in the C lattice once puckered by the local sp3rehybridization of the C atoms binding hydrogen. Moreover, for epitaxial Gr on metals, the substrate-induced Gr corrugation might modulates periodically H adsorption. In this respect, the Gr/Ni(111) interface appears much more favorable than other graphene/metal systems, as the limitations due to the presence of the moirè supercell vanish due to commensurate relation between the Gr and Ni(111) lattices. Moreover, hydrogenation might be favored by the peculiar reactivity of Gr/Ni(111).This issues motivated a re-investigation of the interaction of this particular interface with hydrogen.

In this study [1]we used x-ray photoelectron spectroscopy (XPS) and near edge x-ray absorption fine structure spectroscopy (NEXAFS) to follow the RT hydrogenation of Gr/Ni(111) and determined the configuration of the hydrogenated interface by scanning tunneling microscopy (STM). We found that hydrogenation proceeds through a dual path that includes hydrogen chemisorption on top of the graphene followed by a slow but continuous intercalation below graphene. At low coverage H atoms predominantly adsorb as monomers and chemisorption saturates when ≈ 25% of the surface is hydrogenated. The formation of C−H bonds determines new components in the C 1s core level spectrum that are attributed by DFT calculations to C atoms directly bonded to H and to their first neighbors. In parallel with chemisorption, with a much lower rate, H atoms intercalate below Gr and bind to Ni surface sites. Thermal programmed desorption measurements showed that chemisorbed hydrogen is released around 600 K, whereas the intercalated phase desorbs abruptly slightly below 400 K. Then the Gr cover, besides offering a storage volume for the intercalated H, stabilizes it above room temperature rising by a few tens of kelvins the H2 release temperature with respect to the bare Ni(111) surface.

The effectiveness of these results can be expanded by using Ni substrates with large specific surface, as nanoparticles or nanostructured foils, which, when covered with Gr, might become media where hydrogen can be loaded and stored above room temperature.

[1] D. Lizzit et al. ACS Nano 13 (2019) 1828

2:40pm **2D+AP+EM+MI+MN+NS+PS+TF-MoA4 Assembly of Arrays of Predefined Monolayer Features into vdW Heterostructure by a Continuous Exfoliate-align-Release Process***, **Vu Nguyen**, H. Taylor,* University of California at Berkeley

One of the major challenges of van der Waals (vdW) integration of 2D materials is the high-yield and -throughput assembly of pre-defined sequence of monolayers into heterostructure arrays. Although a variety of techniques have been developed to exfoliate the 2D materials from the source and deterministically place them onto a target substrate, they typically can transfer only either a wafer-scale blanket or a small flake at a time with uncontrolled size and shape. Here we present a method to exfoliate arrays of lithographically defined monolayer MoS_2 and WS_2 features from multilayer sources and directly transfer them in a deterministic manner onto target substrates. The continuous exfoliate-align-release process, without the need of an intermediate carrier substrate, was enabled by a new transfer medium fabricated by spin-coating a low-crosslinked and transparent adhesive on a transparent, electrostatically active backing material with low surface energy. MoS_2/WS_2 vdW heterostructure arrays produced by this method were characterized, showing coupled photoluminescence between the monolayers. Light-emitting devices using WS_2 monolayer were also demonstrated, proving the functionality of the fabricated materials. This method promises to produce large-area monolayer and multiplex heterostructure arrays with capability to integrate with existing semiconductor manufacturing equipment.

3:00pm **2D+AP+EM+MI+MN+NS+PS+TF-MoA5 van der Waals Heterojunction Photothermoelectric Effect in MoS_2/Graphene Monolayers***, **Yunqiu Kelly Luo**,* The Ohio State University*; T. Zhou,* University at Buffalo, State University of New York*; M. Newburger,* The Ohio State Univesity*; R. Bailey-Crandell, I. Lyalin,* The Ohio State University*; M. Neupane,* U.S. Army Research Laboratory*; A. Matos-Abiague,* Wayne State University*; I. Zutic,* University at Buffalo, State University of New York*; R. Kawakami,* The Ohio State University

Two-dimensional (2D) van der Waals (vdW) heterostructures provide a vast playground for exploring new phenomena due to its unique ability to tailor and combine dissimilar materials with atomic precision. In particular, the combination of graphene and transition metal dichalcogenides (TMDC) garners immense interest due to their novel optoelectronic, valleytronic and spintronic properties. Here, we report the observation of a highly tunable vdW heterojunction photothermoelectric effect (HPTE) in dual-gated MoS_2/graphene heterostructures, identified by a signature six-fold photocurrent pattern as a function of heterojunction bias and carrier density. In stark contrast to photovoltaic and photothermionic effects, we discover a new mechanism arising from photoexcitation of hot electrons in graphene and subsequent thermoelectric transport across the vdW junction. While analogous to lateral photothermoelectric effects at quasi-1D junctions in single layers, the vertical geometry of HPTE offers area scaling of 2D active regions and establishes, for the first time, the photothermoelectric response in vdW heterostructures. Operating at both low (18 K) and room temperatures, the discovery of HPTE creates new

possibilities for electrically-tunable broadband photodetectors and atomically-thin spin caloritronic devices.

3:20pm **2D+AP+EM+MI+MN+NS+PS+TF-MoA6 Formation of Edge-bonded MoS_2-graphene Nanoribbons by On-surface Synthesis***, **Mark Haastrup**, M. Mammen, J. Rodríguez-Fernández, J.V. Lauritsen,* Aarhus University, Denmark

2D materials exhibiting unique material properties have the potential for a huge impact on our future. Graphene, as the first discovered truly 2D material, has been extensively studied. However, the lack of an intrinsic band gap makes it inadequate for electronic and optical devices. MoS_2 from the family of transition metal dichalcogenides has been intensively investigated for its possibility to be used in future applications. The vision is to integrate various 2D materials to realise an actual device. However, the actual assembly of these materials with high controllability remains a challenge. Vertical heterostructures, supported by Van der Waals interactions, have already been realised by manually stacking 2D materials on top of each other[1]. An ultimate thin device can be realised by creating lateral heterostructures with atomically sharp interfaces where each material is directly bonded to another. Currently, methods for in-plane bonding of MoS_2 to other materials (e.g. graphene) are limited due to poor structural match. One possible solution is to develop selective bottom-up methods for synthesis of molecular nanostructures by self-assembly.

This study aim to investigate the fundamental nature of bonding of graphene nanoribbons (GNRs) to the edges of MoS_2 nanoparticles by scanning tunnelling microscopy (STM). The aim is to synthesise GNRs from precursor molecules through a thermally activated Ullmann reaction already used elsewhere[2,3]. After initial growth of MoS_2, it is necessary to anneal in a hydrogen atmosphere to activate the edges to facilitate the attachment of an intermediate structure of poly(para-phenylene) (PPP) wires. STM reveals the PPP wires have an affinity for the corners of the MoS_2 nanoparticles with a distance, obtained from line scans across the adsorption site, consistent with a covalent C-S bond.

[1]: Pant et al., Nanoscale, 2016, 8, 7, 3870-3887

[2]: Cai et al., Nature, 2010, 466, 7305, 470–473

[3]: Basagni et al., J. Am. Chem. Soc., 2015, 137, 5, 1802-1808

4:00pm **2D+AP+EM+MI+MN+NS+PS+TF-MoA8 The Effects of Metal-modification and Two Dimensional (2D) Lamellar Structure on Catalytic Performance of MFI Zeolite for Ethylene Conversion into Liquid Aromatics***, **Laleh Emdadi**, L. Mahoney, D. Tran, I. Lee,* US Army Research Laboratory

The effects of two dimensional (2D) meso-/microporous structure and metal modification with gallium or zinc on catalytic performances of lamellar MFI zeolites in ethylene conversion reaction to liquid aromatics were investigated. Dual template technique was used to synthesize the 2D zeolite and metal modification of the zeolite was carried out by wet impregnation method. The results of multiple analysis techniques such as TEM, XRD, Ar adsorption-desorption, UV-Visible spectroscopy, and H_2-TPR showed that the zeolite structure is a pivotal factor for controlling the type of metal dopant species forming on zeolite, their size, and their distribution. Adding metal dopants to 2D zeolite structures improved the yield of liquid aromatics and selectivity for mono-benzene alkylated aromatics compared to their microporous commercial MFI analogies while decreased the coke formation rate. Zinc loaded lamellar MFI had the most efficient catalytic performance among all studied catalysts with lowest amount of total coke and highest fraction of light coke including mono-benzene alkylated aromatics determined by combination of different techniques such as FTIR, UV-Vis, MS-temperature programmed oxidation (TPO), FTIR-TPO, and GC-MS. This can be explained by higher accessibility of reactants to active sites and facilitated transport of products and coke precursors from lamellar structure of this zeolite and the lower Brønsted/Lewis acid site ratio of this catalyst provided by metal modification which is more suitable for ethylene aromatization and suppresses the formation of heavy coke species. The catalytic performance of zeolite catalyst can be tuned by modulating both the textural and acidity properties of the zeolite structure. The metal modified 2D lamellar MFI zeolites as bifunctional catalysts open an avenue for converting large reactant molecules to desired products by designing a catalyst with an optimal structure, acidity, and dispersion of metal dopants.

4:20pm **2D+AP+EM+MI+MN+NS+PS+TF-MoA9 Structural Stability of Graphene Nanoflakes:From the View Point of Aromaticity***, M. Ushirozako, H. Matsuyama, A. Akaishi, **Jun Nakamura**,* The University of Electro-Communications (UEC-Tokyo), Japan

Recently, nano-scale graphene nanoflakes (GNFs) have attracted great attention as one of the promising materials for electronics and spintronics. Kim *et al*. have successfully fabricated GNFs with various sizes up to 35 nm and have reported that the photoluminescence property of GNFs depends on the size and the edge shape [1]. From the view point of the structural stability of GNFs, we have not yet acquired the systematic comprehension with regard to effects of shapes and sizes of GNFs on the stability. In the present study, we have examined how the stability of GNFs is dominated by the edge shape and the size of GNFs, using first-principles calculations within the density functional theory.

In order to evaluate the stability of GNFs, we calculated the edge formation energy. First, we consider GNFs with the six-fold symmetry (D_{6h}) and classify them into zigzag GNFs (ZZGNFs) and armchair GNFs (ACGNFs). ACGNFs have two subtypes, AC(1) and AC(2), depending on whether carbon atoms are just at the corner of the outermost envelope hexagon of GNFs. We define the edge purity as the ratio of the number of carbon atoms at the edge unambiguously regarded as the armchair to the total number of edge atoms. The purity of AC(1) is higher than that of AC(2). The chemical formulae associated with ZZ, AC(1), and AC(2) are $C_{6n^2}H_{6n}$, $C_{18n^2-18n+6}H_{12n-6}$, $C_{18n^2-30n+12}H_{12n-12}$, respectively. In addition, we also evaluate the structural stabilities of triangular and rhombus GNFs.

We calculated the edge formation energy of the GNFs having up to 1200 carbon atoms as a function of the number of edge carbon atoms [3]. The formation energy of ZZGNFs is higher than that of ACGNFs irrespective of the size of GNFs. This instability of ZZGNFs is attributed to the presence of the so-called edge state. Indeed, it has also been shown that the formation energy of the zigzag graphene nanoribbon is higher than that of the armchair one [4]. It is noted that AC(2) is slightly more stable than AC(1), whereas the purity of AC(2) is lower than that of AC(1). Such peculiar stabilization can be reasonably explained in terms of the aromaticity of GNFs. The Nucleus Independent Chemical Shifts (NICS) values, which is averaged for the six-membered rings in GNFs, for AC(2) are lower than those for AC(1). This means AC(2) is more aromatic than AC(1). We will discuss the quantitative relationship between the stability and the aromaticity of GNFS.

[1] S. Kim et al., ACS Nano, **6**, 9, 8203 (2012)

[2] W. Hu *et al*., J. Chem. Phys. **141**, 214704 (2014)

[3] A. Akaishi, M. Ushirozako, H.Matsuyama, andJ.Nakamura, Jpn.J.Appl.Phys. **57**, 0102BA(2018)

[4] S. Okada. Phys. Rev. B, **77**, 041408 (2008)

4:40pm **2D+AP+EM+MI+MN+NS+PS+TF-MoA10 Wafer-scale 2D-3D Mixed Heterostructures Enabled by Remote Epitaxy through Graphene***, **Jeehwan Kim**,* Massachusetts Institute of Technology **INVITED**

The current electronics industry has been completely dominated by Si-based devices due to its exceptionally low materials cost. However, demand for non-Si electronics is becoming substantially high because current/next generation electronics requires novel functionalities that can never be achieved by Si-based materials. Unfortunately, the extremely high cost of non-Si semiconductor materials prohibits the progress in this field. Recently our team has invented a new crystalline growth concept, termed as "remote epitaxy", which can copy/paste crystalline information of the wafer remotely through graphene, thus generating single-crystalline films on graphene [1,2]. These single-crystalline films are easily released from the slippery graphene surface and the graphene-coated substrates can be infinitely reused to generate single-crystalline films. Thus, the remote epitaxy technique can cost-efficiently produce freestanding single-crystalline films including III-V, III-N, and complex oxides. This allows unprecedented functionality of flexible device functionality required for current ubiquitous electronics. I will also present detailed mechanism behind remote atomic interaction through graphene [2]. In addition, we have recently demonstrated a manufacturing method to manipulate wafer-scale 2D materials with atomic precision to form monolayer-by-monolayer stacks of wafer-scale 2D material heterostructures [3]. In this talk, I will discuss the implication of this new technology for revolutionary design of next generation electronic/photonic devices with combination of 3D/2D mixed heterostructures.

[1] Y. Kim, et al, and J. Kim, “Remote epitaxy through graphene enables two-dimensional material based layer transfer” ***Nature***, Vol. 544, 340 (2017)

[2] W. Kong, et al, and J. Kim, “Polarity govern atomic interaction through two-dimensional materials”, ***Nature Materials***, Vol. 17, 999 (2018)

[3] J. Shim, S. Bae, et al, and J. Kim, “Controlled crack propagation for atomic precision handling of wafer-scale two-dimensional materials” ***Science***, 362, 665 (2018)

2D Materials
Room A216 - Session 2D+AP+EM+MI+NS+PS+TF-MoA
2D Materials Growth and Fabrication

Moderator: Sarah Haigh, University of Manchester, UK

2:00pm **2D+AP+EM+MI+NS+PS+TF-MoA2 Synthesis of High Quality Monolayer Transition Metal Dichalcogenides using Direct Liquid Injection***,* ***Kathleen M. McCreary****, E.D. Cobas, A.T. Hanbicki, M.R. Rosenberger, H.-J. Chuang, B.T. Jonker,* U.S. Naval Research Laboratory

In recent years, interest in monolayer transition metal dichalcogenides (TMDs) has rapidly increased, spurred by the possibility for integration into a variety of technologies such as photodetection, flexible electronics, and chemical sensing. While fundamental investigations can be performed on exfoliated flakes or chemical vapor deposition synthesized isolated islands, the limited size resulting from these techniques poses a significant barrier forimplementation of TMDs in technological applications. To overcome these obstacles, new synthesis avenues should be explored. Here, we outline a novel technique that utilizes a commercially available Anneal Sys growth chamber equipped with direct liquid injection (DLI) heads for all precursors. The use of liquid, rather than solid precursors, provides fine control of both metal and chalcogen precursors leading to the synthesis of monolayer MoS_2 across cm^2 areas. Photoluminescence, Raman, XPS, and conductive AFM are used to evaluate DLI grown MoS_2, and indicate high quality material having low defect density, with metrics comparable to or better than exfoliated and chemical vapor deposition grown MoS_2.

2:20pm **2D+AP+EM+MI+NS+PS+TF-MoA3 Understanding and Controlling the Growth of 2D Materials with Non-Equilibrium Methods and in situ Diagnostics***,* ***David Geohegan****, Y-C. Lin, Y. Yu,* Oak Ridge National Laboratory*; C. Liu, G. Duscher,* University of Tennessee Knoxville*; A. Strasser,* University of Texas at Dallas*; A.A. Puretzky,* Oak Ridge National Laboratory*; K. Wang,* Intel Corporation, USA*; M. Yoon, C.M. Rouleau,* Oak Ridge National Laboratory*; S. Canulescu,* DTU Nanolab, Technical University of Denmark*; P.D. Rack,* University of Tennessee Knoxville*; L. Liang, W. Zhang, H. Cai, Y. Gu, G. Eres, K. Xiao,* Oak Ridge National Laboratory **INVITED**

Atomically-thin two-dimensional (2D) materials, including layered 2D transition metal dichalcogenide (TMD) semiconductors and their heterostructures, exhibit remarkable quantum properties that are envisioned for energy-efficient photovoltaics, flexible optoelectronics, catalysis, and quantum information science. However, significant synthesis and processing challenges currently limit the technologic development of these “all-surface” materials, including wafer-scale, bottom-up synthesis of uniform layers of crystalline 2D materials that are comparable in quality to exfoliated flakes of bulk materials. As-synthesized crystals of 2D TMDs display remarkable heterogeneity on both the atomistic level (e.g., vacancies, dopants, and edge terminations) and on the mesoscopic length scale (e.g., misoriented grains, layer orientations, and interactions with substrates and adsorbates) that can strongly influence the structure and electronic properties in 2D materials. This heterogeneity offers a serious challenge for synthesis and processing, yet offers a tremendous opportunity to tailor functionality.

Here we describe several approaches that are being developed for in situ diagnostic analysis and control of synthesis and heterogeneity. In addition to conventional vapor transport techniques, progress in laser-based approaches for 2D synthesis and modification, such as pulsed laser deposition (PLD) and pulsed laser conversion of precursors, are presented that permit control of the growth environment using time-resolved in situ diagnostics. The non-equilibrium advantages of PLD to form alloys and vertical heterojunctions are demonstrated using the tunable kinetic energy and digital nature of the process. Correlated atomic-resolution electron microscopy and atomistic theory are used to understand the size and stoichiometry of the “building blocks” deposited for synthesis and the forces that guide assembly. 2D crystals are grown directly on TEM grids within custom chambers and transmission electron microscopes where the ability to ‘see’ every atom in these atomically-thin crystals permits a unique opportunity to understand the forces governing their synthesis and functionality. In situ optical spectroscopy techniques are described to characterize the material’s evolving structure and properties, offering the opportunity to ‘close the loop’ between synthesis and optoelectronic functionality of 2D materials and heterostructures.

Research sponsored by the U.S. Dept. of Energy, Office of Science, Basic Energy Sciences, Materials Science and Engineering Div. (synthesis science) and Scientific User Facilities Div. (characterization science).

3:00pm **2D+AP+EM+MI+NS+PS+TF-MoA5 Area-Selective Atomic Layer Deposition of 2D WS_2 Nanolayers***,* ***Shashank Balasubramanyam*** [1]*,* Eindhoven University of Technology, The Netherlands, Noord Brabant*; M.J.M. Merkx,* Eindhoven University of Technology, The Netherlands*; W.M.M. Kessels,* Eindhoven University of Technology, The Netherlands, Netherlands*; A.J.M. Mackus,* Eindhoven University of Technology, The Netherlands, Nederland*; A.A. Bol,* Eindhoven University of Technology, The Netherlands, Netherlands

With continued downscaling of device dimensions, ultra-thin two dimensional (2D) semiconductors like WS_2 are considered as promising materials for future applications in nanoelectronics. At these nanoscale regimes, device fabrication with precise patterning of critical features is challenging using current top-down processing techniques. In this regard, area-selective atomic layer deposition (AS-ALD) has emerged as a promising candidate for bottom-up processing to address the complexities of nanopatterning. Till date, AS-ALD of metals[1] and dielectrics[2] have been successfully demonstrated. However, AS-ALD of 2D materials has remained elusive. In this contribution, we demonstrate area-selective deposition of 2D WS_2 nanolayers by using a three-step (ABC-type) plasma-enhanced ALD process.

AS-ALD of WS_2 was achieved by using acetylacetone (Hacac) inhibitor (A), bis(tertbutylimido)-bis(dimethylamido)-tungsten precursor (B), and H_2S plasma (C) pulses. This process resulted in immediate growth on SiO_2 while a significant nucleation delay was observed on Al_2O_3, as determined from *in-situ* spectroscopic ellipsometry (SE) and *ex-situ* X-ray photoelectron spectroscopy (XPS) measurements. The surface chemistry of this selective process was analysed by *in-situ* Fourier transform infrared spectroscopy (FTIR). The analyses revealed that the inhibitor adsorbed on the Al_2O_3 surface, blocking precursor adsorption, while little or no inhibitor adsorption was detected on the SiO_2 surface where WS_2 was readily deposited. Furthermore, the area-selective growth was demonstrated on SiO_2 samples with patterned Al_2O_3 on top. On SiO_2, WS_2 could be deposited with angstrom-level thickness control.

To improve the crystallinity, the AS-ALD WS_2 films were annealed at temperatures within the thermal budget of industrial semiconductor processing (≤ 450°C). The annealed films exhibited sharp Raman peaks, which is a fingerprint of highly crystalline WS_2. Furthermore, Raman line scans over the patterns showed very sharp peak intensity transitions at the SiO_2-Al_2O_3 interface which confirmed that annealing had no impact on selectivity.

To summarize, this work pioneered the combination of two key avenues in atomic-scale processing: area-selective growth and ALD of 2D materials. It is expected that the results of this work will lay the foundation for area-selective ALD of other 2D materials.

[1] R. Chen and S.F. Bent, *Adv. Mater.* (2006).

[2] A. Mameli, M.J.M. Merkx, B. Karasulu, F. Roozeboom, W.M.M. Kessels and A.J.M. Mackus, *ACS Nano* (2017).

3:20pm **2D+AP+EM+MI+NS+PS+TF-MoA6 Growth Behavior of Hexagonal Boron Nitride on Cu-Ni Binary Alloys***,* ***Karthik Sridhara,*** Texas A&M University*; J.A. Wollmershauser,* U.S. Naval Research Laboratory*; L.O. Nyakiti,* Texas A&M University*; B.N. Feigelson,* U.S. Naval Research Laboratory

Controlled growth of large area n-layered chemical vapor deposited (CVD) hexagonal boron nitride (h-BN) is of great interest as a tunnel dielectric, and substrate for graphene and transition metal dichalcogenides (TMDs). The CVD growth of h-BN has been demonstrated on various transition metal catalytic substrates such as Cu, Ni, Pt and Fe. Of these metal substrates, Cu and Ni are frequently used due to their relative abundance and low cost. However, h-BN growth on Cu leads to monolayer films, and growth on Ni yields thicker, substrate grain-dependent films. Therefore, a

[1] **TFD James Harper Award Finalist**

cost-effective transition metal substrate is needed that will facilitate controlled n-layered h-BN growth.

In this work, we prepare isomorphous Cu-Ni binary alloys from 10-90 wt.% Ni by creating Ni-rich (Ni-Cu) and Cu-rich (Cu-Ni) alloys using electroplating of Cu on Ni foils and Ni on Cu foils, respectively. The electroplated foils are then annealed at ~1030° C for >5 hours to create Ni-Cu and Cu-Ni alloys. The alloys are subsequently polished mechanically to create a planarized surface suitable for h-BN growth. The surface morphology before and after polishing is assessed using a scanning electron microscope (SEM). Energy dispersive spectroscopy (EDS) characterization of the alloys confirms a designed stoichiometry at every weight percent. h-BN is grown on the alloys using atmospheric pressure chemical vapor deposition (APCVD) at 1030° C, with ammonia borane as the precursor, and H_2/N_2 as the carrier gas flowing at ~200 sccm. Cu and Ni foils are used as control samples for this study. Fourier transform infrared reflection absorption spectroscopy (FT-IRRAS) is used to confirm and characterize h-BN growth directly on Cu, Ni and alloy substrates. SEM is performed to evaluate the h-BN film and crystal morphology. The results indicate that the h-BN growth behavior on Ni-Cu is different than on Cu-Ni alloys. A trend of decreasing h-BN amount with reducing Ni concentration is observed on Ni-Cu alloys while no such trend is observed on Cu-Ni alloys. Additionally, there are large (~20 µm) multilayer and monolayer single crystals of h-BN on Ni-Cu alloys, and predominantly monolayer crystals and films of h-BN on Cu-Ni alloys. The difference in growth behavior is studied using x-ray photoelectron spectroscopy (XPS) and electron backscattering diffraction (EBSD), which reveal that the alloy surface composition determines the h-BN growth. This work demonstrates how Cu-Ni alloy substrate of different compositions, along with CVD growth conditions, can be used to control h-BN growth.

4:20pm **2D+AP+EM+MI+NS+PS+TF-MoA9 Controlled Growth of Transition Metal Dichalcogenide Monolayers for Applications in Nanoelectronic and Nanophotonic Devices**, *A. George, C. Neumann, D. Kaiser, R. Mupparapu,* Friedrich Schiller University Jena, Germany*; U. Hübner,* Leibniz Institute of Photonic Technology, Jena, Germany*; Z. Tang, A. Winter, I. Staude,* ***Andrey Turchanin,*** Friedrich Schiller University Jena, Germany

Controlling the flow rate of precursors is highly essential for the growth of high quality monolayer crystals of transition metal dichalcogenides (TMDs) by chemical vapor deposition. Thus, introduction of an excess quantity of precursors affects the reproducibility of the growth process and results in the multilayer growth. Here, we demonstrate the use of Knudsen-type effusion cells for controlled delivery of sulfur precursor for the large area, high density, size-controlled and highly reproducible growth of monolayer TMD crystals [1]. The size of the grown crystals can be tuned between 10 - 200 µm. We grow MoS_2, WS_2, $MoSe_2$ and WSe_2 monolayer crystals as well as $MoSe_2$-WSe_2 lateral heterostructures and characterize them by optical microscopy, atomic force microscopy, Raman spectroscopy, photoluminescence spectroscopy and electrical transport measurements. It has been found that they possess a high crystalline, optical and electrical quality based on their single crystalline nature. We demonstrate their implementation in novel field-effect and nanophotonic devices and discusse an influence of the point defect density on their functional characteristics [2-3]. Moreover, we present a novel synthetic route for the integration of TMDs into lateral heterostructures with other 2D materials [4].

[1] A. George et al., *J. Phys.: Mater.* 2 (2019) 016001.

[2] T. Bucher et al., *ACS Photonics* 6 (2019) 1002.

[3] R. Meyer et al., *ACS Photonics* 6 (2019) DOI: 10.1021/acsphotonics.8b01716

[4] A. Winter et al., *Carbon* 128 (2018)106.

4:40pm **2D+AP+EM+MI+NS+PS+TF-MoA10 Atomic Layer Deposition of BN as a Novel Capping Barrier for B_2O_3**, ***Aparna Pilli,*** *J. Jones, J.A. Kelber,* University of North Texas*; A. LaVoie, F. Pasquale,* Lam Research Corporation

The deposition of boron oxide (B_2O_3) films on Si and SiO_2 substrates by atomic layer deposition (ALD) is of growing interest in microelectronics for shallow doping of high aspect ratio transistor structures. B_2O_3, however, forms volatile boric acid (H_3BO_3) upon ambient exposure, requiring a passivation barrier, for which BN was investigated as a possible candidate. Here, we demonstrate, deposition of BN by sequential BCl /NH reactions at 600 K on two different oxidized boron substrates: (a) B O deposited using BCl /H O ALD on Si at 300 K (“B O /Si”); and (b) a boron-silicon oxide formed by sequential BCl /O reactions at 650 K on SiO followed by annealing to 1000 K (“B-Si-oxide”). X-ray photoelectron spectroscopy (XPS) data demonstrate layer-by-layer growth of BN on B_2O_3/Si with an average growth rate of ~1.4 Å/cycle, accompanied by some B_2O_3 removal during the first BN cycle. In contrast, continuous BN growth was observed on B-Si-oxide without any reaction with the substrate. XPS data also indicate that the oxide/nitride heterostructures are stable upon annealing in ultrahigh vacuum to >1000 K. XPS data, after the exposure of these heterostructures to ambient, indicate a small amount of BN oxidation at the surface NH species, with no observable hydroxylation of the underlying oxide films. These results demonstrate that BN films, as thin as 13 Å, are potential candidates for passivating boron oxide films prepared for shallow doping applications.

5:00pm **2D+AP+EM+MI+NS+PS+TF-MoA11 Atomic Layer Deposition of SiO_2 on Group VIII Metals: Towards Formation of a 2D Dielectric**, *T. Suh, R. Yalisove,* ***James Engstrom,*** Cornell University

The atomic layer deposition (ALD) of many metals, particularly Group VIII (now known as Groups 8, 9 and 10), on SiO_2 has been an active area of research in many fields, which include microelectronics and heterogeneous catalysis. There have been many fewer studies of the inverse—the deposition of SiO_2 on many of these same metals. One possible reason to explore the ALD growth of SiO_2 on transition metals is that it might provide a route to an atomically thick SiO_2 dielectric, *silicatene*. Silicatene is a 2D material that consists of a bilayer of Si_2O_3 linked to each other by bridging oxygen atoms (giving SiO_2), where there are no dangling bonds or covalent bonds to the underlying substrate on which it is grown. For example, an established route to form silicatene involves deposition of elemental Si in UHV and subsequent high-temperature annealing on various single-crystalline metal surfaces including, but not limited to, Ru(0001), Pt(111), and Pd(100). Such a process, unfortunately, is likely not compatible with high-volume manufacturing. With this motivation we embarked on a study of the plasma-assisted ALD of SiO_2 on e-beam deposited polycrystalline thin films of Ru, Pt and Pd using a commercial ALD reactor. We analyzed both the thin films and the starting substrates using a combination of techniques including contact angle, spectroscopic ellipsometry (SE) and X-ray photoelectron spectroscopy. Thin films of SiO_2 were deposited using tris(dimethylamido)silane and an oxygen plasma at a substrate temperature of 200 °C, and we examined growth for 5, 10, 20, 50 and 100 cycles. Contact angle measurements showed immediate evidence for SiO_2 deposition on all metal surfaces, and the contact angle decreased and remained constant and < 10° from 5 to 100 cycles of ALD. From SE we found little evidence of an incubation period, and growth was linear for the range of sample examined and the thickness deposited per cycle was remarkably constant at a value of 0.76-0.78 Å-cycle^{-1}. Analysis of these films using angle-resolved XPS was consistent with the formation of a thin film of SiO_2 with uniform thickness. Having characterized the thin film thickness-ALD cycle relationship we subjected SiO_2 thin films with thickness of ~ 7-15 Å to post-deposition high-temperature anneals in oxygen furnace. Initial attempts to form silicatene with an anneal at 800 °C, produced a structure suggesting possible interfacial reaction between the SiO_2 and Ru, perhaps involving silicide formation. We will end our presentation with a discussion of recent work involving a more extensive examination of the post-deposition annealing step, and deposition on patterned wafers.

Electronic Materials and Photonics Division
Room A214 - Session EM+PS+TF-MoA

New Devices and Materials for Logic and Memory
Moderator: Rehan Kapadia, University of Southern California

1:40pm **EM+PS+TF-MoA1 Short-term Plasticity to Long-term Plasticity Transition Mimicked by High Mobility InP FETs with TiO_2 Trapping Layer**, ***Jun Tao,*** *R. Kapadia,* University of Southern California

Memory is widely believed to be encoded and stored in the central nervous system by altering the synapse strength via activity-dependent synaptic plasticity between millions of neurons in vertebrates. Consolidations from short-term plasticity (STP) to long-term plasticity (LTP) not only transform the important external stimuli to permanently stored information but release storage space for accepting new coming signals. Although memristor technology (e.g. RRAM) has been reported to mimic the STP and LTP characteristics and exhibited its merit in density comparing to traditional CMOS based SRAM technology, some conventional memristors suffer non-ideal operation speed, small dynamic range, and high resistance variation.

In our work, the single crystal Indium Phosphide (InP) based synaptic devices demonstrated its advantages not only in the emulation of the synaptic functions for both STP and LTP characteristics but also in the controllability of transition from STP to LTP. Since we interpret gate voltage pulses as the pre-synaptic action potentials, the source-drain current as post-synaptic current, and the channel conductance as synaptic weight, the consolidations from STP to LTP are elaborately demonstrated through mediating multiple action potential parameters like pulse numbers, pulse intervals (or rates), and pulse durations. The synaptic devices we demonstrated here are essentially single crystal channel InP Field Effect Transistors (FETs) fabricated on Si/SiO_2 substrates with the templated liquid-phase (TLP) method. In addition, TiO_2 trapping layer is inserted into the gate dielectric layer to provide extra deeper trap states. The 'ratchet' mechanism is utilized to have the charges 'fall' into the TiO_2 well and implement the transition from STP to LTP effectively.

2:00pm **EM+PS+TF-MoA2 Magnetic Domain Wall Devices for Artificial Neural Network***, **Saima Siddiqui**, S. Dutta, A. Tang, L. Liu, M. Baldo, C. Ross,* MIT

Magnetic domain wall devices are promising candidates for logic [1] and storage class memory [2]. Due to the non-volatility and energy-efficient switching, this type of device is one of the prime candidates for in memory computing and brain-inspired computing. In-memory computing is a non-von-Neumann architecture where data computation and storage are done locally to reduce the data movement between the processor and the storage memory [3]. The layer-by-layer operations of data require synapses (i.e. variable resistors whose resistance vary linearly with the input) and activation function generators between layers (i.e. variable resistors whose resistance vary non-linearly with the input current).

Domain walls' motion in a magnetic wire is a function of applied current due to spin-orbit torque from an adjacent heavy metal (Fig. 1). The current density and spin orbit torque can be modified along the wire by adjusting the width of the heavy metal. The spin orbit torque then becomes a function of the domain wall position, which makes the domain wall motion a nonlinear function of the applied current (Fig. 2). Linear and nonlinear domain wall motion can be detected via magnetoresistance by using a magnetic tunnel junction in which the magnetic wire forms the free layer. The electrical detection is necessary for the analog matrix multiplication in neuromorphic accelerator. However, domain walls are pinned due to the magnetostatic energy minima on the sides of the MTJ. The synaptic (Fig. 3) and activation function (Fig 4) like magnetoresistive behavior can still be generated by using multiple MTJs in parallel. In this study, we demonstrate linear and nonlinear domain wall motion in magnetic wires and modify the design of magnetic tunnel junctions to convert these motions into magnetoresistance. The experimental observations of the device characteristics agree with both analytical and micromagnetic modeling.

[1] J. A. Currivan-Incorvia, S. Siddiqui, S. Dutta, E. R. Evarts, J. Zhang, D. Bono, C. A. Ross, and M. A. Baldo, Nat Commun., 7, 10275 (2016).

[2] Stuart S. P. Parkin, Masamitsu Hayashi, and Luc Thomas, Science, Vol. 320, Issue 5873, pp. 190-194 (2008)

[3] Jacob Torrejon, Mathieu Riou, Flavio Abreu Araujo, Sumito Tsunegi, Guru Khalsa, Damien Querlioz, Paolo Bortolotti, Vincent Cros, Kay Yakushiji, Akio Fukushima, Hitoshi Kubota, Shinji Yuasa, Mark D. Stiles & Julie Grollier, Nature volume 547, pp. 428–431 (2017).

2:20pm **EM+PS+TF-MoA3 Ferroelectric Devices for Non-von Neumann Computing***, **Zheng Wang**, A. Khan,* Georgia Institute of Technology **INVITED**

Excitation and inhibition go hand in hand in neuronal circuits in biological brains. For example, neurons in the visual and the auditory cortices provide excitatory responses to visual and auditory stimuli, respectively. On the other hand, interneurons in the central nervous system provide inhibitory signals to downstream neurons thereby imparting regulation and control in neuronal circuits—the loss of which often causes neurodegenerative disorders. These neuro-biological facts have inspired the bio-mimetic computational perspective that artificial, excitatory neurons need to be paired with inhibitory connections for functional correctness and efficient compute models such as spiking neural networks.

In this talk, we will introduce a ferroelectric neuromorphic transistor platform [1,2] which can (1) efficiently incorporate both excitatory and inhibitory inputs in the simple two transistor topology of an artificial, ferroelectric spiking neuron, and (2) emulate several classes of biological spiking dynamics (such as regular, fast, Thalamo-Cortical spiking and so on). We will discuss the recent experimental demonstrations of ferroelectric spiking neurons. The talk will end with a simulation experiment where a full-scale spiking neural network was implemented using experimentally calibrated ferroelectric circuit models and the network was benchmarked analog CMOS and other emerging device technologies.

References:

[1] Z. Wang, B. Crafton, J. Gomez, R. Xu, A. Luo, Z. Krivokapic, L. Martin, S. Datta, A. Raychowdhury, A. I. Khan, "Experimental Demonstration of Ferroelectric Spiking Neurons for Unsupervised Clustering," *The 64th International Electron Devices Meeting (IEDM 2018)*, 2018.

[2] Z. Wang, S. Khandelwal & A. I. Khan, "Ferroelectric oscillators and their coupled networks," IEEE Electron Dev. Lett. 38, 1614 (2017).

3:00pm **EM+PS+TF-MoA5 Ultrafast Measurement of Nanoseconds Polarization Switching in Ferroelectric Hafnium Zirconium Oxide***, **Mengwei Si**, P. Ye,* Purdue University

Ferroelectric (FE) hafnium oxides (HfO_2) such as hafnium zirconium oxide (HZO) is the promising thin film ferroelectric material for non-volatile memory applications. The ultrafast measurements of polarization switching dynamics on ferroelectric (FE) and anti-ferroelectric (AFE) hafnium zirconium oxide (HZO) are studied, with the shortest electrical pulse width down to as low as 100 ps. The transient current during the polarization switching process is probed directly. The switching time is determined to be as fast as 10 ns to reach fully switched polarization with characteristic switching time of 5.4 ns for 15 nm thick FE HZO and 4.5 ns for 15 nm thick AFE HZO by Kolmogorov−Avrami−Ishibashi (KAI) model. The limitation by parasitic effect on capacitor charging is found to be critical in the correct and accurate measurements of intrinsic polarization switching speed of HZO. The work is in close collaborations with Xiao Lyu, Wonil Chung, Pragya R. Shrestha, Jason P. Campbell, Kin P. Cheung, Haiyan Wang, Mike A. Capano and was in part supported by SRC and DARPA.

3:20pm **EM+PS+TF-MoA6 Interfacial Charge Engineering in Ferroelectric-Gated Mott Transistors***, XG. Chen, Y. Hao, L. Zhang, **Xia Hong**,* University of Nebraska-Lincoln

Ferroelectric field effect transistors (FeFETs) built upon Mott insulator channel materials have been intensively investigated over the last two decades for developing nonvolatile memory and logic applications with sub-nanometer size scaling limit. However, the intrinsically high carrier density of the Mott channel (10^{22}-10^{23}/cm^3) also imposes significant challenges in achieving substantial modulation of the channel conduction. In this work, we exploit the intricate interplay between interfacial charge screening and transfer effects in epitaxial heterostructures composed of two strongly correlated oxide layers, one layer of rare earth nickelate RNiO$_3$ (R = La, Nd, Sm) and one layer of (La,Sr)MnO$_3$ (LSMO), to realize a giant enhancement of the ferroelectric field effect in Mott-FeFETs with a Pb(Zr,Ti)O$_3$ gate. For devices with 1-5 nm single layer RNiO$_3$ channels, the room temperature resistance switching ratio $(R_{off}-R_{on})/R_{on}$ increases with decreasing channel thickness till it reaches the electrical dead layer thickness. For devices built upon RNiO$_3$/LSMO bilayer channels, the resistance switching ratio is enhanced by up to two orders of magnitude compared with the single layer channel devices with the same channel thickness. Systematic studies of the layer thickness dependence of the field effect show that the LSMO buffer layer not only tailors the carrier density profile in RNiO$_3$ through interfacial charge transfer, but also provides an extended screening layer that reduces the depolarization effect in the ferroelectric gate. Our study points to an effective strategy for building high density nanoelectronic and spintronic applications via functional complex oxide heterointerfaces.

4:00pm **EM+PS+TF-MoA8 The Interface of Transition Metal Dichalcogenides and Ferroelectric Oxides***, **Maria Gabriela Sales**, S. Jaszewski, S. Fields, R. Christopher, N. Shukla, J. Ihlefeld, S. McDonnell,* University of Virginia

Transition metal dichalcogenides (TMDs) are an interesting class of materials because of their unique properties owing to their 2D nature, wherein layers that are covalently bonded in-plane are held together by van der Waals forces in the out-of-plane direction, similar to graphene. However, unlike graphene, semiconducting TMDs have a band gap that is tunable with layer thickness, allowing control over its properties depending on specific applications. One such application is in ferroelectric-based transistors, which have high potential for use in memory and logic, but whose major drawback in integration is the poor semiconductor-ferroelectric interface when using silicon as the semiconducting channel, due to issues such as interdiffusion across the interface. Thus, a promising alternative route is using a TMD as the channel with a ferroelectric material as the gate dielectric. This is expected to have an improved interface

quality because of the fact that TMDs have no dangling bonds at the surface and are highly stable in-plane. In this study, we focus on a mixture of hafnium oxide and zirconium oxide as our ferroelectric material, with zirconium stabilizing the ferroelectric phase in hafnia. We explore the TMD/ferroelectric structure, addressing certain integration issues in growth, and looking at their interface chemistry and thermal stability. Specifically, we look at commercially available geological MoS_2 and molecular beam epitaxy-grown WSe_2 interfaced with an atomic layer deposited $Hf_xZr_{1-x}O_2$ ferroelectric. Our report will focus on the results of our investigations of this interface carried out using a combination of X-ray photoelectron spectroscopy (XPS) and X-ray diffraction (XRD) techniques.

4:20pm **EM+PS+TF-MoA9 Electronic and Thermal Properties of 2D Materials***, **Connor McClellan**, E. Yalon, K. Smithe, C. English, S. Vaziri, C. Bailey, A. Sood, M. Chen, E. Pop,* Stanford University

This talk will present recent highlights from our research on two-dimensional (2D) materials and devices including graphene, and transition metal dichalcogenides (TMDs). The results span from fundamental measurements and simulations, to devices, to system-oriented applications which take advantage of unusual 2D material properties.

Using the low cross-plane thermal conductance, we found unexpected applications of graphene as an ultra-thin electrode to reduce power consumption in phase-change memory [1]. We have also demonstrated wafer-scale graphene systems for analog dot product computation [2]. We have grown monolayer 2D semiconductors by chemical vapor deposition over cm^2 scales on amorphous oxides, including MoS_2 with low device variability [3], WSe_2, and $MoSe_2$.

Using a self-aligned process, we demonstrated 10 nm gate-length monolayer MoS_2 transistors with excellent switching characteristics and approaching ballistic limits [4]. Using sub-stochiometric oxides, we achieved high electron doping to reduce electrical contact resistance down to 480 Ω·µm and increase on-current up to a record of 700 µA/µm in monolayer MoS_2 [5]. We also directly measured the saturation velocity in monolayer MoS_2, finding it is thermally-limited (i.e. by device self-heating and phonon scattering) to about one-third that of silicon and about one-tenth that of graphene [6]. Using Raman thermometry, we uncovered low thermal boundary conductance (~15 $MW/m^2/K$) between MoS_2 and SiO_2, which could limit heat dissipation in 2D electronics [7]. We are presently exploring unconventional applications including thermal transistors [8], which could enable nanoscale control of heat in "thermal circuits" analogous with electrical circuits. These studies reveal fundamental limits and new applications of 2D materials, taking advantage of their unique properties.

References: [1] A. Behnam et al., Appl. Phys. Letters. 107, 123508 (2015). [2] N. Wang et al., IEEE VLSI Tech. Symp., Jun 2016, Honolulu HI. [3] K. Smithe et al., ACS Nano 11, 8456 (2017). [4] C. English et al., IEEE Intl. Electron Devices Meeting (IEDM), Dec 2016. [5] C. J. McClellan et al., IEEE Device Research Conference (DRC), June 2017. [6] K. Smithe et al., Nano Lett. 18, 4516 (2018). [7] E. Yalon, E. Pop, et al., Nano Lett. 17, 3429 (2017). [8] A. Sood, E. Pop et al. Nature Comm. 9, 4510 (2018).

4:40pm **EM+PS+TF-MoA10 Electronics in Flatland***, **Sanjay Banerjee**,* University of Texas at Austin **INVITED**

2D materials such as graphene, transition metal dichalcogenides and topological insulators have opened up avenues in beyond-CMOS device concepts. We will discuss our work involving single or many-particle 2D-2D tunneling, leading to transistors with negative differential resistance. We also explore spintronics in these systems for novel logic and memory devices. We will also discuss the use of these materials in less esoteric, but more practical high frequency, mechanically flexible FETs for IoT applications.

Plasma Science and Technology Division
Room B130 - Session PS+AS+EM+SS+TF-MoA

Plasma-Surface Interactions

Moderators: Sebastian Engelmann, IBM T.J. Watson Research Center, Sumit Agarwal, Colorado School of Mines

2:00pm **PS+AS+EM+SS+TF-MoA2 Plasma Resistance of Sintered Yttrium Oxyfluoride (YOF) with Various Y, O, and F Composition Ratios***, **Tetsuya Goto**, Y. Shiba, A. Teramoto,* Tohoku University, Japan*; Y. Kishi,* Nippon Yttrium Co., Ltd, Japan*; S. Sugawa,* Tohoku University, Japan

Yttrium oxyfluoride (YOF) has been received much attention as the material for various functional components used in the plasma process chamber for semiconductor manufacturing. This is because, as compared to the widely used Y_2O_3, YOF is stable against various corrosive plasmas using halogen gases which is frequently used in the etching processes and/or chamber cleaning processes. We have reported that YOF (1:1:1) film has the higher resistance to various plasma conditions (N_2/Ar, H_2/Ar, NH_3/Ar, NF_3/Ar, O_2/Ar) than the Y_2O_3 and YF_3 films [1, 2]. In this presentation, we report the effect of ion bombardment on the surface structure of sintered yttrium oxyfluoride (YOF) with various Y, O, and F composition ratios. By combining the starting materials of YOF, $Y_5O_4F_7$, and YF_3 in sintering, the YOF samples with different Y, O, and F composition ratios were prepared. In these samples, the oxygen composition ratio was changed from 33 at% to 7at%. According to this, the fluorine composition ratio was changed from 33at% to 66at%, and thus, the samples became from Y_2O_3 rich to YF_3 rich. Ar ion beam with 500 eV was irradiated to these YOF samples. It was found that the sputtering etching rate was monotonically decreased as the oxygen composition ratio was decreased. It was also found that the surface roughness was relatively smaller for the samples with the composition ratios of Y:O:F=1:1:1 and 5:4:7 (both correspond to the stable composition) than those with other composition ratios. The results indicated that the atomic composition ratio is an important parameter to obtain YOF with good stability against plasmas.

Acknowledgement

The plasma irradiation and inspection were carried out in Fluctuation-Free-Facility in Tohoku University.

1. Y. Shiba, A. Teramoto, T. Goto, Y. Kishi, Y. Shirai and S. Sugawa, J. Vac. Sci. Technol. A, 35 (2), 021405 (2017).

2. A. Teramoto, Y. Shiba, T. Goto, Y. Kishi and S. Sugawa p. 16, AVS 65th International Symp., Long Beach, 2019.

2:20pm **PS+AS+EM+SS+TF-MoA3 Understanding Atomic Layer Etching: Thermodynamics, Kinetics and Surface Chemistry***, **Jane P. Chang** [1],* University of California, Los Angeles **INVITED**

The introduction of new and functionally improved materials into silicon based integrated circuits is a major driver to enable the continued down-scaling of circuit density and performance enhancement in analog, logic, and memory devices. The top-down plasma enhanced reactive ion etching has enabled the advances in integrated circuits over the past five decades; however, as more etch-resistive materials are being introduced into these devices with more complex structures and smaller features, atomic level control and precision is needed in selective removal of these materials. These challenges point to the growing needs of identifying and developing viable etch chemicals and processes that are more effective in patterning complex materials and material systems such as multiferroics, magnetic materials and phase change materials, with tailored anisotropy and selectivity.

In this talk, a universal chemical approach is presented, combining thermodynamic assessment and kinetic validation to identify and validate the efficacy of various plasma chemistries. Specifically, potential reactions between the dominant vapor phase/condensed species at the surface are considered at various temperatures and reactant partial pressures. The volatility of etch product was determined to aid the selection of viable etch chemistry leading to improved etch rate of reactive ion etching process. Based on the thermodynamic screening, viable chemistries are tested experimentally to corroborate the theoretical prediction. Some of the above mentioned material systems such as complex oxides and metallic material systems used in logic and memory devices are used as examples to demonstrate the broad applicability of this approach.

[1] **PSTD Plasma Prize Winner**

3:00pm **PS+AS+EM+SS+TF-MoA5 Comparison of Silicon Surface Chemistry between Photo-Assisted Etching and Ion-Assisted Etching**, ***Emilia Hirsch**, L. Du, V.M. Donnelly, D.J. Economou,* University of Houston

Etching of p-Si in 60 mTorr Cl_2/Ar Faraday-shielded inductively coupled plasmas was investigated under both ion-assisted etching (IAE) and photo-assisted etching (PAE) conditions. Real-time etching rate and after-etch Si surface chemical composition were characterized by laser interferometry and vacuum-transfer X-ray photoelectron spectroscopy (XPS), respectively. By varying the duty cycle of a pulsed negative DC bias applied to the sample stage, it was found that the IAE rate scaled with the ion current integrated over the bias period, and the total etching rate was simply the sum of PAE and IAE rates. Consequently, little or no synergism occurred between VUV photon- and ion-bombardment stimulated etching. The PAE rate was ~ 210 nm/min at 60 mTorr. Above the 25 eV threshold, the IAE etching rate increased with the square root of the ion energy. Compared to RF bias, a more monoenergetic IED was obtained by applying pulsed DC bias, allowing precise control of ion energy near the low-energy IAE threshold. XPS spectra showed that, when compared to IAE, the chlorinated layer on the surface of samples etched under PAE conditions had significantly lower chlorine content, and it was composed of SiCl only. Under IAE conditions, however, Si· dangling bonds, $SiCl_2$, and $SiCl_3$ were found, in addition to SiCl, with relative abundance of SiCl>$SiCl_2$>$SiCl_3$. The absence of higher chlorides and Si· dangling bonds under PAE conditions suggested that VUV photons and ions are interacting with the Si surface very differently. When PAE and IAE occurred simultaneously, energetic ion bombardment dictated the surface chemistry that resulted in the formation of higher chlorides.

3:20pm **PS+AS+EM+SS+TF-MoA6 Chemical Reaction Probabilities in the Etching of Si by Fluorine Atoms Produced in a Mixture of NF-$_3$/SF_6 Plasma**, ***Priyanka Arora**[1], T. Nguyen,* University of Houston*; S. Nam,* Samsung Electronic Company, Republic of Korea*; V.M. Donnelly,* University of Houston

Reaction probabilities in the absence of ion bombardment, defined as the number of silicon atoms removed per incident fluorine atom, have been investigated in mixtures of NF_3 and SF_6 plasmas in an inductively-coupled plasma reactor. Fluorine atom densities were measured by optical emission actinometry, and isotropic etching rates were measured by the degree of undercutting of SiO_2-masked silicon, using cross-sectional scanning electron microscopy (SEM). In addition, atomic force microscopy (AFM) was used to examine surface roughness after etching. The F atom reaction probabilities derived from these measurements indicate ~30-fold higher reaction probability in SF_6 plasma compared with values in NF_3 plasma. Surfaces etched in SF_6 plasma were much smoother than those etched in NF_3 plasma. Addition of only 10% SF_6 to an NF_3 plasma produced a much higher reaction probability (~10-fold) than in a pure NF_3 plasma. This surprising enhancement of reaction probabilities for F with Si in SF_6 plasma will be shown to be due to adsorbed sulfur acting as a catalyst to greatly enhance the etching rate of Si. By allowing sulfur in isopropyl alcohol to evaporate on the masked Si samples, sulfur could be preferentially deposited in relatively high concentrations near mask edges in ~2 mm diameter periodic "strings of beads". When this sample is placed side by side with one not exposed to sulfur, the sulfur dosed sample etched several times faster at the center of each bead, while sulfur-free surface exhibited the expected slower rate.

4:00pm **PS+AS+EM+SS+TF-MoA8 John Thornton Memorial Award Lecture: Low Temperature Plasma-Materials Interactions: Foundations of Nanofabrication And Emerging Novel Applications At Atmospheric Pressure**, ***Gottlieb S. Oehrlein**[2],* University of Maryland, College Park **INVITED**

Our ability to understand and control the interactions of non-equilibrium plasma with surfaces of materials has been an exciting frontline and enabled the realization of new applications and technologies. The plasma-surface interactions (PSI) field has grown rapidly because of a number of reasons. First, plasma-assisted etching (PE) is one of the foundations of micro- and nanofabrication where increasingly atomistic precision in materials processing is required. By enabling the realization of intricate material features that semiconductor circuits and microstructures consist of, PE makes possible our technological tools that form modern society. This exceedingly complex procedure begins with the transfer of a resist mask in a directional and chemically selective fashion into various materials. Controlling profile shape, critical dimensions, surface roughness, and electrical integrity are crucial, and determined by PSI. Second, development of novel low temperature plasma sources operating at atmospheric pressure has enabled advances in areas where use of PSI has historically been limited, e.g. biology. In this talk I will present a brief review of contributions that I and my collaborators have been honored to make to our understanding of PSI, in particular in the areas of surface processes that are essential for achieving the objectives of plasma etching processes in current semiconductor fabrication that are approaching the atomic scale, and interaction of low temperature atmospheric pressure plasma sources with model polymers and biomolecules aimed at disinfection and sanitation of biological materials.

4:40pm **PS+AS+EM+SS+TF-MoA10 Determining Surface Recombination Probabilities during Plasma-enhanced ALD using Lateral High Aspect Ratio Structures**, ***Karsten Arts**,* Eindhoven University of Technology, The Netherlands, Netherlands*; M. Utriainen,* VTT Technical Research Centre of Finland, Finland*; R.L. Puurunen,* Aalto University School of Chemical Engineering, Finland*; W.M.M. Kessels,* Eindhoven University of Technology, The Netherlands, Netherlands*; H.C.M. Knoops,* Eindhoven University of Technology, The Netherlands

In this work we measure surface recombination probabilities r of plasma radicals, which is essential for the modeling and understanding of radical-driven plasma processes. Such quantitative information on r is scarcely reported in the literature and typically obtained by difficult and indirect measurement techniques. Here, we determine r using plasma-enhanced atomic layer deposition (ALD) on high aspect ratio (AR) structures, where the AR up to which film growth is obtained gives direct insight into r corresponding to the growth surface. This is demonstrated by measuring the recombination probabilities of O atoms on SiO-$_2$, TiO_2, Al_2O_3 and HfO_2, revealing a surprisingly strong material-dependence. Aside from studying different materials, our method can for instance be used to investigate the impact of pressure and temperature on r. This can provide valuable information for e.g., device fabrication, plasma source design and simulations, in the context of plasma-enhanced ALD but also relevant outside this field.

For this study, we use microscopic lateral-high-aspect-ratio (LHAR) structures[1] supplied by VTT (PillarHall® LHAR4). These chips have extremely high AR trenches (AR<10000) such that film growth is limited up to a certain penetration depth for even the most conformal processes. In the case of plasma ALD, where the film conformality is typically limited by surface recombination,[2] we show that the achieved penetration depth can be used to determine r. Furthermore, the LHAR structures allow for comparison of growth behavior with and without an ion component.

These opportunities are demonstrated by plasma ALD of SiO-$_2$, TiO_2, Al_2O_3 and HfO_2, using an O_2/Ar plasma and $SiH_2(N(C_2H_5)_2)_2$, $Ti(N(CH_3)_2)_4$, $Al(CH_3)_3$ and $HfCp(N(CH_3)_2)_3$, respectively, as precursors. It is observed that an exponential increase in plasma exposure time is required to linearly increase the film penetration depth. This relation, which solely depends on r, has been used to determine r=(6±2)· 10^{-5}, (6±3)· 10^{-5}, (1-10)· 10^{-3} and (0.1-10)· 10^{-2} for oxygen radicals on SiO-$_2$, TiO_2, Al_2O_3 and HfO_2, respectively. Corresponding to these large differences in r, growth of SiO_2 and TiO_2 penetrated extremely deep up to AR~900, while deposition of Al_2O_3 and HfO_2 was achieved up to AR~90 and AR~40, respectively. This strong material-dependence illustrates the importance of our quantitative research on surface recombination of plasma radicals.

1. Arts, Vandalon, Puurunen, Utriainen, Gao, Kessels and Knoops, J. Vac. Sci. Technol. A **37**, 030908 (2019)
2. Knoops, Langereis, van de Sanden and Kessels, J. Electrochem. Soc. **157**, G241 (2010)

5:00pm **PS+AS+EM+SS+TF-MoA11 Study of Plasma-Photoresist Interactions for Atomic Layer Etching Processes**, ***Adam Pranda**[3], K.-Y. Lin, G.S. Oehrlein,* University of Maryland, College Park

The emergence of atomic layer etching (ALE) processes has enabled improved control of surface profiles. Whereas the implementation of ALE processes on hard mask materials has been well established, the effects of these processes on photoresist materials is not well known. With the advent of next generation extreme ultraviolet (EUV) photoresists, there is the potential to utilize ALE processes with photoresist materials for fabrication of sub-10 nm feature sizes.

[1] **Coburn & Winters Student Award Finalist**
[2] **John A. Thornton Memorial Award Winner**
[3] **Coburn & Winters Student Award Finalist**

The plasma processing of photoresist materials induces several key physical and chemical modifications which affect material properties such as the etching behavior and surface roughness. In this work, we utilize in-situ ellipsometry, atomic force microscopy (AFM), x-ray photoelectron spectroscopy (XPS), and Fourier transform infrared (FTIR) spectroscopy to interpret the relationships between the aforementioned material properties, the photoresist chemical composition, and plasma ALE parameters such as ion energy and precursor gas type. By comparing these relationships between baseline continuous plasma etching processes and ALE processes, which include the introduction of chemically reactive surface passivation, we elucidate the intrinsic photoresist behaviors under plasma exposure and how an ALE process specifically impacts these behaviors.

Under nonreactive plasma chemistries, a universal response among photoresist materials is the development of a surface dense amorphous carbon (DAC) layer due to energetic ion bombardment. We have found that the photoresist etch rate is inversely proportional to the DAC layer thickness.[1] However, photoresists with UV sensitive pendant groups, such as 193 nm photoresists, develop a greater surface roughness due to the stresses in the surface generated by synergistic ion and UV photon interactions.

With depositing fluorocarbon (FC)-based ALE gas chemistries, the deposited FC layer reacts with the DAC layer and converts it into a mixed layer. This incorporation of FC into the DAC layer reduces the surface roughness without impacting the etch rate of the underlying photoresist as long as a sufficient DAC layer thickness remains.[2] This behavior is potentially advantageous for maximizing the photoresist to SiO_2 selectivity while maintaining an adequate surface roughness.

The authors acknowledge S.A. Gutierrez Razo, J.T. Fourkas, R.L. Bruce, S. Engelmann, and E.A. Joseph for collaborations on aspects of this work, and financial support by the National Science Foundation (NSF CMMI-1449309) and Semiconductor Research Corporation (2017-NM-2726).

[1] A. Pranda et al., J. Vac. Sci. Technol. A **36**, 021304 (2018).

[2] A. Pranda et al., Plasma Process. Polym. e1900026 (2019).

Thin Films Division
Room A124-125 - Session TF+2D+AP+EL+SS-MoA

ALD and CVD: Nucleation, Surface Reactions, Mechanisms, and Kinetics

Moderators: Adrie Mackus, Eindhoven University of Technology, The Netherlands, Qing Peng, University of Alabama

1:40pm **TF+2D+AP+EL+SS-MoA1 ALD on Particles: What is Different from Wafers?**, ***Ruud van Ommen***, Delft University of Technology, Netherlands **INVITED**

Advanced materials, often relying on nanostructured particles as building blocks, are crucial in meeting grand challenges in energy and health. Atomic layer deposition (ALD) is an excellent technique to make such nanostructured particles: particles of which the surface is either covered by an ultrathin film or by nanoclusters. Although the underlying mechanisms are similar, there are quite some differences between ALD processing of wafers and ALD processing of particles. This presentation will discuss recent developments and insights in the field of applying ALD to particles, with an emphasis on reactor technology, precursor utilization, operating conditions, and scaling up. I will show that ALD is suited to produce nanostructured particles with very high precision. Moreover, it is scalable such that large amounts of such particles can be produced.

2:20pm **TF+2D+AP+EL+SS-MoA3 Insights into Particle ALD Peculiarities from In- and Ex-Situ Characterization**, ***Benjamin Greenberg***, American Society for Engineering Education; *J.A. Wollmershauser, B. Feygelson,* U.S. Naval Research Laboratory

Particle atomic layer deposition (pALD) is an increasingly popular technique for mass production of core/shell nanoparticles (NPs). In a typical pALD process, NP powders are agitated in a fluidized bed or rotary reactor, and conformal coating of the entire powder surface—often > 100 m^2 in lab-scale reactors—is attempted via prolonged precursor exposures and purges. Over the past 2+ decades there have been many reports of highly encouraging results, including TEM images of NPs individually encapsulated by shells of uniform thickness. Nevertheless, several fundamental questions about pALD mechanisms and behavior remain challenging to answer. For example, how does the pALD growth per cycle (GPC) deviate from the corresponding ALD GPC on a flat substrate, and why? Or more importantly, what conditions are required to maximize the fraction of powder that attains an ideal core/shell structure (individual NP encapsulation) rather than a coated-agglomerate structure in which cores are glued together? In this work, using a commercial rotary pALD reactor to coat various NPs with oxide shells, we employ a wide array of characterization techniques to shed light on these issues and inform process optimization. In situ, we experiment with relatively uncommon techniques such as high-speed video analysis and pyrometry of the agitated NP powder, as well as conventional techniques such as mass spectrometry (RGA). High-speed videos in particular reveal aspects of the process often undiscussed (and sometimes difficult to convey) in the pALD literature, including changes in the powder motion as surface chemistry evolves. Ex situ, we characterize the coated NPs via TEM, XRD, SAXS, XPS, and N_2-adsorption surface area measurements (BET method).

3:00pm **TF+2D+AP+EL+SS-MoA5 Controlling the Nucleation of CVD Cobalt Films on SiO_2: Combining an Amido-based Nucleation Promotor with an Amine-based Growth Inhibitor to Afford Atomically-smooth Surfaces**, ***Zhejun Zhang***, *G.S. Girolami, J.R. Abelson,* University of Illinois at Urbana-Champaign

Cobalt films are of interest for the back-end metallization and transistor contact in microelectronics because cobalt has a greater electromigration resistance and a lower diffusion rate in dielectrics compared with copper. However, few-nanometer thick Co films deposited by CVD on dielectrics are usually non-continuous – they consist of islands with pinholes and significant roughness – which renders them unsuitable for nanoscale device fabrication. A nucleation layer, such as TiN, can be pre-deposited to improve the area density of Co nuclei; this approach eliminates the problem of islanding, but it subtracts cross-sectional area from the plug or line, thus increasing the electrical resistance.

Here, we solve the Co nucleation problem in CVD using a two-pronged approach. First we expose the SiO_2 surface to a tetrakis(dimethylamido)(transition metal) precursor at low temperature. This affords a self-limiting, submonolayer coverage of an intermediate, similar to the behavior of such molecules in ALD processes. The adsorbate layer then enhances the nucleation of cobalt from the $Co_2(CO)_8$ precursor, such that a large area density of nanoscale islands forms with essentially no nucleation delay. Using this approach, the rms surface roughness for a 1.5-nm-thick Co film decreases from 2.5 to 1.0 nm.

Second, we further improve the surface morphology by adding a co-flow of ammonia together with the carbonyl precursor; this serves as a growth inhibitor that reduces the steady-state growth rate of Co films by 50 %. The presence of the inhibitor does not alter the nucleation rate, however, the rms roughness of a 1.5-nm-thick film is further reduced to only 0.4 nm. We suggest that the roughness is due to a better valley-filling at low precursor reaction probability, consistent with the literature. In summary, our approach enables the use of CVD to afford excellent Co films for nanofabrication.

3:20pm **TF+2D+AP+EL+SS-MoA6 Plasma-assisted Atomic Layer Epitaxy of Indium Aluminum Nitride Studied Using *in situ* Grazing Incidence Small-angle X-ray Scattering**, ***Jeffrey M. Woodward***, ASEE (residing at US Naval Research Laboratory); *S.G. Rosenberg,* American Society for Engineering Education (residing at US Naval Research Laboratory); *S.D. Johnson, N. Nepal,* U.S. Naval Research Laboratory; *Z.R. Robinson,* SUNY Brockport; *K.F. Ludwig,* Boston University; *C.R. Eddy,* U.S. Naval Research Laboratory

Indium aluminum nitride (InAlN) is an attractive material for power electronic applications. However, conventional methods of epitaxial growth of InAlN are challenged by a large miscibility gap and the significant differences in optimal growth conditions for the constituent aluminum nitride (AlN) and indium nitride (InN) binary compounds. Despite these challenges, the epitaxial growth of InAlN alloys throughout the entire compositional range has been demonstrated using plasma-assisted atomic layer epitaxy (ALEp)[1], a variant of atomic layer deposition in which relatively higher temperatures are utilized. In the ALEp growth of InAlN, the desired alloy compositions are achieved by forming ultra-short period superlattices of alternating InN and AlN layers, referred to as digital alloys (DA). In order to further advance these empirical efforts, significant research is needed to better understand the nucleation and growth kinetics of ALEp DA growth. To this end, we employ *in situ* grazing incidence small angle X-ray scattering (GISAXS) for the real-time study of the evolving ternary InAlN surfaces as has been done previously for binary InN[2] and AlN[3].

Here we present *in situ* GISAXS studies of ALEp growth of InN, AlN, and a range of InAlN DAs on GaN (0001) substrates, which were performed at Brookhaven National Laboratory's NSLS-II using a custom reactor. The InAlN DAs studied include $In_{0.19}Al_{0.81}N$ (3 AlN cycles and 2 InN cycles per supercycle), $In_{0.5}Al_{0.5}N$ (1 AlN cycle and 3 InN cycles per supercycle), $In_{0.64}Al_{0.36}N$ (1 AlN cycle and 5 InN cycles per supercycle) and $In_{0.83}Al_{0.17}N$ (1 AlN cycle and 14 InN cycles per supercycle). Preliminary analysis of the data suggests that while the pure InN and AlN grew in 3D and 2D modes, respectively, the InAlN growth mode did not follow a simple trend as the nominal composition was tuned from InN to AlN. Instead, select compositions (50% and 83% In) exhibited predominantly 3D growth, while others (19% and 64% In) exhibited 2D growth. We also present complementary ALEp growth studies using a commercial Ultratech/Cambridge Nano Tech Fiji 200 and *ex situ* characterization methods, including high resolution X-ray diffraction, X-ray reflectivity, and atomic force microscopy.

[1] N. Nepal, V.R. Anderson, J.K. Hite, and C.R. Eddy, Thin Solid Films **589**, 47 (2015)

[2] J.M. Woodward, S.G. Rosenberg, A.C. Kozen, N. Nepal, S.D. Johnson, C. Wagenbach, A.H. Rowley, Z.R. Robinson, H. Joress, K.F. Ludwig Jr, C.R. Eddy Jr, J. Vac. Sci. Technol. A **37**, 030901 (2019)

[3] V.R. Anderson, N. Nepal, S.D. Johnson, Z.R. Robinson, A. Nath, A.C. Kozen, S.B. Qadri, A. DeMasi, J.K. Hite, K.F. Ludwig, and C.R. Eddy, J. Vac. Sci. Technol. A **35**, 031508 (2017)

4:00pm **TF+2D+AP+EL+SS-MoA8 Real-time Monitoring of the Surface Chemistry of Atomic Layer Deposition by Ambient Pressure X-ray Photoelectron Spectroscopy***,* ***Joachim Schnadt****, P. Shayesteh,* Lund University, Sweden*; R. Tsyshevskiy,* University of Maryland*; J.-J. Jean-Jacques, F. Bournel,* Sorbonne Université, France*; R. Timm,* Lund University, Sweden*; A.R. Head,* Brookhaven National Laboratory*; G. D'Acunto, F. Rehman, S. Chaudhary,* Lund University, Sweden*; R. Sánchez-de-Armas,* Uppsala University, Sweden*; F. Rochet,* Sorbonne Université, France*; B. Brena,* Uppsala University, Sweden*; A. Mikkelsen, S. Urpelainen, A. Troian, S. Yngman, J. Knudsen,* Lund University, Sweden **INVITED**

Atomic layer deposition (ALD) and chemical vapour deposition (CVD) are very important methods that enable a highly controlled growth of thin films [1]. The surface chemis-try of the underlying processes remains, however, little understood. While idealised reac-tion mechanisms have been developed, they represent postulates rather than models based on the factual identification of surface species and kinetics [2]. New *in situ* and *operando* methods offer the prospect of gaining a much more thorough understanding of the involved molecular and atomic surface processes and (dynamic) structures, which, in turn, means that a much better knowledge basis can be achieved for the future improvement of materials and growth recipes (see, e.g. [3,4]). One such *operando* method, which can be applied to the investigation of ALD and CVD, is synchrotron-based ambient pressure x-ray photoelectron spectroscopy (APXPS). While conventional x-ray photoelectron spectroscopy (XPS) is limited to vacuum pressures of 10^{-5} mbar and below, APXPS can be carried out at realistic pressure. Today, most APXPS machines can operate at pressures up to the 10 mbar regime, which is an ideal match to the pressure regime used in standard ALD reactors.

Here, I will report on our recent efforts to apply density functional theory (DFT)-assisted synchrotron-based APXPS to the ALD/CVD of oxides (TiO_2, SiO_2, and HfO_2) on semiconductor (InAs and Si) and oxide surfaces (TiO_2, RuO_2) [3-5]. I will show that APXPS allows the identification of the surface species occurring during thin film growth and the real-time monitoring of their evolution with a time resolution of down into the millisecond regime. Here, DFT is an important tool for pinpointing the nature of the chemical species and for providing deeper insight in the surface chemical processes. I will also report on our efforts to further improve instrumentation with the goal of achieving a much closer match of the APXPS sample environment with the geometries used in conventional ALD reactors. The development will also open for the use of a wider range of precursors and growth protocols.

[1] V. Miikkulainen et al., J. Appl. Phys. 113 (2013) 021301.

[2] F. Zaera, Coord. Chem. Rev. 257 (2013) 3177.

[3] B. A. Sperling et al. Appl. Spectrosc. 67 (2013) 1003.

[4] K. Devloo-Casier et al., J. Vac. Sci. Technol. 32 (2014) 010801.

[3] S. Chaudhary et al. , J. Phys. Chem. C 119 (2015) 19149.

[4] A. R. Head et al. , J. Phys. Chem. C 120 (2016) 243.

[5] R. Timm et al., Nature Commun. 9 (2018) 412.

4:40pm **TF+2D+AP+EL+SS-MoA10 Kinetics during TMA-H_2O ALD: The Possible Role of Cooperative Surface Reactions***,* ***Brent Sperling****, B. Kalanyan, J.E. Maslar,* National Institute of Standards and Technology (NIST)

Until recently, the CH_3 groups produced by surface reactions of trimethylaluminum (TMA) during atomic layer deposition were widely believed to always be highly reactive toward H_2O, but *in situ* measurements have shown this is not the case below about 200 °C.[1] At these temperatures, some CH_3 groups react slowly, and a significant amount persists from cycle to cycle under typical growth conditions. Interestingly, these persistent CH_3 groups are not incorporated as carbon impurities. We have observed these CH_3 groups using *in situ* reflection infrared spectroscopy and have confirmed low carbon concentrations in our films using *ex situ* XPS. Furthermore, we have measured the kinetics of the reaction with H_2O and have found them to be well-described by a double-exponential decay function. A simple Monte Carlo simulation that incorporates cooperative effects by clustered surface reactants (as suggested by DFT calculations[2]) reveals that a double-exponential decay of coverage can result even when only one species of reactant is present. Furthermore, the short-range distributions of coverage that result in the simulation differ from purely random ones. This difference implies that measurements sensitive to dipole-dipole interactions when combined with an independent measurement of surface coverage could be used to confirm or disprove the cooperative reaction model.

[1] V. Vandalon and W. M. M. Kessels, *J. Vac. Sci. Techol. A***35** (2017) 05C313

[2] M. Shirazi and S. D. Elliott, *Nanoscale***7** (2015) 6311.

5:00pm **TF+2D+AP+EL+SS-MoA11 Atomic Layer Deposition of Metal Sulfides: Growth and Surface Chemistry***,* ***Xinwei Wang****,* Shenzhen Graduate School, Peking University, China

Atomic layer deposition (ALD) of metal sulfides has recently aroused great interest, and many new sulfide ALD processes have emerged during the past several years. Surface chemistry plays a key role in ALD, but it remains yet to be investigated for many recently developed sulfide ALD processes. In this representation, I will report our study on the growth and surface chemistry of the ALD of nickel, iron, and cobalt sulfides, using various in situ characterization techniques of X-ray photoelectron spectroscopy (XPS), low-energy ion scattering (LEIS), quartz crystal microbalance (QCM), and quadrupole mass spectrometry (QMS). For instance, nickel sulfide (NiS) can be deposited from a Ni amidinate precursor ($Ni(amd)_2$) and H_2S by ALD (*Chem. Mater.* (2016) 28, 1155), but the surface chemistry of this process is found to deviate from the conventional ligand-exchange ALD scheme, and a formation of a nonvolatile acid-base complex from acidic surface sulfhydryl and basic amidine is suggested during the H_2S half-cycle (*J. Phys. Chem. C* (2018) 122, 21514). The initial ALD growth of NiS on a SiO_x surface is also intriguing, as the initial growth mechanism is found to be rather different from that in the later steady film growth. In the initial ALD cycles, the XPS results show a drastic cyclic variation of the signals for the Ni−O bonds, with prominently observable Ni−O signals after each $Ni(amd)_2$ dose but almost negligible after the subsequent H_2S dose. These results suggest that the Ni−O bonds are first formed on the surface in the $Ni(amd)_2$ half-cycles and then mostly converted to NiS in the following H_2S half-cycles. To describe this initial ALD growth process, a reaction-agglomeration mechanistic scheme is proposed (*Chem. Mater.* (2019) 31, 445). Surface thermolysis study of the Ni amidinate precursor further reveals the temperature-dependent behavior of the film growth.

Thin Films Division
Room A122-123 - Session TF+SE-MoA
HiPIMS and Reactive HiPIMS for Novel Thin Films

Moderators: Joe Becker, Kurt J. Lesker Company, Megan Holtz, Cornell University

1:40pm **TF+SE-MoA1 The Influence of the Magnetic Field on the Deposition Rate and Ionized Flux Fraction in the HiPIMS Discharge**, *H. Hajihoseini,* University of Iceland, Iceland*; M. Cada, Z. Hubicka,* Academy of Sciences of the Czech Republic, Czech Republic*; S. Unaldi,* LPGP Université Paris-Sud, France*; M.A. Raadu, N. Brenning,* KTH Royal Institute of Technology, Sweden*; **Jon Tomas Gudmundsson**,* University of Iceland, Iceland*; D. Lundin,* LPGP Université Paris-Sud, France

Three different ways to quantify the degree of ionization in sputtering magnetrons are discussed [1]. Then we move on to explored the effect of the magnetic field strength |**B**| and geometry (degree of balancing) on the deposition rate and ionized flux fraction F_{flux} in dc magnetron sputtering (dcMS) and high power impulse magnetron sputtering (HiPIMS) when depositing titanium. The HiPIMS discharge was run in two different operating modes. The first one we refer to as 'fixed voltage mode' where the cathode voltage is kept fixed at 625 V while the pulse repetition frequency is varied to achieve the desired time average power (300 W). The second mode we refer to as 'fixed peak current mode' is carried out by adjusting the cathode voltage to maintain a fixed peak discharge current and by varying the frequency to archive the same average power. Our results indicate that the dcMS deposition rate is weakly sensitive to variations in the magnetic field while the deposition rate during HiPIMS operated in fixed voltage mode changes from 30% to 90% of the dcMS deposition rate as |**B**| decreases [2]. In contrast, when operating the HiPIMS discharge in fixed peak current mode the deposition rate increases only slightly with decreasing |**B**|. In fixed voltage mode, for weaker |**B**| the higher the deposition rate, the lower the F_{flux}. The measured quantities, the deposition rate and ionized flux fraction, are then related to the ionization probability α_t and the back attraction probability of the sputtered species β_t. We show that the fraction of the ions of the sputtered material that escape back attraction increases by 30% when |**B**| is reduced during operation in fixed peak current mode while the ionization probability of the sputtered species increases with increased discharge current when operating in fixed voltage mode.

[1] A. Butler, N. Brenning, M. A. Raadu, J. T. Gudmundsson, T. Minea and D. Lundin, *Plasma Sources Science and Technology*, **27**(10) (2018) 105005

[2] H. Hajihoseini, M. Čada, Z. Hubička, S. Unaldi, M. A. Raadu, N. Brenning, J. T. Gudmundsson and D. Lundin, *Plasma*, submitted for publication, April 2019

2:00pm **TF+SE-MoA2 HIPIMS and Magnetron Sputtering of Niobium for use in Josephson Junctions**, ***George Major**, M.R. Linford,* Brigham Young University

Niobium (Nb) is a technology-critical element with superconductive properties, and applications in electronics, superconductors, and particle accelerators. Thin film niobium is commonly deposited by magnetron sputtering. Properties of Nb thin films must be precisely tuned for applications, e.g., Josephson Junctions, as surface roughness, crystallite size, and apparent elastic modulus can affect superconducting film properties. To create a Josephson Junction, a thin film of Al (4 to 10 nm) is deposited on top of a smooth Nb film (ca. 100 nm). The functionality of this Al film is inversely related to its thickness. The smoother the film onto which the Al is deposited, the thinner it can be. High-power impulse magnetron sputtering (HIPIMS) is an emerging method for physically depositing thin films. HIPIMS produces a high degree of ionization of sputtered material and a high rate of molecular gas dissociation, which results in high density films. Various metals, including Ti and Ta, have been successfully deposited by HIPIMS, showing dense, smooth microstructures free of large-scale defects. Here, Nb thin films are deposited using magnetron sputtering and HIPIMS. These films are characterized by AFM, TEM, XPS, and SEM. Ellipsometry is used to study their optical properties and to determine their optical constants. HIPIMS should result in lower surface roughness compared to magnetron sputtering. The resulting films will lead to improved superconductive devices.

2:20pm **TF+SE-MoA3 Thin Film Crystal Growth of Oxides, Nitrides and Carbindes using High Impulse Magnetron Sputtering**, ***Jon-Paul Maria**,* The Pennsylvania State University **INVITED**

This presentation will discuss thin film crystal growth using reactive pulsed magnetron sputtering specifically in the region referred to as high power impulse magnetron sputtering, or HIPIMS. HIPIMS is characterized by duty cycles less than approximately 10%, and magnetron power densities in excess of 1 kW/cm^2. These intense impulses produce high ionization fractions of both the gas and sputtered species, they can be sustained in atmospheres containing substantial fractions of O_2 or N_2 with only modest re-sputtering, and they can be tuned so as to minimize target poisoning. Pulsed dc plasmas have been applied routinely to promote thin film adhesion, to achieve high deposition rates, and to produce extremely hard and wear resistant coatings. Their introduction to electronic materials has been much less rapid.

The intent of this presentation is to demonstrate the utility of pulsed dc plasmas, and specifically the HIPIMS regime, for electronic materials, including oxides, nitrides and carbides which require reactive environments that can in many cases can be challenging to realize. Three case studies will be presented: 1) epitaxial growth of CdO thin films for IR optoelectronic applications, 2) epitaxial growth of GaN thin films for wide bandgap applications, and 3) entropy-stabilized carbides for extreme environments. The basic instrumentation of this interesting plasma method will be discussed, and how it offers advantages for controlling defect chemistry, and this transport properties, in CdO, for enabling epitaxy at surprisingly low temperatures in GaN, with excellent control of surface morphology, and for achieving high carbon content in rocksalt carbides, and thus high hardness. In all cases the specific connections between plasma parameters, temperature, pressure, growth mode, and ultimately physical properties will be stressed. The intent is to demonstrate how this less-well explored region of plasma processing space offers possible advantages to crystal growth of electronic materials of contemporary interest.

3:00pm **TF+SE-MoA5 Reactive Bipolar High Power Impulse Magnetron Sputtering (B-HiPIMS) for Deposition of High Entropy Carbides**, ***Trent Borman**, M.D. Hossain, J.-P. Maria,* The Pennsylvania State University

Sputtered carbide thin films frequently feature significant carbon sub-stoichiometry irrespective of the source materials, while amorphous-C or a-C:H secondary phases begin to precipitate with as many as 1/3 or more of the carbon sites vacant in the rock salt structure. In reactive sputtering it is often necessary to sputter in the compound regime in order to achieve a higher carbon stoichiometry, however this comes with the penalty of reduced sputter yield. Reactive HiPIMS can avoid carburization of the target through gas rarefaction and high target etch rates. While this is beneficial for process stability, carbide microstructural evolution is still limited by the low homologous temperature achievable in thin film deposition (0.25-0.3T_{melt}). Recently, bipolar-HiPIMS has been discussed as a means of tailoring the bombardment in order to drive microstructural development through momentum transfer and thermalization of kinetic energy.

The authors will discuss the reactive synthesis of high entropy carbide films from metal alloy targets using Bipolar High-Power Impulse Magnetron Sputtering (B-HiPIMS) in a mixed Ar/CH_4 atmosphere. The effects of bipolar pulse voltages and lengths on microstructural, compositional, and phase development will be discussed. Additionally, the impacts of order of magnitude changes in sputter pulse length on the formation of carbide thin films will be reported. This work investigates a broad range of carbon stoichiometries: from metallic films and carbon deficient carbides to near stoichiometric carbides and carbide/amorphous-carbon nanocomposites. This enables investigation of the property trends as a function of carbon content, as it is presently unclear if the diverse trends observed in the binary carbides persist in a high entropy system or are overshadowed by the high entropy metal sublattice.

This material is based upon work supported by the National Science Foundation Graduate Research Fellowship (DGE-1252376) and the Office of Naval Research (N00014-15- 1-2863).

3:20pm **TF+SE-MoA6 High Density Titanium Oxide and Silicon Oxide Films Deposited by Current-Controlled High Power Impulse Magnetron Sputtering**, ***Arutiun P. Ehiasarian**, P.Eh. Hovsepian, D.A. Loch,* Sheffield Hallam University, UK

High density transparent oxide layers on glass can improve the environmental viability of photovoltaics, displays, and low emissivity layers in glazing as well as aid the photocatalytic deactivation of organic contaminants. High Power Impulse Magnetron Sputtering (HIPIMS)

produces high density microstructures and high hardness due to the delivery of an ionised metal and dissociated oxygen deposition flux to the substrates.

TiOx and SiOx films were produced in a cluster tool by reactive HIPIMS of a pair of metallic targets in an Ar-Oxygen atmosphere. The HIPIMS process was carried out by controlling the current within the pulse. This resulted in the elimination of stability issues associated with runaway currents for all target poisoning states from metallic to fully poisoned. TiOx was deposited by a fast plasma ignition and a constant current during pulses of up to 200 microseconds. Electron cooling and gas rarefaction were observed sequentially during the initial stages if the pulse. These were followed by a steady increase in metal ion emission at constant power input. SiOx was deposited using a current ramp and shorter pulses of up to 20 microseconds and a bipolar operation. In the transition mode oxygen was emitted mainly from the target whilst in the filly poisoned mode it was detected in the gas phase by time-resolved optical emission spectroscopy. TiOx films deposited without additional heating or substrate biasing had good transparency and a refractive index which increased continuously as the oxygen flow reduced from 45 to 13% reaching a maximum value of 2.55 at a wavelength of 550 nm. The films comprised a mixture of rutile and anatase phase with HIPIMS deposition producing higher fractions of rutile compared to bipolar pulsed DC operation. The HIPIMS films reached higher refractive index of 2.55 compared to 2.47 for bipolar pulsed DC. The hardness of the films and its relation to process conditions are discussed. The morphological density was extremely high as confirmed by a 2 orders of magnitude reduction in corrosion current in potentiodynamic polarisation tests on 304 stainless steel substrates. SiOx microstructural density, refractive index and hardness are discussed.

4:00pm **TF+SE-MoA8 Epitaxial Growth and Surface Morphology of Thin Film GaN via HiPIMS**, ***Kevin Ferri**, E. Runnerstrom,* Pennsylvania State University*; A. Klump, Z. Sitar, R. Collazo,* North Carolina State University*; J.-P. Maria,* The Pennsylvania State University

GaN is a desirable wide bandgap semiconductor for applications as blue and UV emitters as well as high temperature, high power, and high frequency electronic devices. In order to overcome the low reactivity of gallium with nitrogen at low temperatures, thin film GaN deposition techniques such as Metal Organic Chemical Vapor Deposition often use high pressure growth at temperatures in excess of 1000 °C. While higher temperatures allow for high crystal quality thin film GaN with favorable morphology, this presents challenges to abrupt junction formation due to fast diffusion rates that cause dopant migration during deposition. It is thus advantageous to find avenues to lower the deposition temperature for GaN to a region where controlled doping can occur. While doing so, it is imperative to maintain epitaxy and growth morphology for device fabrication.

In this presentation, we demonstrate that reactive High-Power Impulse Magnetron Sputtering (HiPIMS) is an effective low temperature alternative for depositing high quality, epitaxial GaN thin films. In contrast to conventional direct current (DC) or radio frequency (RF) sputtering, pulsed DC provides the needed kinetic energy and ionization fraction to establish a sufficiently reactive environment to promote full nitridation. This can be challenging with many other Ga sources. More specifically, the low duty cycle regime of pulsed DC known as HiPIMS provides access to kW/cm^2 peak power densities without target degradation and thus dramatically increased gallium reactivity. In addition, adding an opposite polarity voltage pulse between the target bombarding events, known as a kick pulses, further allows one to tailor both the adatom landing energy on the substrate surface, and mitigate target poisoning.

This unique capability set enables us to prepare high crystal quality epitaxial GaN thin films with smooth surface morphologies characterized by c/2 steps and terraces at temperatures below 500 °C. The presentation will focus on the relationships between sputtering parameters including voltage, kick pulse, pulse length, and duty cycle, on GaN thin film crystal quality, surface morphology, and growth rate. Preliminary transport properties will be reported.

4:20pm **TF+SE-MoA9 Reactive HiPIMS Deposition of a Thick Cu:CuCNx Multilayered Nano-composite Coating Material for Improving Machining Process Performance in Rough Turning**, ***Md.Masud-Ur Rashid**, C.M. Nicolescu,* KTH Royal Institute of Technology, Plasmatrix Materials AB, Sweden*; A. Archenti,* KTH Royal Institute of Technology, Sweden*; G. Shuai,* KTH Royal Institute of Technology*; R. Tomkowski,* KTH Royal Institute of Technology, Sweden

Vibrations in metal cutting process such as turning have detrimental effect on productivity, finished surface roughness of workpiece and cutting insert life. During machining process high frequency vibration (equal to or above 10000 Hz) causes micro cracks to the cutting insert, which facilitate the failure of cutting insert and consequently resulted in higher roughness on workpiece surface. In this study a reactive high power impulse magnetron sputtering (R-HiPIMS) deposition process was used to deposit a thick copper and copper-carbon nitride (Cu:CuCNx) multilayered nano-structured composite coating, with higher stiffness and damping properties, on the shim. This coated shim was then used to suppress the high frequency vibration during rough turning operation. Scanning electron microscopy (SEM) of the coating cross section as well as energy dispersive x-ray spectroscopy (EDS) mapping of the cross-section confirms the multilayered structure with the presence of different rations of copper (Cu), carbon (C), and nitrogen (N). The Cu:CNx coating thickness was measured to be approximately 100 µm. The average surface hardness (SH) and cross-sectional hardness (CSH), measured by Vickers-microhardness indention, were found to be 353.2 HV and 149.5 HV respectively. Insert wear measurement after 30 minutes of rough turning process, reveals that the studied 100 µm Cu:CuCNx multi-layered composite coating material can reduce the tool wear by 60.5%. The average roughness value (Ra) of the work piece material is also reduced by 8.76% in case of using Cu:CNx coated shim comparing to conventional shim.

4:40pm **TF+SE-MoA10 The Residual Stress Control in Hard Metal Films by Energetic Deposition**, ***Y.G. Li**, Y.Z. Qu, Z.T. Jiang, M.K. Lei,* Dalian University of Technology, China

For energetic deposition, ion bombardment was an important factor independent of grain size for influencing the residual stress, and the energy and flux were critical parameters to determine the residual stress evolution. In this work, modulated pulsed power magnetron sputtering (MPPMS) and deep oscillation magnetron sputtering (DOMS) were employed to control the energy and flux with or without bias to modulate the ion bombardment for intrinsic stress generation. The films thickness was selected at 0.2, 0.5, 1.5 and 3.0 µm to give a comparative study of the intrinsic stress, and thermal stress was not considered since the effect of thermal stress made no major influences. It was found that the thin films all showed compressive residual stress with thickness under 1 µm, and the residual stress of Cr thin film was lower than that of the Nb thin film under similar thickness. The residual stress of DOMS Nb thin film was always higher than MPPMS Nb thin film, however the residual stress of DOMS Cr thin film was equivalent to MPPMS Cr thin film. The ion irradiation effect should be the dominating effect responsible for the difference between Nb and Cr thin films, since Nb generated more Nb^{2+} ions than Cr in energetic deposition. For Cr thin films, the grain size and deposition rate were also important influencing factors, fine grain size and high deposition rate promoted the formation of compressive residual stress. For energy deposition, the effect of secondly charged ions in the film growing front should be concentrated to establish a proper kinetic model for intrinsic stress generation.

5:00pm **TF+SE-MoA11 Advanced HIPIMS Coatings Through Kick Pulse Technology**, ***Jason Hrebik**,* Kurt J. Lesker Company

HIPIMS coating technology has been rapidly growing over the past few years due to the availability of R&D scale supply offerings. This has resulted in many new breakthroughs in application enhancement, production scalability, and efficiency. The number of applications where HIPIMS is now considered is also advancing. Breakthroughs in HIPIMS controllability have enabled researchers to find a variety of ideal operating parameter sets for various performance requirements. One of the most significant technical advances is a reverse positive kick pulse. This option provides a significant variable for driving out film stress in HIPIMS applications and increasing yield rates, which have been a major downside to HIPIMS in the past. These advances open up new possibilities for the technology and the enhancement of many thin film applications. This presentation will highlight examples of these applications along with the advantages associated with HIPIMS and the Kick pulse technology. It will show how these advances can be scaled to larger scale production applications and provide examples of what enhancements can be expected.

Thin Films Division
Room A124-125 - Session TF+AP-TuM
ALD and CVD: Precursors and Process Development

Moderators: Paul Poodt, Holst Centre / TNO, The Netherlands, Erwin Kessels, Eindhoven University of Technology, The Netherlands

8:00am **TF+AP-TuM1 Mechanism-Based Precursor Design for CVD of Metal Oxides and Sulfides***, **Lisa McElwee-White**,* University of Florida **INVITED**

Aerosol-assisted chemical vapor deposition (AACVD) of WO_x was demonstrated using the oxo tungsten(VI) fluoroalkoxo single-source precursors, $WO[OC(CF_3)_2CH_3]_4$ (**1**) and $WO[OC(CH_3)_2CF_3]_4$ (**2**). Mechanistic studies of the decomposition of **1** and **2** were consistent with gas phase decomposition to yield tungsten (VI) dioxo intermediates during growth of WO_x materials. The dioxo tungsten alkoxide precursors $WO_2[OC(CF_3)_2CH_3](DME)$ (**3**) and $WO_2[OC(CF_3)_3](DME)$ (**4**) were then prepared as a means of independently generating intermediates involved in deposition of WO_x materials from **1** and **2**. Further experimental and computational mechanistic studies have led to synthesis of related precursors with other O-bound ligand types, including β-diketonates, β-ketoesterates, β-ketoiminates, and β-diketiminates, which have been used for deposition of WO_x films and nanostructures. Similar mechanism-based design strategies using S-bound ligands have been extended to precursors for deposition of MoS_2 and WS_2. Precursor syntheses, mechanistic studies, deposition of films under AACVD and CVD conditions, and characterization of the resulting materials will be discussed.

8:40am **TF+AP-TuM3 Improved Control of Atomic Scale Processing: Characterization and Optimization of Precursor Mass Delivery Utilizing a Novel Thermal Sensor***, **Daniel Alvarez**, J. Spiegelman, C. Ramos, Z. Shamsi,* RASIRC

ALD precursor utilization is a long-standing problem in semiconductor manufacturing. In general, precursors are quite expensive ($5-$25/gram), particularly where utilization is estimated as low as 5-10%. Thus far, chip manufacturers have been burdened by precursor costs and low wafer throughput. A non-optimized process consumes excess material and requires longer purge time.

For Area Selective Deposition (ASD), control of precursor mass delivery is even more critical to process viability. Here, excessive precursor material can initiate growth on "Non-growth" surfaces, leading to a need for intermittent etch steps.

More process control may make problematic processes viable for semiconductor manufacturing. Recently RASIRC introduced a novel dry hydrogen peroxide (H_2O_2) precursor. A novel H_2O_2 mass flow sensor was developed to aid in product characterization. This thermal sensor accurately measures heat of decomposition for minute amounts of H_2O_2:

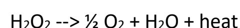

H_2O_2 --> ½ O_2 + H_2O + heat

Our work uses this device to characterize H_2O_2 delivery parameters to:

1. Minimize total precursor mass required
2. Maximize precursor mass delivered in shortest time
3. Limit purge time for increased throughput
4. Minimize nucleation of "Non-growth" surfaces

Quantitative experimental methods are used to understand the effects of:

1. Ampoule headspace pressure
2. Carrier gas flow rate
3. Liquid precursor temperature
4. Precursor pulse time
5. Saturation efficiency of carrier gas with precursor vapor
6. Binary interactions for multicomponent liquids
7. System heat transfer
8. Ampoule design

An ALD simulation manifold was built to re-create typical ALD conditions. An automated test program controls valves and sensors to simulate process recipes. Initial results indicate highly variable mass delivery w.r.t. pressure. An ampoule outlet pressure of 20 torr results in 33.22 mg/min H_2O_2 mass delivery, vs 15.11 mg/min at 70 torr and 1.22 mg/min at 760 torr. Results are less affected by flow rate, where 0.5 slm at 22 torr leads to 33mg/min H_2O_2 vs 1.0 slm at 34 torr leads to 42 mg/min, and 2.0 slm at 57 torr leads to 44 mg/min. Here, increased mass delivery from higher flow rate is offset by a corresponding increase in pressure. In addition, while increased flow rate does not result in significant mass delivery increase for 2 slm, there is a significant decrease in precursor concentration, where the molar ratio of H_2O_2/N_2 is decreased by 70% vs 0.5 slm. Concentration effects are significant to film uniformity in ALD and have ramifications in ASD.

Mass delivery vs pulse time was also examined. Data will be presented for 3s, 1s, 0.3 sec, and 0.1s pulses. Application to process optimization will also be discussed.

9:00am **TF+AP-TuM4 Effect of Co-Reactant on the Atomic Layer Deposition of Copper Oxide***, **Jason Avila**, N. Nepal, V.D. Wheeler,* U.S. Naval Research Laboratory

Atomic layer deposition (ALD) of copper oxide presents a powerful opportunity to grow p-type semiconductor material for a wide variety of applications such as transparent conducting oxide, solar fuels catalysis, and power devices. There are, however, very few ALD processes to facilitate the growth of copper oxide. Cu(II) bis(dmiethylamino-2-propoxide) (Cudmap) has previously been used to grow copper metal using a reducing source such as tertiary butyl hydrazine.[1,2] Cudmap has also been demonstrated to grow Cu_2O using water as a co-reactant, self-reducing from Cu(II) to Cu(I) in the presence of water.[3] This study will examine the effect of ALD co-reactants, ozone and water, on the copper oxidation state of copper oxide films grown using Cudmap.

Copper oxide films were grown in a Veeco Savannah ALD reactor using Cudmap and ozone or water at 150 °C on Si and c-plane sapphire. This is the first experimental demonstration of CuO films using Cudmap and ozone. Using ozone, a growth rate of 0.18 Å/cycle was achieved at 150 °C, far higher than the measured growth rate of 0.04 Å/cycle when using water. Since growth rates are still quite slow, a vapor assisted precursor delivery system for the Cudmap was implemented and its ability to achieve higher growth rates will be presented.

XPS was able to confirm the presence of only the Cu(II) oxidation state with a Cu/O ratio of 1, verifying the deposition of CuO films. For comparison, films grown with water show the presence of only Cu(I) oxidation state and have a nearly stoichiometric with a Cu/O ratio of 2:1, confirming the deposition of Cu_2O films. AFM also indicated uniform, continuous film growth, independent of co-reactant, for films as thin as 2 nm. However, for a similar thickness, CuO films deposited with ozone were rougher than Cu_2O films grown with water. In addition to these initial results, comparison of the optical and electrical properties of the different copper oxide films for p-type semiconductor applications will be presented.

References

(1) Väyrynen, K.; Mizohata, K.; Räisänen, J.; Peeters, D.; Devi, A.; Ritala, M.; Leskelä, M. Chemistry of Materials 2017, 29, 6502.

(2) Kalutarage, L. C.; Clendenning, S. B.; Winter, C. H. Chemistry of Materials 2014, 26, 3731.

(3) Avila, J. R.; Peters, A. W.; Li, Z.; Ortuno, M. A.; Martinson, a. B. F.; Cramer, C. J.; Hupp, J. T.; Farha, O. Dalton Transactions 2017, 46, 5790.

9:20am **TF+AP-TuM5 Electron Enhanced Atomic Layer Deposition (EE-ALD) of Cobalt Films and Development of New Hollow Cathode Plasma Electron Source***, **Zachary Sobell**,* CU Boulder*; A.S. Cavanagh, S.M. George,* University of Colorado at Boulder

Cobalt films were grown with electron enhanced atomic layer deposition (EE-ALD) at room temperature using sequential surface reactions. The Co film growth was performed using sequential cobalt tricarbonyl nitrosyl (CTN, $Co(CO)_3NO$) exposures and low energy (75-175 eV) electrons. A hot filament electron flood gun was used as the electron source. The electrons desorb the CO and NO ligands from CTN on the surface and produce active sites for additional CTN adsorption. The maximum growth rate was 0.5 Å per cycle at an electron energy of 125 eV. Cobalt is important as an advanced interconnect material to replace copper or tungsten. Because the electron flux is normal to the substrate, Co EE-ALD may be used to facilitate bottom-up-fill of trenches and vias.

One difficulty with Co EE-ALD using the electron flood gun is the long cycle times of 540 seconds. Much of this cycle time is consumed protecting the flood gun filament from precursor exposures and the long duration of the electron exposure due to the limited current of the gun. 42% of the cycle time is needed for the warm up and cool down of the filament of the electron flood gun between CTN exposures. Another 44% of the cycle time is required for the electron exposures. An additional 14% of the cycle time is needed to reduce the precursor pressure in the chamber following CTN exposures. The cycle time could be reduced significantly using a more robust and higher flux electron source.

A new hollow cathode plasma electron source (HC-PES) has been developed to reduce the cycle time during EE-ALD. The HC-PES has a >100X increase in electron flux compared with the electron flood gun. The HC-PES also eliminates the warm-up and cool-down time of the filament of the electron flood gun. The electron current from the HC-PES can be switched from nanoamps to miliamps in < 10 ms. The HC-PES is also chemically insensitive and reduces the need for pumping out the chamber following CTN exposures. This presentation will report on the characterization of this new HC-PES and its use for Co EE-ALD.

9:40am **TF+AP-TuM6 Surface Science Studies of GaN Substrates Subjected to Plasma-Assisted Atomic Level Processes***, **Samantha G. Rosenberg,*** American Society for Engineering Education (residing at U.S. Naval Research Laboratory)*; D.J. Pennachio, E.C. Young, Y.H. Chang, H.S. Inbar,* University of California at Santa Barbara*; J.M. Woodward,* U.S. Naval Research Laboratory*; Z.R. Robinson,* SUNY Brockport*; J. Grzeskowiak,* University at Albany - SUNY*; C.A. Ventrice, Jr.,* SUNY Polytechnic Institute*; C.J. Palmstrøm,* University of California at Santa Barbara*; C.R. Eddy, Jr.,* U.S. Naval Research Laboratory

III-N semiconductors are well suited for applications in several important technological areas, including high current, normally-off power switches.[1,2] Such devices require heterostructures not readily achievable by conventional growth methods. Therefore, we have developed a technique adapted from atomic layer deposition (ALD), called plasma-assisted atomic layer epitaxy (ALEp).[2] Using surface science techniques, we strive to develop not only a fundamental understanding of the ALEp growth process but also complimentary atomic level processes (ALPs) that will result in the best preparation method for a pristine GaN starting surface for ALEp.

Here we employ *in-situ* and *in-vacuo* surface science studies of GaN substrate preparation to advance fundamental understanding of the ALEp process. Having optimized our GaN surface preparation (gallium flash off ALP),[3] we conduct *in-vacuo* X-ray photoelectron spectroscopy (XPS), reflection high-energy electron diffraction (RHEED), and scanning tunneling microscopy (STM) studies in the Palmstrøm Lab at UCSB to further refine both our process and our understanding. Preliminary XPS results show that a GFO ALP conducted at 250°C for 12 cycles reduces the oxygen content by 5% but shows no reduction in the carbon content, while a GFO ALP conducted at 400°C for 30 cycles reduces the carbon content by 60% but shows no reduction in the oxygen content. Other XPS results show that our previously reported optimal GFO ALP results in a ~25% reduction of carbon, while a similar 25% reduction of oxygen was achieved using a GFO ALP with or without TMG. We have also conducted comparable temperature program desorption (TPD) and low energy electron diffraction (LEED) experiments at SUNY Polytechnic Institute to correlate structural and chemical changes that occur on GaN surfaces treated with our GFO ALP. TPD shows that NH_3 is released from GaN surfaces not subjected to GFO ALP as it is heated past 150°C, while GFO ALP GaN surfaces show no NH_3 release upon subsequent TPD experiments. Both GaN surfaces, before and after TPD, show an unreconstructed 1x1 diffraction pattern in LEED.

1. N. Nepal, et al., Appl. Phys. Lett. 103, 082110 (2013)

2. C. R. Eddy, Jr, et al., J. Vac. Sci. Technol. A 31(5), 058501 (2013)

3. S. Rosenberg, et. al., J. Vac. Sci. Technol. A 37, 020908 (2019)

11:00am **TF+AP-TuM10 Reaction Pathways in Photolytic CVD of Platinum on Organic Thin Films***, **Bryan G. Salazar,*** University of Texas at Dallas*; H. Liu, L. McElwee-White,* University of Florida*; A.V. Walker,* University of Texas at Dallas

Chemical vapor deposition (CVD) is widely used to deposit materials including metals, oxides, and sulfides. However, CVD is generally unsuitable for use on organic substrates because it often requires high temperatures (> 200 °C). In this work we investigate photolysis as an alternative to thermal activation for CVD of metals on organic thin films. To study the role of precursor chemistry on the Pt CVD process we use three different precursors: $(COD)Pt(CH_3)_2$, $(COD)PtCl(CH_3)$, and $(COD)PtCl_2$. We also investigate the role of substrate functionality on the CVD process using three different self-assembled monolayers (SAMs) with carboxylic acid-, hydroxyl-, and methyl- terminal groups to model organic thin films. Solution-phase photochemistry studies and residual gas analysis indicate that the photolytic activation of $(COD)Pt(CH_3)_2$ and $(COD)PtCl(CH_3)$ occurs via the loss of a methyl radical, while the $(COD)PtCl_2$ occurs via the loss of a chlorine. Subsequently these radicals abstract ligands from the gas phase precursor and the organic surface leading to the formation of methane, chloromethane, chlorine and ethane. Using X-ray photoelectron spectroscopy and time-of-flight secondary ion mass spectrometry (TOF SIMS), we also investigated the reaction pathways involved on the organic surfaces. The data indicates that the deposition is highly dependent on the wavelength of light, the Pt precursor, and the SAM terminal group. Using $(COD)Pt(CH_3)_2$, we observe a small amount of Pt deposition on –OH and –COOH terminated SAM surfaces. In TOF SIMS we observe Pt- and O-containing ions indicating that Pt has inserted into the terminal group. Little, or no, deposition is observed on the $–CH_3$ terminated SAMs. In agreement with previous studies, the data also shows that the neutral polyhapto ligand, COD, is difficult to remove; there are Pt- and COD-containing species present on the surface. Further, the data indicates that there is some SAM decomposition during the deposition. In contrast, for $(COD)PtCl(CH_3)$ and $(COD)PtCl_2$ little, or no, Pt deposition is observed and the data indicates that the SAM layers decompose to form polyaromatic hydrocarbons. The damage appears to be caused by the formation of chlorine radicals during the photolysis, which can penetrate through and react with the SAM. In contrast, the methyl radical is larger leading to less SAM damage because it cannot penetrate through the SAM layer. These studies provide insight into the reaction pathways involved in photolytic CVD and the role of radicals in the subsequent deposition and interaction with organic layers. Such studies therefore aid in the rational design of photolytic CVD on organic substrates.

11:20am **TF+AP-TuM11 Process Development and Mechanism Analysis of Low Temperature ALD TiN with $TiCl_4$/Monomethylhydrazine***, **Taiki Kato**, Z. Ni, M. Matsukuma, H. Nakamura, Y. Ideno, Y. Serizawa,* Tokyo Electron Technology Solutions Limited, Japan

TiN is an important barrier metal for semiconductor devices. Nevertheless, it is difficult to form low-electrical-resistance TiN films at low temperature with existing thermal $TiCl_4/NH_3$ ALD processes. To overcome this difficulty, we tried a new azotizing gas MMH (Monomethylhydrazine: CH_3NHNH_2) instead of NH_3 and achieved low electrical resistance TiN (~1 mW.cm) under 300 deg C deposition temperature. XPS and AFM observations revealed that the film deposited with $TiCl_4$/MMH has smaller Cl concentration and is smoother than the one deposited with $TiCl_4/NH_3$. In this study, we analyzed the $TiCl_4$/MMH ALD reactions to clarify the process improvement mechanism when using MMH. Furthermore, we also analyzed the reactivity of $TiCl_4$ with NH_3 and with novel azotizing gases HZ (Hydrazine: H_2NNH_2) and UDMH (Unsymmetrical dimethylhydrazine: $(CH_3)_2NNH_2$) for future process development.

To analyze surface azotizing reactions, we used density functional theory calculation software, DMol[3]. Surface reaction analysis of $TiCl_2$ termination revealed that the azotizing reactions removed Cl from the substrate by HCl gas generation and MMH was more reactive as an azotizing gas than NH_3. These results explained the experimental phenomenon in which MMH can remove Cl from a TiN film more efficiently than NH_3 and improve the film's roughness and electrical resistance. HZ and UDMH are also more reactive than NH_3 and are candidates for future azotizing gases.

Next, we analyzed gas phase decomposition reactivity of these agents for clarification of ALD process windows. This analysis is conducted by GRRM (Global Reaction Route Mapping) program which can search for reaction paths automatically. Gas decomposition reaction paths search revealed that ALD processes of $TiCl_4$ / HZ, MMH and UDMH are feasible under 400 deg C.

Furthermore, we analyzed azotizing gas chain reactivity for safe conservation estimation. This analysis is calculated by a molecular dynamics simulator, ADF ReaxFF. We inspected the chain reactivity of HZ, MMH, and UDMH densely packed in a tight container at high temperature. Reaction MD simulations showed that UDMH is the safest, followed by MMH then HZ.

In summary, we developed a new thermal TiN ALD process with $TiCl_4$/MMH instead of existing NH_3. Our simulation studies suggest that MMH, HZ and UDMH can remove Cl from TiN film more efficiently than NH_3 and improve the film roughness and the electrical resistance. Other reaction paths analyses show that the novel azotizing agents also have ALD temperature process windows under 400 degC and that the safe conservation trend HZ < MMH < UDMH. These hydrazine-like agents are promising azotizing precursors for low temperature ALD.

11:40am **TF+AP-TuM12 Atomic Layer Deposition of Aluminum, Hafnium and Zirconium Oxyfluoride Films with Tunable Stoichiometry***, **Neha Mahuli**, J.M. Wallas, S.M. George,* University of Colorado at Boulder

Metal oxyfluoride films are chemically robust and resistant to plasma corrosion. This study explored the atomic layer deposition (ALD) of various metal oxyfluorides including aluminum oxyfluoride (AlO_xF_y), hafnium oxyfluoride (HfO_xF_y) and zirconium oxyfluoride (ZrO_xF_y). Different deposition techniques were developed to obtain tunable stoichiometry of

these metal oxyfluoride films. The complicating factor was fluorine/oxygen exchange and the diffusion of fluorine in the oxyfluoride film.

For the metal oxyfluoride deposition, H_2O and HF were used as the oxygen and fluorine sources. $Al(CH_3)_3$ was used as the Al source. Hf and Zr alkylamide precursors were used as the Hf and Zr sources. The metal oxyfluorides were deposited using either (1) the halide-exchange method or (2) the nanolaminate method. These two methods gave rise to tunable stoichiometry from pristine metal oxide to adjustable oxyfluoride to pristine metal fluoride.Both methods were evaluated using *in situ* quartz crystal microbalance (QCM) measurements and *ex situ* X-ray photoelectron spectroscopy (XPS) analysis.

The halide-exchange method is based on the facile exchange of oxygen by fluorine from HFbased on following equation (MO_x + yHFàMF_y + xH_2O). HF exposures after deposition of the metal oxide easily replaced oxygen with fluorine. The fluorine also diffused into the underlying metal oxide film as a function of time and temperature. The compositional control is achieved either using metal oxide layers of various thicknesses or different HF pressures. The rate of fluorine diffusion determined by *in-situ* QCM as well as *ex-situ* XPS was assigned as AlO_xF_y>ZrO_xF_y>HfO_xF_y.

The stoichiometry was also tuned using the nanolaminate method with different numbers of metal oxide ALD and metal fluoride ALD cycles. One supercycle (of ratio n:m) here consists of 'n' layers of metal oxide followed by 'm' layers of metal fluoride. The F:O ratios in the metal oxyfluoride films using this mechanism could be controlled over the full range of compositional ratios. The rate of fluorine diffusion in these systems was also found to be AlO_xF_y>ZrO_xF_y>HfO_xF_y.

12:00pm **TF+AP-TuM13 ALD on Thermally and Chemically Treated Fused Silica and Glass Surfaces***, **Tahereh Gholian Avval**, G. Hodges, V. Carver, M.R. Linford,* Brigham Young University

Silanol (SiOH) and surface hydroxyl (OH) groups strongly affect the absorption behavior of species onto silica (SiO_2) surfaces. The density of hydroxyl (OH) groups on these surfaces are important for initiating and producing conformal thin films by atomic layer deposition (ALD). The combination of chemical and thermal treatments of surfaces in ALD increases insight into their chemistry. Different chemical treatments, including cleaning solutions of industrial importance, affect surface silanol density and consequently subsequent thin film growth by ALD. In this work, we describe the density of hydroxyl (OH) groups on fused silica surfaces and their effect on ALD. In particular, we hydroxylated pieces of fused silica with hydrofluoric acid (HF) and then heat treated it at 200, 500, 700 and 900 °C. The samples then underwent different numbers of ALD cycles to produce thin films of Al_2O_3. As expected, analysis of these surfaces by X-ray photoelectron spectroscopy (XPS) showed that higher temperatures lead to lower aluminum loading/deposition. As a result, heat-treated samples at 900 °C appear to be significantly depleted in surface silanols and lagged behind in thickness compared to the other samples. Other chemical treatments of industrial relevance for silica and glass were also considered in this study, including hydrochloric acid (HCl), tetramethylammonium hydroxide (TMAH), and a detergent. This information is important for ALD deposition of this important material.

Thin Films Division
Room A122-123 - Session TF+EM+MI-TuM
Thin Films for Microelectronics, Photonics, and Optoelectronic Applications

Moderators: John F. Conley, Jr., Oregon State University, Halil Akyildiz, Uludag University, Turkey

8:00am **TF+EM+MI-TuM1 Monolithic Integration of III-Vs on Si for Electronic and Photonic Applications***, P. Staudinger, S. Mauthe, N. Vico Trivino, N. Sousa, C. Convertino, Y. Baumgartner, P. Tiwari, H. Schmid, **Kirsten Moselund**,* IBM Research Zurich, Switzerland **INVITED**

For more than half a century researcher have been working on monolithic integration of III-V materials on Si in order to achieve seamless integration of III-V with Si CMOS. Progress has been made in recent years for example on nanowires [1], aspect ratio trapping (ART) [2] and other selective growth techniques suitable for III-V device integration. Here, I will discuss our work on Template-Assisted Selective Epitaxy (TASE) [3], as a novel epitaxial technique where III-V nanostructures are grown within an oxide template.

In this method we first use a combination of lithography and etching to define our structures in Si. These might be vertical or lateral nanowires, or more exotic shapes such as hall-bars, rings and disks. The Si features are covered by an oxide, which is opened locally, and the Si is partially etched exposing a Si nucleation seed within a hollow oxide cavity (template). The template is subsequently filled by metal-organic chemical vapor deposition (MOCVD) grown III-V material. The geometries of the III-V features are lithographically defined by the shape of the hollow template and to a large extent independent of growth conditions.

The versatility of this technique will be shown through several experimentally demonstrated devices, such as InGaAs MOSFETs [4], heterojunction tunnel FETs [5] and monolithically integrated room temperature optically pumped GaAs [6] and InP microdisk lasers [7].

The quality of the TASE-grown material is assessed by high-resolution scanning transmission electron microscopy (HR-STEM). Devices are free from propagating defects and dislocations, but stacking faults are present as expected for selective epitaxy. By controlling the twinning, we were successful in demonstrating pure wurtzite InP micro-substrates for the first time. We also compare lasing performance to that of devices based on defect-free bonded material, which currently represents the state-of-the-art in terms of photonic integration.

This work received funding from H2020 ERC project PLASMIC (Grant No. 678567), SiLAS (Grant No. 735008) and the SNF (Project 200021_156746).

1. B. Mayer et al., Nano Lett., vol. 16, no. 1, pp. 152–156, 2016.

2. Z. Wang et al., Nat. Photonics, vol. 9, pp. 837–842, 2015.

3. H. Schmid et al. Appl. Phys. Lett. 2015, *106* (23), 233101.

4. L. Czornomaz et al., Symp. VLSI Tech., 2015, pp. T172–T173, 2015.

5. Cutaia, D. et al., Symp. VLSI Tech., pp. 403-407, (2016).

6. S. Wirths et al., ACS Nano 12 (3), pp. 2169, 2018.

7. S. Mauthe et al., submitted to IEEE J. Sel. Top. Quantum Electron. (2019).

8. M. Sousa et al. , 2018 IEEE Nano, DOI: 10.1109/NANO.2018.8626223

9. P. Staudinger et al., Nano Letters, vol. 18 (12), 7856, 2018.

8:40am **TF+EM+MI-TuM3 A Scheme for Better Future Technology by developing AlGaN based Highly Responsive Photosensing Devices***, **Neha Aggarwal**, S. Krishna, L. Goswami, G. Gupta,* CSIR-National Physical Laboratory, India

All species on Earth are affected by UV radiation, from environment-to-humans, industrial-to-residential, defense-to-technology; a number of current & futuristic applications of detecting UV radiation exist. For fabricating UV photodetectors (PDs), III-Nitrides are promising candidates due to their superior material properties such as wide-direct bandgap, high thermal conductivity, good radiation hardness, etc. Also, III-nitrides are intrinsically blind to the visible region of EM spectrum; thus, do not require expensive optical filters unlike existing Si-based UV PDs. Among nitrides, AlGaN based heterostructures have gained huge interest in optoelectronic applications due to their ability to tune the bandgap by modulating Al concentration which allows them to select the cut-off wavelength depending upon the application. Further, to facilitate the integration of AlGaN based devices with existing Si technology, Si substrates were utilized for growing AlGaN heterostructures. However, large lattice mismatch between AlGaN & Si may restrict the growth of defect-free AlGaN, thus a nucleation layer is needed to avoid cracking due to tensile strain. Incorporation of AlN as interlayer reforms the tensile stress in AlGaN layer directly grown on Si into compressive stress which yields the desired crack-free epitaxial structure. In this work, extensive efforts are employed to grow AlN on Si (111) substrate via PAMBE & successfully accomplished best quality AlN with lowest HRXRD FWHM of 15 arcmin having screw dislocation density of 8.5×10^8 cm^{-2}. Then, we have performed hetero-epitaxial growth of $Al_xGa_{1-x}N$ on AlN buffered Si (111) for x in 0.30-0.45 range & discusses the compositional fluctuations associated with changes in buffer growth parameters. As the buffer growth conditions changes, Al composition varies from 0.30-0.45 & FWHM is reduced from 55.6 to 36.4 arcmin. To realize a highly responsive UV PD, uniformly oriented AlGaN nano-islands are grown aimed to efficiently absorb photons due to increased surface-to-volume ratio. On this, we also implemented interdigitated (ID) electrode configuration to collect higher photo-generated charge carriers. The fabricated AlGaN UV PDs having cut-off wavelength of 284 nm yielded a significant enhancement in responsivity from 36.4 to 140.5 A/W at 2 V bias upon changing electrodes from non-ID to ID. However, the developed UV detection device exhibit high response towards UV with responsivity value of 182 mA/W under 2.5 V bias which is better than the commercially available UV detectors. Conclusively, the

highly responsive AlGaN UV-PD on Si displays potential application in the development of advanced optoelectronic devices.

9:00am **TF+EM+MI-TuM4 Correlating the Optical Property Evolution in the Au-Ni Binary Thin Films: From Metastable Solid Solution to Phase Separated Alloy**, ***Robyn Collette***, *Y. Wu, P.D. Rack,* University of Tennessee Knoxville

Surface plasmon resonances can be sustained by metallic nanostructures and have been explored for potential optoelectronic device applications. Metallic alloys provide a pathway to tune the plasmonic response of a material. Additionally, alloying may allow for multifunctional materials to be realized. For example, Au-Ni alloys may combine the magnetic properties of ferromagnetic Ni with the plasmonic properties of Au. However, limited studies have been conducted on Au-Ni alloys for use in plasmonic devices. Since the behavior of the alloys depends on the structure, it is first critical to understand the relationship between the structure and the optical properties of the alloy.

In this study, the optical properties of $Au_{1-x}Ni_x$ alloy thin films are investigated by employing a combinatorial sputtering approach. The dielectric function is measured using spectroscopic ellipsometry and is correlated to the composition (energy dispersive x-ray spectroscopy), and phases present (x-ray diffraction). As-deposited alloys form a metastable solid solution, however, annealed alloys exhibited phase separation into Au-rich and Ni-rich phases due to the large miscibility gap in the Au-Ni material system. The optical properties are then rationalized by modeling the dielectric function of the solid solution alloys with a Drude-Critical Point analytical model. Lastly, the efficacy of the model is demonstrated which shows that the dielectric function of the phase separated alloys may be approximated using a composition-weighted average of two solid solution dielectric functions.

9:20am **TF+EM+MI-TuM5 Integration of Electro-optically Active $BaTiO_3$ and $Ba_xSr_{1-x}TiO_3$ with Buffered Si (001) by Chemical Methods**, ***John G. Ekerdt***, *B.I. Edmondson, E. Lin,* University of Texas at Austin; *S. Kwon,* University of Texas at Dallas; *A.A. Demkov,* University of Texas at Austin; *M.J. Kim,* University of Texas at Dallas

Recent investigations into thin film $BaTiO_3$ (BTO) show it is a promising candidate for on-chip photonic devices due to its large linear electro-optic (EO) coefficient (r > 100-1000 pm/V) relative to more conventional photonic materials such as $LiNbO_3$ (~30 pm/V) or strained Si (~2 pm/V). However, such high coefficients are achieved only by costly and inherently un-scalable physical vapor deposition techniques. In recent studies, we have investigated chemical routes to the integration of electro-optically active BTO thin films with Si, which offer faster and more scalable methods of deposition. Specifically, atomic layer deposition (ALD) of 40 nm BTO films and chemical solution deposition (CSD) of 85 nm BTO films on $SrTiO_3$ (STO) templates on Si (001) prepared by molecular beam epitaxy (MBE) yield epitaxial BTO films with microstructure and defect nature markedly different from physical deposition techniques. Furthermore, we explored CSD of *c*-axis in-plane $Ba_xSr_{1-x}TiO_3$, which is difficult to achieve by physical methods and offers unique insight into the EO behavior of this highly tunable dielectric. X-ray diffraction and scanning transmission electron microscopy confirmed epitaxial, distorted tetragonal structures with a range of structural defects, and electrical and electro-optical measurements showed diminished ferroelectricity and EO response compared to MBE-grown thin films or bulk BTO. ALD-grown films exhibited optical hysteresis with coercivity of ~10 kV/cm, an effective linear EO coefficient of 26 pm/V for 40 nm films, and leakage currents caused by oxygen vacancies. CSD-grown films did not show evidence of ferroelectric hysteresis but maintained EO response with a coefficient of 25 pm/V and had very low leakage current. Past reports of chemical vapor deposited films yielded an EO coefficient of 7 pm/V. These results provide further understanding into the relationship between film structure and linear EO behavior.

9:40am **TF+EM+MI-TuM6 Nonlinear Optical Properties of TiO_2-based ALD Thin Films**, ***Theodosia Gougousi***, *R. Kuis, I. Basaldua, P. Burkins, J.A. Kropp, A.M. Johnson,* University of Maryland, Baltimore County

Nonlinear materials in thin film form are highly desirable for the development of ultrafast all-optical system on-a-chip platforms, optical frequency converters and optical limiting applications. Conventional nonlinear optical (NLO) materials are usually cut from bulk crystals or are liquids that are not suitable for integration with the contemporary semiconductor industry process flow. The third order nonlinear response of ALD TiO_2-based films is investigated using thermally managed Z-scan technique. Some of the as-deposited films exhibit very high nonlinear response which is orders of magnitude higher than conventional nonlinear optical materials such as silica fibers and CS_2. Thermal treatment of the films at 450°C for 3 hours in an oxygen rich atmosphere affects the films' optical properties and results in the loss of the high nonlinear optical response. TiO_2 films deposited by Physical Vapor Deposition (PVD) from a 99.9% TiO_2 target at room temperature are used as control samples and their nonlinear optical response is found below the detection limit of the Z-scan setup. This extraordinary nonlinear optical behavior of the TiO_2 ALD films is linked to the presence of a very small at. % of TiN bonding in the film. We will present detailed characterization of these films by x-ray photoelectron spectroscopy, x-ray diffraction and UV-Vis absorption. The high level of control of the nonlinear index of refraction, n_2, using the deposition process coupled with the ability of ALD to coat nonplanar geometries with atomic level precision and the fact that these processes are CMOS compatible have the potential to provide a breakthrough in optical device design and applications.

11:00am **TF+EM+MI-TuM10 Atomic Layer Deposition on Hexagonal Ge and SiGe Nanowires for Surface Passivation**, ***Willem-Jan Berghuis***, Department of Applied Physics, Eindhoven University of Technology, Postbus 513, 5600 MB Eindhoven, The Netherlands; *W.M.M. Kessels,* Eindhoven University of Technology, The Netherlands, Netherlands; *J.E.M. Haverkort, E.P.A.M. Bakkers, A. Dijkstra, E.M.T. Fadaly, M.A. Verheijen,* Eindhoven University of Technology, The Netherlands

Semiconductor nanowires (NWs) are nanoscale rods with a typical length of a few microns. They are made of materials such as Ge, Si, InP, GaAs. Due to their high aspect ratio, nanowires have a very high surface-to-volume-ratio, which leads to a large influence of the surface on their electronic and optical properties. Surface states facilitate recombination of electron-hole pairs, which reduces the photovoltaic conversion efficiency of NW solar cells [1] or which decreases the output of NW based LEDs or lasers. The surface can also induce space charge regions in the nanowires, which greatly affects their conductivity and which can be critical in for example sensing applications [2]. To reach the desired performance of nanowires in their applications, it is important to control the surface effects.

Atomic layer deposition (ALD) is a deposition technique that allows for preparation of ultrathin films with sub-nanometer thickness control and with an excellent conformality on high aspect ratio structures such as nanowire arrays. For these reasons ALD is a suitable technique to cover nanowires with thin films to control the surface properties.

Recently, nanowires have enabled the growth of Ge and SiGe in the hexagonal diamond crystal phase [3]. In contrast to the cubic crystal phase of these materials, the hexagonal crystal phase leads to a direct bandgap. The latter makes this material an interesting candidate to realize solid-state lasers that are compatible with the current silicon-based electronics. One of the important steps to accomplish this is to reduce the surface recombination losses; i.e. to passivate the surface.

The aim of this work is to explore the surface passivation of these hexagonal Ge and SiGe nanowires. We do so by covering the nanowires with ultrathin films of Al_2O_3 prepared by thermal and plasma-assisted ALD (PE-ALD). Secondly, we cover the wires with a stack of PO_x/Al_2O_3. The latter is a relatively new passivation scheme that has proven very successful for the surface passivation of InP nanowires [4] and Si wafers [5]. The change in photoluminescence (PL) of the nanowires as a function of the ALD films has been studied to assess the surface passivation and the influence of various pre- and post-treatments. Conformal coating of hexagonal Ge nanowires has been realized and we have observed an improvement of the photoluminescence for NWs covered with PE-ALD Al_2O_3 and PO_x/Al_2O_3.

11:20am **TF+EM+MI-TuM11 Oxidation Studies of Silicon Germanium (SiGe) using In-Situ Steam Generated (ISSG) and Plasma Enhanced Atomic Layer Deposited (PEALD) Oxides**, ***Yi Song***, *S. Siddiqui, C. Durfee, A. Pana, J. Li, M. Belyansky, S. Naczas, E.P. Stuckert, L. Jiang, J. Demarest, V. Basker, D. Guo, H. Bu,* IBM Research Division, Albany, NY

SiGe is a versatile material for the semiconductor industry for sub-7 nm node technology development; it can be used as a high mobility channel material in FinFET, and as multiple sacrificial layers to form channel regions in gate all around (GAA) nanosheet device architecture. Understanding SiGe film oxidation is important for matching oxidation rates between SiGe layers with different Ge% in nanosheet applications [1]. In this paper, a study of ISSG (800 °C) and PEALD (room temperature to 300 °C) oxidation processes is performed on blanket $Si_{1-x}Ge_x$ films ranging from x = 0.25 to 0.80. We establish the boundaries of three distinct regions of oxidation behavior for the ISSG process (Region I: $0 < x < 0.5$, Region II: $0.5 < x < 0.67$,

and Region III: $x > 0.67$). Historically, low Ge oxidation has been extensively studied [2-4]. Here, we show for Region I, the ISSG oxidation rate is very small (1.7 nm of oxide growth in 5 sec). The oxidation rate rapidly increases in Region II as x increases, where it reaches a maximum (13.8 nm in 5 sec) at the Region II/Region III boundary, then abruptly drops in Region III as x increases due to complete sublimation of Ge (see Figure 1). The abrupt increase in the ISSG oxidation rate between Regions I and II makes it difficult to match oxide thicknesses for the wide range of Ge% utilized by nanosheet device architecture. Therefore, we studied a lower temperature oxidation process (PEALD) which has a lower oxidation rate. We found that PEALD oxidation rates are unchanged across the Region I/II boundary, even for higher temperatures up to 300 °C as shown in Figure 2. This enables oxide thickness matching for a wide range of Ge%. These results are applicable to the development of various nanotechnologies such as nanosheet and high mobility channel FinFET devices.

11:40am **TF+EM+MI-TuM12 Precision Defect Engineering of Metal/Insulator/Metal (MIM) Diodes using Localized ALD Transition Metal Impurities in Al_2O_3 Tunnel Barriers**, ***Konner Holden***[1], *Y. Qi, J.F. Conley, Jr.,* Oregon State University

Thin film MIM tunnel diodes are receiving increased interest for high-speed applications such as THz detection and rectenna based energy harvesting. Traditionally, current density vs. field (J-$\mathcal{E}$) asymmetry ($f_{asym} = J^-/J^+$) with MIM diodes has been achieved through metal work function differences ($\Delta\Phi_M$). Recently, nanolaminate insulator tunnel barrier MIIM diodes enabled by ALD showed improved f_{asym}, non-linearity, and responsivity at low voltage by step tunneling through the wider bandgap (E_G) insulator to the conduction band of the narrow E_G insulator.[1] *Intrinsic defects* present in narrow E_G insulators were later demonstrated to further improve low $\mathcal{E}$ asymmetry via defect enhanced direct tunneling, when paired with an insulator dominated by tunneling.[2,3] In this work, we investigate the impact of localized *extrinsic defects* by using ALD to intentionally introduce Ni at precise intervals in an Al_2O_3 tunnel barrier.

ALD of Al_2O_3 on TiN was performed at 200 °C using TMA and H_2O. Five samples were prepared in which a 100 cycle Al_2O_3 ALD sequence was interrupted by two cycles (c) of $Ni(^{tBu2}DAD)_2$ and O_3 after 25, 50, 75, and every 25 c of Al_2O_3. As-deposited MIM devices were tested with bias applied to an Al top electrode (Fig. 1).

DC J-$\mathcal{E}$ sweeps of the 100 c device show Fowler-Nordheim tunneling (FNT) at high $\mathcal{E}$, with $f_{asym} > 1$ due to $\Delta\Phi_M \approx 0.2$ eV (Fig. 1). The addition of Ni cycles in all cases leads to an increase in J at low $\mathcal{E}$ vs. the 100 c Al_2O_3 device, suggesting defect related conduction. At high $\mathcal{E}$, however, J of all Ni devices is lower than the 100 c device, suggesting suppression of FNT. The 25/2/75 and 75/2/25 (Al_2O_3/Ni/Al_2O_3) devices show f_{asym} *opposite* of the 100 c device, while the 50/2/50 and 25/(2/25)x3 devices are roughly symmetric (Fig. 1). The greater reduction in J at large negative $\mathcal{E}$, f_{asym} reversal, and reduced J-$\mathcal{E}$ slope for the 25/2/75 and 75/2/25 devices suggest that FNT is suppressed more for emission from the smaller Φ_M electrode (Al) than for TiN. FNT suppression appears greatest for the 75/2/25 device in which Ni is closest to the Al, pointing to an increase in effective barrier height, likely due to negative charge in the Al_2O_3. Capacitance (*C) vs.* $\mathcal{E}$ sweeps (Fig. 2) reveal a positive voltage shift in C_{min} for all Ni devices, consistent with negative charge.

The asymmetry reversal demonstrates the possibility of precision defect engineering of MIM tunnel devices using ALD. An in-depth discussion of J-$\mathcal{E}$ and C-$\mathcal{E}$, temperature-*IV*, frequency-*CV*, other impurities, and annealing will be presented.

1. Alimardani et al., APL 102 143501 (2013).

2. Alimardani et al., JAP 116, 024508 (2014).

3. Alimardani and Conley, Jr., APL 105, 082902 (2014).

12:00pm **TF+EM+MI-TuM13 Improvement in the Electrical Characteristics of a-ZTO based TFTs *via* Microwave Assisted Annealing of Channel Layer**, ***Sunil Uprety***, *M.P. Khanal, H. Lee, S. Sarwar,* Auburn University; *A. Subramanian,* Stony Brook University; *E. Hassani, T.S. Oh, X. Zhang,* Auburn University; *C.Y. Nam,* Brookhaven National Laboratory; *M. Park,* Auburn University

In this research, we have investigated the effect of microwave-assisted annealing of amorphous zinc tin oxide (a-ZTO) channel layers on the electrical characteristics of the thin film transistors (TFTs). A multi-stacked a-ZTO layer was deposited on the oxidized Si wafer using sol-gel process. The precursor solution was prepared by dissolving zinc acetate dihydrate and tin chloride dihydrate into methoxyethanol. The solution was spin coated and calcined in a hot plate at 285°C. The as-calcined a-ZTO wafers were microwave annealed. The microwave (MW) annealing was carried on a commercial microwave oven at different power levels with the sample placed in a kiln which acts as a susceptor. The films remained amorphous even after MW annealing, which was evidenced by X-ray diffraction. The devices were fabricated using the microwave-annealed and as-calcined samples. Hall measurement is being carried out to study the concentration and mobility of charge carries. The performance of the TFTs with as-calcined and MW annealed channel layers were compared. Improvement in the electrical characteristics of the TFTs with MW annealed films were noted. It is believed that the microwave irradiation may promote the enhancement of the electrical characteristics of TFTs. Further research is being pursued to elucidate the role of microwave annealing in improvement of the device performance.

[1] **TFD James Harper Award Finalist**

Atomic Scale Processing Focus Topic
Room B130 - Session AP+EL+MS+PS+SS+TF-TuA

Advancing Metrology and Characterization to enable Atomic Layer Processing

Moderators: Eric A. Joseph, IBM T.J. Watson Research Center, Jessica Kachian, Intel Corporation

2:20pm **AP+EL+MS+PS+SS+TF-TuA1 In Situ Ellipsometry Characterization Of Atomic Layer Processes: A Review*, James Hilfiker*,** *G.K. Pribil, J. VanDerslice,* J.A. Woollam Co., Inc. **INVITED**

Atomic layer processes such as atomic layer deposition (ALD) and atomic layer etch (ALE) provide monolayer-level thin film deposition or etch. Spectroscopic ellipsometry (SE) is ideally suited for the characterization requirements of such very thin layers. In situ SE provides real-time feedback, which is invaluable for establishing new atomic layer processes. In situ SE characterization has been adopted by many researchers due to its versatility. SE measurements are sensitive to deposition or etch at the (sub)monolayer level. The real-time evolution of film thickness provides details on nucleation periods or delays, the growth or etch rates per cycle, and verifies the self-limiting nature of a process. Multiple experiments can be performed within a single run by modifying the process conditions, allowing quick qualification of deposition temperatures, chemical exposure times, plasma influences, and purge times. In this paper, we will review the areas where in situ SE has been applied to both atomic layer deposition and etch.

We will also discuss the applications of in situ SE that benefit from a broad wavelength range. SE is best known for determining film thickness and optical constants. This characterization can be accomplished for many types of materials – dielectrics, semiconductors, organics, and even metals – provided the layer remains semi-transparent. Other material properties affect the optical constants and can be determined via this relationship. In situ SE has been used to estimate the crystal structure, composition, and even conductivity of thin films. We will discuss the advantages and limitations of in situ SE, which in many ways has proven to be an ideal partner for atomic layer processes.

3:00pm **AP+EL+MS+PS+SS+TF-TuA3 Elucidating the Mechanisms for Atomic Layer Growth through In Situ Studies*, Jeffrey Elam,*** Argonne National Laboratory **INVITED**

Atomic Layer Deposition (ALD) provides exquisite control over film thickness and composition and yields excellent conformality over large areas and within nanostructures. These desirable attributes derive from self-limiting surface chemistry, and can disappear if the self-limitation is removed. Understanding the surface chemical reactions, i.e. the ALD mechanism, can provide insight into the limits of self-limitation allowing better control, successful scale up, and the invention of new processes. In situ measurements are very effective for elucidating ALD growth mechanisms. In this presentation, I will describe our recent investigations into the growth mechanisms of ALD nanocomposite films comprised of conducting (e.g. W, Mo and Re) and insulating (e.g. Al_2O_3, ZrO_2 and TiO_2) components using in situ measurements. These ALD nanocomposites have applications in particle detection, energy storage, and solar power. We have performed extensive in situ studies using quartz crystal microbalance (QCM), quadrupole mass spectrometry (QMS), Fourier transform infrared (FTIR) absorption spectroscopy, and current-voltage measurements. These measurements reveal unusual ALD chemistry occurring upon transitioning between the ALD processes for the two components. This results in unique reaction products that affect the properties of the films in beneficial ways. The knowledge gained from our in situ studies of the ALD nanocomposite films has helped us to solve problems encountered when we scaled up the ALD processes to large area substrates.

4:20pm **AP+EL+MS+PS+SS+TF-TuA7 Surface, Interface, or Film: A Discussion of the Metrology of ALD Materials in Semiconductor Applications*, G. Andrew Antonelli,*** *N. Keller,* Nanometrics **INVITED**

Atomic layer deposition, etching, and interface engineering are enabling technologies for semiconductor manufacturing. These processes have led to an explosion in the use of laboratory techniques such as transmission electron microscopy and the need to bring such instruments closer to or into the fab itself. However, there remains a need for in-line, non-destructive, non-contact metrology capable of quickly characterizing and monitoring these extremely thin films on test structures, on product, or in device as these data are the only meaningful method for monitoring of ultimate device performance. Indeed, in cases such as the use of selective deposition or etching, no test vehicle other than the ultimate product may be relevant. A variety of measurement techniques with a focus on x-ray and optical probes as applied to this class of problems will be reviewed. Examples will be provided on relevant logic such as the Gat-All-Around FET and memory devices such as 3D NAND.

5:00pm **AP+EL+MS+PS+SS+TF-TuA9 In Line and Ex Situ Metrology and Characterization to Enable Area Selective Deposition*, Christophe Vallee,*** *M. Bonvalot, B. Pelissier, J-H. Tortai, S. David, S. belahcen, V. Pesce, M. Jaffal, A. Bsiesy,* LTM, Univ. Grenoble Alpes, CEA-LETI, France*; R. Gassilloud, N. Posseme,* CEA-LETI, France*; T. Grehl, P. Bruner,* IONTOF GmbH, Germany*; A. Uedono,* University of Tsukuba, Japan

Innovation in materials, architectures (3D), gap filling technologies, lithography and etch processes are mandatory at every node of CMOS or memory devices. These challenging integration issues can be facilitated by the use of an integration scheme currently being intensively investigated known as area selective deposition (ASD). Criteria for an adequate area selective deposition process are: growth only on specific regions, high throughput compatible with industrial demands, no so-called mushroom profiles into adjacent features as well as no nuclei defectivity on undesired sites. Several routes can be developed to achieve an ASD process with ALD. The one discussed here concerns the deposition/etch approach which takes benefit from an *in situ* etching step inserted in a standard ALD cycle [1]. By incorporation of anisotropic or isotropic etching steps in the ALD process, "surface" selective deposition, as well as topographically selective deposition (TSD) have been obtained [2, 3]. The major current shortcoming of this approach lies in the deep insight which is required regarding elementary atomic-scale reaction mechanisms. Indeed, in the case of an ALD/ALE Area Selective Deposition process, a highly precise control of etching and its selectivity at the atomic scale is needed. Controlling the nature and density of defects induced by etching or passivation steps and understanding their impact on the physical and electrical properties of selectively deposited films are of course also required. Moreover, in order to optimize these processes, an accurate understanding of the underlying reasons why passivation after a low number of ALD cycles, is no more effective. Thus, *in situ* as well as *ex situ* monitoring and metrology are mandatory.

In this presentation, we will discuss how to optimize and understand atomic-scale reaction mechanisms in an ALD/ALE ASD process using combined *in situ* or *ex situ* measurements, such as ellipsometry, XPS, XRR, LEIS, FIB-STEM, and positron annihilation. We will show that when crosslinked, these technics are very effective to perform atomic scale metrology and characterization. As an example, we will discuss F atom localization and density in selectively deposited oxides thanks to a F-based ALE chemistry incorporated in the ALD process. In the case of a topographically selective deposition (TSD) process attempts will be presented to understand ion/surface interactions when low energetic ions are extracted from the plasma of the PEALD reactor both during deposition and plasma-ALE steps.

[1] R. Vallat et al, JVSTA **35** (2017) 01B104

[2] R. Vallat et al, JVSTA **37** (2019) 020918

[3] A. Chacker et al, APL **114** (2019)

5:20pm **AP+EL+MS+PS+SS+TF-TuA10 Recent Progress in Thin Film Conformality Analysis with Microscopic Lateral High-aspect-ratio Test Structures*, Riikka Puurunen,*** Aalto University, Finland **INVITED**

Conformal thin films which cover complex 3D shapes with a film of uniform properties (thickness, composition, etc.) are increasingly demanded applications such as semiconductor devices, microelectromechanical systems, energy conversion/storage and catalysis. Atomic layer deposition (ALD) and its counterpart atomic layer etching (ALE) [together known as atomic layer processing (ALP)], are increasing in usage largely thanks to their known conformal character.

A question that needs to be asked in the R&D of 3D applications using conformal ALD/ALE processes is: how conformal is conformal; is the conformality sufficient to meet the specs? In semicon industry, vertical vias and cross-sectional transmission electron microscopy (TEM) are standardly used for conformality analysis. Recently, microscopic lateral high-aspect-ratio (LHAR) test structures have been developed to improve the conformality analytics capabilities. LHAR structures e.g. enable detailed conformality analysis at arbitrarily high aspect ratios (e.g., >5000:1), where no film can coat the 3D structure fully, thereby exposing the saturation

profile characteristic for the process. This, in turn enables the kinetic analysis of the process and e.g. extraction of the sticking coefficients related to the growth reactions.

This invited talk will address recent progress related to the fabrication and the use of microscopic LHAR conformality test structures. After the breakthrough with the first prototypes (PillarHall LHAR1; Gao et al. 2015, Mattinen et al. 2016; reviewed in Cremers et al., 2019), third and fourth generation prototypes have been developed (PillarHall LHAR3 and LHAR4). This work will review the conformality analysis progress enabled by the microscopic LHAR structures and discuss the benefits and challenges of this approach. Recent published progress includes the conformality modelling by Ylilammi et al. (2018) and experimental extraction of sticking coefficient by Arts et al. (2019). In addition, several other ongoing conformality analysis cases will be presented.

References

Arts, Vandalon, Puurunen, Utriainen, Gao, Kessels, Knoops, J. Vac. Sci. Technol. A 37, 030908 (2019); https://doi.org/10.1116/1.5093620

Cremers, Puurunen, Dendooven, Appl. Phys. Rev. 6, 021302 (2019); https://doi.org/10.1063/1.5060967

Gao, Arpiainen, Puurunen, J. Vac. Sci. Technol. A 33, 010601 (2015); https://doi.org/10.1116/1.4903941

Mattinen, Hämäläinen, Gao, Jalkanen, Mizohata, Räisänen, Puurunen, Ritala, Leskelä, Langmuir, 32, 10559 (2016); http://doi.org/10.1021/acs.langmuir.6b03007

Ylilammi, Ylivaara, Puurunen, J. Appl. Phys. 123, 205301 (2018); https://doi.org/10.1063/1.5028178

6:00pm **AP+EL+MS+PS+SS+TF-TuA12 *In operando*XPS Study on Atomic Layer Etching of Fe and Co Using $Cl_2$and Acetylacetone or Hexafluoroacetylacetone***, **Zijian Wang**, O. Melton, D. Angel, B. Yuan, R.L. Opila,* University of Delaware

Etching of transition metals is one of the major challenges in magnetoresistive random-access memory (MRAM) device fabrication. In this work, atomic layer etching of iron and cobalt surfaces with halogen and an organic molecule was studied. We successfully performed etching of Fe and Co thin films via forming volatile metal complexes at low temperature with cyclic sequential reactions of Cl_2 and acetylacetone (acac) or hexafluoroacetylacetone (hfac) . The etching reaction mechanism of acac and hfac reacting with Clorine-modified Fe and Co surfaces was investigated: the surface was first activated with Cl_2 gas, and subsequently, the top layer of chlorinated metal was removed by reaction with a diketone (acac/hfac). The extent of Cl_2 reaction determines the etching rate of the metal. At substrate temperatures lower than 135°C, acac could remove the chlorinated Fe metal layer from Fe surfaces, but not chlorinated Co from Co surfaces. *In-operando* x-ray photoelectron spectroscopy (XPS) and density functional theory (DFT) simulation shows that the reaction of acac or hfac with Chlorinated Fe or Co surfaces is likely following a complex reaction pathway instead of simple diketone substitution for the metal chloride. Diketone decomposition may play an important role in the etching process.

Electronic Materials and Photonics Division
Room A214 - Session EM+OX+TF-TuA

Nikolaus Dietz Memorial Session: Wide and Ultra-wide Band Gap Materials and Devices

Moderators: Seth King, University of Wisconsin - La Crosse, David Aspnes, North Carolina State University

2:20pm **EM+OX+TF-TuA1 Nitride-Based Semiconducting Materials: A Long Pathway to Advanced Nuclear Detection Capabilities***, **Vincent Woods**, L. Hubbard,* Pacific Northwest National Laboratory*; Z. Sitar,* North Carolina State University*; A.Y. Kozhanov,* Georgia State University **INVITED**

This energetic talk will focus primarily on the development of advanced nitride-based avalanche photodiode devices but will also highlight the many contributions that Nikolaus Dietz made to the field of real-time optical characterization, materials development and advanced growth techniques. Iterative development and advances in growth techniques and characterization have allowed sufficient improvement in materials quality to show demonstrable g ain in Avalanche Photodiode Detector (APD) device structures currently being produced for nuclear detection applications. This contribution will present the structural and optoelectronic properties of GaN/AlGaN heterostructures grown by Metal Organic Chemical Vapor Deposition (MOCVD) on AlN, GaN and sapphire templates/substrates. The target parameters for the materials heterostructures have been modeled for utilization in APD structures operating in the UV region. Optical modeling has improved absorption within the heterojunction as well as maximized light trapping within the device. Electronic modeling has determined the optimal dopant concentrations for maximum impact ionization rate, as well as tolerance to defects and unintentional doping. This application required advances in the defect densities, surface morphology, and interfaces. Surface morphological and structural properties of the GaN/AlGaN heterostructures are analyzed by Atomic Force Microscopy (AFM), and high resolution transmission electron microscopy (TEM). Recent results related to the gain of the final APD device will be presented.

3:20pm **EM+OX+TF-TuA4 Low Temperature Growth of InN by Atomic Layer Epitaxy***, **Charles R. Eddy, Jr.**,* U.S. Naval Research Laboratory*; S.G. Rosenberg, J.M. Woodward,* American Society for Engineering Education (residing at U.S. Naval Research Laboratory)*; K.F. Ludwig,* Boston University*; N. Nepal,* U.S. Naval Research Laboratory

Wurtzite indium nitride (InN) has direct bandgap of about 0.7 eV with large phonon gap and is an attractive semiconductor material for application in various areas, e.g. optical, electrical, optoelectronic, and spintronic device technologies [1]. InN and its alloys with GaN and AlN (III-N) have therefore found application in a variety of technologies such as high power transistors, emitters, detectors, and solar-cells. The relatively high growth temperature of common III-N synthesis techniques has impeded further development and application of the materials due to challenges with miscibility gaps and strain related to thermal expansion mismatch with non-native substrates. To address these challenges, plasma assisted atomic layer epitaxy (PA-ALEp) offers a new approach to low temperature III-N growth and can be used to epitaxially grow InN by using alternative pulses of trimethylindium and nitrogen plasma [2]. We report on development of the PA-ALEp process for InN growth on sapphire and gallium nitride substrates demonstrating the self-limited growth windows as a function of temperature and pulse durations in the process. We benchmark the quality of our films compare to those grown by Dietz et al. by high pressure CVD [3]. The process produces quality, crystalline semiconductor films with properties comparable to those grown by conventional methods at temperatures roughly 2X higher. Beyond that, the PA-ALEp process affords realization of InN containing ternary nitrides with aluminum and gallium that are not possible with conventional growth methods. Further, the unique, non-thermal equilibrium process enables realization of cubic (rock salt) phases on InN. In order to better understand nucleation and growth mechanisms involved in the PA-ALEp process, we employ in situ X-ray scattering methods using synchrotron radiation. We have determined that the growth proceeds largely by a Stranski-Krastinov process on either sapphire or gallium nitride. Further, we have investigated the impact of components of the PA-ALEp cycle on the growth process [4], in particular the plasma pulse time. Here we see that pulse time can affect the nature of nucleation from bimodal nucleation to single mode nucleation to degraded growth as pulse time increases from 15 seconds to 30 seconds. These and other nucleation and growth behaviors will be highlighted.

[1] O. Ambacher, J. Phys. D: Appl. Phys. 31, 2653 (1998).

[2] N. Nepal, et al., Cryst. Growth Design 13, 1485 (2013).

[3] N. Dietz, et al., Phys. Status Solidi B 242, 2985 (2005).

[4] N. Nepal, et al., J. Vac. Sci. Technol. A 37, 020910 (2019).

4:20pm **EM+OX+TF-TuA7 Stochiometry- and Orientation-Dependent Native Point Defects of MOCVD-Grown $ZnGeN_2$ Films***, **Micah Haseman**, D. Ramdin, R. Karim,* The Ohio State University*; D. Jayatunga,* Case Western Reserve University*; H. Zhao,* The Ohio State University*; K. Kash,* Case Western Reserve University*; L.J. Brillson,* The Ohio State University

Heterovalent ternary II-IV-nitrides like $ZnGeN_2$ are attracting increased interest due to their close relation to technologically important III-nitrides such as GaN. Unlike many III-nitrides, the constituents of $ZnGeN_2$ are more earth-abundant with potential for more versatile optoelectronic lattice matching. Essential to II-IV-nitride device application is the control of native point defects and subsequent manipulation of doping and carrier compensation. In many wide band gap binary semiconductors such as GaN or ZnO the most thermodynamically stable defects are cation or anion vacancies whereas stable defects in ternary alloys may include antisites, interstitials, and their complexes as well as H interstitials and complexes. Thus identification of native point defects in $ZnGeN_2$ and other ternaries can be challenging. Using depth-resolved cathodoluminescence spectroscopy (DRCLS), we have observed multiple deep level defects in

MOCVD-grown $ZnGeN_2$ films. Excitation depths obtained via Monte Carlo simulations for varying incident electron beam energies provide depth-resolution for the cathodoluminescence spectra which reveal defects that extend throughout the deposited $ZnGeN_2$ film and are not localized near the free surface nor the film-substrate interface, therefore, unless these defects are unintentional impurities, they must be native point defects. Density functional theory (DFT) predicts the most thermodynamically stable native point defects are in fact Zn_{Ge} and Ge_{Zn} antisites and the n-type nature of the films studied suggests that Zn_{Ge} acceptor is the most favorable defect to form [1]. We used off-stoichiometric films to identify luminescence features due to gap state transitions from specific defects. For Zn-rich films (Zn/Ge = 1.15), we observe an additional defect feature at 2.4 eV corresponding to a near mid-gap state. DFT band structures for $ZnGeN_2$ show that Zn_{Ge} antisites create gap states just below mid-gap, consistent with the n-type Fermi level and with the Zn-rich films. In addition, we observe strong variation in these mid-gap states with Al_2O_3 vs GaN substrate growths as well as an Al_2O_3 orientation dependence. DRCLS's ability to probe electronic structure on a near-nanometer scale enables us to probe defect variations with stoichiometry as growth conditions are varied within the outer tens of nanometers - a nanoscale testbed to identify defects. Identifying and controlling such defects using growth processes can enable advances in $ZnGeN_2$ for next generation electronic device applications. The authors gratefully acknowledge support from NSF grants DMR-18-00130 and DMREF 1533957.

[1]Skachkov et. al. Phys. Rev. B 93, 155202 (2016)

4:40pm **EM+OX+TF-TuA8 Low-temperature Growth of Wide Bandgap Nitride and Oxide Thin Films via Plasma-assisted Atomic Layer Deposition: Influence of rf-plasma Source and Plasma Power***, **Necmi Biyikli**, S. Ilhom, A. Mohammad, D. Shukla,* University of Connecticut

Plasma-assisted atomic layer deposition (PA-ALD) provides an alternative way to grow wide bandgap materials at substantially reduced substrate temperatures (lower than 400°C) when compared to conventional epitaxial growth techniques. While majority of the published literature indicate polycrystalline or amorphous films, recent results depict preferred crystal orientation and even single crystalline nitride and oxide films obtained mainly by delicate substrate in-situ cleaning and careful plasma condition tuning and optimization.

In this talk, we will give an overview of the current state-of-the-art in PA-ALD research on wide and ultra-wide bandgap semiconductors, focusing mainly on wide bandgap III-nitrides (AlN, GaN) and III-oxides (Ga_2O_3). Subsequently, we'll share our recent research efforts on growing crystalline GaN and Ga_2O_3 thin films via PA-ALD utilizing two different plasma sources: inductively coupled plasma (ICP) and capacitively-coupled hollow-cathode plasma (CCHCP) source. We show that for III-nitride films, CCHCP source provides significant improvement in terms of oxygen impurity incorporation and structural film quality, while using a compact vacuum reactor with reduced source-to-substrate distance leads to reduced plasma power levels needed for self-limiting growth saturation curves. Both sources will also be compared in terms of film quality for ultra-wide bandgap Ga_2O_3.

We will present how the choice of plasma source and rf-plasma power affects the structural, chemical, optical, and electrical properties of the grown wide bandgap nitride and oxide films. Detailed x-ray diffraction (XRD), x-ray photoelectron spectroscopy (XPS), transmission electron microscopy (TEM), spectroscopic ellipsometer (SE), Hall measurements (HM) results and analyses will be presented. In addition to these ex-situ characterization results, we'll provide our real-time in-situ ellipsometric film growth monitoring results which provide valuable information about the single chemisorption, ligand-exchange/removal, and nitrogen/oxygen incorporation reactions.

We'll present proof-of-concept electronic and opto-electronic device demonstration based on GaN and Ga2O3 films grown via PA-ALD and will conclude with a future outlook in terms of how to further improve material quality and device performances.

5:00pm **EM+OX+TF-TuA9 Wide Bandgap Dilute Magnetic Semiconductors for Room Temperature Spintronic Applications***, V.G. Saravade, A. Ghods,* Missouri University of Science and Technology, Rolla, MO, USA*; N. Ben Sedrine,* Universidade de Aveiro, Portugal*; C. Zhou, **Ian Ferguson**,* Missouri University of Science and Technology **INVITED**

Wide bandgap dilute magnetic semiconductors (DMS) are promising materials for spintronic applications due to their theoretically predicted and experimentally observed ferromagnetic properties at room temperature (RT) [1]. Spintronics is an enabling technology for devices that will meet current and future computing needs through quantum computing, neuromorphic applications, and artificial intelligence.

Gallium nitride doped with rare earth or transition metals have exhibited ferromagnetic behavior for spintronic applications although its mechanism is still not well understood [1]. In order to build spin-based devices, it is necessary to understand, control, and manipulate their magnetic properties. MOCVD-grown GaGdN shows RT ferromagnetism as evidenced in vibrating sample magnetometry and anomalous Hall Effect (AHE) measurements. Also, AHE measurement showed that the mechanism for the ferromagnetism is intrinsic and likely mediated by free carriers, which is conducive for spintronic applications [2]. However, ferromagnetism is only observed with a Gd precursor, $(TMHD)_3Gd$, which contains oxygen in its organic ligand that appears to be incorporated into the GaGdN. As per density functional theory calculations, oxygen and carbon could introduce deep localized states close to the Fermi level in GaGdN that couple with Gd states to render ferromagnetism [3, 4]. To achieve a clarity and control of this phenomenon, O and C are intentionally implanted into GaGdN grown using oxygen-free Cp_3Gd source. In this case, as-grown GaGdN is not ferromagnetic, but post-implantation with O or C does result in ferromagnetism. X-ray diffraction exhibits low damage and good crystal quality for the implanted GaGdN with peak shifts as compared to the GaGdN before implantation, showing signs of O or C incorporation. Annealing the implanted GaGdN activates the dopant, improves the crystal quality, and shows clear signs of AHE. This indicates that the intrinsic and potentially free carrier-mediated RT ferromagnetism in GaGdN is activated by band states introduced by O or C. A better understanding of the mechanism for RT ferromagnetism will enable using these materials to build spintronic devices, and processors for high speed computing applications.

References

1. M. Kane, S. Gupta and I. Ferguson, "Transition metal and rare earth doping in GaN", Woodhead publishing, 2016

2. V. Saravade, C. Ferguson, A. Ghods, C. Zhou, and I. Ferguson, MRS Adv. 3 (3), p. 159, 2018

3. Z. Liu, X. Yi, J. Wang, J. Kang, A. Melton, Y. Shi, N. Lu, J. Wang, J. Li, and I. Ferguson, Appl. Phys. Lett. 100 (23), 232408, 2012

4. R. Xie, H. Xing, Y. Zeng, Y. Liang, Y. Huang and X. Chen, AIP Adv. 7, 115003, 2017

5:40pm **EM+OX+TF-TuA11 Processing and Characterization of Schottky and Ohmic contacts on (100) β-Ga_2O_3***, **Luke Lyle**, K. Jiang, E. Favela, D. Moody, T. Lin, P. Chung,* Carnegie Mellon University*; K. Das,* North Carolina State University*; Z. Galazka, A. Popp, G. Wagner,* Leibniz-Institut für Kristallzüchtung, Germany*; L.M. Porter,* Carnegie Mellon University

Over the past decade beta-gallium oxide (β-Ga_2O_3) has accrued increased interest due to its ultrawide bandgap of around 4.6 eV, superior figures of merit for numerous electronic and optoelectronic applications, and the ability to produce single-crystal melt-grown substrates. Considering these factors, β-Ga_2O_3 has been primarily pursued for applications as high-power electronics, of which the understanding and development of Schottky and ohmic metal contacts is critical. In this study we characterized the electrical properties of electron-beam evaporated Ni, Mo, Au and other metal Schottky contacts to (100) β-Ga_2O_3 substrates. Prior to deposition of the metals, the Ga_2O_3 surface was cleaned via a 10% HCl solution followed by a clean in boiling 30% H_2O_2 solution at 85°C. Ti/Au was deposited via electron-beam evaporation and annealed at 400°C in an Ar atmosphere for use as ohmic contacts. The ideality factors, barrier heights, and doping densities were calculated from I-V and C-V measurements, which showed excellent agreement in most cases; I-V-T measurements are also planned as a complementary method to determine electrical transport behavior as a function of temperature. From our measurements it was observed that the Schottky barrier heights tended to increase as a function of the metal workfunction. These results are in contrast to our prior measurements of Schottky contacts on (-201) β-Ga_2O_3, which showed little to no correlation between Schottky barrier height and metal workfunction. In this presentation we will compare the electrical behavior of the various metal contacts on (100) β-Ga_2O_3, including the extracted ideality factors (~1.05–1.2) and Schottky barrier heights (~0.9–2 eV). The results will be discussed in the context of important processing conditions, as well as structural, optical, and morphological characteristics of (100) and (-201) -Ga_2O_3 substrates as determined from x-ray diffraction, UV-visible spectroscopy, atomic force microscopy, and other techniques.

6:00pm **EM+OX+TF-TuA12 III-Nitrides: Enabling Applications with Wide to Ultra-Wide Bandgap Materials and Devices***, **Erica Douglas,** A.G. Baca, B.A. Klein, A.A. Allerman, A.M. Armstrong, A. Colon, C.A. Stephenson, R.J. Kaplar,* Sandia National Laboratories

Though now commercially available, wide band gap semiconductors (WBG) such as GaN were pursued due to immense potential for high frequency, light-emission, and power electronic applications. Due to high breakdown voltages, which have been achieved due in part to intrinsic material properties and device engineering, as well as low on-state resistance, wide bandgap semiconductors have found significant success in the commercial application regime. The critical electric field that a material can withstand can be significantly increased through bandgap engineering due to critical field scaling as $E_g^{2.5}$ [1]. Thus, moving from WBG materials with bandgaps ~3 eV, to UWBG with bandgaps above 3.4 eV, alloying GaN with Al can increase the bandgap from 3.4 eV (GaN) to 6.2 eV (AlN) and result in a critical electric field approaching 5X that of GaN.

Since the first AlGaN-channel transistor was reported in 2008 [2], development and progress on devices with increasing Al content has been pursued, including high electron mobility transistors with channel concentrations as high as 85% Al [3]. Though a corollary can be drawn to GaN, there are still a significant number of challenges to overcome for AlGaN-channel devices, ranging from epitaxial growth to fabrication. This talk will describe the latest results at Sandia National Laboratories in AlGaN-channel HEMTs, including recent advances in: enhancement-mode operation, current density, device performance over temperature, and RF operation.

This work was supported by the Laboratory Directed Research and Development program at Sandia National Laboratories. Sandia National Laboratories is a multi-mission laboratory managed and operated by National Technology and Engineering Solutions of Sandia, LLC., a wholly owned subsidiary of Honeywell International, Inc., for the U.S. Department of Energy's National Nuclear Security Administration under contract DE-NA-0003525.

[1] R. J. Kaplar, *et al.*, *ECS J. Solid State Science and Technology*, vol. 6, p. Q3061 (2017).

[2] T. Nanjo, *et al.*, *Appl. Phys. Lett.***92**, 263502 (2008).

[3] A.G. Baca, *et al.,Appl. Phys. Lett.***109**, 033509 (2016).

Complex Oxides: Fundamental Properties and Applications Focus Topic
Room A220-221 - Session OX+EM+HC+MI+NS+SS+TF-TuA

Complex Oxides: Catalysis, Dielectric Properties and Memory Applications

Moderators: Alexander Demkov, University of Texas at Austin, Jeffry Kelber, University of North Texas

2:20pm **OX+EM+HC+MI+NS+SS+TF-TuA1 Novel Multiferroic and Ferroelectric Ferrite Thin Films***, **Peter A. Dowben,** C. Binek, X. Xu,* University of Nebraska-Lincoln **INVITED**

Ferroelectricity and ferromagnetism are foundational to numerous technologies, yet the combination of ferroelectricity and ferromagnetism, namely multiferroicity, may be even more desirable. Multiferroic materials are believed to be a route to voltage controlled spintronic devices. Yet very few single phase materials are known to be ferroelectric and ferromagnetic at the same time, i.e. multiferroic. Even fewer materials are fewer materials are magneto-electric, that is to say materials with magneto-electric coupling, i.e. voltage control of magnetization, but without separate order parameters for magnetism (or antiferromagnetism) and ferroelectricity. This talk will review the electronic structure of the tri-rutile magneto-electric antiferromagnets, like Fe_2TeO_6, as well as rare earth ferrites like $ReFeO_3$ (Re = rare earth) stabilized in the hexagonal phase. Both types of materials are frequently antiferromagnetic, and, in principle, both can exhibit magneto-electric coupling. The surface termination affects the measured spin polarization of the surface and the interface with other materials. This will have a significant influence on the voltage control of magnetization. We have investigated the structural and electronic properties at the surface of these more unusual multiferroic materials using angle-resolved x-ray photoemission spectroscopy (ARXPS), complemented by x-ray diffraction (XRD), x-ray photoemission electron microscopy (X-PEEM), and X-ray circular dichroism. We find that the low local symmetry, especially at surfaces, will split the electronic states, via spin–orbit coupling. In some cases, the result is a net spin polarization at the surface, under electric field cooling. Because of the strongly preferential surface termination of these types of materials, the boundary polarization is roughness insensitive, in some cases making spintronic device applications plausible.

3:00pm **OX+EM+HC+MI+NS+SS+TF-TuA3 Potential Applications and Challenges for Complex Oxides in Advanced Memory and Computing Applications***, **Sebastian Engelmann,** T. Ando, V. Narayanan,* IBM T.J. Watson Research Center **INVITED**

As the semiconductor industry continues to push for and develop higher performance computing systems, there is also a growing trend of redeveloping or optimizing fundamental computing approaches to be more energy efficient. The development of hardware for novel AI systems is no exception. New integration schemes, novel materials, multi-component materials or even nanoscale materials and the ability to integrate all of these approaches together becomes the compounded challenge. Deposition and etch technologies that offer differentiating solutions to these issues therefore need to meet somewhat conflicting demands, such as low damage processing as well as high rate processing beside many other issues.

Novel thin films, thin film laminates and alloys promising unprecedented performance are very interesting candidates to enable such computing paradigm shifts. In particular the class of complex oxides is a very interesting area of research as they offer new phenomena such as ferroelectricity, ferromagnetism or high temperature conductivity. While new phenomena are being discovered, unraveling the fundamental physics behind these properties is a critical element for an industrial exploitation of these properties.

In addition, these new and complex materials are growing the need for the ultimate process solution: atomic layer precision processing. Atomic layer etching is a promising path to answer the processing demands of new devices at the Angstrom scale. Self-limiting reactions, discrete reaction and activation steps or extremely low ion energy plasmas are some of the pathways being pursued for precise material removal control and maintaining the original film performance. Depending on the nature of the material, the etch response may be either too much or not enough chemical modifications of the material. Resulting modifications of the films is an important variable to consider in the readiness of material systems. In particular synergy to deposition approaches such as atomic layer deposition has been proposed as a solution, but more work is needed.

4:20pm **OX+EM+HC+MI+NS+SS+TF-TuA7 Epitaxial Design of Complex Oxides for Catalysis and Electrocatalysis***, **Yingge Du,*** Pacific Northwest National Laboratory **INVITED**

Predictive synthesis of highly active and cost-effective catalysts and electrocatalysts for energy conversion and storage is critical for leveraging intermittently available energy sources. Transition metal oxides with perovskite (ABO3) and perovskite-related structures (e.g., Brownmillerite and Ruddlesden-Popper) have been identified as robust catalysts with high oxygen reduction reaction (ORR) and/or oxygen evolution reaction (OER) activities that rival the performance of noble metals and their compounds. The study of perovskites as epitaxial thin films enables measurement of their intrinsic catalytic activity, deconvolved from the effects of surface roughness and polycrystalline defects (e.g., grain boundaries and edges between facets). In addition, epitaxial growth facilitates accurate control over the composition, crystallographic orientation, and strain in thin films.

In this talk, our recent efforts in the design of epitaxial complex oxides for catalysis and electrocatalysis will be highlighted. Using $LaNiO_3$, a bi-functional electrocatalyst, as an example, I will show how isovalent substitution, aliovalent substitution, and interfacial strain can be used to tune the structural, electronic, and optical properties of the resultant films, and how these observed changes correlate with their (electro)catalytic performance. The use of complex oxide thin films as support or anti-corrosion layers during catalytic reactions will also be discussed.

5:20pm **OX+EM+HC+MI+NS+SS+TF-TuA10 Vanadia/Tungsten Oxide on Anatase TiO2(101): a Model Catalyst Study by STM and XPS***, **Tao Xu,** J.V. Lauritsen, K.C. Adamsen,* Aarhus University, Denmark*; S. Wendt,* iNANO, Aarhus University, Denmark

Nitrogen oxides (NOX) from flue gas are in concern as major sources of air pollution. Increasingly stricter NOX emission control policies (e.g. Euro VI) demand innovation and better performance of NOX reduction technology. The Selective Catalytic Reduction (SCR) of NOX by vanadia supported on anatase titania, with tungsten oxide (WO3) as promoter, has been widely

used for this service and attracted much research attention. However, many aspects of the SCR catalysis process remain poorly understood at the atomic level. Particularly, the synergistic effect of tungsten oxide and vanadia remain elusive in literature, despite intensive RAMAN and infrared spectroscopy studies.

In this work, we use mineral a-TiO2 single crystals exposing the (101) facets as the model surface and deposit V2O5 and WO3 in our ultrahigh vacuum chamber (UHV) chamber by e-beam evaporation in oxygen. Combining Scanning Tunneling Microscope (STM) and X-ray photon-electron Spectroscopy (XPS), we systematically investigated the morphology and oxidation state changes of the model catalyst upon heating and reactant adsorption.

The STM results illustrate the distribution of V2O5 and WO3 on anatase TiO2(101) at the atomic level. It is found that both species are highly dispersed in the sub-monolayer region. For the deposition of surface oxide species, we explored different methods to achieve the highest oxidation state of vanadium (5+) and tungsten (6+). The thermal stability of the as-deposited V2O5 and WO3 are investigated by XPS and STM systematically. We found that when V2O5 and WO3 co-exist on the a- TiO2 surface the stability of V2O5 is improved. This work provides atomic level understanding on the V2O5/WO3/TiO2 SCR catalyst and new insights into the synergistic interactions between vanadia and tungsten oxide on the a-TiO2 surface.

5:40pm **OX+EM+HC+MI+NS+SS+TF-TuA11 Observation of Memory Effect and Fractal Surface in $SrRuO_3$ Epitaxial Thin Films**, ***Ratnakar Palai,*** University of Puerto Rico; *H. Huhtinen,* University of Turku, Finland

Integration of multifunctional oxide materials (ferroelectrics and multiferroics) into silicon technology is of great technological and scientific interests. The current interest in functional oxides is largely based on engineered epitaxial thin films because of their superior properties compared to the bulk and polycrystalline thin films and their technological applications in dynamic random access memories, magnetic recording, spintronics, and sensors. Most of these applications require bottom and top electrodes to exploit the electronic properties of the functional materials.

SrRuO3 (SRO) has been found to be very useful for electrodes and junctions in microelectronic devices because of its good electrical and thermal conductivities, better surface stability, and high resistance to chemical corrosion, which could minimize interface electrochemical reactions, charge injection in oxide, and other detrimental processes, thus improving retention, fatigue resistance, and imprint. It also has good work function to produce the required large Schottky barrier on most ferroelectric oxide capacitors.

The bulk SRO exhibits several useful properties, such as extraordinary Hall effect, strong magnetocrystalline anisotropy, itinerant ferromagnetism, and spin-glass behavior. Spin-glass materials are currently frontier field of research and the most complex kind of condensed state of matter encountered so far in solid-state physics. Despite of the enormous importance of spin-glass models in neural networks, our knowledge of the underlying mechanistic processes involved is extremely limited. Although memory effect has been reported in bulk SRO, to our knowledge, the behavior is not well understood and there was no such report in thin films.

In this work, we report on the observation of memory effect and strong magnetic anisotropy in extremely smooth 1–3 Å roughness epitaxial (110) and (010) SrRuO3 thin films. The observation of non-zero imaginary susceptibility and frequency dependent cusp at freezing temperatures confirms the spin-glass behavior, which agrees well with the dc magnetization measurement. The origin of memory effect can be attributed to the magnetic frustration and random interaction, which is affected by dynamics of cooling and will be discussed in details.

6:00pm **OX+EM+HC+MI+NS+SS+TF-TuA12 *In situ* Auger Electron Spectroscopy of Complex Oxide Thin Film Surfaces Grown by Pulsed Laser Deposition**, ***Thomas Orvis,*** *M. Surendran, Y. Liu, A. Cunniff, J. Ravichandran,* University of Southern California

Complex oxides can enhance the functionality of electronic and photonic devices by supplementing them with interesting properties such as ferroelectricity, superconductivity, and magnetoresistivity. Furthermore, low dimensionality in these materials can result in additional useful properties, inspiring the continued study of complex oxides in thin film form. However, the deposition of these materials is typically governed by notoriously complex growth mechanisms, revealing the need for *in situ* probes to observe and understand their precise nature. To this end, we report the *in situ* observation of chemical composition of complex oxide thin film surfaces with Auger electron microscopy during growth by pulsed laser deposition. Our implementation of real-time monitoring techniques for complex oxide thin films sheds an important light on the intricacies of the relationships between processing conditions and resulting composition.

Thin Films Division
Room A124-125 - Session TF+PS-TuA
Epitaxial Thin Films

Moderator: Robert Grubbs, Micron Technology

2:40pm **TF+PS-TuA2 Van der Waals Layer Promoted Heteroepitaxy in Sputter-deposited Transition-metal Carbide and Sulfide Thin Films**, ***Koichi Tanaka***[1], *P. Arias, M.E. Liao, Y. Wang, H. Zaid, A. Aleman,* University of California, Los Angeles; *K. Hojo,* Nagoya University, Japan; *A. Deshpande, M.S. Goorsky, S. Kodambaka,* University of California, Los Angeles

Over the past decade, two-dimensional (2D) layered materials such as graphene, MoS_2, etc., have attracted considerable attention for a variety of applications, primarily in nanoelectronics and optoelectronics. An exciting and relatively little explored application of these van der Waals (vdW) layered materials is their use as templates for crystal growth. In the recent years, vdW layers present at the substrate-film interface have been shown to promote 'remote epitaxy', by relaying the epitaxial registry between the film and the substrate.

Here, we demonstrate that the crystallinity of sputter-deposited thin films can be significantly improved using vdW layered materials as buffer layers on growth substrates. Using 2D hexagonal boron nitride (hBN, a = 0.250 nm and c = 0.667 nm) as the buffer layer, we grow hexagonal-MoS_2 (a = 0.315 nm and c = 1.23 nm), trigonal-structured Ta_2C (a = 0.310 nm and c = 0.494 nm), and NaCl-structured TaC (a = 0.446 nm) of desired thickness on Al_2O_3(0001) substrates via ultra-high vacuum direct current magnetron sputtering of Mo and TaC targets respectively, in Ar/C_2H_4 and Ar/H_2S gas mixtures. hBN layers are deposited in the same system via pyrolytic cracking of borazine (~600 L) onto the substrates at prior to the growth of the thin films. The as-deposited films are characterized using a combination of *in situ* using Auger electron spectroscopy and low-energy electron diffraction and *ex situ* X-ray diffraction (XRD), X-ray photoelectron and Raman spectroscopies, and transmission electron microscopy (TEM) based techniques.

We find notable differences in the layers deposited on hBN-covered Al_2O_3(0001) compared to those grown on bare substrates: significantly stronger 0002 (or 111 in case of TaC) reflection intensities and observation of Laue oscillations in ω-2θ XRD scans and higher intensity of MoS_2 characteristic peaks in Raman spectrum. Furthermore, we show that inserting hBN layers at regular intervals results in highly-0002-oriented growth and suppression of polycrystallinity in thicker Ta_2C films. Our results indicate that hBN layers enhance the crystallinity, irrespective of the crystal structure, of sputter-deposited thin films.

3:00pm **TF+PS-TuA3 Molecular Beam Epitaxy Applied to Tensile-Strained Quantum Dots for Quantum Optics and Band-Structure Engineering**, ***Paul Simmonds,*** Boise State University **INVITED**

Since the early 1990s, solid-state self-assembled quantum dots (QDs) have been the subject of intensive research for devices and technologies ranging from high-stability lasers, to intermediate band solar cells. Driven by compressive strain, semiconductor QDs form spontaneously on the (001) surfaces of both III-V and group IV materials during growth by molecular beam epitaxy (MBE). But several years ago, I became interested in the question of why QD self-assembly seemed to be limited to materials with this specific combination of compressive strain, and a (001) surface orientation. For example, why could we not grow QDs under *tensile* rather than compressive strain or on non-(001) surfaces, especially since QDs with these characteristics are predicted to be highly desirable for certain applications. The low fine-structure splitting of (111) QDs should make them ideal entangled photon sources; tensile-strained QDs would have dramatically reduced semiconductor band gaps, with implications for infrared optoelectronics and nanoscale band structure engineering.

The first step towards answering this question was to understand how the competition between plastic and elastic strain relief mechanisms made it enormously challenging to synthesize non-(001) or tensile-strained QDs without the formation of crystallographic defects. The outcome of this

[1] **National Student Award Finalist**

analysis was the discovery of a robust new approach to QD self-assembly based on MBE that overcomes these difficulties, and enables the reliable, controllable growth of defect-free, tensile-strained QDs on (111) and (110) surfaces.

I will describe the model upon which tensile-strained QD self-assembly is founded, and then discuss the application of this novel growth mode to several different material systems. I will present data confirming that the (111)-oriented QDs we can now grow do indeed show promise as entangled photon sources. I will highlight the possibilities for band structure engineering that are now available with tensile-strained QDs, using the example of transforming germanium into a direct band gap semiconductor.

In summary, I hope to demonstrate that tensile-strained self-assembly represents a powerful new tool for heterogeneous materials integration, and nanomaterial development.

5:00pm **TF+PS-TuA9 Low-temperature Homoepitaxial Growth of N-type Superlattices for Ultrastable, Ultrafast X-Ray and Charged Particle Detectors***, **April Jewell**,* Jet Propulsion Laboratory, California Institute of Technology*; M.E. Hoenk,* Jet Propulsion Laboratory*; Q. Looker, M.O. Sanchez, B.D. Tierney,* Sandia National Laboratories*; A.G. Carver,* Jet Propulsion Laboratory*; S. Nikzad,* Jet Propulsion Laboratory, California Institute of Technology

We present a low-temperature process for the homoepitaxial growth of antimony superlattices in silicon. The all low temperature superlattice doping process is compatible as a post-fabrication step for device passivation. We have used low-temperature molecular beam epitaxy (MBE) to embed atomically thin (2D), highly concentrated layers of dopant atoms within nanometers of the surface. This process allows for dopant densities on the order of 10^{13}-10^{14} cm^{-2} (10^{20}-10^{21} cm^{-3}); higher than can be achieved with three-dimensional (3D) doping techniques. This effort builds on our prior work with n-type delta doping; we have optimized our growth processes to achieve delta layers with sharp dopant profiles. By transitioning from a standard effusion cell to a valved cracker cell for antimony evaporation, we have achieved carrier densities approaching 10^{21} cm^{-3} with peak distribution at ~10 Å FWHM for single delta layers. We will discuss details related to growth optimization, and show results from in situ monitoring by electron diffraction. We will also report on elemental and electrical characterization of our films.

The performance of our low-temperature 2D-doping processes has been validated by applying both p-type and n-type superlattice-doping to fully depleted photodiodes. The superlattice-doped devices show significantly higher responsivity than the equivalent ion-implanted devices. Additionally, when exposed to pulsed X-rays the superlattice-doped devices exhibit fast response and recovery times required for use in pulsed power experiments.

5:20pm **TF+PS-TuA10 Epitaxial Growth of Ultrathin Molybedenum Nitrides on Ru(0001) and Ag(100)***, **Asim Khaniya**, M. Sajid, A. Kara, W.E. Kaden,* University of Central Florida

Molybdenum-nitrides are known to possess interesting mechanical, electronic, and catalytic properties. For example, (i) hexagonal δ-MoN exhibits mechanical elasticity and hardness values comparable to cubic BN and diamond, (ii) both hexaganol and cubic phases of molybdeumn nitrides are known to be superconducting, and (iii) mixed-phase structures have been shown to outperform commercial hydrotreatment catalysts for selective nitrogen removal from heterocyclic organic feedstocks. To better understand these properties, many groups have worked to create improved recipes to grow different phase-pure crystallographic phases of the material. To-date, the most successful procedures have leveraged epitaxy to improve long-range bulk order, but have lacked the well-defined, planar terminations suitable for controlled surface-science investigations. To establish such samples, our group has opted to use low energy nitrogen ions in tandem with molybdenum physical vapor deposition to grow and characterize molybdenum-nitride films on Ru(0001) and Ag(100) supports, which have been chosen to template the growth of hexaganol and cubic phases of the nitride. At the time of this abstract submission, we have succeeded in the growth of a δ-MoN-like film that appears to grow layer-by-layer and in registry with the Ru(0001) support, and are now in the early stages of repeating the process to create γ-Mo_2N on Ag via an analogous process. This talk will focus on the interesting aspects of these materials (particularly those relevant to catalysis), our approach to film preparation, and a thorough analysis of the physical properties of the resultant films and growth modes via: XPS, LEED, He^+ Ion Scattering Spectroscopy, STM, and DFT.

5:40pm **TF+PS-TuA11 Using Time and Temperature of the Purge Step to Control Crystallinity, Phase Assemblage, and Epitaxy in Atomic Layer Deposited (ALD) Thin Films***, **Mark Losego**, B.D. Piercy, R.J. Petrie,* Georgia Institute of Technology

The purge step between precursor and co-reactant doses in an atomic layer deposition (ALD) process is often viewed as a process liability. The goal for most manufacturing processes is to make this purge step as short as possible without disrupting the quintessential self-limited growth of ALD. In our lab, we have instead viewed this purge step as a potential opportunity to influence the crystallinity and phase assemblage of our materials. In actuality, each of these purge steps are an opportunity to allow surface diffusion to rapidly reform the film's microstructure before the next layer is deposited. Throughout the literature are interesting, but often conflicting reports of how ALD films crystallize with temperature and thickness. In our recent work, we have asked some simple questions, like how does the onset of such crystallinity change with purge time? We have found, for example, that the onset of anatase formation in the $TiCl_4$-H_2O ALD system can be reduced by more than 40 °C by simply extending the purge time between each cycle. While potentially time intensive, these results have implications for depositing crystalline materials on temperature-sensitive substrates, like polymers. We also find that often an initial seeding of the crystallinity can lead to accelerated growth of crystalline phases with subsequent cycles. In a second paradigm to be discussed, we have introduced a high-temperature pulsed heating source to an ALD system to intentionally crystallize materials and drive epitaxial growth. As proof-of-concept, we have studied epitaxial growth of ZnO on c-plane sapphire using a diethylzinc (DEZ) / water chemistry. DEZ is known to decompose above about 180˚C, and the DEZ-H_2O system cannot be grown epitaxially on c-sapphire with traditional thermal ALD approaches. Here, we show that heating pulses up to 900˚C can be used to drive epitaxy. Interestingly, we find that a template layer of only 20 pulsed heating ALD cycles is sufficient to template ZnO epitaxy with subsequent low temperature ALD growth (180 °C) to film thicknesses of up to 100 nm.

6:00pm **TF+PS-TuA12 The Role of Template Layers in Heteroepitaxial ALD Growth of Crystalline La_2O_3 on GaN(0001)***, **Pei-Yu Chen**, T. Hadamek,* University of Texas at Austin*; S. Kwon,* University of Texas at Dallas*; F. Al-Quaiti, A. Posadas,* University of Texas at Austin*; M.J. Kim,* University of Texas at Dallas*; A.A. Demkov, J.G. Ekerdt,* University of Texas at Austin

The high switching frequency, operating temperatures and voltages make GaN the material of choice for higher power applications and instrumental to reducing power consumption. In many of these applications, there is a need for a high quality gate dielectric. Lanthanum sesquioxide, La_2O_3, is one of the promising gate insulator candidates. In this work, we compare La_2O_3 thin films grown by atomic layer deposition (ALD) and molecular beam epitaxy (MBE), and explore the formation of ALD-La_2O_3 films on GaN(0001). An island growth mode (Volmer-Weber growth) was observed when La_2O_3 films were deposited directly on GaN(0001) at 250 °C by ALD using tris(N,N'-diisopropylformamidinato)-lanthanum as the precursor and H_2O as the co-reactant. Only with use of a thin template layer, 2 nm-thick hexagonal La_2O_3 grown by MBE or 3 nm-thick cubic Er_2O_3 grown by ALD, can a 2-dimensional ALD-La_2O_3 thin film be formed. The 2-dimensional ALD-La_2O_3 growth on templated-GaN(0001) was confirmed by RHEED and AFM. The macrostructure and microstructure of ALD-La_2O_3 films were verified with XRD, STEM, and atomic structure modeling. The ALD-La_2O_3 film retains a cubic structure on ALD-Er_2O_3 templated-GaN(0001) while it transforms from the cubic phase to mixture of cubic and hexagonal phases on MBE-La_2O_3 templated-GaN(0001) when the film is thicker than 15 nm. Hexagonal La_2O_3 is more thermodynamically stable than cubic bixbyite La_2O_3; the stabilization of cubic ALD-La_2O_3 on ALD-Er_2O_3 templated-GaN(0001) can be attributed to the use of the cubic ALD-Er_2O_3 template and relatively low growth temperature. Analogies are presented for the In_2O_3 system, which has similar cubic bixbyite and hexagonal structures as La_2O_3, except the phases are reversed in In_2O_3. We calculate the surface energy of hexagonal In_2O_3 and compare the result with reported cubic In_2O_3 values to explore the relative contribution of bulk and surface energies in stabilizing the structure of thin crystalline films. Stabilization of thin cubic ALD-La_2O_3 on hexagonal MBE-La_2O_3 templated-GaN(0001) is attributed to likely surface energy differences between cubic and hexagonal La_2O_3.

Thin Films Division
Room A122-123 - Session TF-TuA
Emerging Applications for Thin Films

Moderators: Emily McGuinness, Georgia Institute of Technology, Jesse Jur, North Carolina State University

2:20pm **TF-TuA1 Flexible Hybrid Electronics Process Maturation using Printed Inks*, John D. Williams,*** The Boeing Company **INVITED**

Flexible hybrid electronics (FHE) are at the intersection of additive electronics and printed electronics. This is achieved through the utilization of additive methods on flexible and/or stretchable substrates. FHE leverages the low manufacturing cost of additive manufacturing due to fast processing time and low material waste. There are many applications that benefit from small low-cost sensor arrays and wireless networks, including new data collection devices on both manufacturing floors and aerospace systems to enable big data analytic capabilities.

In 2016, Boeing joined the NextFlex Manufacturing Innovation Institute established by U.S. Department of Defense Manufacturing Technology Program to support industry-wide improvements in the manufacturing readiness level (MRL) of Flexible Hybrid Electronics. Boeing's Radio Frequency Manufacturing and Sensing Technologies (RFMaST) laboratory in Huntsville, AL is working in concert with a dozen companies and university partners on seven different NextFlex efforts to improve manufacturing processes and produce industrially relevant technology demonstrators.

The results to date, document an MRL 6 or higher capability for flexible hybrid electronics technologies. Current and previous work has improved the design interface for the nScrypt additive liquid dispense tool, and pushed the industrial supply chain for thinned Integrated Circuits. Additionally, we have documented repeatable printing processes multilayer passive elements on 2D and 3D surfaces, generated Flexible Antenna Array Technologies (FAAT) for GHz frequency applications, and developed in-situ monitoring approach for FHE print processes. Most recently, Boeing and its partners have shown a demonstrator for the Condition Monitoring Sensor Array (CMSA) project that combines a flexible battery, Bluetooth Low Energy, edge processing, and four sensors onto a single flex circuit. Over the next two years, our team will widen these efforts to include UAV flight applications, composite health monitoring, multilayer flexible PCBs and dozens of other sensing applications.

Coupling these achievements with materials characterization, in-situ process monitoring, and large area digital printing will provide Boeing and the US industrial base with MRL 7 small-scale production capabilities for the next generation of electronic sensors. Today, our company has the manufacturing readiness to vertically implement new FHE products and help establish the supply chain required for utilization in commercial and military products.

3:00pm **TF-TuA3 Large-Area Atmospheric Pressure Spatial ALD for Flexible OLED Display Applications***, C. Frijters, J. Smeltink,* ***Huib Heezen****, P. Poodt,* SALDtech B.V., Netherlands

Atmospheric pressure Spatial ALD (sALD) is able to deliver high deposition rates while maintaining the advantages of conventional ALD, such as low defect density, high conformality and thickness uniformity. First industrial applications of Spatial ALD include passivation of c-Si solar cells and roll-to-roll manufacturing of flexible barrier foils. An emerging application for Spatial ALD is flat panel (OLED) displays. Examples include semiconducting and dielectric layers for use in thin-film transistors, and thin-film encapsulation for flexible OLED displays. As today's displays are fabricated using glass panels in the order of several square meters, a remaining challenge is the development of large-area Spatial ALD deposition technology that is able to combine high throughput with uniform performance across very large areas.

We are developing large-area Spatial ALD technology, and as a first step between the lab and the display fab, we have installed a large area Spatial ALD sheet-to-sheet tool which can handle up to 400x325 mm^2 sized substrates. With this tool we are able to deposit uniform films across a deposition width of 400 mm. The whole tool is operated under an atmospheric pressure but inert N_2 environment. The tool can be used to deposit a variety of materials using both thermal and plasma-enhanced Spatial ALD.

We will present the basic deposition performance of the tool in terms of thickness- and compositional uniformity. Large-area thickness non-uniformities of less than 1% are achieved for several oxide materials. Next, we will focus on two display-related applications: thin-film encapsulation of OLED devices, and high mobility InZnO and InGaZnO semiconductors for thin-film transistors. We will explain the requirements, the deposition process and the performance of the deposited films. Finally, the challenges in up-scaling Spatial ALD to plate sizes of 1.5 m and beyond will be discussed.

3:20pm **TF-TuA4 Printed Polymer Heat Sinks for High-Power, Flexible Electronics*, Katherine Burzynski,*** University of Dayton*; N.R. Glavin, E.M. Heckman,* Air Force Research Laboratory*; C. Muratore,* University of Dayton

Consumers and military personnel alike are demanding ubiquitous electronic devices which require enhanced flexibility and conformality of electronic materials and packaging, while maintaining device performance. Whether it be high-power devices for faster data speeds, such as fifth generation (5G) wireless communication technology or wearable sensors to facilitate the Internet of Things (IoT), the age of flexible, high performance electronic devices has begun. Managing the heat from flexible electronics is a fundamental challenge. Even on rigid substrates with significantly higher thermal conductivity than polymeric and other flexible substrates, the full potential of semiconducting materials is often thermally limited. The flexible gallium nitride (GaN) high electron mobility transistors (HEMTs) employed in this work are conventionally processed devices that can be released from their growth substrate and transferred to a variety of rigid and flexible substrates. Characterization of the GaN device behavior on the as-grown sapphire wafers (prior to transfer) provide a baseline for evaluation of the thermal performance of engineered interfaces and substrates. With conventional substrates, device performance (specifically, the saturation current) is reduced when the device is transferred to polymeric substrates. The thermal dissipation is further restricted due to the addition of an adhesive layer to the substrate. Thermal imaging of devices in operation reveals that the current passing through an as-grown GaN transistor on a sapphire wafer reaches the target operating temperature at approximately five times the power of the same device transferred to a flexible substrate. Printable, thermally conductive nanocomposites integrating 1D, 2D, and 3D forms of carbon in a flexible polymer matrix, as well as metal nanoparticles, were developed to maximize heat transfer from electronic devices. The thermal conductivity of the candidate substrate materials was measured experimentally to have more than a 900 percent increase in thermal conductivity (from 0.2 to 1.7 W/mK), while maintaining desirable mechanical properties. The performance of devices transferred to these novel flexible composite substrates was characterized and used in computational simulations to predict flexible substrate architectures that effectively promote point-to-volume heat transfer to further improve device performance. Additive manufacturing for engineered architectures of the flexible, thermally conductive substrate materials was demonstrated to substantially reduce the thermal limitation of high-power flexible electronics.

4:20pm **TF-TuA7 Selective Deposition by Fast-ALD of Transparent Conductive Metal Oxides for Application in Organic (opto)electronic Devices***, M. Granados, D. Munoz-Rojas,* LMGP, France*; c. fontelaye, G. Nonglaton,* ***Tony Maindron,*** CEA-LETI, France

Future's demands for new TCOs are driven by new developments made toward the realization of displays onto temperature-sensitive plastic substrates, transparent displays, as well as sensor arrays for bio-healthcare applications. With regard to the realization of TCOs, the Atomic Layer Deposition (ALD) technology is well adapted since it allows the realization of high quality materials at low temperatures, together with a digital control of thickness. In the meantime, multicomponent film growth can be reproducible and highly controllable even on large substrates, with the self-limiting reaction of ALD offering great benefits to many materials. The mainstream TCO deposited by ALD today is by far ZnO, as well as its derivatives (ZnO:Al; ZnO:Sn; ZnO: In…). Unfortunately, the ALD of ZnO suffers from two major drawbacks: (i) ALD is a very low throughput technique and (ii) ZnO-based materials are very sensitive to moisture (environmental and during microfabrication processes). Fast-ALD is an alternative new generation high-throughput process that will be approached in this work to make TCO films, to solve issue (i). In the meantime, Area Selective Deposition (ASD) strategies based on the use of vapor-deposited SAMS (Self Assembled Monolayers) will be investigated to selectively deposit the materials. Doing so, this work will leverage the use of intensive photolithography/etching processes of ZnO, to solve issue (ii). A future perspective of this work is to provide innovative fast-ASD deposited TCO-based TFT architectures.

4:40pm **TF-TuA8 Photocatalytic Antibacterial Activity of ALD Thin Films on Fibrous Materials**, ***Halil Akyildiz**, S. Diler,* Uludag University, Turkey

Semiconductor metal oxide thin film materials show photocatalytic properties, which can achieve various reactions for a variety of applications such as degradation of organic pollutants. Using similar mechanism, elimination of bacteria is also presented in the literature mostly on planar substrates. Since increase in the photocatalytic performance is expected with increasing surface area, thin films of ZnO and TiO_2 were deposited onto fibrous Nylon 66 surfaces via Atomic layer deposition (ALD) were tested for the elimination of bacteria. Tests were conducted at various thicknesses of ALD films for both types of materials. Formation and morphology of the films were investigated via electron microscope techniques TEM, FTIR, and SEM. Furthermore the structural analysis of the films were conducted via XRD and AFM while optical properties of the films were investigated via UV-Vis and PL spectrophotometers. Photocatalytic activity of the coated fiber materials was investigated by measuring methylene blue degradation. Antibacterial performance of the ALD films on fibers was tested using standard methods ISO 20645 and AATCC 100 against S. Aureus (ATCC 6538) and E. Coli (ATCC 35218) bacteria. As deposited ZnO samples showed better antibacterial performance compared to the TiO_2 films which is attributed the higher crystallinity of ZnO films.

5:00pm **TF-TuA9 A Kinetic and Thermodynamic Study of Aromatic Compounds Interacting with Metal-Organic Framework Thin Films**, *J. Shankwitz, D. Speed, D. Sinanan,* ***Greg Szulczewski**,* University of Alabama

Metal-organic frameworks (MOFs) are a class of highly porous materials that can be synthesized using a variety of inorganic nodes and organic linkers, which enables MOFs for emerging application in gas sensing, gas storage and gas separations. In this talk, we will describe the synthesis of MOF thin films of the UiO-66-X type, where X = H, NH_2 and NO_2 grown on Au-coated Si wafers and Au-coated quartz microbalance crystals using a vapor-assisted conversion method. The thin films were characterized by XPS, XRD, RAIRS and SEM. The thin films were activated by heating under high vacuum and exposed to a saturation pressure of benzene, toluene, ethyl benzene and xylene isomers (BTEX family) while recording the frequency change of the crystal at different temperatures. The Sauerbrey equation was used to convert the frequency change to accumulated mass, followed by calculation of the Henry's constant at each temperature for the BTEX family of compounds. The results show that UiO-66-NO_2 had the highest affinity for all of the aromatic compounds studied. In addition, the kinetics of adsorption have been modeling by a Fickian diffusion process to estimate the diffusion coefficients of the molecules in the MOFs.

5:20pm **TF-TuA10 Carbon's Role in Reducing Alumina's Resistivity Through Catalytic Carbon Nanotube Growth**, ***Berg Dodson**, R.C. Davis, R.R. Vanfleet,* Brigham Young University

Alumina is used as a diffusion barrier in the catalytic synthesis of carbon nanotubes (CNTs). Prior to CNT growth, the alumina film is electrically insulating, but becomes conductive following a CNT growth process. Electrical resistance measurements show how this change in conductivity correlates principally with a carbon CVD process. Low resistances are observed even when no iron is present for the CNT growth and when deposited carbon layers are etched off. TEM (and SIMS) data demonstrate that both iron and carbon can diffuse into the alumina layer during processing. Additionally, I will discuss at how predicted doping levels compare to the observed conductivity of the samples.

5:40pm **TF-TuA11 Ferroelectricity in Hafnia-Zirconia based Thin Films: Characterization and Applications**, ***Vineetha Mukundan**,* SUNY Polytechnic Institute*; S. Consiglio, D.H. Triyoso, K. Tapily, R.D. Clark, G.J. Leusink,* TEL Technology Center, America, LLC*; J.H. Hazra, K. Beckmann, N.C. Cady, A.C. Diebold,* SUNY Polytechnic Institute, Albany

Hafnia-based materials have tremendous potential to replace perovskites in FeRAM applications due to their unique ferroelectric properties and potential for scalability [1]. Implementation of hafnia-based thin films in FeRAM has recently been demonstrated by Mikalojick *et al* [1]. With hafnia's high coercive field, enhanced endurance and memory window achieved by encapsulation with different electrodes, it is advantageous to also integrate it into a FET device [2]. For use in neuromorphic computing, Jerry *et al.*have employed electric-field controlled partial polarization switching in atomic layer deposited ferroelectric hafnia-zirconia films to demonstrate a FeFET based analog synapse [3]. Ferroelectricity in hafnia doped with Si was recently discovered by Böscke e*t al* [4] and it has been well established that the orthorhombic Pca21 is responsible for its ferroelectric properties. The factors leading to the formation and stabilization of this metastable phase are unclear. Structural modification and stabilization of different metastable states are being investigated by alloying hafnia with ZrO_2, doping with Si and Al, various annealing schemes and different processing schemes including different semiconductor substrates. We study the long range structure of hafnia-zirconia films by grazing incidence in-plane x-ray diffraction (GI-I-XRD) and local structure by extended x-ray absorption fine structure spectroscopy (EXAFS) along with polarization measurements to study their electrical properties. An important part for advancing these ultra-thin films for application as both FeRAM and NCFET devices necessitates studying capacitive stacks in the form of metal-insulator-metal (MIM) and metal-insulator-semiconductor (MIS) [5]. Further, we estimate the percentage content of the different phases including the non-centrosymmetric orthorhombic phases in these stacks varying in composition and thickness. With increasing zirconia content in these stacks, the monoclinic phase decreases and it exhibits anti-ferroelectric property. With increasing thicknesses, it is found that the monoclinic phase increases in content, which should give rise to a decrease in the polarization of these stacks. We observed no change in the structure with annealing after it has been encapsulated by the TiN electrode, even up to 1000°C suggesting the confinement plays an active role in its structural evolution. Additional studies are underway to understand the influence of processing conditions, electrical cycling, annealing temperature, types of electrodes, and substrates on the structure and electrical properties of Hafnia-zirconia based thin films [6].

6:00pm **TF-TuA12 Atomic Layer Deposition-enabled Formation of Laser-Induced Graphene for Charged Membrane Applications**, ***David Bergsman**, B.A. Getachew, J.C. Grossman,* Massachusetts Institute of Technology

Membrane-based processes are becoming increasingly popular for water treatment due to their relatively high energy efficiency and low cost compared to other treatment methods. However, the advantages of membranes are mitigated by the need for additional pre-treatment steps that are required to maintain their effective operation. The treatment and prevention of membrane fouling, in particular, constitutes a large fraction of typical membrane operational costs. One potential approach to combat fouling is to design conductive membrane coatings that can prevent the attachment and growth of biofoulants both electrostatically and via electrochemical generation of reactive oxygen species. Despite their potential, these conductive membrane coatings are often expensive, requiring additional chemicals and non-scalable methods to produce, e.g. carbon nanotube mats or other graphitic coatings deposited by vacuum filtration.

In this work, we explore the use of laser-induced graphene (LIG) for the creation of conductive ultrafiltration membranes. Porous polyethersulfone (PES) membranes are first coated in a thin layer of alumina using atomic layer deposition (ALD) before being irradiated with an infrared laser. We show that this alumina film, which can be scalably produced using spacial ALD, can localize LIG formation to the surface of the membrane, preventing the buried, un-lased areas of PES from melting and losing their porosity during the lasing process. This allows the top-most layer of the PES to be a conductive coating that can be used to charge the membrane surface and used to improve membrane performance (e.g. fouling mitigation). The formation of LIG is verified by scanning electron microscopy and Raman spectroscopy. The conductive layer is also shown to possesses relatively high conductivity, which is important for reducing power consumption in devices. Insight into the mechanism behind the improved stability to melting provided by ALD is provided by thermogravimetric analysis, differential scanning calorimetry, and Fourier-transform infrared spectroscopy. The effect of ALD film thickness and the use of sequential infiltration synthesis will also be explored. These insights are used to discuss the potential application of this approach to creating conductive coatings on other polymers using ALD-based approaches.

Energy Transition Focus Topic
Room A226 - Session TL+AS+SS+TF-TuA

Breakthroughs and Challenges in Applied Materials for Energy Transition (ALL INVITED SESSION) & Panel Discussion

Moderators: Jason Avila, U.S. Naval Research Laboratory, Devika Choudhury, Argonne National Laboratory

2:20pm **TL+AS+SS+TF-TuA1 Interface Science and Engineering for Energy-Water Systems***, **Seth Darling**,* Argonne National Laboratory **INVITED**

Driven by climate change, population growth, development, urbanization, and other factors, water crises represent the greatest global risk in the coming decades. Advances in materials represent a powerful tool to address many of these challenges. Understanding—and ultimately controlling—interfaces between materials and water are pivotal [1]. In this presentation, we will lay out the challenges and present several examples based on materials science strategies for addressing applications in water. In each instance, manipulation of interfacial properties provides novel functionality, ranging from selective transport to energy transduction to pollution mitigation.

[1] J. Appl. Phys. 124 (2018) 030901

3:00pm **TL+AS+SS+TF-TuA3 Atomic Dynamics of Noble Metal Surface in Gases Revealed by Time Resolved Environmental Transmission Electron Microscopy***, **Seiji Takeda**, N. Kamiuchi, R. Aso, H. Yoshida, T. Tamaoka,* Osaka University, Japan **INVITED**

The surface of noble metals in gas has been extensively studied in the field of surface science. The surface has been investigated in both ultra high vacuum and various gases of high pressure and under various stimuli, for instance the illumination of intense light, the electric and/or magnetic field and the irradiation of charged particles. A microscopy study is potentially useful to provide us with the imaging data on the surface in real space and time at the resolution that is available in a microscopy apparatus to use. Among various methodologies for microscopy, atomic resolution environmental transmission electron microscopy has advanced greatly in the time resolution recently, allowing us to explore the dynamic surface and to elucidate the mechanism of the dynamic phenomena that are related to various energy transition processes. We show recent our studies, including the self-activated surface dynamics of gold catalysts in reaction environments [1] and the unexpected gas (nitrogen) -solid (palladium) transition [2] that is occurring on the surface under a strong electrostatic field. We demonstrate that the surface dynamics that is associated with the energy transition processes needs to be visualized at atomic scale for understanding the electronic excitations behind the surface dynamics.

References

[1] N. Kamiuchi et al., Nat. Commun. **9** (2018) 2060.

[2] T. Tamaoka, R. Aso et al., Nanoscale (2019) .

4:20pm **TL+AS+SS+TF-TuA7 Totally Organic and Organic-Inorganic Hybrid Batteries***, **Burak Esat**[1],* Fatih University, Turkey, Rutgers University*; S. Bahceci, S. Akay,* Fatih University, Turkey*; A. Momchilov,* Bulgarian Academy of Science, Bulgaria

We hereby represent novel polymers and reduced graphene oxide with pendant electro-active groups such as TEMPO and quinones.

The first example of polymers with pendant anode-active groups studied in our group is a polymethacrylate derivative carrying anthraquinone moieties (pMAntrq). This anthraquinone based anode-active material has proven to show a quite good reversible electrochemical reduction behavior in both aqueous and non-aqueous electrolytes in our studies. pMAntrq|1M $LiClO_4$ in EC:DEC=1:1|Li battery system has been constructed. The initial discharge capacity of the cell obtained was 151 mAh/g when cycled between 4.2 and 1.2V at 0.25C rate and 79.2 mAh/g when cycled between 4.0 and 1.5V at 0.3C rate during subsequent cycles.

This material was also used in an aqueous battery, pMAntrq |5M KOH aq.|$LiMn_2O_4$. Although an initial discharge capacity of 37.7 mAh/g was obtained, it deteriorated quickly due to the solubility of the reduced form of the polymer in this electrolyte system. This is the first reported example of such organic-inorganic hybrid battery.

An anode material based on reduced graphene oxide (RGO) functionalized with anthraquinone is also investigated and a battery against Li metal revealed a quite reversible capacity of 200 mAh/g based on the weight of electro-active anthraquinone moieties when cycled between 3.2 and 1.8 V at 0.3C rate. The energy density was found to be around 450 mWh/g.

We have also synthesized and characterized polyacetylene polymers with pendant TEMPO radicals which are electrochemically oxidizable in a reversible manner at around 3.5-3.6V vs. Li. These materials have been proven to be cathode-active materials for rechargeable batteries. We have demonstrated that a mixture of Tempo radical polymer with $LiMn_2O_4$ (1:1) can be used as a hybrid cathode material. Typically, this polymer may be expected to act as a polymeric electro-active binder and a stability improver for the inorganic cathode-active material.

Studies toward construction of all organic batteries using these anode and cathode materials are currently in progress.

4:40pm **TL+AS+SS+TF-TuA8 Electrochemical Strategies for Designing Interfaces of Battery Materials***, **Betar Gallant**,* Massachusetts Institute of Technology **INVITED**

Future generations of energy-storage devices require advances beyond state-of-the-art materials and redox systems. Rechargeable batteries, specifically today's Li-ion batteries, have largely been dominated by transition metal oxide cathodes; advanced conversion systems with higher theoretical energy densities, such as Li-S and Li-O_2, have received significant attention as "beyond Li-ion" batteries, but have their own challenges and limitations. Looking at the periodic table invites one to wonder, "Is there more beyond sulfur and O_2?" This talk will focus on challenges and opportunities related to a different chemical family: fluorine, or more specifically, active fluoride. Fluoride-containing additives, electrolytes, solid electrolyte interphases (SEI), and intercalation materials represent a recurring motif in many proposed next-generation battery chemistries, but current understanding of the behavior of fluorinated interfaces and materials remains largely phenomenological. In addition, controlling the incorporation of fluoride into materials still remains a major challenge owing to safety issues of fluorine and the intransigence of fluoride-containing precursors, hindering design in this space.

In this talk, I describe our group's exploration of several applications where fluoride-forming reactions can be harnessed and tailored for benefit in advanced batteries. First, I describe our efforts to develop high-energy density redox systems based on the electrochemical reduction of fluorinated gases. We show that fundamental knowledge and the experimental framework developed in the field of Li-O_2batteries in recent years can be successfully translated to the development of new gas-to-solid conversion reactions with high energy densities. Next, I will discuss the opportunities presented by the ability to generate fluoride *in situ* in working batteries from these reactions, creating new possibilities to fluorinate interfaces in tailorable and precise ways. I will present our findings relevant to two examples where fluoride has been suggested to play a critical and enabling role: Li anode interfaces, and oxyfluoride-based intercalation cathodes. Using our gas-based fluoridation architecture, we explore the fundamental role that fluoride plays in each of these applications. Finally, I will highlight future challenges and opportunities in the characterization of fluoridated materials.

[1] **Scholar Rescue Fund Fellow**

Atomic Scale Processing Focus Topic
Room B130 - Session AP+BI+PS+TF-WeM

Surface Reaction Analysis and Emerging Applications of Atomic Scale Processing

Moderator: Eric A. Joseph, IBM T.J. Watson Research Center

8:00am **AP+BI+PS+TF-WeM1 Open Spaces in Al_2O_3 Film Deposited on Widegap Semiconductors Probed by Monoenergetic Positron Beams***, **Akira Uedono**,* University of Tsukuba, Japan*; T. Nabatame,* NIMS, Japan*; W. Egger, T. Koschine,* Universität der Bundeswehr München, Germany*; C. Hugenschmidt, M. Dickmann,* Technische Universität München, Germany*; M. Sumiya,* NIMS, Japan*; S. Ishibashi,* AIST, Japan **INVITED**

Positron annihilation is a useful technique for characterizing vacancy-type defects in semiconductors, and it has been successfully used to detect defects in GaN. This technique is also useful for detecting open spaces in thin amorphous films deposited on semiconductor substrates. When a positron is implanted into condensed matter, it annihilates with an electron and emits two 511-keV gamma quanta. The energy distribution of the annihilation gamma rays is broadened by the momentum component of the annihilating electron-positron pair. A freely diffusing positron may be localized in a vacancy-type defect because of Coulomb repulsion from positively charged ion cores. Because the momentum distribution of the electrons in such defects differs from that of electrons in the bulk material, these defects can be detected by measuring the Doppler broadening spectra of the annihilation radiation. Because the electron density in open spaces or vacancy-type defects is lower than that in the bulk, the lifetime of positrons trapped by such regions is longer than that of positrons in the delocalized state. Thus, the measurement of the positron lifetime also provides information of open spaces and vacancies in solid. In the present work, open spaces and defects in the Al_2O_3(25 nm)/GaN structure were probed by using monoenergetic positron beams.

Al_2O_3 films were deposited on GaN by atomic layer deposition at 300ºC. Temperature treatment above 800°C leads to the introduction of vacancy-type defects in GaN due to outdiffusion of atoms from GaN into Al_2O_3. The width of the damaged region was determined to be 40-50 nm from the Al_2O_3/GaN interface, and some of the vacancies were identified to act as electron trapping centers. In the Al_2O_3 film before and after annealing treatment at 300-900ºC, open spaces with three different sizes were found to coexist. The density of medium-sized open spaces started to decrease above 800°C, which was associated with the interaction between GaN and Al_2O_3. Effects of the electron trapping/detrapping processes of interface states on the flat band voltage and the defects in GaN were also discussed.

The present research suggests that the interaction between amorphous Al_2O_3 and GaN introduces not only vacancy-type defects in GaN but also changes the matrix structure of Al_2O_3 film. We also revealed that the electron trapping/detrapping processes of interface charge states are influenced by the defects introduced in GaN.

8:40am **AP+BI+PS+TF-WeM3 Surface Reaction Analyses of Atomic-layer Etching by Controlled Beam Experiments***, **Kazuhiro Karahashi**, T. Ito, S. Hamaguchi,* Osaka University, Japan

In manufacturing of modern advanced semiconductor devices such magnetoresistive random-access memories (MRAMs), phase-change random-access memories (PRAMs), and three-dimensional integrated circuit (3D IC) devices, damage-free high-precision etching for various materials is an indispensable process technology. Halogenation of a surface layer combined with low-energy ion bombardment or ligand-exchange of organic molecules for the formation of metal complexes is a surface reaction that may be used for such highly selective etching processes with atomic-scale precision. A better understanding of surface reactions taking place during the etching process often allows one to control and optimize the process more effectively. In this study, we have developed a new surface-reaction analysis system with highly controlled beams of various species and examined surface reaction mechanisms of plasma-assisted or thermal atomic-layer etching (ALE) processes for silicon (Si), copper (Cu), and nickel (Ni) films. The beam experiment of this system offers an experimental “simulation” of actual ALE surface reactions. The system is equipped with differentially-pumped multiple beam sources that can irradiate the sample set in an ultra-high-vacuum (UHV) chamber with different types of beams, i.e., low-energy ions, thermal molecules, metastable radicals, and atomic/molecular clusters, independently. During the beam irradiation, scattered and desorbed species may be measured by a differentially pumped quadrupole mass spectrometer (QMS). Time-resolved measurements of QMS synchronized with pulsed beam irradiation facilitate detailed analysis of the beam-surface interactions. Chemical states of adsorbed species on the sample surface may be measured by X-ray photoelectron spectroscopy (XPS). In this presentation, we discuss the mechanisms of halogenated-layer formation on the Si, Cu, or Ni surfaces by their exposure to XeF2 or Cl2 gases and the removal mechanisms of halogenated species from the surface by low-energy ion irradiation or surface heating. Thermal desorption mechanisms of Cu or Ni by the metal-complex formation with organic molecules (such as diketones) from its oxidized surface are also discussed

9:00am **AP+BI+PS+TF-WeM4 Surface Reaction Analysis of Fluorine-based Reactive Ion Etching (RIE) and Atomic Layer Etching (ALE) by Molecular Dynamics (MD) Simulation***, **Erin Joy Tinacba**, M. Isobe, K. Karahashi, S. Hamaguchi,* Osaka University, Japan

Plasma etching has always been a useful process in semiconductor device fabrication. There are several ways of using plasma etching such as reactive ion etching (RIE), wherein the material surface is bombarded with energetic ions while it also exposed to chemically reactive radicals from the plasma. Because of the energy provided by bombarding ions and high chemical reactivity on the surface, the surface is etched even at a relatively low temperature due to the combination of physical and chemical sputtering effects. RIE is often suited to fast etching processes of high aspect ratio structures since it can provide high etching yields. Another application of plasma etching is plasma-assisted atomic layer etching (ALE), wherein chemical and sputtering effects of typical plasma etching are separated into two steps. In a typical ALE process, the first step is an adsorption step wherein chemically reactive molecules or radicals from a plasma are used to modify the material surface. The modified monolayer or a thin layer on the material surface is then etched during the subsequent desorption step (second step) where low-energy ions bombard the surface. The etching reaction stops when the modified layer is depleted. This cycle is repeated many times until the desired etched depth is reached. The ALE process might be slow but it can provide tight control in the etch variability for sub-10 nm technology applications.

In this paper, molecular dynamic (MD) simulation is used to understand the effects of ions and radicals of high fluorine (F) content on etching reactions of silicon (Si), silicon dioxide (SiO_2), and silicon nitride (Si_3N_4), which may be observed in RIE processes based on, e.g., SF_6, C_2F_6, or NF_3 plasmas. If such a plasma is used as a radical source and ion bombardment steps by inert gas ions are separated from the radical exposure steps, an ALE process may be performed with similar surface reactions. In typical RIE, a supply of a large amount of fluorine to the surface by increasing the flux of energetic ions containing multiple F atoms (such as SF_5^+, $C_2F_5^+$ and NF_2^+ ions) and/or by increasing a F radical flux to the surface results in high etch rates. It has been found that the etching rates by such highly fluorinated ions obtained from MD simulations are in good agreement with experimental observations and the deep fluorination of the surface accounts for their high etch rates. Although fluorine may be considered too corrosive to be used for ALE, we also analyzed by MD simulation an ALE process by fluorine-containing radicals such as NF2 and compared the results with experimental observations.

9:20am **AP+BI+PS+TF-WeM5 Analysis of Metal Surface during Atomic Layer Etching with Gas Cluster Ion Beam and Organic Acid***, **Noriaki Toyoda**, K. Uematsu,* University of Hyogo, Japan

Surface states of metal surface after atomic layer etchings (ALE) with gas cluster ion beam (GCIB) and organic acid were investigated using surface analysis tools (mainly X-ray photoelectron microscopy). In recent years, we have reported the usage of GCIB irradiation for the removal steps of ALE. Since GCIBs are aggregates of thousands of gas atoms or molecules, the energy/atoms or energy/molecules can be easily reduced to several eV even though the total energy of GCIB is several keV. This characteristic is beneficial for low-damage irradiation. In additions, since GCIBs induce dense energy deposition, the bombarded area experiences transient high-temperature and high-pressure conditions. As a result, chemical reactions are enhanced at low-temperature. These characteristics are suitable for the removal step in ALE.

In this study, we have investigated the surface state of metal (Ni, Cu) after ALE with GCIB and organic acid using in-situ XPS. Prior to GCIB irradiation, metal surfaces were cleaned by Ar ions. Then Ni or Cu surface were exposed to acetic acids or acetylacetones. The surface layer with adsorbed organic acid on metals were removed by subsequent GCIB irradiation. The difference of the surface states of metal between Ar and O_2-GCIB

irradiation are compared with in-situ XPS results. Etching mechanism by GCIB in the presence of the adsorbed organic acid will be discussed.

9:40am **AP+BI+PS+TF-WeM6 In-situ Characterization of Growth Kinetics of Piezoelectric Films Grown by Atomic Layer Deposition Utilizing an Ultra-high Purity Process Environment**, ***Nicholas Strnad,*** General Technical Services, LLC; *D.M. Potrepka,* U.S. Army Research Laboratory; *N. O'Toole, G.B. Rayner,* Kurt J. Lesker Company; *J.S. Pulskamp,* U.S. Army Research Laboratory

Recently, $PbZr_xTi_{1-x}O_3$ (PZT) was grown by atomic layer deposition (ALD) in a piezoelectric film stack that was micro-machined into electrically actuated cantilever beams. [1] ALD PZT is a process technology that may drive 3D PiezoMEMS that utilizes piezoelectric films deposited on micro-machined sidewall structures. AlN is also a desirable piezoelectric for 3D PiezoMEMS but integration has been hampered by its sensitivity to reactive background gases resulting in oxygen contamination of several atomic percent and above. [2] Reactive background gases can also impact oxide films by skewing the non-uniformity and growth-per-cycle (GPC). Thus, individual reactor conditions play a significant role in both the growth kinetics, and resulting quality of thin films grown by ALD. To address both of these issues there exists the need for ultra-high purity (UHP) process capability. Here, we present how the transition from non-UHP to UHP process environment affects ALD AlN and the constituent oxide films in ALD PZT. The UHP process environment also enables the rapid characterization of the reaction kinetics of ALD processes by in-situ ellipsometry. The reaction kinetics of several constituent oxides for ALD PZT are presented based on empirical in-situ observations.

References

[1] Strnad, N.A. (2019) Atomic Layer Deposition of Lead Zirconate-Titanate and Other Lead-Based Perovskites (Doctoral Dissertation) https://doi.org/10.13016/8dqx-7pev

[2] Chen, Z. (2019) Thermal atomic layer deposition of aluminum nitride thin films from AlCl3 (Master's Dissertation)

11:00am **AP+BI+PS+TF-WeM10 Nanoscale Surface Modification of Medical Devices using Accelerated Neutral Atom Beam Technology**, ***Dmitry Shashkov,*** *J. Khoury, B. Phok,* Exogenesis Corp. **INVITED**

Controlling surface properties of biomaterials is vital in improving the biocompatibility of devices by enhancing integration and reducing bacterial attachment. We use Accelerated Neutral Atom Beam (ANAB) technology, a low energy accelerated particle beam gaining acceptance as a tool for nanoscale surface modification of implantable medical devices. ANAB is created by acceleration of neutral argon atoms with very low energies under vacuum which bombard a material surface, modifying it to a shallow depth of 2-3 nm. This is a non-additive technology that results in modifications of surface topography, wettability, and chemistry. These modifications are understood to be important in cell-surface interactions on implantable medical devices. Similarly, ANAB could be used to modify surfaces of medical device coatings (small molecules and proteins)., creating a native drug elution barrier. In this study, we characterize the effects of ANAB on several materials including metals (Ti, CoCr) and polymers (PEEK, PP, PVC) and measure the differential ability of eukaryotic versus prokaryotic cell attachment on these modified surfaces. We also study the ability of ANAB to create an elution barrier on a drug coating without the use of binding polymers. We identified that eukaryotic cells including mesenchymal stem cells (MSC) and osteoblasts increase attachment and proliferation on treated surfaces as measured by MTS assay and cell visualization by microscopy. MTS assay shows that by day 14, control PEEK has 9,925±1,994 cells while ANAB-treated PEEK has 88,713±6,118 cells ($n=3$; $p<0.0014$). At the same time, we find that bacterial cells including *S.aureus* and *P.aeruginosa* have a decreased ability to bind on the ANAB-treated surface. This dichotomy of cellular attachment may be attributed to the nano-scale surface topography, favoring larger eukaryotic cells while inhibiting attachment of smaller bacterial pathogens. In studies focusing on drug elution, rapamycin was spray-coated on the surface of CoCr bare metal stents and either left as control or ANAB-treated the surface of the drug. These stents were then placed in a plasma elution assay for up to 7 days. We found that untreated stents eluted off most of the drug within 24 hours, and 100% of it by 48 hours post-elution. The ANAB-treated stents, however, showed a favorable elution profile slowly releasing the drug over the 7 day period. ANAB, therefore, has many possible uses in medical device technology in increasing integration, decreasing bacterial attachment and potentially biofilm formation, and, if desired, create an elution profile for a combination drug-device without the use of binding polymers.

11:40am **AP+BI+PS+TF-WeM12 Chemically Enhanced Patterning of Nickel for Next Generation EUV Mask**, ***Xia (Gary) Sang,*** *E. Chen,* University of California, Los Angeles; *T. Tronic, C. Choi,* Intel Corporation; *J.P. Chang,* University of California, Los Angeles

The ever-increasing demand in high-precision pattern definition and high-fidelity pattern transfer in the IC manufacturing industry calls for continuous advancement in lithography technology. Extreme Ultra-Violet (EUV) lithography is being widely adopted for defining sub-10 nm nodes. Due to its ideal optical properties, Ni is under active research as the future absorbing layer material in EUV masks, the profile of which determines the quality of resulting lithographic patterns. Contemporary techniques for patterning Ni rely on noble ion beam milling, which leaves considerable amounts of re-deposition on feature sidewall. Finding chemically selective patterning technique is thus of critical importance. Due to the etch-resistant nature of Nickel, removal at an atomic level is enabled by chemical modification of the surface through plasma exposure and subsequent introduction of organic ligands. Plausible chemicals are first screened by thermodynamic assessments from available databases, experiments were then conducted to validate the theoretical predictions.

Both blanket and patterned Ni thin films were studied using this reaction scheme. Organic chemistries, such as acetic acid and formic acid were first investigated to determine the feasibility of metal-organic formation through direct exposure. The efficacy of acetic acid and formic acid etching chemistries were confirmed through solution-based studies on Ni, the formation of Ni(CH3COO)2 and Ni(HCOO)2 were confirmed through mass spectrometry. Nickel oxide formation and subsequent removal were confirmed by quantifying the change in the relative intensities of peaks of metallic Ni (852.6 eV) and oxidized Ni (853.7 eV) by X-Ray Photoelectron Spectroscopy (XPS).

The chemical reactivity difference between Ni0 and Ni2+ was quantified in the work to explore the attainable etch selectivity. Due to the decrease in radical concentration and flux, vapor phase etching of metallic Ni resulted in small thickness reduction (~ 0.4 nm/cycle). It is then tested that surface modification, particularly oxidation, is capable of promoting subsequent reactions by lowering reaction energy barrier through metal oxide formation. An oxygen plasma treatment is added prior to acid vapor exposure, and this cyclic approach results in a relatively linear etch rate of ~ 2 nm/cycle, which translates to a 50:1 etching selectivity of NiO over Ni. The same cyclic approach was then applied to patterned samples, post-etch sidewall angle of ~ 85° is measured, which closely conserves the initial feature profile (~ 87°).

12:00pm **AP+BI+PS+TF-WeM13 Surface Reactions of Low Energy Electrons and Ions with Organometallic Precursors and their Relevance to Charged Particle Deposition Processes**, ***Rachel Thorman,*** Johns Hopkins University; *E. Bilgilisoy,* FAU Erlangen-Nürnberg, Germany; *S. Matsuda, L. McElwee-White,* University of Florida; *D. Fairbrother,* Johns Hopkins University

Focused electron beam induced deposition (FEBID) and focused ion beam induced deposition (FIBID) are nanofabrication techniques where beams of charged particles (electrons or ions) create metal-containing nanostructures by decomposing organometallic precursors in low pressure environments. Consequently, the interactions of electrons and ions with surface-bound organometallic precursors are fundamental processes in these deposition processes. Previously performed ultra-high vacuum (UHV) studies on low energy (below 100 eV) electron interactions with adsorbed precursors (e.g. $Pt(PF_3)_4$, $MeCpPtMe_3$, and $Co(CO)_3NO$) have revealed that electron-induced reactions of surface bound precursors occurs in two sequential steps: (1) an initial step characterized by precursor decomposition/deposition and partial ligand desorption followed by (2) decomposition of the residual ligands. However, a similar level of understanding does not exist for low energy ion interactions with organometallic precursors. In this presentation, I will show that a low temperature, UHV surface science approach can serve as a platform to study the reactions of both low energy electrons (500 eV) and low energy ions (<1kV Ar^+ ions) with organometallic precursors. Results from *in situ* X-ray photoelectron spectroscopy (XPS) and mass spectroscopy (MS) clearly show that low energy electron and ion-induced reactions of several surface-adsorbed species, including $(\eta^5\text{-}Cp)Fe(CO)_2Re(CO)_5$, $Ru(CO)_4I_2$, $Fe(CO)_5$, and $Co(CO)_3NO$, are markedly different. Similarly to electron-induced reactions, low-energy ion-induced reactions proceed in a two-step process with an initial decomposition step primarily characterized by ligand loss. However, ligand loss is typically must more extensive than is observed for electron-induced reactions; for example, in the case of $(\eta^5\text{-}Cp)Fe(CO)_2Re(CO)_5$ and $Fe(CO)_5$, all CO ligands desorb in this initial step. The second step in the ion induced reactions can be described as a regime

primarily characterized by physical sputtering. These contrasting results are discussed in the context of different deposition mechanisms proposed for FEBID and FIBID.

Spectroscopic Ellipsometry Focus Topic
Room A212 - Session EL+AS+EM+TF-WeM
Optical Characterization of Thin Films and Nanostructures

Moderators: Eva Bittrich, Leibniz Institute of Polymer Research Dresden, Tino Hofmann, University of North Carolina at Charlotte

8:00am **EL+AS+EM+TF-WeM1 Enhanced Strong Near Band Edge Emission from Lanththanide Doped Sputter Deposited ZnO***, C.L. Heng,* Beijing Institutute of Technology, China*; W. Xiang, T. Wang,* Beijing Institutete of Technology, China*; W.Y. Su,* Beijing Instititute of Technology, China*; P.G. Yin,* Beihang University, China*; **Terje G Finstad**,* University of Oslo, Norway

Research on ZnO films and nanostructures have increased steadily in the last decades being motivated by many applications including photonic applications. Incorporation of rare earth (RE) elements for the purpose utilize transition therein for conversion or manipulation of the wavelength spectrum. That was also our original motivation, however we observed the REs also can provide an enhancement of near band gap emission,NBE. This has been observed for Tb, Ce, Yb and Eu. The ZnO films were co-sputtered with RE elements onto Si wafers in an Ar+O_2 ambient yielding oxygen rich films as observed by RBS and XPS. The films were annealed in an N_2 ambient for various temperatures from 600 to 1100 °C. The luminescence behavior was studied emission and excitation spectroscopy as well luminescence decay measurements. Both undoped and RE doped films showed a large increase in emission with increasing annealing temperature, while the increase was largest for the RE doped samples. The crystallinity and microstructure of the films were studied by XPS, SEM, XRD and HRTEM. It is observed that the increase in UV NBE is correlated with crystalline improvements of ZnO. At the temperature for maximum PL emission intensity there is silicate formation due to interaction with the substrate. The maximum occurs for an annealing temperature where not all the ZnO has been consumed in the silicate reaction. This maximum appears to be 1100 °C for the thicker films and 1000 °C for thinner films. For samples having maximum NBE there seem to be random lasing occurring indicated by the intensity dependence of UV PL emission. A hypothesis for the main reason behind the increase in NBE intensity with RE doping is that the RE ions influence the film structure during nucleation early in the deposition process by influencing the mobility of atoms. The initial grain structure will have an affect on the development grain structure for the whole film and an influence on the grain growth. This influences the presence of non-radiative defect centers in the film and the grain surface and grain boundaries. As a side effect, we observe that there is very little transfer of excitation energy to the RE ions. This supports the notion that oxygen deficient centers may be necessary to have efficient energy transfer to RE ions in ZnO. Finally we remark that strong UV light from ZnO films have been sought particularly because they could offer a low temperature production for some application. The present method is still a high temperature method, but it is very simple and can be directly combined with Si technology which can be advantage for certain applications.

8:20am **EL+AS+EM+TF-WeM2 Ellipsometry Study of PLD based Temperature Controlled Thin Film Depositions of CdSe on ITO Substrates***, **Flavia Inbanathan**,* Ohio University*; M. Ebdah,* King Saud University, Kingdom of Saudi Arabia*; P. Kumar,* Gurukula Kangri Vishwavidyalaya, India*; K. Dasari,* Texas State University*; R.S. Katiyar,* University of Puerto Rico*; W.M. Jadwisienczak,* Ohio University

Cadmium Selenide(CdSe), a n-type semiconductor with a direct bandgap of 1.73eV has been explored widely for its suitability in various applications including photovoltaics and optoelectronics, because of its optical and electrical properties. The literature presents various deposition methods for CdSe thin films out of which this work is based on pulsed laser deposition(PLD)[1]. The optoelectronic applications of CdSe thin films depend on their structural and electronic properties that depends on deposition and process parameters[2]. The stability of the thin films at various temperatures is an important factor to improve the efficiency and durability of photosensitive devices. The present work aims to fabricate the high quality CdSe thin films using PLD method and affirms the optimal deposition temperature at 250°C as validated by the films surface roughness and ellipsometry studies[3][4]. The effect of different *in-situ* deposition temperature on structural, morphological and optical properties through XRD, AFM, SEM, optical absorption/transmission and ellipsometry spectroscopy have been investigated. CdSe thin films with thickness close to 200nm were deposited on the Indium Tin Oxide (ITO) coated glass substrates at temperatures ranging from 150 to 400°C. The light absorption spectrum analysis of all the CdSe films confirmed well defined direct energy band gap from 2.03 to 1.83eV. The ITO substrate is modelled using a two sub-layers model that consists of 130nm graded ITO on top of a 0.7mm bulk ITO layer, and the experimental ellipsometry spectra agreed very well with the fitting spectra. The ellipsometry study confirmed that CdSe thin films show an increase of 44% in refractive index(n) in the violet spectrum, and a constant value in blue-yellow spectral range but with significant changes in red spectrum for increase in temperature upto 350°C; beyond which resulted in constant value, possibly due to the stagnation in the grain growth. The extinction coefficient(k) value of CdSe approaches zero in the red spectrum region for 150°C and 300°C temperatures whereas it showed a value of 0.25 and 0.7 for 250°C and 400°C temperatures, respectively. The peaks observed around 650nm and 750nm in ellipsometry spectra are assigned to excitonic transitions. The collected data will be critically analysed in terms of CdSe optical properties engineered for optoelectronic and photovoltaic applications.

References: **[1]**Z.Bao *et al.,*J.Mater.Sci.:Mater Electron(2016)27,7233-7239; **[2]**S.Mahato, *et al*., J.Scien.: Adv.Mater. Devices, (2017)2,165-171; **[3]**A.Evmenova *et al.,*Advan. Mater. Scien.Eng. (2015), ID 920421,11; **[4]**B.T.Diroll *et al*., Chem. Mater.,(2015)27,6463-6469.

8:40am **EL+AS+EM+TF-WeM3 The Application of Mueller Matrix Spectroscopic Ellipsometry to Scatterometry Measurement of Feature Dimension and Shape for Integrated Circuit Structures***, **Alain C. Diebold**,* SUNY Polytechnic Institute **INVITED**

One of the most difficult measurement challenges is non-destructively determining the feature dimensions and shape for complicated 3D structures. This presentation will review Mueller Matrix Spectroscopic Ellipsometry based scatterometry which uses the Rigorous Coupled Wave Approximation (RCWA) to solve Maxwell's equations for a model structure and the resulting Mueller Matrix elements are compared to experimental results. Here we use the structures used in GAA transistors fabrication as an example of challenging measurements.(1, 2, 3) In this talk, we present simulations aimed at understanding the sensitivity to changes in feature shape and dimension for the structures used to fabricate GAA transistors. Simulations of the multi-layer fins show a clear sensitivity to fin shape and Si layer thickness which is enhanced by the use of the full Mueller Matrix capability vs traditional spectroscopic ellipsometry. We also discuss experimental measurement of nanowire test structure demonstrating the ability to measure the etching of mutiple sub-surface features. [3]

References

[1] Alain C. Diebold, Anthony Antonelli, and Nick Keller, Perspective: Optical measurement of feature dimensions and shapes by scatterometry, APL Mat. **6**, (2018), 058201. doi: 10.1063/1.5018310.

[2] Sonal Dey, Alain Diebold, Nick Keller, and Madhulika Korde, Mueller matrix spectroscopic ellipsometry based scatterometry simulations of Si and Si/SixGe1-x/Si/SixGe1-x/Si fins for sub-7nm node gate-all-around transistor metrology, Proc. SPIE 10585,

Metrology, Inspection, and Process Control for Microlithography XXXII, 1058506 (6 June 2018); doi: 10.1117/12.2296988

[3] Madhulika Korde, Subhadeep Kal, Cheryl Pereira, Nick Keller, Aelan Mosden, Alain C. Diebold, Optical Characterization of multi-NST Nanowire Test Structures using Muller Matrix Spectroscopic Ellipsometry (MMSE) based scatterometry for sub 5nm nodes, Proc. SPIE Metrology, Inspection, and Process Control for Microlithography XXXIII, (2019), in press.

9:20am **EL+AS+EM+TF-WeM5 Optical Constants and Thickness of Ultrathin Thermally Evaporated Iron Films***, **Nick Allen**, D.S. Shah, R.R. Vanfleet, M.R. Linford, R.C. Davis,* Brigham Young University

Carbon nanotube templated microfabrication (CNT-M) is a technique that uses a patterned iron catalyst to grow 3-D structures for device applications. Iron catalyst thickness strongly affects carbon nanotube (CNT) growth heights and the straightness of the CNT-M structures. Atomic force microscopy has been used to directly measure the thicknesses of such iron/iron oxide films, but this technique is slow and not easily scalable. A faster method is ellipsometry, but for very thin films, the optical constants and thickness are not easily separated, thus standard ellipsometry approaches are inadequate. The 2-6 nm thick iron films used as CNT growth catalysts are in this challenging region. The absorptive nature of the iron/iron oxide films adds further difficulty. In this study, a multi-sample

ellipsometry analysis using iron films of various thicknesses was performed to obtain the optical constants of thermally evaporated iron. We used contrast enhancement by incorporating a silicon dioxide layer under the film being analyzed to enhance sensitivity to the optical constants.

9:40am **EL+AS+EM+TF-WeM6 Birefringent Photonic Crystals for Polarization-discriminatingInfrared Focal Plane Arrays*, Marc Lata*,** *Y. Li, S. Park, M.J. McLamb, T. Hofmann,* University of North Carolina at Charlotte

Infrared optical materials fabricated using direct laser writing have received substantial interest since the emergence

of this technology which is based on the two-photon polymerization of suitable monomers [1, 2]. We have

demonstrated that direct laser writing allows the fabrication of structured surfaces to reduce Fresnel reflection

loss in the infrared spectral range while two-dimensional photonic crystals enable optical filters with high spectral

contrast [3, 4]. In combination with the ability to fabricate large scale arrays of uniform structures, two-photon

polymerization could be a disruptive technology for enhancing focal plane arrays in IR imaging systems.

So far, photonic crystals which provide polarization selectivity have not been used for the pixel-based enhancement

of infrared focal plane arrays. Here we explore the form-birefringence found in photonic crystals composed

of arrays of subwavelength-sized slanted micro wires (Fig. 1) for this purpose. The photonic crystals investigated

here were fabricated in a single fabrication step using direct laser writing of an infrared transparent photoresist.

The lateral dimensions of the photonic crystals are comparable to the pixel size of infrared focal plane arrays which

is on the order of some tens of micrometers [5]. We observe a strong contrast under cross-polarized illumination

in the mid-infrared spectral range at w = 1550 cm-1. Finite-element-based techniques are used to optimized the

geometry of the constituents of the photonic crystals to minimize edge effects. We envision laser direct writing as

a suitable technique for the enhancement of focal plane arrays to enable focal-plane polarimeters for the infrared

spectral range.

11:00am **EL+AS+EM+TF-WeM10 Relevance of hidden Valleys in the Dequenching of Room-temperature-emitting Ge Layers***, T. Sakamoto, Y. Yasutake,* University of Tokyo, Japan*; J. Kanasaki,* Osaka City University, Japan*; **Susumu Fukatsu**,* University of Tokyo, Japan

Ge offers a unique advantage of gaining a deeper insight into the intervalley coupling of *hot* electrons [1], which is arguably of importance in the context of controlling the optoelectronic and photonic functionalities [2]. In view of the complicated valley degeneracy in the near-band-edge region, such intervalley coupling of electrons plays a pivotal part even when strain-engineering pseudomorphic Ge-based quantum structures.

The capability of direct-gap emission at room temperature is of considerable practical significance of Ge, for which an added advantage is that emission wavelengths fortuitously fall within the telecom bands. Moreover, Ge is particularly interesting from the device physics point of view as it outperforms many semiconductor allies in the sense that thermal *dequenching* occurs near room-temperature: the emitted light intensity increases with increasing temperature, which is convenient but nevertheless logic-defying.

Such a rather counterintuitive “thermal roll-up”, as opposed to thermal roll-off which is usually more relevant, has been interpreted in terms of two-level electron kinetics assuming local thermal equilibrium; long-lived electrons populating the indirect conduction-band bottom, i.e., L-valleys, are excited up into the direct-gap Γ-valley by absorbing phonons, which seems to fit a fairly standard phenomenological picture reasonably well. To the contrary, this model system fails in the case of Ge layers, the quality of crystallinity of which is compromised because of a low growth temperature. In fact, they only show steady thermal roll-off, viz. *quenching*, without a trace of the anticipated dequenching.

These apparently conflicting observations can be reconciled only by considering another otherwise invisible *hidden* conduction-band valley that comes in between the L andΓ valleys to decouple them. A three-level scheme is naturally invoked thereby. Indeed, it explains not only the missing dequenching but the lost local thermal equilibrium in low-quality layers. As a proof of such a conjecture, an attempt was made to directly capture the *hidden* valleys by means of time- and angle-resolved two-photon photoemission [3]. Preliminary results indicate the relevance of X(Δ)-valleys, which are slightly above the Γ-valley, in the dequenching of room-temperature emission as a result of ultrafast coupling of L-X(Δ)-Γ valleys by phonons taking up large crystal momenta. These are consistent with theory and luminescence study.

1. T. Sakamoto *et al.*, Appl. Phys. Lett. **105**, 042101 (2014).

2. Y. Yasutake and S. Fukatsu, Spoken at 2018 APS March Meeting (Los Angeles, 2018), P07.00012.

3. J . Kanasaki *et al.*, Phys. Rev. B **96**, 115301 (2017).

11:20am **EL+AS+EM+TF-WeM11 Spectroscopic Ellipsometry on Organic Thin Films - From in-situ Bio-sensing to Active Layers for Organic Solar Cells***, **Eva Bittrich**, P. Uhlmann, K.-J. Eichhorn,* Leibniz Institute of Polymer Research Dresden, Germany*; M. Schubert,* University of Nebraska-Lincoln, Linköping University, Sweden, Leibniz Institute of Polymer Research Dresden, Germany*; M. Levichkova, K. Walzer,* Heliatek GmbH, Germany **INVITED**

Nanostructured surfaces and thin films of small organic molecules, polymers or hybrid materials are promising interfaces for versatile applications like sensing, water purification, nanoelectronics, energy production and energy storage devices. Ellipsometry, as non-invasive method, is well suited to contribute to the understanding of structure – property – relationships in organic thin films, but can also act as probing technique for hybrid sensing elements. Aspects from our research ranging from switchable responsive polymer brush interfaces for biosensing to thin films of small organic molecules for organic solar cells will be presented. On the one hand, swelling of polymer brushes grafted to slanted columnar thin films of silicon will be visualized by anisotropic optical contrast microscopy, as an example for a new class of hybrid sensing materials with unique sensitivity on the nanoscale. On the other hand the effect of template molecules on the morphology and optical properties of semiconducting thin films will be discussed, emphasizing the correlation of ellipsometric data with structural analysis by grazing incidence wide angle X-ray scattering (GIWAXS).

12:00pm **EL+AS+EM+TF-WeM13 Optical Dielectric Function of Si(bzimpy)2 – A Hexacoordinate Silicon Pincer Complex Determined by Spectroscopic Ellipsometry***, **Yanzeng Li**, M. Kocherga, S. Park, M. Lata, M.J. McLamb, G.D. Boreman, T.A. Schmedake, T. Hofmann,* University of North Carolina at Charlotte

Tang and VanSlyke demonstrated light emission from the first practical electroluminescent device based on a double-organic-layer structure of tris(8-hydroxyquinoline)aluminum, Alq_3, and a diamine film in the late 80's. Since then, organic light emitting diodes (OLED) based on metal chelates such as Alq3 have been widely studied. Despite the widespread use of Alq_3, there has been a broad search for new materials with improved properties, in particular, with respect to their chemical and electrochemical stability. We have recently reported on the successful synthesis of a neutral, hexacoordinate silicon-based fluorescent complex $Si(bzimpy)_2$. Our results indicate that $Si(bzimpy)_2$ exhibits inherent advantages such as the tunability of the luminescence in the visible spectrum, greater thermal stability, and high charge mobility that is comparable to that of Alq_3. Despite the successful synthesis and encouraging electroluminescence at 560 nm the complex dielectric function of the water stable complex has not been reported yet. Here we present spectroscopic ellipsometry data which were obtained from a Si(bzimpy)2 thin-film in the spectral range from 300~nm to 1900~nm. A parameterized model dielectric function composed of a Tauc-Lorentz and Gaussian oscillators is employed to analyze the experimental ellipsometry data. We find a good agreement between the critical point energies observed experimentally and our density functional theory calculations reported recently.

Electronic Materials and Photonics Division
Room A214 - Session EM+2D+AS+MI+MN+NS+TF-WeM

Nanostructures and Nanocharacterization of Electronic and Photonic Devices

Moderators: Sang M. Han, University of New Mexico, Jason Kawasaki, University of Wisconsin - Madison

8:00am **EM+2D+AS+MI+MN+NS+TF-WeM1 Photonic Thermal Conduction in Semiconductor Nanowires**, *E.J. Tervo, M.E. Gustafson, Z.M. Zhang, B.A. Cola, **Michael A. Filler**,* Georgia Institute of Technology

We present a practical material system—chains of infrared plasmonic resonators situated along the length of semiconductor nanowires—where near-field electromagnetic coupling between neighboring resonators enables photonic thermal transport comparable to the electronic and phononic contributions. We model the thermal conductivity of Si and InAs nanowires as a function of nanowire diameter, resonator length, aspect ratio, and separation distance by combining discrete dipolar approximation calculations, to determine the relevant dispersion relations, with thermal kinetic theory. We show that photonic thermal conductivities exceeding 1 W m^{-1} K^{-1} are possible for 10 nm diameter Si and InAs nanowires containing repeated resonators at 500 K, more than an order of magnitude higher than existing materials systems and on par with that possible with phonons and electrons. These results highlight the potential for photons in properly engineered solids to carry significant quantities of heat and suggest new ways to dynamic control thermal conductivity.

8:20am **EM+2D+AS+MI+MN+NS+TF-WeM2 Electric Field-Induced Defect Migration and Dielectric Breakdown in ZnO Nanowires**, ***Hantian Gao**, M. Haseman,* Department of Physics, The Ohio State University; *H. von Wenckstern, M. Grundmann,* Universität Leipzig, Felix-Bloch-Institut für Festkörperphysik; *L.J. Brillson,* The Ohio State University

Nanowires of the II-VI compound semiconductor ZnO have generated considerable interest for next generation opto- and microelectronics . Central to nanowire electronics is understanding and controlling native point defects, which can move[1] and lead to dielectric breakdown under applied electric fields. We used nanoscale lateral and depth-resolved cathodoluminescence spectroscopy (DRCLS) with hyperspectral imaging (HSI) in a scanning electron microscope (SEM) to observe defect migration and redistribution directly under applied electric fields and after dielectric breakdown. HSI maps represent lateral intensity distributions of specific features acquired pixel by pixel across SEM-scanned areas and normalized to near band edge (NBE) emissions. A pulsed layer deposited (PLD) ZnO microwire (3 µm diameter) exhibited homogeneous distributions of common luminescence features at 2.0 eV (V_{Zn} cluster) and 2.35 eV (Cu_{Zn}) as well as 2.7 and 2.9 eV (V_{Zn}) peaks near the wire surface. With increasing electrical bias up to 3x10^5 V/cm between two Pt contacts, these defects systematically redistribute, even at room temperature, moving toward and under one of the contacts, draining the "bulk" nanowire, especially its near-surface region. Since ionized V_{Zn}-related and Cu_{Zn} antisite defects are acceptors, their removal reduces the compensation of electron density in the typically n-type ZnO and thus its resistivity.

Besides HSI lateral maps, DRCLS vs. incident beam energy yields depth profiles radially of defects at specific locations along the nanowire. These exhibit high near-surface and wire core densities that biasing reduces. Current voltage measurements with increasing field gradients show a gradual resistivity decrease until an abrupt dielectric breakdown of the microwire at 300 kV/cm (150 V/5 µm). The acceptor removal between the contacts and their accumulation under one of the contacts can both contribute to this breakdown due to the decrease in resistivity and higher current conduction between the contacts and possible defect-assisted tunneling[2] across the increased defect density under the contact, respectively. These electric field-induced defect movements may be of more general significance in understanding dielectric breakdown mechanism not only in ZnO nanostructures but also bulk semiconductors in general.

HG, MH, and LJB gratefully acknowledge support from AFOSR Grant No. FA9550-18-1-0066 (A. Sayir). HVW and MG acknowledge Deutsche Forschungsgemeinschaft (Gr 1011/26- 1).

1. G. M. Foster, et al., Appl. Phys. Lett. **111**, 101604 (2017).

2. J.W.Cox, et al., Nano Lett, **18**, 6974 (2018).

8:40am **EM+2D+AS+MI+MN+NS+TF-WeM3 Characterization of SiGe/Si Multilayer FIN Structures using X-Ray Diffraction Reciprocal Space Maps**, ***Roopa Gowda**, M. Korde,* SUNY Polytechnic Institute; *M. Wormington,* Jordan Valley Semiconductors Inc.; *A.C. Diebold, V. Mukundan,* SUNY Polytechnic Institute

Nanowire and Nanosheet FET's are potential replacements for FinFET's, mainly beyond sub-10nm CMOS technology nodes, as gate-all-around (GAA) FET device architecture provides improved electrostatics in higher on current (*I* on) and better subthreshold swing. As GAA is one of the best promising device for logic applications for future technology nodes, there is an increased need of characterization technique for such multilayer $Si_{1-x}Ge_x$/ Si complex structures. We studied $Si_{1-x}Ge_x$/Si/Si_{1-x}Gex/Si/$Si_{1-x}Ge_x$/Simultilayer FIN structures using X-Ray Diffraction Reciprocal Space Maps (RSM). RSM is one of the most popular technique to study epitaxial thin-films nanostructures due to straightforward analysis of the data. We found RSM simulations showing sensitivity of nanosheet fin structures dimensions such as pitch-walk (PW), Nanosheet thickness (NST), composition and shape. RSM's provide better means to interpret more complex diffraction measurements than real space constructions. RSMs of $Si_{1-x}Ge_x$/Si multilayer structure has been simulated using Bruker JV-RADS v6.5.50/HRXRD software. 1D line profiles extracted from RSMs was also used for the analysis of nanostructures dimensions. We obtained multilayer structure dimensions from the published information. We studied the influence of nanostructure parameters PW, NST, Composition and shape on RSMs. Imperfect periodic structures impact the intensity modulation of the grating rods (GRs). We observed that satellite peaks intensity reduces and harmonics peaks intensity enhances as PW increases. Rate of intensity change in higher order peaks is much faster than the lower harmonic peaks. We observed that the spacing between adjacent interference fringes in RSMs is related to the thickness of the layers. The period of fringes is inversely proportional to the thickness of the layer, hence total FIN height can be determined. 1D line profiles along Q_z shows decreased angular width and increase in intensity of the layer peak and interference fringes as NST increases. Symmetric 004 longitudinal RSMs and their line profiles clearly show layer peak shift from substrate peak as composition increases due to increase of SiGe lattice spacing along the growth direction. Cross-shaped GR pattern in RSMs is observed which is due to trapezoidal surface grating caused by SWA. Line profiles indicate that fin shapes influence the modulation of the GRs as a function of Q_x. We demonstrate the characterization of complex $Si_{1-x}Ge_x$/ Si multilayers using RSMs and their line profiles which are relevant for lateral nanowire and nanosheet FETs. Above findings from RSM simulations clearly indicate the influence of variations in structural dimensions.

9:00am **EM+2D+AS+MI+MN+NS+TF-WeM4 Nanoscale Depth and Lithiation Dependence of V_2O_5 Band Structure by Cathodoluminescence Spectroscopy**, ***Mitchell Walker**, N. Pronin,* The Ohio State University; *A. Jarry, J. Ballard, G.W. Rubloff,* University of Maryland, College Park; *L.J. Brillson,* The Ohio State University

Vanadium pentoxide (V_2O_5) has attracted considerable interest for its potential use as a cathode for solid state lithium ion batteries. While researchers have studied the V_2O_5 lithiation charge/discharge cycle for over two decades, we are only now able to measure directly its electronic band structure from the surface to the thin film bulk and its changes with Li intercalation on a near-nanometer scale. We used depth-resolved cathodoluminescence spectroscopy (DRCLS) to monitor the changes in electronic structure from the free surface to the thin film bulk several hundred nm below. DRCLS measures optical transitions at 1.8-2, 3.1-3.2, 3.6-3.7, 4.0-4.1, and 4.6-4.7 eV between multiple conduction bands to the pristine (α) V_2O_5 valence band maximum in excellent agreement with $V_{3d}t_{2g}$ conduction band densities of states (DOS) predicted by density functional theory (DFT).[1] Triplet conduction band states at 1.8, 1.9, and 2 eV correspond to predicted V $3d_{xy}$–O_c $2p_x$/$2p_y$ hybridized states resulting from strong deviations of the unit cell VO_6 octahedra from cubic coordination correspond to optical absorption edges along the 3 crystallographic axes. With excitation depth increasing from < 10 to 125 nm calibrated by Monte Carlo simulations, the relative amplitudes and energies of these states change, signifying gradual changes in octahedral distortion. The band structure changes significantly with Li intercalation into $Li_xV_2O_5$ for x = 0, 1, and 2. Lithiation gradually removes the hybridized band and introduces a 2.4-2.7 eV V_{3d} t_{2g} band extending 50 nm (x=1) or 25 nm (x=2) into the surface. Higher (4.0 and 4.4 eV) features possibly related to a secondary phase dominate the spectra deep inside all V_2O_5 films near the battery electrode. Delithiation reintroduces the 1.8-2 eV split-off band although significantly narrowed by octahedral distortions. Overall, DRCLS shows that

the lithiation cycle alters the V_2O_5 band structure on a scale of 10-100's of nm with lithiation. The direct measure of V_2O_5's electronic band structure as a function of lithiation level provided by DRCLS can help guide future battery engineering work as more efficient lithium ion batteries are developed. In particular, these unique electrode measurements may reveal in what ways lithiation changes V_2O_5 irreversibly, as well as reveal methods to extend solid state battery life. MW and LJB acknowledge support from NSF grant DMR-18-00130. AJ and GR acknowledge Nanostructures for Electrical Energy Storage (NEES), a Department of Energy Office of Science Frontier Research Center.

1. V. Eyert and K.-H. Höck, "Electronic structure of V_2O_5: Role of octahedral deformation," Phys. Rev. B 57, 12727 (1998).

11:00am **EM+2D+AS+MI+MN+NS+TF-WeM10 Hot Electron Emission from Waveguide Integrated Graphene***, **Ragib Ahsan**, F.R. Rezaeifar, H.U. Chae, R. Kapadia,* University of Southern California

From free electron laser sources to electronic structure measurements, electron emission devices play an important role in a wide range of areas. Photoemission is one of the basic processes exploited in modern electron emission devices. However, higher-order processes like multiphoton absorption or optical field induced emission are necessary for efficient photoemission from high workfunction metallic emitters. Our work demonstrates a graphene emitter integrated on a waveguide that can evanescently couple with the photons delivered from a CW laser (405 nm) and registers photoemission at a peak power that is orders of magnitude lower than previously published results based on multiphoton and optical field induced emission processes. Coupling FDTD analysis of the waveguide to a rigorous quantum mechanical study of the scattering mechanisms and the tunneling processes in graphene, we have been able to model the emission current from the graphene emitter with good agreement to the experimental data. Our investigation reveals that the photoexcited electrons can go through three mutually competitive processes: (i) electron-electron scattering (ii) electron-phonon scattering and (iii) directly emission into the vacuum. Absorption of a photon causes a reduction in the tunnel barrier seen by the electron and the emission rate increases exponentially. Integration of graphene to the waveguide enables evanescent coupling between electrons and the photons causing almost 100% absorption of the photons. Our integrated photonics approach demonstrates an emission efficiency that is three orders of magnitude greater than free space excitation. These results suggest that integrating photonic elements with low dimensional materials such as 2D materials, nanoparticles, quantum dots, etc. can provide a new domain of efficient electron emission devices and integrated photonics.

11:20am **EM+2D+AS+MI+MN+NS+TF-WeM11 Imaging Candidate Nanoelectronic Materials with Photoemission Electron Microscopy (PEEM)***, **Sujitra Pookpanratana**, S.W. Robey,* National Institute of Standards and Technology (NIST)*; T. Ohta,* Sandia National Laboratories

The drive to produce smaller and lower power electronic components for computing is pushing the semiconductor industry to consider novel nanoscale device structures, not based solely on crystalline silicon. Continued innovation and progress towards novel nanoelectronic materials and devices in turn requires metrologies sensitive to electronic properties at these length scales. Tip-based imaging techniques provide electronic contrast with sub-nanometer resolution, however it is a local, scanning-based technique. Photoemission (or photoelectron spectroscopy) is the dominant technique to provide detailed electronic band structure information- level energies, dispersion, polarization dependence, etc. – but typically requires materials with millimeter, or larger, length scales. Photoemission electron microscopy (PEEM) can be employed to allow access to this vital information, providing full-field imaging capabilities sensitive to a variety of electronic contrast mechanisms at 10's of nanometers length scales. Here, we will present our results on imaging the impact of molecular dopants on multilayer tungsten disulfide (WS_2) employing the PEEM at the Center for Integrated Nanotechnologies within Sandia National Laboratories. We will also discuss the commissioning of a recently installed PEEM to perform complementary measurements at NIST-Gaithersburg.

Technological commercialization of transition metal dichalcogenides (TMDs) in nanoelectronics devices requires control of their electronic properties, such as charge carrier type and density, for specific device functionality. Conventional techniques for doping are problematic for atomically thin 2D materials. The sensitivity of mono- to few-layer (TMDs) to their local environment and interfaces can be employed *via* surface doping of molecules on TMDs to provide a promising route toward controllable doping. Investigations of surface doping for one to few layer WS_2 were performed using mechanically exfoliated WS_2 on a SiO_2/Si substrate that was then exposed to tris(4-bromophenyl)ammoniumyl hexachloroantimonate, a p-dopant molecule. PEEM was performed before and after p-dopant exposure. After doping, we find that the contrast of the surface WS_2 physical features change and valence band edge shifts about 0.8 eV away from the Fermi energy, consistent with p-doping. We will discuss the effects of molecular doping in terms of homogeneity and surface features across multiple WS_2 flakes. Lastly, we will discuss commissioning of a new PEEM instrument installed at NIST in 2019, using results of graphene to demonstrate imaging capability and energy resolution of this instrument.

11:40am **EM+2D+AS+MI+MN+NS+TF-WeM12 Comparison of Features for Au and Ir Adsorbed on the Ge (110) Surface***, **Shirley Chiang**,* University of California, Davis*; R.K. Xie, H.Z. Xing,* Donghua University, China*; T.S. Rahman,* University of Central Florida*; C.Y. Fong,* University of California, Davis

Two ad-atoms of Au and Ir adsorbed, respectively, on the Ge(110) surface are studied by a first-principles algorithm based on density functional theory. The surface is modeled by a slab consisting of 108 Ge atoms with a 10 Å vacuum region. Hydrogen atoms are used to saturate the dangling orbitals at the other side of the vacuum region. Two cases of Au adsorption and one case of Ir are reported. The case of Ir has a large binding energy because of its small atomic size compared with the Ge atom, and the partially filled d-states. The total energy for each case is given, as are the energies for removing one ad-atom at a time and also both ad-atoms. The binding energy of each case is obtained by simply taking the energy difference between these configurations; this method is more realistic because the experimental data measured by LEEM and STM indicate that the collective motions of the ad-atoms do not allow the surface to relax to its equilibrium state.[1] For a large separation in the case of two Au atoms, there is a smaller binding energy than for one ad-atom. This can relate to the fact that the collective motions seen experimentally do not happen at a full monolayer coverage of ad-atoms.[1] Additional comparisons will be made to an atomic model for Ir/Ge(111) from STM measurements.[2]

[1] B. H. Stenger et al., Ultramicroscopy, 183, 72 (2017).

[2] M. van Zijll et al., Surf. Sci. 666, 90, (2017).

Support from NSF DMR-1710748 (SC, CYF); NSF DMR-1710306 (TSR); National Natural Science Foundation of China Grants 61376102, 11174048 and computational support from Shanghai Supercomputer Center (RKX, HZX).

12:00pm **EM+2D+AS+MI+MN+NS+TF-WeM13 Reference Materials for Localization Microscopy***, C.R. Copeland, R.G. Dixson, L.C.C. Elliott, B.R. Ilic,* National Institute for Science and Technology (NIST)*; D. Kozak, K.-T. Liao,* FDA, National Institute for Science and Technology (NIST)*; J.A. Liddle,* NIST Center for Nanoscale Science and Technology*; A.C. Madison,* National Institute for Science and Technology (NIST)*; J.-H. Myung,* FDA*; A. Pintar, **Samuel Stavis**,* National Institute for Science and Technology (NIST)

As the diffraction limit fades away into the history of optical microscopy, new challenges are emerging in super-resolution measurements of diverse systems ranging from catalysts to therapeutics. In particular, due to common limitations of reference materials and microscope calibrations, many localization measurements are precise but not accurate. This can result in gross overconfidence in measurement results with statistical uncertainties that are apparently impressive but potentially meaningless, due to the unknown presence of systematic errors that are orders of magnitude larger. To solve this fundamental problem in measurement science, we are optimizing and applying nanofabrication processes to develop reference materials for localization microscopy, and demonstrating their use in quantitative methods of microscope calibration.

Our program consists of two complementary approaches. In the first, involving applied metrology, we are developing reference materials such as aperture arrays that can serve as standalone artifacts for widespread deployment. This approach will require the application of critical-dimension metrology to establish the traceability of master artifacts, and their use to calibrate a super-resolution microscope for high-throughput characterization of economical batches of reference materials. In the second approach, involving fundamental research, we are demonstrating the application of reference materials and calibration methods in our own experimental measurements. Most interestingly, achieving vertical integration of our two approaches and the unique capabilities that result, we are building reference materials into measurement devices for in situ calibration of localization measurements for nanoparticle characterization.

.

New Challenges to Reproducible Data and Analysis Focus Topic
Room A124-125 - Session RA+AS+CA+PS+TF-WeM

Reproducibility in Science and Engineering, Including Materials and Energy Systems

Moderators: Karen Gaskell, University of Maryland, College Park, Svitlana Pylypenko, Colorado School of Mines

8:00am **RA+AS+CA+PS+TF-WeM1 Reproducibility and Replicability in Science and Engineering: a Report by the National Academies*, Dianne Chong,*** Boeing Research and Technology (Retired) **INVITED**

One of the pathways by which scientists confirm the validity of a new finding or discovery is by repeating the research that produced it. When a scientific effort fails to independently confirm the computations or results of a previous study, some argue that the observed inconsistency may be an important precursor to new discovery while others fear it may be a symptom of a lack of rigor in science. When a newly reported scientific study has far-reaching implications for science or a major, potential impact on the public, the question of its reliability takes on heightened importance. Concerns over reproducibility and replicability have been expressed in both scientific and popular media.

As these concerns increased in recent years, Congress directed the National Science Foundation to contract with the National Academies of Science, Engineering, and Medicine to undertake a study to assess reproducibility and replicability in scientific and engineering research and to provide findings and recommendations for improving rigor and transparency in research.

The committee appointed by the National Academies to carry out this task included individuals representing a wide range of expertise: methodology and statistics, philosophy of science, science communication, behavioral and social sciences, earth and life sciences, physical sciences, computational science, engineering, academic leadership, journal editors, and industry expertise in quality control. Individuals with expertise pertaining to reproducibility and replicability of research results across a variety of fields were included as well.

This presentation will discuss the committee's approach to the task and its findings, conclusions, and recommendations related to factors that influence reproducibility, sources of replicability, strategies for supporting reproducibility and replicability, and how reproducibility and replicability fit into the broader framework of scientific quality and rigor.

8:40am **RA+AS+CA+PS+TF-WeM3 Directly Assessing Reproducibility in Materials Chemistry Research Using Literature Meta-analysis*, David Sholl,*** Georgia Institute of Technology **INVITED**

While it is widely agreed that making reported research more reproducible is a desirable goal, less is known about how reproducible current work in materials chemistry is. I will discuss using literature meta-analysis as a tool to obtain quantitative insight into the reproducibility of materials chemistry experiments. Case studies will be discussed involving measurements of gas adsorption in metal-organic frameworks and the synthesis of metal-organic framework materials. These are useful examples to study because comprehensive databases of information from the open literature are available, but they share features that are common in many areas of material chemistry. Insights from these case studies suggest possible paths towards improving data reproducibility for individual researchers, for academic departments and for professional organizations.

9:20am **RA+AS+CA+PS+TF-WeM5 Reproducibility in Fundamental and Applied Science*, George Crabtree,*** Argonne National Laboratory, University of Illinois at Chicago **INVITED**

The scientific enterprise operates via a few basic features, including questions, insight, hypotheses, critique, reproducibility, elaboration and revision. All contribute to the process of discovery, none can be taken as the single signature of scientific truth. Discovery science is a dynamic process informed by new observations and continuous refinement of the precision, accuracy, principals and scope of our collective scientific knowledge. History has many examples of significant revisions of previously accepted dogma based on new observations (the earth is flat, matter is infinitely divisible, the stars are fixed). New insights lead to new fundamental principles (energy is conserved, nothing can go faster than light, germs cause disease) that open new opportunities for advancing the scientific frontier and raising the quality of life. Examples of advances of the frontiers of energy science and their implications for reproducibility will be given.

11:00am **RA+AS+CA+PS+TF-WeM10 Representativeness of a TEM image for Revealing New Phenomenon in Energy Storage Materials*, Chongmin Wang,*** Pacific Norththwest National Laboratory*; D.R. Baer,* Pacific Northwest National Laboratory

Transmission electron microscopy (TEM), as a imaging technique with high spatial resolution, appears to be a routine tool for showcasing, often viewed as an enlightening figure, the structural and chemical information of materials at multiscale of down to single atomic column. One of a very common questions that raised by the viewer, not necessarily suspicious, is the representativeness of the image to the real situation as considering the sampling scale of the TEM imaging method. This question is further elevated for the case of in-situ and operando observation as which naturally couples in another dimension of “time” in addition to the “spatial” scale. In addition, beam effect can be coupled in for artifacts. In this presentation, we will check into the reproducibility of TEM imaging of both in-situ and ex-situ for revealing new phenomenon in energy storage materials, while certain cautions may also be necessary for interpreting new observations based on TEM.

11:20am **RA+AS+CA+PS+TF-WeM11 Reproducibility Issues when Developing Catalysts for Fuel Cell Applications**, *M.J. Dzara, S.F. Zaccarine,* Colorado School of Mines*; K. Artyushkova,* Physical Electronics and University of New Mexico*; **Svitlana Pylypenko,*** Colorado School of Mines

This talk will discuss reproducibility issues encountered during the development of novel catalysts for low temperature fuel cell performance (PEMFC) as replacements of state-of-the-art catalysts that contain Pt-based nanoparticles supported on a high surface area carbon support. Examples across several catalytic systems will be shown, including low platinum-group metal (low-PGM) catalysts with extended surfaces derived from nanowire templates, and PGM-free catalysts based on N-doped carbon with an atomically dispersed transition metal.

Reproducibility issues related to the synthesis of these catalytic materials and their impact on the performance of these catalysts will be reported first following by discussion of challenges in characterization. Specifically, the need for complementary characterization will be highlighted along with issues that arise when materials are characterized by different groups using different techniques. Another set of reproducibility issues arises when conducting characterization of catalysts under in-situ and in-operando conditions.[1] The time constraints imposed by the availability of instrumentation result in datasets that have a limited number of samples, areas per samples and replicate measurements on the same sample.

(1) Dzara, M. J.; Artyushkova, K.; Shulda, S.; Strand, M. B.; Ngo, C.; Crumlin, E. J.; Gennett, T.; Pylypenko, S. Characterization of Complex Interactions at the Gas − Solid Interface with in Situ Spectroscopy : The Case of Nitrogen-Functionalized Carbon. *J. Phys. Chem. C***2019**, *123* (14), 9074–9086.

11:40am **RA+AS+CA+PS+TF-WeM12 Challenges in Multimodal Spectroscopic Analysis of Energy Storage Materials*, Vijayakumar Murugesan,*** Pacific Norththwest National Laboratory*; K.T. Mueller,* Joint Center for Energy Storage Research (JCESR) **INVITED**

Charge transfer across heterogeneous interfaces facilitated by redox reactions is the basis of energy storage technology. Capturing the interfacial processes over broad scales both spatially (ranging from angstroms up to 100 nm) and temporally (lasting from fs up to a few minutes) is a major challenge. This is one origin of the existing knowledge gaps in energy storage materials, which impede our ability to predict and control the emergent behaviors at electrochemical interfaces. As part of Joint Center for Energy Storage Research (JCESR) center, we developed a multi-modal in situ characterization tool set based on X-ray absorption, photoelectron and multinuclear NMR spectroscopy in combination with computational modelling that can access a range of the important complex processes. This multimodal approach helps us gain critical insights of the charge transfer process, but also presented unique challenges in data collection, analysis and reproducibility. The multitude of constituents and varying surface chemistry combined with external stimuli (applied potential and temperature) challenges the traditionally conceived time and spatial resolution limitations of the probes. For example, establishing reference systems and base line measurements for electrochemical process where combinatorial constituents react and depend on the charge state is a major challenge in spectroscopic studies and complicates subsequent corroboration with computational analysis. In this talk, we will discuss

overcoming these challenges and apply the methods to critically analyzing solid-electrolyte interphase (SEI) evolution in Li-metal based batteries, multivalent ion transport across membranes and chemical stability of redox flow battery electrolytes.

Thin Films Division
Room A122-123 - Session TF1-WeM

Vapor Deposition of Functional Polymer Thin Films and Composites

Moderators: Adrienne Stiff-Roberts, Duke University, John (Jack) Lyons, U.S. Naval Research Laboratory

8:00am **TF1-WeM1 Durable Surface Energy Control with Initiated Chemical Vapor Deposited (iCVD) Polymers***, **Karen Gleason**,* Massachusetts Institute of Technology **INVITED**

Multiple iCVD homopolymer and co-polymer compositions have been employed for the tuning of surface energy from ultrahydrophobic to ultrahydrophilic and for fine-tuning the surface energy over much narrow ranges as well. The iCVD approach is particularly valuable for insoluble materials, including low-surface energy fluoropolymers and durable crosslinked networks. The iCVD surface modification layers can be ultrathin (<20 nm) and are able to conformally cover geometric features in the substrate. For iCVD poly(divinylbenzene) (PDVB), this combination of features enabled the controlled wetting and directed self-assembly of block co-polymers inside of confined features. Ultrathin and conformal iCVD fluoropolymers on aligned carbon nanotube stamps prevent densification of the stamp upon drying, enabling high-speed flexographic printing with nanoparticle inks.

Since film growth proceeds upwards from the substrate, iCVD offers the opportunity for interfacial engineering prior to beginning iCVD synthesis. Indeed, linker-free graftingcan be achieved in situ immediately prior to the iCVD growth on substrates from which hydrogen atoms can be abstracted. Linker-free grafted cross-linked PDVB layers display outstanding robustness and have served as a base layer for a covalent attached top layer of iCVD fluoropolymers. The grafted PDVB/fluoropolymer bilayers provide resistance against the attachment of ice and natural gas hydrates and even proved durable when sandblasted. Grafting is essential for tethering swellable hydrophilic surface modification layers. Indeed the durability of iCVD hydrogels and zwitterionic layers is greatly enhanced by grafting for the prevention of delamination.

8:40am **TF1-WeM3 Initiated Chemical Vapor Deposition of poly(N-vinylcaprolactam)-based Cross-linked Smart Hydrogel Thin Films with Tunable Temperature-responsive Swelling Behavior***, **Fabian Muralter**, A. Perrotta, A.M. Coclite,* Graz University of Technology, Austria

Initiated Chemical Vapor Deposition (iCVD) makes it possible to deposit smart hydrogel thin films conformally into 3D-nanostructures for sensor applications. For this contribution, cross-linked p(N-vinylcaprolactam)-based (pNVCL) thin films were synthesized by iCVD for the first time. In aqueous environment, the phase transition of these polymeric systems between a “hydrophilic” swollen state below to a “hydrophobic” shrunken state above their lower critical solution temperature (LCST) was investigated via spectroscopic ellipsometry. As previously shown for other polymers, the amount of cross-linking has been used to tune the temperature-responsive behavior of the deposited pNVCL-based systems. Interestingly, pNVCL is also reported to show decreased transition temperatures for higher molecular weight systems. Thus, by changing the filament temperature during iCVD, it was possible to lower the LCST by almost 20°C, without changing the (nominal) composition. Overall, degrees of maximum swelling of the polymer below the transition temperature of up to 250% of the dry thickness could be achieved and the LCST could be tuned in the range of 16-40°C. For probing the applicability in sensor setups, these systems were also investigated in terms of swelling in humid environment (relative humidity, RH). There, three regions could be identified: First, in rather dry environment, the systems respond by mainly filling porosity, but not showing a temperature-responsive behavior. Second, up to ~80% RH, the response in swelling is close to linear to the measured RH. Third, in very humid environment, the swelling is highly non-linear and temperature-dependent. Moreover, the film thickness approaches the value that can be observed also when the polymer is immersed in water at the respective temperature. Furthermore, the response of the polymer in water as well as in humid environment has been shown to be very fast, as, for example, it responds faster than the commercial sensor used for monitoring the RH in the measurement cell. Together with the biocompatibility reported for pNVCL, the knobs of filament-temperature and cross-linking to tune the described features of the temperature-responsive swelling behavior of these systems make them highly promising for biomedical or environmental (sensor) applications.

9:00am **TF1-WeM4 Promotion of Crystalline Polyfluorene Domains in Thin Films Deposited by RIR-MAPLE***, **Spencer Ferguson**, B. Zhang, A.D. Stiff-Roberts,* Duke University

An important goal for functional polymer thin film deposition is to selectively deposit semi-crystalline phases to enable unique properties. As a specific example, semi-crystalline β-polyfluorene (β-PFO) could improve the performance of blue polymer light emitting diodes (LEDs) due to better color purity and enhanced charge conduction. However, it has been challenging to directly investigate the impact of this crystalline phase on the performance of PFO-based LEDs films deposited by spin-casting due to poor surface quality with prominent pinholes resulting from the poor solvents or additives used to promote β-PFO[1,2]. Previous work[3] has shown that emulsion-based, resonant infrared matrix-assisted pulsed laser evaporation (RIR- MAPLE) enables deposition of pinhole-free thin films containing β-PFO.

In order to further study the ability of the emulsion target used in RIR-MAPLE to promote the deposition of β-PFO, the emulsion surfactant will be investigated to study the impact of the polarity difference between the primary PFO solvent (trichlorobenzene) and the water within the emulsion. The standard surfactant used in RIR-MAPLE is sodium dodecyl sulfate, and it has a single hydrophobic tail. In a reported study on PFO, phospholipids were used to form a lamellar structure within an emulsion to drop cast films with high concentrations of β-PFO[4]. In contrast to SDS, the phospholipid surfactant has multiple hydrophobic tails, which could significantly impact the formation of β-PFO by RIR-MAPLE. In addition, sodium alkyl aryl sulfonate will be investigated as a surfactant to determine the impact of aromatic rings on the promotion of β-PFO. As a second study, the annealing of deposited films below the glass transition temperature of PFO will be investigated to determine the impact on β-PFO concentration and the overall film morphology.

For each study, UV-Vis absorbance, photoluminescence, and surface morphology will be characterized. This work will provide a path to the fabrication of thin films containing greater concentrations of β-PFO for inclusion as the active region in blue polymer LEDs.

This material is based upon work supported by the National Science Foundation under Grant No. NSF CMMI-1727572.

1. J. Peet, E. Brocker, Y. Xu, and G. C. Bazan, Adv. Mater. **20**, 1882 (2008).

2. B. Liu, T. Li, H. Zhang, T. Ma, J. Ren, B. Liu, J. Lin, M. Yu, L. Xie, and D. Lu, J. Phys. Chem. C **122**, 14814 (2018).

3. S. Ferguson, C. V. Williams, B. Mohapi, and A. D. Stiff-Roberts, J. Electron. Mater. **48**, 3388 (2019).

4. M. J. Tapia, M. Monteserín, H. D. Burrows, J. S. Seixas De Melo, J. Pina, R. A. E. Castro, S. García, and J. Estelrich, J. Phys. Chem. B **115**, 5794 (2011).

9:20am **TF1-WeM5 Conductive Directly Fused Poly (Porphyrin) Coatings by an Oxidative Chemical Vapour Deposition Approach***, **Kamal Baba**, G. Bangasi, G. Frache, D. El Assad, J. Desport,* Luxembourg Institute of Science and Technology, Luxembourg*; K. Heinze,* Johannes Gutenberg University of Mainz, Germany*; N.D. Boscher,* Luxembourg Institute of Science and Technology, Luxembourg

Thanks to their remarkable functional properties, porphyrinic compound led to the development of various technological applications, including photovoltaic[1] catalysis[2] and sensing.[3] Among this porphyrinic compounds, conjugated and directly fused porphyrins attracted strong attention.[4] Indeed, the high conjugation of these systems provides additional interesting functional properties such as two photon absorption, near infrared absorption and enhanced electro-catalytic activity.[5,6] However, while the solution-phase synthesis of directly fused porphyrin coatings has been successfully developed in recent years, the deposition of these promising compounds in thin film form has remained a challenge.

In this work, we report the simultaneous synthesis and deposition of conductive directly fused poly(porphyrin) coatings based on a substrate independent and up-scalable oxidative chemical vapor deposition (oCVD) approach. The direct fusion of nickel(II) 5,15-(diphenyl)porphyrin (NiDPP) is successfully achieved using different oxidants, such as iron(III) chloride ($FeCl_3$), copper(II) chloride ($CuCl_2$) and copper(II) perchlorate hexahydrate ($Cu(ClO_4)_2{\cdot}6H_2O$). The decisive reactions and side reactions during the oCVD

process are evidenced by Lased Desorption Ionization High Resolution Mass Spectroscopy (LDI-HRMS) and UV-Vis-NIR absorption. $FeCl_3$ is demonstrated to be the most suitable oxidant, allowing the formation of singly-fused poly(NiDPP) or conductive doubly or triply-fused poly(NiDPP) that strongly absorb in the near-infrared spectral region. Owing to the highly conjugated structure of the fused tapes, the deposited coatings films exhibit electrical conductivity up to 7×10^{-1} S cm^{-1} and strong absorption in the visible to near-infrared spectral region.

The described approach is not specific to NiDPP, providing the fact that meso-position remains available, other porphyrins can be fused and deposited in thin film form. Interestingly, the developed approach is inherently scalable and readily allows the deposition and patterning of conductive fused porphyrin thin films on sensitive substrates, such as printer paper or polymer foils, paving the way to the integration of directly fused porphyrin into advanced optoelectronic devices.

References:

1. S. Mathew, A. Yella, P. Gao et al., Nat. Chem. 2014, 6(3), 242–7

2. W. Zhang, W. Lai, R. Cao, Chem. Rev. 2017, 117(4), 3717–3797

3. Y. Ding, WH. Zhu, Y. Xie, Chem. Rev. 2017, 117(4), 2203–2256

4. T. Tanaka, A. Osuka, Chem. Soc. Rev. 2015, 44, 943–969

5. H. Mori, T. Tanaka, A. Osuka, J. Mater. Chem. C. 2013, 1, 2500–2519

6. D. Khusnutdinova, B.L. Wadsworth, M. Flores et al., ACS Catal. 2018, 8, 9888–9898

9:40am **TF1-WeM6 Molecular Design and Vapor Phase Synthesis of Crown-Ether-Based Thin Film Materials***, **Darrin Liau**, G.W. Rubloff, S.B. Lee, K. Gregorczyk,* University of Maryland, College Park

Ion transport in materials and at their interfaces plays a profound role in a wide spectrum of applications. These include: energy generation (solar-driven water splitting and fuel cells); energy storage (batteries and capacitors); environmental management (water desalination and purification, and nuclear waste management and remediation); solid-state ionic devices (neuromorphic computing); and a variety of biological systems (ion channels)**.** Here we present an MLD synthesis route to incorporating ion-selective moieties into a thin film, concentrating on the crown ether (CE) family of molecules for their well understood and characterized affinity to selectively bind metal cations in the electron-rich center of the molecule.

Two commercially available crown-ether materials (CE), 1,4,10-Trioxa-7, 13-diazacyclopentadecane(2A15C5) and for 1,4,10,13-tetraoxa-7,16-diazacyclooctadecane (2A18C6), were measured using differential scanning calorimetry (DSC) and thermogravimetric analysis (TGA) to assess their suitability as precursors. The results for both molecules show that vaporization begins at ~100-150C in both cases, leading to evaporation of essentially all the material by ~200-250C. The DSC curves for both materials show heat flow indicative of phase changes in the range of the vaporization temperatures ~100-150°C. Malonyl chloride (MC) was used as an organic linker precursor. In-situ spectroscopic ellipsometry (SE) was used to probe the MLD process parameters, showing a wide temperature window between 75°C-150°C with a linear growth rate ~5-6 Å/cycle. Detailed cycle-by-cycle SE show step-wise growth corresponding to the discrete precursor pulses for the CE and the MC. This allows estimates of thickness added per precursor dose, which include an increase in thickness of ~0.295 nm during the MC pulse and ~0.343 for the 2A15C5 CE pulse, for a total thickness added of ~0.622 nm for a full MLD cycle.

Chemical analysis of the as-grown MLD films was conducted by in-vacuo X-ray photoelectron spectroscopy (XPS). The presumed molecular configuration of CE and MC film is confirmed by the presence of all expected elements in the expected ratios. The O 1s spectrum indicates the presence of two species, consistent with expectations based on the presence of both C-O-C oxygen in the CE ring and C=O oxygen in the MC. The N 1s spectrum shows a single species of N in the film, as predicted from the CE moiety. The C 1s spectrum is more complex but consistent with the structure: on the higher binding energy side, we see a peak associated with N-C=O at ~290 eV, an overlapping C-N and C-O at ~288 eV, and a C-C peaks at ~285eV.

11:00am **TF1-WeM10 Chemical Insolubility of Vapor Phase Infiltrated Poly(methyl methacrylate) / AlOx Hybrid Materials***, **Emily McGuinness**, C.Z. Leng, M.D. Losego,* Georgia Institute of Technology

Vapor phase infiltration (VPI) is a relatively new processing technique used for transforming polymers into organic-inorganic hybrid materials. VPI has been used to improve polymer mechanical properties, protect fabrics from UV and thermal degradation, dope conducting polymers, and act as a contrasting agent in electron microscopy for imaging phases of polymer blends. Recently, our group has explored a new application for VPI, the protection of thermoplastic polymers from solvent dissolution. In this study, poly(methyl methacrylate) (PMMA) thin films were infiltrated with trimethylaluminum (TMA) and water at different temperatures and to different depths of infiltration. The resultant AlO_x / PMMA hybrid films were then exposed to a variety of solvents to explore their stability. Chemical stability was found to vary non-linearly, with infiltration temperature. Films infiltrated at lower temperatures (70˚C and 100˚C) swelled or partially dissolved in good solvents for neat PMMA, such as toluene or chloroform, and partially dissolved in isopropanol and water, which are not good solvents for PMMA (Fig 1). In comparison, films infiltrated at higher temperatures (130˚C) showed enhanced solvent stability in most solvents, even those that dissolved neat PMMA. The increased solvent resistance is likely due to crosslinking between PMMA functional groups and TMA molecules, a reaction that has been reported to vary with temperature. Due to this variability, PMMA films infiltrated at low temperatures are only partially crosslinked while those infiltrated at high temperatures are fully crosslinked, making them more solvent resistant. The increased dissolution of hybrid films in certain alcohols and polar solvents is hypothesized to result from an interaction between the inorganic crosslinker and the solvent. We also found that complete transformation of the polymer into hybrid material was unnecessary for dissolution resistance at higher temperatures. An infiltration depth of 0.5 mm was sufficient for complete resistance to toluene dissolution at room temperature. For proof-of-concept, we applied this treatment to a quarter inch thick laser-etched PMMA sheet and then exposed it to toluene at 60˚C for 10 minutes. While the design on the neat PMMA version rapidly dissolved, the sheet with a 0.5 mm AlOx / PMMA subsurface layer showed nearly complete retention of its design (Fig 2). In this talk, we will explore these findings and discuss the differences in solvent stability of AlOx / PMMA hybrid materials as a function of temperature as well as investigate the underlying chemical and structural variations that yielded these results.

11:20am **TF1-WeM11 Atomic and Molecular Layer Deposition of Hybrid Mo-thiolate Thin Films***, **Jingwei Shi**, C. MacIsaac, L. Zeng, S.F. Bent,* Stanford University

As a member of the two-dimensional transition-metal dichalcogenides (TMDs) family, MoS_2 has attracted great attention since it possesses unique and desirable properties for optical, electrical, and electrochemical applications. MoS_2 derives many of its interesting properties from its bonding structure, such as its direct band gap from the lack of interlayer interactions, and its good electrocatalytic performance from defect and edge Mo-S sites. Therefore, a material that contains Mo-S motifs while also lacking the long-range order found in MoS_2 may be an interesting system to study.

To this end, we recently reported the synthesis of a Mo-thiolate thin film utilizing a combination of atomic layer deposition (ALD) and molecular layer deposition (MLD) with molybdenum hexacarbonyl and 1,2-ethanedithiol as precursors. ALD and MLD are vapor deposition techniques that may allow engineering of thickness dependent properties through its inherent angstrom-level control. The Mo-thiolate class of materials synthesized previously contained Mo-S bonding as well as aliphatic ethyl carbon chains. In this work, we extend and compare that system with the deposition of Mo-thiolate films containing butyl and benzyl organic linkers. The new process utilizes molybdenum hexacarbonyl and 1,4-butanedithiol or 1,4-benzenedithiol as precursors. The 1,4-butanedithiol and 1,4-benzenedithiol contains the S-R linkages, and the Mo-S linkages are created during each half-cycle reaction. Ellipsometry measurements of film thickness with precursor pulse time show that this system has a saturating growth rate. The measured growth rate is 1.0 Å per cycle for Mo-butanethiolate and 1.5 Å per cycle for Mo-benzenethiolate, at a deposition temperature of 170 °C. X-ray photoelectron spectroscopy (XPS) shows that the material is compositionally similar to the predicted elemental ratios. XPS analysis also shows the presence of Mo(VI) as well as oxygen contamination, suggesting some non-idealities to the process.

Key differences between the Mo-thiolate hybrids and MoS_2 are revealed when post-deposition annealing treatments are performed on the Mo-thiolate films. Due to the existence of carbon linkages in the Mo-thiolate films, the annealed films show signatures in Raman spectroscopy not only of crystalline MoS_2 but also of graphitic carbon. We further explore the differences in optical properties between the three compositionally distinct Mo-thiolates. Through this systematic comparison study, we aim to understand the role of different molecular linkages in the Mo-thiolate

framework, which may be beneficial for the deliberate design of hybrid thin films based on their desired properties.

11:40am **TF1-WeM12 Electroactive Thin Films of Conjugated Polymers: Energy Conversion and Storage***, **Shayan Kaviani**, E. Tavakoli, S. Nejati,* University of Nebraska-Lincoln

Platinum group metals (PGM), transition metals, and metal oxides have been extensively studied as efficient catalysts in electrochemical energy conversion devices. Nonetheless, these catalysts have the drawbacks of susceptibility to poisoning and the high cost. To realize widespread application of cost-effective, clean and renewable energy conversion devices–based on electrocatalytic reactions, e.g. metal-air batteries–there is a need to develop alternative electrocatalysts. Conjugated polymers, as carbon-based metal-free materials possess electroactive properties with tunable optoelectronic properties. Here, we demonstrated a successful method to design and apply thin coats of these polymers on a high surface area gas diffusion layers to develop efficient air-cathode electrode for zinc-air batteries. We use oxidative chemical vapor deposition (oCVD), as a unique liquid-free and substrate-independent technique, and enable cross-coupling reaction of heterocyclic monomers and doping of the resulting films in a single step with high precision. We investigated the properties of a series of thiophene-based conjugated polymers. We used volatile liquid oxidants such as antimony pentachloride and gained control over dehydrocoupling polymerization reactions rate of thiophene derivatives. We showed that our oCVD processing conditions have a direct influence on the properties of the deposited films. By adjusting the oCVD settings, we deposited smooth (roughness factors < 1 nm) and conformal coatings of conjugated polymers on a variety of substrates. We showed that by tailoring the chemistry of monomers, we can tune the electrochemical properties of the oCVD-polymers. For instance, in the case of poly(thiophene) and poly(3,4-ethylenedioxythiophen) (PEDOT), the onsets of the oxygen reduction reaction (ORR) overpotential are measured to be 0.61 V and 0.76 V vs reversible hydrogen electrode (RHE) [1]. Populating the monomer structure with heteroatoms, we recorded an enhanced electroactivity–comparable to Pt/C–for polymeric domains of poly(3,4-ethylenedithiathiophene) (PEDTT). The electron transfer number for ORR in these polymers, follows the trend of electrocatalytic activity; the higher electroactivity, the higher number of electrons transferred. More interestingly, PEDTT shows high electroactivity toward oxygen evolution reaction (OER) with overpotential onset of 1.72 V vs RHE. This observation makes oCVD PEDTT, the first conjugated polymer with bifunctional electroactivity in oxygen reactions.

1. Kaviani, S., et al., *Electroactive and Conformal Coatings of oCVD Polymers for Oxygen Electroreduction.* ACS Applied Polymer Materials, 2019 1 (3), 552-560.

12:00pm **TF1-WeM13 Enhancing the Key Properties of CVD Polymer Thin Films for Device Fabrication***, **Xiaoxue Wang**,* The Ohio State University*; K.K. Gleason,* Massachusetts Institute of Technology

In the last decade, the rapid development of the flexible and stretchable (soft) electronics has been largely fueled by the fundamental breakthrough in soft materials synthesis and new fabrication technologies. Among the soft electronic materials, polymers stand out due to their merits of high stretchability, biocompatibility, light weight, scalability and cost-efficiency. However, despite the great prospects of electronic polymers, several critical challenges still need to be addressed: (1) Key electrical properties, such as electrical conductivity (σ) and carrier mobility (μ) of polymers are still relatively low compared with conventional rigid semiconductors, and result in higher power consumption and lower operation speed; (2) Low thermal conductivity (κ) makes heat dissipation a critical issue; (3) Conventional solution-based processing technologies may pose wettability and compatibility issues for device fabrication on flexible substrates. Here we will present a synergistic approach to combat these challenges by using Chemical Vapor Deposition (CVD) technology as an effective tool. First, record high electrical conductivity (σ) and charge carrier mobility (μ) are achieved in poly(3,4-ethylenedioxythiophene) (PEDOT), with engineered crystallization and morphology implemented by CVD. We also build wafer-scale PEDOT-Si rectifier arrays operating at 13.56 MHz for RFID readers by direct CVD synthesis. Second, record high cross-plane thermal conductivity (>10x common polymers) is demonstrated in intrinsic poly(3-hexylthiophene) (P3HT) thin films by using a self-assembling CVD growth method. This method generates an extended chain structure with π- π stacking, and thereby significantly facilitates the thermal transport. Lastly, CVD's powerful capability in device application, with gas sensors as an example, will be presented. In summary, this work establishes an innovative method to effectively tune the key physical properties of polymers by CVD-based structure-property engineering on the molecular level. In addition, this work also has the potential to facilitate novel device fabrication technologies and applications in artificial skin, bio-degradable sensors, stretchable photovoltaics and light emitting diodes (LEDs).

Thin Films Division
Room B131 - Session TF2-WeM
Thin Film Late News Session

Moderator: Virginia Wheeler, U.S. Naval Research Laboratory

11:00am **TF2-WeM10 Peter Mark Memorial Award Lecture: Molecular Beam Epitaxial Growth of Novel Plasmonic Materials: Heavily-doped Semiconductors and Topological Insulators***, **Stephanie Law**[1],* University of Delaware **INVITED**

Plasmonic devices have great potential to advance the science and technology of photonics by confining light to subwavelength volumes. Traditional plasmonic devices in the visible spectral range have been made using metals like gold, silver, and aluminum. However, in order to create plasmonic devices at infrared and terahertz frequencies, we must look to alternative materials and heterostructures. In this talk, I will discuss our recent results on the molecular beam epiatxy growth of heavily-doped semiconductors for infrared plasmonics and topological insulators for terahertz plasmonics. We find that the morphology of heavily-doped semiconductors is significantly improved with the use of a bismuth surfactant. These improved materials are then incorporated into layered heterostructures that function as infrared hyperbolic metamaterials. These hyperbolic metamaterials show large mode indices and relatively high quality factor simultaneously, laying the groundwork for new infrared plasmonic devices. In addition to our work on semiconductors, I will also discuss our efforts on the growth of topological insulators (TIs) for terhertz plasmonics. We have found that the unintentional doping density can be reduced by a factor of two in TI thin films by growing a trivially-insulating lattice-matched buffer layer between the film and the substrate. These films can then be used as terahertz plasmonic films, which are then able to confine light into spaces 200 times smaller than the free space wavelength. Finally, I will discuss our recent efforts to grow self-assembled TI nanoparticles for use as quantum dots.

11:40am **TF2-WeM12 Impact of Interface Quality on the Strength of Volume Plasmon Polaritons in Hyperbolic Metamaterials***, **Patrick Sohr**, D. Wei,* University of Delaware*; S. Tomasulo, M.K. Yakes,* U.S. Naval Research Laboratory*; S. Law,* University of Delaware

In this work, we investigate doped and undoped semiconductors as alternative materials for hyperbolic metamaterials (HMMs) for applications in the mid to long wave infrared regimes. HMMs are artificial materials composed of subwavelength metallic and dielectric structures. In this work, we focus on layered HMMs, where the metal and dielectric layers are deposited on top of one another. These materials are highly anisotropic with a positive permittivity along one axis and a negative permittivity along the perpendicular axis. This behavior results in an open hyperbolic isofrequency surface, which is theoretically capable of supporting infinitely large wavevectors and a large photonic density of states. These materials have the potential to increase the emission rate of radiative emitters and permit for subwavelength imaging. These capabilities and others have made HMMs an interesting area of study for the fields of optics and optoelectronics.

Initially, HMMs were made using traditional metals (i.e. gold and silver) and paired with traditional dielectrics (i.e. silica and alumina). These materials have been shown to work exceptionally well in the visible to near infrared range. However, in the mid- to long wave infrared, these materials are no longer viable, and an alternative material system is required. One alternative is using doped and undoped semiconductors as the metallic and dielectric layers, respectively. Not only are semiconductors a promising material for the infrared, but also allow for easy integration with current optoelectronic devices.

In this work, we investigate three material systems for use as a semiconductor HMM: Si:InAs/AlSb, Si:InAs/GaSb, and Si:InGaAs/InAlAs. These materials are all grown by molecular beam epitaxy and characterized using Fourier Transform Infrared Spectroscopy. We show that the quality of the high wavevector modes is strongly dependent on the conduction band

[1] **Peter Mark Memorial Award Winner**

offset at the interface of the metal and dielectric layers. The Si:InAs/AlSb, which has the largest conduction band offset, exhibits the strongest and highest quality modes. While the Si:InGaAs/InAlAs and Si:InAs/GaSb, which have smaller conduction band offsets, exhibit weaker modes. This is due to the large wavevector modes within the HMM being comprised of coupled surface plasmon polaritons (SPPs) that exist at the interface of the metal and dielectric layers. When the electronic confinement at the interface is weak, the SPPs are less confined and do not couple as efficiently. Now that we have shown that we can grow high quality semiconductor HMMs, we can investigate some of their phenomenon in the infrared regime.

12:00pm **TF2-WeM13 Transparent Microelectrode Arrays made by Ion Beam Assisted Deposition for Neuronal Cell *in vitro* Recordings***, Tomi Ryynänen,* Tampere University, Finland*; R. Mzezewa, E. Meriläinen, T. Hyvärinen, J. Lekkala, S. Narkilahti, P. Kallio,* Tampere University

Microelectrode arrays (MEAs) are a common measurement platform in various biological *in vitro* studies where neuronal cells or cardiomyocytes are applied e.g. for drug screening, toxicity testing, cell model development or simply for increasing understanding of cell behavior. The field potential or impedimetric measurements, or stimulation performed with MEA are usually complemented with fluorescence imaging or microscopic inspection while or after the MEA recordings. The use of an inverted microscope is preferred, as imaging from the top side is often impossible because of the cell culturing medium and its reservoir placed on top of the MEA. With the inverted microscope there exists, however, another challenge. Typically, the tracks and the electrodes of the MEA are opaque and thus they prevent the full visibility of the cells from the bottom side. Partial solution is to make the tracks from transparent indium tin oxide (ITO) material. However, ITO electrodes are rare, simply because of their relatively high impedance and noise level. Instead, opaque low impedance Pt black or titanium nitride (TiN) electrodes are usually used with ITO tracks. Transparent low impedance graphene or conducting polymer electrodes have been demonstrated, but usually with challenges related to the ease of fabrication and stability. A recent approach is to use a very thin TiN layer made by atomic layer deposition (ALD) [1] or reactive sputtering [2] in the electrodes. The idea is to take benefit from TiN's columnar structure and thus capability of decreasing impedance, but still maintain the transparency, at least to some extent.

In this study, we show that ion beam assisted electron beam deposition (IBAD) is a valid alternative for sputtering and ALD in depositing both transparent ITO tracks and very thin transparent TiN layers for the MEA electrodes. We evaluate the performance of different combinations of ITO tracks and ITO or TiN electrodes, both from imaging and impedance point of view. In the first version, both tracks and electrodes were made of ITO to guarantee full transparency and thus optimal imaging capability. In the 2nd version, ITO electrodes were coated with thin TiN layer to decrease impedance but still maintain (partial) transparency. In the third version the measurement capability was optimized by thick opaque TiN electrodes. The optical transmission and electrical impedance of these three versions were characterized and the biocompatibility of the MEAs was verified by cell experiments with human embryonic stem cell-derived (hESC) neuronal cells.

[1] Ryynänen et al. doi: 10.3389/fnins.2019.00226

[2] Mierzejewski et al. doi: 10.3389/conf.fncel.2018.38.00027

Electronic Materials and Photonics Division
Room A214 - Session EM+2D+NS+TF-WeA

THEME Session: Electronics and Photonics for a Low-Carbon Future

Moderators: Michael A. Filler, Georgia Institute of Technology, Stephen McDonnell, University of Virginia

2:20pm **EM+2D+NS+TF-WeA1 Uncovering the Materials Paradigm for Solar Absorbers through In situ Imaging and Characterization*, Mariana Bertoni,*** Arizona State University **INVITED**

The behavior of solar cells is very often limited by inhomogeneously distributed nanoscale defects. This is the case throughout the entire lifecycle of the solar cell, from the distribution of elements and defects during solar cell growth as well as the charge-collection and recombination during operation, to degradation and failure mechanisms due to impurity diffusion, crack formation, and irradiation- and heat-induced cell damage This has been known for a while in the field of crystalline silicon, but inhomogeneities are far more abundant in polycrystalline materials, and are the limiting factor in thin-film solar cells where grain sizes are often on the order of the diffusion length.

We will show that the high penetration of hard X-rays combined with the high sensitivity to elemental distribution, structure, and spatial resolution offers a unique avenue for highly correlative studies at the nanoscale. We will present results on CdTe and $Cu(In,Ga)Se_2$ where carrier collection is directly correlated to the compositional and structural properties of the material under a large variety of synthesis and operating conditions. The segregation of copper at the grain boundaries of both solar absorbers will be discussed in detail as well as the defects impact to carrier collection efficiency. Furthermore, the kinetics of copper segregation during growth and processing will be presented.

3:00pm **EM+2D+NS+TF-WeA3 Atomic Layer Deposition's Potential in Sustainability*, Karen Buechler,*** ALD NanoSolutions **INVITED**

Atomic layer deposition (ALD) is an exciting thin film deposition technique which holds the promise to permit enormous material innovations. These material innovations are currently enabling advanced catalysts, high capacity energy storage, advanced manufacturing technologies and many other products. Many of these products work towards reducing energy needs. This talk will highlight several examples of advanced material development through ALD which lead to advanced products which in turn are reducing the carbon footprint of consumers and manufacturers.

4:20pm **EM+2D+NS+TF-WeA7 Challenges in Materials and Processing to Implementation of Energy Efficient SiC Technology*, Mei-Chien Lu,*** Monte Rosa Technology

Energy and sustainability have been the main driving forces for the implementation of silicon carbide technology for efficient energy conversion in recent applications in electrical vehicles, hybrid electrical vehicles, data center power management, and photovoltaic and wind power. The decades-long research and development efforts are attributed to the complexity of polytypes of crystal structures of silicon carbide. Reducing these inherent defects from crystal growth and epitaxial layer growth are crucial and continuing tasks. Device architectures are found to be more efficient along selected crystal planes. Innovative processing technologies have to be developed to make these devices built by compound semiconductors with strong covalent bonding manufacturable. Fundamental challenges in materials, devices, and processing technologies will first be briefed. A patent landscape analysis is then conducted herein to reveal the past trends to pave the paths for future research and development. Implementations of silicon carbide devices are in its infancy with some full SiC inverter adopted by a commercial electrical vehicle manufacturer. Market shares and momentum of silicon carbide power electronics as well as the expectations from perspectives of department of energy and industry major players will be discussed. The continuous efforts to address the challenges in materials and processing are encouraged to support the full scale implementation of energy efficient silicon carbide technology.

4:40pm **EM+2D+NS+TF-WeA8 High Efficiency of Hot Electron Transfer at a Metal-Insulator-Semiconductor to Electrolyte Interface*, Hyun Uk Chae,*** *R. Ahsan, Q. Lin, R. Kapadia,* University of Southern California

Hot electrons generated from metal has drawn considerable interest in recent years due to the potential for lowering the high-barrier chemical reactions. The majority of hot electron controlling strategy at present have been plasmonic devices using localized surface plasmon resonance (LSPR). Several works have been done using plasmons to induce the hot electron generation to use as catalysts for chemical reactions like hydrogen evolution reaction (HER). However, the efficiency of those devices is extremely low and the mechanism behind it is quite complicated and remain unclear until now. To take advantage of hot electrons efficiently, properly and simply designed devices are required. Here, we demonstrate the different mechanisms of hot electron transfer in a thin gold film in an Au-Al_2O_3-Si metal-insulator-semiconductor (MIS) junction by modulating Au film thickness, the applied voltage between Au-Si junction. Hot electron injection contributes to modifying the electron distribution inside the Au electrode, which enables HER to be driven more at same overpotential in solution. This work present that the injection of non-equilibrium electrons can shift the onset voltage of HER by ~0.6 V on the gold film in a 0.5 M H_2SO_4 solution. The efficiency of hot electron density efficiency shows ~85% at 2V of MIS junction bias and solution bias of -1.5 V vs Ag/AgCl is also presented. In addition to experimental results, we carried out the 2-D Monte Carlo simulation to track the injected hot electrons to study for the detail behaviors of thermalization mechanism inside the Au region which indicates the rate of HER. Since electrons quickly lose their energy within femtosecond by electron-electron or electron-phonon scattering, it is significant to see how they behave inside the injected medium to understand the reactions more precisely. The high-efficiency of hot electron usage reported here can be an opening towards the creation of practical hot-electron devices, which could be widely applied to the various fields.

5:00pm **EM+2D+NS+TF-WeA9 Integrated Photocathodes for Solar Driven Conversion of Carbon Dioxide to value-added Products***, J.W. Ager,* Lawrence Berkeley Lab, University of California, Berkeley*; **Guru Gurudayal,*** PPG **INVITED**

If renewable power sources such as solar and wind could be used to produce chemical precursors and/or fuels, it would provide an alternative to mankind's unsustainable use of fossil fuels and slow the rate of CO_2 emission into the atmosphere [1,2]. Solar to chemical energy conversion by photoelectrochemical processes is a promising approach to address this challenge. Analogous to photovoltaics [3], driving the uphill redox reactions required for net solar to chemical energy conversion necessitates directional charge transport [4]. Additionally, in order to convert carbon dioxide to hydrocarbons, one must manage multi-electron transfer reactions (e.g. 12 in the case of ethylene and ethanol), and minimize potential losses in all parts of the system [5].

Charge selective contacts can be used to steer direct photo-generated carriers to catalytic sites that perform CO_2 reduction in an integrated photocathode. In contrast to conventional photocathode designs which employ p-type absorbers, we used a back illumination geometry with an n-type Si absorber to permit the use of absorbing metallic catalysts which would otherwise block the light. Back and front interfaces were configured by ion implantation and by surface passivation to achieve carrier selectivity. Surface texturing of the Si was used optimize light absorption on the illuminated side and increase the surface area available for catalysis on the electrolyte side. Selectivity to C-C coupled products was achieved by using hierarchical Au- Ag-Cu nanostructures as electrocatalysts [6].

The photovoltage, 550- 600 mV under simulated 1-sun illumination, confirms the carrier selectivity and passivation of the front and back interfaces. Compared to planar controls, textured photocathodes generate higher current densities, exceeding 30 mA cm^{-2}. Under simulated diurnal illumination conditions, over 60% faradaic efficiency to C_{2+} hydrocarbon and oxygenate products (mainly ethylene, ethanol, propanol) is maintained for several days. By coupling photocathodes to series-connected semi-transparent halide perovskite solar cells, we demonstrated stand-alone, CO_2 reduction with a 1.5% conversion efficiency to hydrocarbons and oxygenates [7].

1. Graves,C.; Ebbesen, S. D.; Mogensen, M.; Lackner, K. S. *Renew. Sustain. Energy Rev.***2011**,*15*, 1–23.

2. Chu, S.; Cui, Y.; Liu, N. *Nat. Mater.***2016**, *16*, 16–22.

3. Wurfel, U.; Cuevas, A.; Wurfel, P. *IEEE J. Photovoltaics***2015**, *5*, 461–469.

4. Osterloh, F. E. *ACS Energy Lett.***2017**, *2*, 445–453.

5. Gurudayal et al. *Energy Environ. Sci.***2017**, *10*, 2222–2230.

6. Lum, Y.; Ager, J. W. *Energy Environ. Sci.***2018**, *11*, 2935–2944.

7. Gurudayal et al. *Energy Environ. Sci.***2019**, *12*, 1068–1077.

5:40pm **EM+2D+NS+TF-WeA11 Modeling of Optical Scattering in White Beetle Scales*, Seung Ho Lee,* *S.M. Han, S.E. Han,* University of New Mexico

Keywords: Light Scattering; Diffusion Approximation

Abstract: Extremely thin "super-white" coatings that reject solar spectrum but radiate through the transparent atmospheric window in mid-infrared have broad implications in heat management and energy savings for diverse sectors, including building construction, ship manufacturing, and space vehicle operation. In our previous work, we were able to create paint-format "super-white" coatings from microsphere-based materials.[1,2] In this work, however, we borrow our inspiration from white beetles in nature that reveal structural ingenuity at the nanometer scale to achieve such white film. White beetle scales display exceptionally strong light scattering power from a thin anisotropic random biopolymer network. While previous studies have revealed that the anisotropy plays an important role in strong light scattering, the physics of anisotropic light propagation remains less than fully understood. In particular, the studies have shown that light scattering in anisotropic random media may deviate significantly from the anisotropic diffusion approximation. This uncertainty in diffusion approximation led to a study interrogating the scale structures by fully solving Maxwell's equations. These calculations yet left questions on their accuracy, as the structural dimensions in perpendicular direction to the incident light were significantly greater than optical wavelengths. In this work, we systematically reduce the structural size in our simulations, using Fourier analysis of the white beetle scale structures. The size reduction enables fast, accurate calculations of light scattering in the biological structures. From these simulations, we find that the diffusion approximation is valid in describing light propagation in the white beetle scales. Further, we derive a light diffusion equation for anisotropic media from the radiative transfer equation and show that the equation for anisotropic diffusion derived in the past studies is inaccurate. We discuss how our newly derived equation can be used for accurate numerical calculations of light scattering and characterizing anisotropic light diffusion.

[1] S. Atiganyanun, J. Plumley, S. J. Han, K. Hsu, J. Cytrynbaum, T. L. Peng, S. M. Han, and S. E. Han, "Effective Radiative Cooling by Paint-Format Microsphere-Based Photonic Random Media," *ACS Photon.* **5,** 1181-1187 (2018).

[2] J. D. Alden, S. Atiganyanun, R. Vanderburg, S. H. Lee, J. B. Plumley, O. K. Abudayyeh, S. M. Han, and S. E. Han, "Radiative Cooling by Silicone-Based Coating with Randomly Distributed Microbubble Inclusions," *J. Photon. Energy* **9,** 032705-1:10 (2019).

Advanced Surface Engineering Division
Room A215 - Session SE+AS+TF-WeA

Nanostructured Thin Films and Coatings

Moderators: Mehran Golizadeh, Montanuniversität Leoben, Austria, Suneel Kodambaka, University of California, Los Angeles

3:00pm **SE+AS+TF-WeA3 Metallic Glass: From Coating to First-Ever Nanotube Arrays*, Jinn P. Chu,*** National Taiwan University of Science and Technology, Taiwan, Republic of China

Thin film metallic glass (TFMG) is a new class of multi-component metallic thin film with unique characteristics, including high strength, high ductility, smooth surface, absence of grain boundaries, low coefficient of friction, and corrosion resistance, though their bulk forms are already well-known for properties because of their amorphous structure. Thin films prepared by physical vapor-to-solid deposition are expected to be further from equilibrium than those prepared by liquid-to-solid melting or casting processes. This is expected to further improve the glass forming ability and widen the composition range for amorphization. In the first part of my talk, I will present some important TFMG properties and applications we have discovered in recent years. Then, the metallic glass nanotubes (MGNTs) on Si fabricated by a simple lithography and sputter deposition process for very large-scale integration is introduced. This first-ever metallic nanotube array is awarded by *American Chemical Society* (ACS) at nano tech Japan 2018 in Tokyo. Like biological nanostructured surfaces, MGNTs show some surprising water repelling and attracting properties. Nanotubes are 500-750 nm tall and 500-750 nm in diameter [1]. The MGNT surface becomes hydrophobic, repelling water. By heating/cooling the array, the surface hydrophobicity is changed. Two examples will be presented in this talk based on modifications of this scheme. First, after modification of biotin, the array acts as a waveguiding layer for an optical sensor. The MGNT sensor waveguide could readily detect the streptavidin by monitoring the shift. The detection limit of the arrays for streptavidin is estimated to be 25 nM, with a detection time of 10 min. Thus, the arrays may be used as a versatile platform for high-sensitive label-free optical biosensing [2]. Second, the array is prepared on a heating device and, with an applied electric voltage to the heating device underneath, so that the arrays are functioned as biomimetic artificial suckers for thermally adhesion response [3].

References

[1] J. K. Chen, W. T. Chen, C. C. Cheng, C. C. Yu and J. P. Chu, Metallic glass nanotube arrays: preparation and surface characterizations, Materials Today, 21 (2018), 178-185.

[2] W. T. Chen , S. S. Li , J. P. Chu , K. C. Feng, J. K. Chen, Fabrication of ordered metallic glass nanotube arrays for label-free biosensing with diffractive reflectance, Biosensors and Bioelectronics, 102 (2018), 129-135.

[3] W. T. Chen, K. Manivannan, C. C. Yu, J. P. Chu and J. K. Chen, Fabrication of an artificial nanosucker device with a large area nanotube array of metallic glass, Nanoscale, 10 (2018) 1366-1375.

3:20pm **SE+AS+TF-WeA4 Tin Oxide Nanoaggregate Fragmentation and Restructuring during Supersonic Impaction based Thin Film Deposition Processes*, Souvik Ghosh,*** *X. Chen, C. Li, B. Olson, C.J. Hogan,* University of Minnesota, Minneapolis

Aerosol deposition (AD) is a versatile technique for printing thin films. During AD, gas-suspended particles are impacted inertially on a target surface at high velocities. Subsonic impaction processes often lead to highly porous, weakly bound depositions. High-speed supersonic deposition, however, can lead to denser, mechanically robust coatings of metals & metal oxides. Supersonic deposition is hence a potential low temperature route to the additive manufacturing of thin films (<1 µm to >10 µm) of a variety of materials.

However, the mechanism of film densification & consolidation remains poorly understood, particularly because AD can function with spherical or fractal-like agglomerated particles, from both dry powder feeds & aerosol synthesis processes. In an effort to better understand AD, we examined the mechanism of thin film formation via supersonic impaction of SnO_2 nanoaggregates on alumina, where we observed the formation of mechanically robust SnO_2 thin films. SnO_2 nanoaggregates were synthesized via flame spray pyrolysis (FSP) of Tin 2-Ethylhexanoate. These nanoaggregates characterized via differential mobility analysis shows a broad size distribution in the 40 nm -300 nm mobility diameter range. X-ray diffraction analysis of as-collected powders confirmed the formation of nano-crystalline SnO_2. To understand morphological changes to aggregates during high speed deposition, a differential mobility analyzer was used prior to deposition to select aggregates within a prescribed mobility diameter. The aggregates were then deposited electrostatically at low velocity (at atmospheric pressure) & supersonic speeds after passing through a 200 µm throat width, slit-type, conically contoured converging-diverging nozzle. With low speed deposition, we observed highly branched, chain like aggregates; while after supersonic deposition, we observed denser aggregates with significantly lower number of particles. Images hence suggest that the aggregates fragment & restructure during supersonic impaction.

Fragmentation & restructuring was quantified by image analysis of TEM images to determine their projected radii of gyration, perimeter, end-to-end distance, & projected area. These four parameters were then compared to those from in-silico projections of quasifractal aggregates, enabling extrapolation of the 3D architectures of deposited particles. Plots of the number of primary nanoparticles in aggregates as functions of their inferred radii of gyration confirmed that supersonic deposition leads to both (1) fewer primary particles per aggregate (fragmentation) & (2) for a given number of primary particles, smaller radii of gyration (restructuring).

4:20pm **SE+AS+TF-WeA7 From Gas-ion to Metal-ion-controlled Irradiation: A Paradigm Shift in the Thin Film Growth by Magnetron Sputtering*, Grzegorz Greczynski,*** Linköping University, Sweden*; I. Petrov, J.E. Greene,* University of Illinois at Urbana-Champaign*; L. Hultman,* Linköping University, Sweden **INVITED**

Ion irradiation is a key tool for controlling the nanostructure, phase content, and physical properties of refractory ceramic thin films grown at low temperatures (T_s) by magnetron sputtering. However, in contrast to gas-ion bombardment, the effects of metal-ion irradiation on properties of these films have not been extensively studied due to (i) low metal-ion concentrations during standard dc magnetron sputtering (DCMS), and (ii) difficulties in separating metal-ion from gas-ion fluxes. These issues were

recently resolved with our development of high–power pulsed magnetron sputtering (HiPIMS), in which pulsed substrate bias is applied in synchronous to the metal-ion-rich portion of each pulse.[1] Careful choice of sputtering conditions allows exploitation of gas rarefaction effects such that the charge state, energy, and momentum of metal ions incident at the growing film surface can be tuned.

The results of time-resolved mass spectrometry analyses performed at the substrate position during HiPIMS and HiPIMS/DCMS co-sputtering of transition-metal (TM) targets in Ar and Ar/N atmospheres are reviewed. Knowledge of the temporal evolution of metal- and gas-ion fluxes is essential for precise control of the incident metal-ion energy and minimizing the role of gas-ion irradiation. Also, covered are the growth of TM nitride and boride alloys by metal-ion synchronized HiPIMS. In contrast to gas-ions, a fraction of which are trapped at interstitial sites, metal-ions are primarily incorporated at lattice sites resulting in much lower compressive stresses. In addition, the closer mass match with the film-forming species results in more efficient momentum transfer and provides the recoil density and energy necessary to eliminate film porosity at low T_s. Several novel film-growth pathways are described: (i) nanostructured N-doped *bcc*-$CrN_{0.05}$ films combining properties of both metals and ceramics, (ii) fully-dense, hard, and stress-free $Ti_{0.39}Al_{0.61}N$, (iii) single-phase cubic $Ti_{1-x}Si_xN$ with the highest reported SiN concentrations, (iv) unprecedented AlN supersaturation in single-phase NaCl-structure $V_{1-x}Al_xN$, (v) a dramatic increase in the hardness, due to selective heavy-metal-ion bombardment during growth, of dense $Ti_{0.92}Ta_{0.08}N$ and $Ti_{0.41}Al_{0.51}Ta_{0.08}N$ films deposited with no external heating, and (vi) simultaneous increase in both hardness and toughness of $Zr_{1-x}Ta_xB_y$ layers deposited with synchronized Ta^+ irradiation.

Finally, $Ti_{1-x}Ta_xN$ alloys grown with no external heating are shown to produce high-quality Cu diffusion barriers and provide excellent corrosion protection for stainless-steel substrates.

[1] G. Greczynski, J. Lu, J. Jensen, I. Petrov, J.E. Greene, S. Bolz, W. Kölker, Ch. Schiffers, O. Lemmer and L. Hultman, J. Vac. Sci. Technol. A 30 (2012) 061504

5:00pm **SE+AS+TF-WeA9 Atomic Layer Deposition of Silver Thin Film on Polydimethylsiloxane (PDMS)**, ***Sarah Hashemi Astaneh**, C. Sukotjo, C.G. Takoudis,* University of Illinois at Chicago

Two types of samples were prepared in this work:

1- Silver coated PDMS

2- Silver coated PDMS with interlayer of TiO_2

For type 1 samples: Silver deposition was done in the costume-built ALD system. (Ag(fod) (Pet_3)) was used as a silver precursor and dimethyl amineborane ((BH_3 ($NHMe_2$)) was used as a reducing agent. Silver bubbler and dimethyl amineborane bubbler temperatures were kept at 96 °C and 50 °C, respectively. The reactor pressure and temperature was kept at 500 mtorr and 115 ˚C during deposition, respectively.

For type 2 samples: prior to silver coating, deposition of TiO_2 on PDMS was done in a commercial ALD system (Kurt J. Lesker 150 LE). Tetrakis (dimethylamido) titanium (IV) (TDMAT™) was used as the metal oxide precursor and maintained at 70 °C in the bubbler during all depositions. Ultra high purity N_2 was used as a carrier gas as well as purging gas. O_3 was used as an oxidizer for this ALD reaction and it was prepared using a UV-ozone generator placed immediately upstream of the deposition chamber to reduce ozone decomposition in delivery line as described in our previous studies. The reactor pressure and temperature was kept at ~1000 mtorr and 120 ˚C during TiO_2 deposition. This process leads to ~9 nm of TiO_2 interlayer on PDMS.

Right after this step, TiO_2 coated PDMS samples were transferred to the custom-built ALD system and silver deposition was carried on in the costume-built ALD system similar to type 1 samples.

In each of the above runs, simultaneously; same thin film was deposited on p-type Si (100) silicon wafer (University wafer Inc, USA) and used as a reference substrate to determine deposited film thickness.

The growth and composition of the silver on top of PDMS samples were analyzed with X-ray photoelectron spectroscopy (XPS) using Kratos AXIS-165 equipped with monochromatic Al Kα X-ray source operating at 15kV and 10 mA. As can be seen in figure 1, Ag 3p, Ag 3d peaks appeared clearly on Si, TiO_2 coated Si and TiO_2 coated PDMS substrates.

5:20pm **SE+AS+TF-WeA10 Use of an Einzel Lens to Enhance Electrohydrodynamic Printing Technology**, ***Matthew Strohmayer*[1]**, *A. Dhall, P. Ramesh, N. Tokranova, C.A. Ventrice, Jr.,* SUNY Polytechnic Institute

Additive manufacturing (AM) shows great promise for both research and industrial applications. The main advantages of AM include limited waste and the ability to build complicated structures. The most common techniques for AM are fused deposition manufacturing, digital light printing, and ink jetting. All of these techniques suffer from resolution and material limitations. Recently, a cost-effective, versatile method of high-resolution printing called electrohydrodynamic (EHD) printing has been introduced. This method allows for spatial resolution in the hundreds of nanometers. This process works similarly to a typical ink jetting system, except instead of the ink/polymer being pushed out of a tip, it is pulled out by an applied electric field. This allows for the resultant droplet to be smaller than the needle diameter. Electrostatic repulsion of the charged droplets limits the ultimate resolution of this technique. To overcome this resolution limitation, we have incorporated an Einzel lens into the system to focus the droplets. This helps the droplets overcome the repulsive Coulomb interaction, leading to better spatial resolution. To validate this approach, simulations were performed to test for different parameters, including droplet size changes and lens optimization. This was then used to build a real system.

Thin Films Division
Room A122-123 - Session TF+EM-WeA

Emerging Thin Film Materials: Ultra-wide Bandgap and Phase Change Materials

Moderators: Cary Pint, Vanderbilt University, Brent Sperling, National Institute of Standards and Technology (NIST), Jin-Seong Park, Hanyang University, Korea

2:20pm **TF+EM-WeA1 MOCVD Growth and Characterization of $ZnGeN_2$-GaN Alloy Films**, ***Benthara Hewage Dinushi Jayatunga**, K. Kash,* Case Western Reserve University*; M.D. Reza, H. Zhao,* The Ohio State University*; O. Ohanaka, R. Lalk,* Case Western Reserve University*; M. Zhu, J. Hwang,* The Ohio State University

$ZnGeN_2$ and GaN are almost lattice matched and both have band gaps of approximately 3.4 eV. A large conduction band offset of ~ 1.4 eV results in a type II band alignment that has great potential for novel device structures. [1,2] For the 50-50 alloy, a slightly positive mixing energy, indicating a tendency toward phase separation, has been predicted. [3] For this mixture the lowest energy configuration is predicted to be an octet-rule-preserving orthorhombic $Pmn2_1$ phase. Other compositions may in principle be made in octet-rule-preserving (and thus lower energy) phases, compared to those that break the octet rule, by random stacking of $ZnGeN_2$ and GaN layers along the orthorhombic *b* axis. [3] Whether random stacking, phase separation, or octet rule violations occur will determine whether, and by how much, the band gap may be tuned with composition, and whether the transport properties are isotropic or anisotropic. The only other work on this alloy reported to date employed a gas reduction nitridation method for synthesis of powders of different compositions, from pure $ZnGeN_2$ to a 50-50 mixture, for photocatalytic applications [4].

Here we report the results of MOCVD growth of this alloy on c-, r-, and a-plane sapphire and c-GaN/sapphire substrates, at temperatures varying from 550 ^{0}C to 700 ^{0}C. Films at the 50-50 composition exhibit better surface morphologies when grown on r-sapphire substrates. Zn incorporation increases with the increase of Ga. The highest growth rate, 3.46 µm/hr, was obtained for a film grown on r-sapphire at 670 ^{0}C and 550 torr, for which a 2θ-ω XRD measurement yielded a wurtzite (110) diffraction peak at 2Ɵ = 57.70^0 with FWHM of 0.76^0 and an RMS surface roughness of ~ 10 nm by AFM. The Hall mobility is 8.19 cm^2/v-s with an n-type carrier concentration of 8.5 x 10^{18} cm^{-3}. Atomic-resolution HAADF-STEM revealed the atomic arrangement of the film near the substrate interface. Introduction of a low-temperature-grown $ZnGeN_2$ buffer layer (480 ^{0}C at 600 torr with low injection of precursors compared to the film growth conditions) led to improved surface morphology and crystal quality, and yielded a room temperature photoluminescence spectrum indicating a band edge at approximately 3.5 eV, close to that predicted for the $Pmn2_1$ phase. [3]

[1] **ASSD Student Award Finalist**

The authors acknowledge support from the National Science Foundation DMREF: SusChEM: grant 1533957.

[1] L. Han, K. Kash, H. Zhao, J Appl Phys **120**, 103102 (2016)

[2] M. R. Karim, H. Zhao, J Appl Phys **124**, 034303 (2018)

[3] B.H.D. Jayatunga, S. Lyu, S. Kumar, K. Kash, W. R. L. Lambrecht, Phys Rev Mat **2** (2018)

[4] T. Suehiro, M. Tansho, T. Shimizu, J Phys Chem **C 121**, 27590 (2017)

2:40pm **TF+EM-WeA2 Device Quality β-Ga2O3 and Related Alloys by MOCVD**, *A. Osinsky, **Fikadu Alema,*** Agnitron Technology, Inc.; *Y. Zhang, A. Mauze, J.S. Speck,* University of California, Santa Barbara; *P. Mukhopadhyay, W. Schoenfeld,* University of Central Florida

We report on the growth of device quality β-Ga_2O_3 and related alloys using MOCVD method. β-Ga_2O_3 thin films are grown using $Ga(DPM)_3$, TEGa and TMGa as Ga sources, and molecular O_2, H_2O vapor, and N_2O as an oxidizer. Films grown from each Ga source had high growth rates with up to 10 m/hr achieved using TMGa [1]. The effect of the oxidizer identity on the growth rate, electron mobility (μ_e), background carrier concentration, surface and crystalline quality of the films will be discussed. Using pure O_2 as an oxygen source, optimal growth conditions have led to the growth of smooth epitaxial UID Ga_2O_3 thin films with a RT μ_e of 176 cm^2/Vs at n~7x10^{15} 1/cm^3 [2]. The highest μ_e of ~3500 cm^2/Vs has been measured at 54 K. C and H impurities have been shown to be below the SIMS detection limit for a wide range of process conditions, whereby films with n~ 2x10^{14} cm^{-3} were demonstrated. We will also present the growth of device quality β-Ga_2O_3 layers doped with Si, Fe, and N impurities. Critical growth conditions influencing the incorporation of these dopants will be discussed. Using optimum growth conditions, controllable doping with a concentration between 10^{15} and 10^{20} 1/cm^3 were obtained for each dopant. In this work, we will also present on the MOCVD growth of $(Al_x, Ga_{1-x})_2O_3$ alloys. The MOCVD process enables the growth of AlGaO at a temperature >800 °C, improving the solubility of Al_2O_3 in β-Ga_2O_3 by preventing the formation of volatile suboxides. The MOCVD reactor used in this work has a unique feature that enables it to minimize premature reaction between the species, thereby improving the Al incorporation. AlGaO alloys with Al content of up to 43 % was obtained. The epitaxial growth of high quality strained β-$(Al, Ga)_2O_3/Ga_2O_3$ heterostructures and superlattices will be discussed. The composition homogeneity, structural quality, surface morphology and electrical properties of the heterostructures will be discussed as a function of growth conditions. Finally, the growth of alloys including β-$(In, Ga)_2O_3$ and ZnGaO using MOCVD and their application for photodetection purposes will be discussed.

[1] F. Alema et al., J. Cryst. Growth, 475, 77(2017).

[2] Y. Zhang et al., APL Materials, 7, 022506 (2019).

3:00pm **TF+EM-WeA3 Development of the β-$(Al_xGa_{1-x})_2O_3$/β-Ga_2O_3 (010) Heterostructures by Plasma-assisted Molecular Beam Epitaxy**, ***James Speck,*** University of California at Santa Barbara **INVITED**

β-Ga_2O_3 is a promising wide bandgap semiconductor for power electronics due to its ~4.8 eV bandgap, reasonable electron mobility, the availability of large area melt grown substrates, and the ability to form heterostructures by alloying on the group III site. In this presentation, we present progress in the plasma-assisted molecular beam epitaxy (PAMBE) growth of β-Ga_2O_3. The presentation will highlight the promise of β-$(Al_xGa_{1-x})_2O_3$/β-Ga_2O_3 heterostructures for lateral devices. We will discuss the growth of β-$(Al_xGa_{1-x})_2O_3$ in the context of the predicted high Al solubility in the β-phase (predicted to be up to ~60-70% for growth temperatures > 800 C). Current experiments limit the Al content to ~25% for coherent growth. We will present detailed analysis of the β-$(Al_xGa_{1-x})_2O_3$ alloys that show the compositions agree between atom probe tomography and high resolution x-ray diffraction. We will highlight a new growth technique, metal oxide catalyzed epitaxy (MOCATAXY), that enables higher growth temperatures due to the addition of an indium catalyst layer that serves both to react with molecular oxygen in the flux and to suppress Ga_2O_3 decomposition via the reaction Ga_2O_3 -> Ga_2O+$^1/_2O_2$. We will demonstrate an increase of growth temperature of ~250 C in comparison to conventional PAMBE growth conditions. We discuss the relative merits and challenges for donor doping in MBE (Si vs. Ge vs. Sn) and options for realizing controllable semi-insulating GaN.

4:20pm **TF+EM-WeA7 Phase-Change Memory: A Quest from Material Engineering Towards the Device Performances**, ***Guillaume Bourgeois**, G. Navarro, M.C. Cyrille, J. Garrione, C. Sabbione, M. Bernard, E. Nolot, E. Nowak,* CEA-LETI, France **INVITED**

In this paper, we provide some examples of how phase–change material engineering can allow targeting specific memory applications. We present the trade-off in Phase–Change Memory between high-speed performance, required in Storage Class Memory applications, and high thermal stability of the amorphous phase at high temperature, mandatory to address automotive embedded applications.

Phase-Change Memory (PCM) is today the most mature among innovative back-end non-volatile memory technologies, thanks to a wide set of interesting features making PCM technology enough versatile to meet different applications' requirements [1]. A PCM device experiences a physical change of a chalcogenide material sandwiched between two electrodes made possible by the current induced Joule heating flowing through the cell. To achieve the amorphous phase, the PCM in the crystalline phase has to be melted, then rapidly quenched (RESET operation). Thanks to the switching phenomenon, the material in the amorphous phase changes abruptly its conductivity starting to be highly conductive, and can recover the crystalline phase thanks to a specific thermal profile during the pulse application, that provides the energy necessary to the atomic reorganization (SET operation). Thereby, PCM thermal stability relies on the magnitude of the activation energy of the crystallization that results from the combination of crystals nucleation and growth phenomena, on which also the device programming speed relies. Thus, a general trade–off exists between the time required for the SET operation and the device data retention performance [2] (Figure 1). Sb-rich GeSbTe compounds are suitable for high-speed performances with a programming time down to tens of ns still ensuring high endurance and scalability, promising for Storage Class Memory applications (SCM) [3]. Reliability at high temperature is the main requirement to target automotive embedded applications. Ge-rich compositions revealed an endurance of 10^7 cycles up to 175 °C and high temperature data retention compatible with embedded standards. We present here the device performance tuning thanks to the phase–change material stoichiometry engineering (Figure 2). Moreover, we highlight the possibility to boost the PCM performances, such as SET speed and Multi Level Cell capability, thanks to dedicated programming strategies [4].

REFERENCES

[1] F. Arnaud et al, "Truly Innovative 28nm FDSOI Technology", IEDM 2018.

[2] G. Navarro et al, "Non-Volatile Resistive Memory", ECS 2016.

[3] V. Sousa et al, "Phase Change Memory", Chapter 7, Springer 2018.

[4] J. Kluge et al, "High Operating Temperature Reliability", IMW 2016.

5:00pm **TF+EM-WeA9 Neuromorphic Materials and Architectures for Dynamic Learning and Edge Processing Applications**, ***Angel Yanguas-Gil,*** Argonne National Laboratory

The ability to dynamically learn and adapt to changes in the environment is one of the hallmarks of biological systems. In the last years there has been a lot of research focused on exploring novel materials, such as those exhibiting memristive behavior, that could enable this type of systems. However, there are comparatively fewer studies focusing on understanding which are the ideal properties that memristive materials should have in order to optimize the performance of architectures capable of dynamic learning. This type of information is crucial to provide design targets for new materials and accelerate the integration of novel devices into architectures optimized for specific applications.

In this work, we identify the subset of the design space of memristive materials that is optimal for dynamic learning applications: in this type of application, a system, in this case a neural network, evolves dynamically and learns as it processes information in real time. This type of behavior is highly desirable for smart sensors or edge processing applications. We have implemented a benchmark architecture consisting of a discrete implementation of spiking neurons where dynamic learning takes place on a set of plastic synapses formed by memristor pairs in a crossbar array. This architecture, which is inspired on the learning center of the insect brain, is capable of dynamically learning standard machine learning datasets such as MNIST and Fashion-MNIST. We have used this model to identify the key properties that memristive materials should have to be optimal dynamic learners, exploring the impact of the kinetics of the memristor's internal state on the system's learning ability, as well as the impact that materials

and device variability and errors in tuning the memristor's internal state have on the system's performance.

The results obtained show that a fine degree of control of the memristor internal state is key to achieve high classification accuracy during dynamic learning, but that, within this optimal region, learning is extremely robust to both device variability and to errors in the writing of the internal state, in all cases allowing for 2σ variations greater than 40% without significant loss of accuracy. Moreover, the dynamics of the internal state can show distinct kinetics depending on the polarity, something that is critical for bipolar memristors. These criteria are significantly different from those required for ReRAM applications or even for neuromorphic applications based on offchip training, where the robustness of reading and writing operations are critical.

5:20pm **TF+EM-WeA10 Atomic Layer Deposited VO_2 Thin Films Towards Modulated Infrared Optoelectronic Devices***, **Virginia Wheeler**, C.T. Ellis, M. Currie, J.R. Avila, M.A. Meeker, A.J. Giles,* U.S. Naval Research Laboratory*; J.D. Caldwell,* Vanderbilt University*; J.G. Tischler,* U.S. Naval Research Laboratory

VO_2 is a phase change material that undergoes a first order crystalline phase transition at a critical temperature (T_c = 68°C), resulting in significant changes in intrinsic electrical and optical properties, especially in the infrared. Optical changes with this phase transition are of particular interest as passive and active components of optoelectronic devices, specifically for thermal regulation and modulated signaling. Realizing this type of device often requires the integration of thin, conformal VO_2 films with complex, non-planar structures (like metamaterials). Thus, atomic layer deposition (ALD) is the ideal deposition method in these cases.

Traditional metal-based plasmonic materials suffer from high optical losses, which has promoted research towards alternative low-loss materials that can support plasmonic-like effects. One such approach employs phonon-mediated collective-charge oscillations (surface phonon polaritons, SPhPs) that are supported by nanostructured polar dielectric materials (SiC, AlN, etc), which inherently are low-loss. Geometric design of the nanostructures enables spectral tuning of resonant features between the longitudinal and tranverse optical phonons of the polar material, typically in the infrared regions. However, the spectral position and amplitude of these resonances remain fixed after fabrication. Integrating phase change materials with these structures provides a way to achieve active modulation of resonances.

In this work, nanopillar arrays were etched into SiC and AlN to create narrowband resonances in the long-wave infrared region. These structures were subsequently coated with ALD VO_2 films with different thicknesses (8-75nm). As-deposited VO_2 films are highly conformal and amorphous, and cause the resonances to shift and broaden due to the different dielectric environment. However, after annealing the films at 525°C in $6x10^{-5}$ Torr, the VO_2 films crystallize resulting in sharper resonances and spectral locations close to the initial uncoated structures. Temperature-dependence reflectance and emission measurements show that by heating through the VO_2 transition temperature, the amplitude of the resonances can be modulated. Full signal modulation (ie. on/off) requires at least a 16nm VO_2 film. This work shows the ability to actively tune surface phonon polariton resonances using ALD phase change materials.

5:40pm **TF+EM-WeA11 Deposition Process for Vanadium Dioxide Thin Films for RF Applications***, **Mark Lust**, S. Chen, N. Ghalichechian,* The Ohio State University

Phase change materials (PCM) are attractive due their tunability, wide range of applications, and quasi-passive actuation as compared to traditional active integrated circuits. Vanadium dioxide (VO_2) is particularly appealing because of its high contrast between dielectric and conductive states and the relatively low temperature (68 °C) at which its metal-insulator transition (MIT) occurs. This work details a process for depositing high quality VO_2 thin films on C-plane sapphire wafers as well as alumina (Al_2O_3) buffer layers using atomic layer deposition (ALD) on silicon substrates. We compare resistivity vs. temperature measurements of VO_2 on sapphire with VO_2 on the Al_2O_3 buffer layers both as-deposited and after rapid thermal annealing (RTA) at temperatures ranging from 950 to 1150°C. The VO_2 thin films yielded ratios of resistivity between conductor (heated) and dielectric (room temperature) states of 9.8×10^4 Ω-cm, 5.2×10^3 Ω-cm, and 1.5×10^4 Ω-cm when deposited on crystalline sapphire, amorphous Al_2O_3 buffer layers, and annealed Al_2O_3 buffer layers, respectively. This corresponds to an improvement by a factor of 2.9 in the annealed buffer layers over the amorphous buffer layers. Moreover, we studied various VO_2 thin films using X-ray diffraction, which showed clear indications that the films are highly pure and have a preferred crystal orientation. The deposition process we have developed will allow us to use high quality VO_2 thin films on silicon substrates, especially millimeter-wave devices such as reconfigurable antennas, sensors, and meta-surfaces.

Atomic Scale Processing Focus Topic
Room B130 - Session AP+PS+TF-ThM

Thermal Atomic Layer Etching

Moderators: Eric A. Joseph, IBM T.J. Watson Research Center, Harutyun Melikyan, Micron Technology

8:00am **AP+PS+TF-ThM1 A Challenge for Selective Atomic Layer Etching of Non-volatile Materials Using Organometalic Complex***, **Yoshihide Yamaguchi**, S. Fujisaki, K. Shinoda,* Hitachi, Japan*; H. Kobayashi, K. Kawamura, M. Izawa,* Hitachi High Technologies, Japan **INVITED**

Remarkable progress on atomic layer etching (ALE) for non-volatile materials has been made in recent years. The typical procedure for thermal ALE of non-volatile materials such as HfO_2 is cyclic repetitions of formation and desorption of the organometallic complex at a constant temperature [1]. The most significant problem in thermal ALE is formation of a volatile organometallic complex layer on the surface. The organometallic complex layer prevents diffusion of etching species into the deep at the formation step and must be easily removed at the desorption step. The thermal ALE of La_2O_3, however, is difficult to apply because the organo-lanthanum complexes are easily decomposed by mild heating (< 200 deg. C) and fail to prevent the diffusion. To solve this thermal instability, the authors have applied a thermal cycle ALE [2,3], which is a combination of a formation of the organo-lanthanum complex at a low temperature and a desorption of the complex at a high temperature. In this paper, several results of our challenge for thermal ALE of non-volatile materials using a selective organo-metallization reaction on the surface will be discussed. Some guiding principles for the organo-metallization reaction will also be explained.

A La_2O_3 thin-film sputtering deposited on a SiO_2/Si wafer was used as a sample. First, the La_2O_3 film was exposed to vapor mixture of a diketone and a stabilizer as the etchant gas at below 150 deg. C. Then the sample was annealed up to 250 deg. C. Temperature dependence in the procedure was also evaluated. After these consecutive processes, the sample was analyzed by scanning electron microscopy, X-ray photoelectron spectroscopy. Formation of the organo-lanthanum complex showed temperature dependent quasi-self-limiting characteristics. In the lower temperature range, the self-limiting characteristics enable precise control of the organo-lanthanum complex formation. In the higher temperature range, the continuous characteristics enable a higher etch amount per cycle with high selectivity. Several differences between chemistry with and without a stabilizer in the etching gas will be discussed. The high etching selectivity of La_2O_3 to HfO_2 was also demonstrated. From these findings, we conclude that practical ALE of La_2O_3 has been successfully demonstrated.

[1] Y. Lee et al., Journal of Vacuum Science & Technology A 36, 061504 (2018).

[2] K. Shinoda et al., J. Phys. D: Appl. Phys. 50, 194001 (2017).

[3] Y. Yamaguchi et al., ALE workshop TuM4 (2018).

8:40am **AP+PS+TF-ThM3 Characterization of Isotropic Thermal ALE of Oxide Films and Nanometer-Size Structures***, **Andreas Fischer**, A. Routzahn, T.B. Lill,* Lam Research Corporation

In this work, we have characterized the reaction of aluminum oxide via the DMAC ligand exchange mechanism.

Fluorination studies of aluminum oxide were performed using NF_3, CF_4 or anhydrous HF, respectively. We also explored various methods of fluorination of the oxide surface such as thermal, in-situ or remote plasma, respectively, and found that a sufficient fluorine concentration could be obtained with either of the methods or reactants to enable atomic layer etching (ALE).

To understand reaction kinetics, we examined the interaction of aluminum fluoride (AlF_3) films with DMAC. We found that AlF_3 etched until it was completely consumed by DMAC. An analysis of its temperature-dependence allowed us to extract activation energies for the ligand exchange mechanism.

In a third part we demonstrated the utility of HF/DMAC reaction for isotropic ALE applied to nanometer-size metal oxide structures on wafers. Various metal oxides were etched and selectivities between oxides and potential mask materials were determined.

9:00am **AP+PS+TF-ThM4 Advanced Selective Chemical Dry Etch for Oxide and Si-based Material***, **Li-Hung Chen**, T. Kato, K. Nakahata, K. Takeya,* Tokyo Electron Technology Solutions Limited, Japan

As device features continuously shrink with introducing complex structures and new materials in semiconductor manufacturing, extremely high selectivity for etch processes have become more and more important. High selective chemical dry etch is developed utilizing a separated damage-free chemical removal chamber and sublimation chamber. The required selectivity is realized by using various chemistries and quantum mechanics analysis.

Firstly, HF/NH3 chemistry is used for oxide etch with high selectivity to SiN, Si, metals and resist. On the other hand, HF mono chemistry can etch SiN with high selectivity to oxide and Si. Quantum mechanics analysis revealed that NH_3 combined with HF enhances the SiO_2 reaction because of its lower activation energy. However, HF mono chemistry enhances the SiN reaction because of its lower activation energy than the oxide reaction[1)]. Secondly, Gas A chemistry is introduced for etching low quality oxide with selectivity >50 to both high quality oxide and SiN. The reaction rate barrier determined by quantum mechanics shows that etch reactivity with ALD-oxide is higher than with Th-SiO2 and SiN in Gas A etch process. Furthermore, Si and SiGe etch are evaluated with different Gas B/C ratio. Etch amount of Si is increased with increasing Gas C flow which can reduce activation energy from quantum mechanics simulation. Moreover, SiGe etching amount is decreased with increasing Gas C flow. This means that selectivity between Si and SiGe can be precisely controlled by Gas flow ratio.

Various applications can be realized by utilizing chemical dry etch with specific chemistries. For oxide etch processes such as fin recess, air gap, hard mask removal and surface clean, HF/NH3 chemistry can be used to meet critical criteria such as oxide selectivity to Si, SiN, resist and metal. CIP HW is developed to enhance throughput with excellent etch selectivity and uniformity. Additionally, HF mono-gas (or F-containing treatment) can dope Fluorine (F) into oxide film which is confirmed by depth profile analysis of secondary ion mass spectrometry (SIMS), and F implantation is known for dielectric breakdown life time improvement[2)]. Also, Gas A can be utilized in Silica oxide removal process, which requires high selectivity between low quality and high quality oxide. Finally, Si mandrel removal and Si or SiGe nanowire fabrication is introduced by controlling gas flow ratio. Further discussion will be presented on AVS 66th.

Reference

[1] T. Kato, et al., AVS 65th Int. Symp. & Exhibit. (2018)

[2] Y. Mitani, et al., Proc. Of IEEE P93-98 (1999)

9:20am **AP+PS+TF-ThM5 Mechanisms of Thermal Atomic Layer Etching (ALE) of Metal by Deprotonation and Complex Formation of Hexafluoroacetylacetone (hfacH)***, **Abdulrahman Basher**[1], I. Hamada,* Osaka University, Japan*; M. Krstic,* Karlsruhe Institute of Technology (KIT), Germany*; M. Isobe, T. Ito,* Osaka University, Japan*; K. Fink,* Karlsruhe Institute of Technology (KIT), Germany*; K. Karahashi, Y. Morikawa,* Osaka University, Japan*; W. Wenzel,* Karlsruhe Institute of Technology (KIT), Germany*; S. Hamaguchi,* Osaka University, Japan

Thermal atomic layer etching (ALE) may be used for precise and damageless etching of difficult-to-etch materials such as Ni, Co, NiFe, MgO, and CoFeB, which can be used as materials for magnetic tunnel junction (MTJ) stacks of magnetic random access memory (MRAM) devices. The goal of this study is to understand the mechanisms of surface chemical reactions during thermal ALE of metal in general with oxidation and exposure to organic molecules. As a model case, we consider a two-step thermal ALE process of nickel (Ni) with an oxidation step and a gas exposure step at an elevated substrate temperature [1]. In the latter step, hexafluoroacetylacetone (hfacH) $CF_3C(OH)=CHC(O)CF_3$ is used as a reactive gas. In the oxidation step, a thin layer of NiO is formed on the Ni film surface and, in the gas exposure step, only (part of) this NiO layer is removed and thus self-limiting etching of Ni is achieved. Our main question is why NiO is etched but Ni is not etched by hfacH. This mechanism is studied with first-principle simulation of interaction of hfacH with Ni and NiO surfaces.

First, we examined interaction of hfacH with a metallic Ni surface, using a simulation code STATE [2,3], which is based on density functional theory (DFT) with pseudo-potentials and a plane wave basis set. Computationally, a metal surface is better represented by a plane wave basis set in general.

[1] **Coburn & Winters Student Award Finalist**

It has been found in our simulation that, as an hfacH molecule approaches a metallic Ni surface with thermal velocity, it is more likely to be decompose and fragmented, rather than forming a hexafluoroacetylacetonate anion (hfac-) by deprotonation. This is consistent with earlier experimental observations [1,4]. The simulation clearly shows an energy threshold for deprotonation of hfacH with a metallic Ni surface.

Second, we examined interaction of enol hfacH with a NiO surface using a simulation code Turbomole [5], which is based on DFT but with Gaussian type orbitals. To better represent a NiO surface, we used the embedded cluster method (ECM) with Turbomole. It has been found that, as an hfacH molecule approaches a NiO surface, it is likely to deprotonate by transferring its hydrogen ion (H+) to an O atom of the NiO surface and the resulting hfac- tends to bond with a Ni atom of the surface because of the highly ionic nature of NiO, where Ni and O atoms are positively and negatively charged, respectively. In this way, volatile $Ni(hfac)_2$ and H_2O can be formed when hfacH molecules interact with a NiO surface. Reaction energies of such interactions have been evaluated from the simulations.

----

[1] T. Ito, et al., AVS 65th International Symposium & Exhibition (2018).

[2] Y. Morikawa, H. Ishii and K. Seki, Phys. Rev. B, **69**, 041403 (2004).

[3] I. Hamada, Physical Rev. B **89**, 121103 (2014).

[4] H. L. Nigg and R. I. Masel, J. Vac. Sci. Techol. A **17**,3477 (1999).

[5] R. Ahlrichs, M. Bär, M. Häser, H. Horn, C. Kölmel, Chem. Phys. Lett. **162**, 165 (1989).

9:40am **AP+PS+TF-ThM6 Thermal Atomic Layer Etching of Amorphous and Crystalline Al_2O_3 Films*, Jessica A. Murdzek*,** *S.M. George,* University of Colorado at Boulder

Thermal atomic layer etching (ALE) can be achieved with sequential, self-limiting surface reactions. One mechanism for thermal ALE is based on fluorination and ligand-exchange reactions. For metal oxide ALE, fluorination converts the metal oxide to a metal fluoride. The ligand-exchange reaction then removes the metal fluoride by forming volatile products. Previous studies have demonstrated the thermal ALE of amorphous Al_2O_3 films. However, no previous investigations have explored the differences between the thermal ALE of amorphous and crystalline Al_2O_3 films.

This study explored the thermal ALE of amorphous and crystalline Al_2O_3 films. HF or XeF_2 was used as the fluorination reactant. Dimethylaluminum chloride (DMAC) or trimethylaluminum (TMA) was employed as the metal precursor for ligand-exchange. The amorphous Al_2O_3 films had a much higher etch rate per cycle than the crystalline Al_2O_3 films. When using HF and TMA at 300 °C, the amorphous Al_2O_3 was removed at 0.78 Å/cycle, whereas the crystalline Al_2O_3 showed no significant thickness removal after 250 cycles (See Supplemental Figure 1). When using XeF_2 and TMA at 300 °C, the etch rate was 0.66 Å/cycle for the amorphous Al_2O_3 film. In comparison, ALE only removed up to 10 Å of the crystalline Al_2O_3 film. XeF_2 may be able to fluorinate the near surface region of the crystalline Al_2O_3 film easier than the crystalline bulk of the film.

The differences between amorphous and crystalline Al_2O_3 are sufficient to obtain selective thermal ALE of amorphous Al_2O_3 in the presence of crystalline Al_2O_3. The investigations also examined the effect of annealing temperature on the etch rate per cycle. Amorphous Al_2O_3 was etched at approximately the same etch rate until the crystallization of amorphous Al_2O_3 at >880 °C. The thermal ALE of crystalline films is important because amorphous films may not crystallize easily when they are too thin. Consequently, amorphous films may have to be grown thicker, crystallized, and then etched back to obtain the desired ultrathin crystalline film thickness.

11:00am **AP+PS+TF-ThM10 Thermal Atomic Layer Etching (ALE) of Germanium-Rich SiGe Films*, Aziz Abdulagatov*,** *S.M. George,* University of Colorado at Boulder

The thermal atomic layer etching (ALE) of germanium-rich SiGe was demonstrated using an oxidation and "conversion-etch" mechanism (See Supplemental Figure 1). In this process, the SiGe surface was oxidized to a SiGe oxide layer using O_2. The SiGe oxide layer was then converted to an Al_2O_3 layer using trimethylaluminum (TMA). The Al_2O_3 layer was fluorinated by HF to an AlF_3 layer prior to the removal of the AlF_3 layer by ligand-exchange using TMA. The thermal ALE of SiGe films will be important for the fabrication of advanced MOSFET devices.

This study explored the thermal ALE of germanium-rich $Si_{0.2}Ge_{0.8}$ films. *In situ* spectroscopic ellipsometry was employed to monitor the thickness of both the $Si_{0.2}Ge_{0.8}$ and the surface oxide layer during ALE. These studies showed that the $Si_{0.2}Ge_{0.8}$ film thickness decreased linearly with number of reaction cycles while the surface oxide thickness remained constant. Using an O_2-HF-TMA reaction sequence, the $Si_{0.2}Ge_{0.8}$ ALE etch rate was 0.57 Å/cycle at 290°C. This etch rate was obtained using optimal reactant pressures of 25, 0.2 and 0.4 Torr, and dose times of 1.5, 1 and 1 s, for O_2, HF and TMA, respectively.

The $Si_{0.2}Ge_{0.8}$ ALE etch rate was lower at lower temperatures. Using an O_2-HF-TMA reaction sequence, the $Si_{0.2}Ge_{0.8}$ etch rate was reduced from 0.57 Å/cycle at 290°C to 0.07 Å/cycle at 225°C. The order of the reactant sequence also affected the $Si_{0.2}Ge_{0.8}$ etch rate. Changing the reactant sequence from O_2-HF-TMA to O_2-TMA-HF reduced the $Si_{0.2}Ge_{0.8}$ etch rate from 0.57 to 0.45 Å/cycle at 290°C. $Si_{0.2}Ge_{0.8}$ could also be etched selectively in the presence of Si and Si_3N_4. The $Si_{0.2}Ge_{0.8}$ etch rate was >10 times faster than the etch rate for Si or Si_3N_4 at 290°C (See Supplemental Figure 2).

11:20am **AP+PS+TF-ThM11 Thermal Atomic Layer Etching of GaN and Ga_2O_3 Using Sequential Fluorination and Ligand-Exchange Reactions*, Nicholas Johnson*,** *Y. Lee, S.M. George,* University of Colorado at Boulder

Atomic layer etching (ALE) of GaN and Ga_2O_3 is important for the fabrication of power electronics devices. Thermal ALE of GaN and Ga_2O_3 was performed using sequential, self-limiting surface reactions. The thermal ALE was accomplished using fluorination and ligand-exchange reactions. XeF_2 and HF were used as the fluorination reactants. BCl_3 was the main metal precursor for ligand-exchange. Ga_2O_3 was also etched using $Al(CH_3)_3$, $AlCl(CH_3)_2$, $TiCl_4$ or $Ga(N(CH_3)_2)_3$ as the metal precursors for ligand-exchange.

Crystalline GaN samples prepared using MOCVD techniques at the US Naval Research Laboratory were etched with sequential XeF_2 and BCl_3 exposures. GaN etch rates varied from 0.18 to 0.72 Å/cycle at temperatures from 170 to 300°C, respectively (see Supplemental Figure 1). Because the GaN etch rates were self-limiting versus BCl_3 exposure and BCl_3 pressure, the GaN etching mechanism is believed to involve XeF_2 fluorination of GaN to GaF_3 and then ligand-exchange between BCl_3 and GaF_3 to yield volatile BCl_wF_x and GaF_yCl_z species. GaN fluorination using a NF_3 plasma was also successful for etching crystalline GaN at 250°C.

Ga_2O_3 samples deposited using ALD techniques were etched with sequential HF and BCl_3 exposures. Ga_2O_3 etch rates varied from 0.59 to 1.35 Å/cycle at temperatures from 150 to 200°C, respectively. The Ga_2O_3 etch rates were self-limiting versus HF and BCl_3 exposure. Ga_2O_3 ALE was also performed using HF for fluorination and a variety of metal precursors for ligand-exchange. Ga_2O_3 etch rates at 250°C were 0.2, 0.8, 1.1 and 1.2 Å/cycle for $Ga(N(CH_3)_2)_3$, $TiCl_4$, $Al(CH_3)_3$ and $AlCl(CH_3)_2$ as the metal precursors, respectively (see Supplemental Figure 2). The wide range of metal precursors that can etch Ga_2O_3 argues that the ligand-exchange reaction with GaF_3 is facile.

11:40am **AP+PS+TF-ThM12 Mechanistic Insights into Thermal Dry Atomic Layer Processing of Metals*, Andrew Teplyakov*,** University of Delaware **INVITED**

The mechanisms of thermally induced reactions of atomic layer deposition (ALD) and atomic layer etching (ALE) can be sometimes viewed as proceeding in opposite directions. However, for atomic layer processing of metals, that would mean that the best designed and most efficient reaction pathways leading to metal deposition would produce insurmountable energy barriers for a reverse process. If ligand detachment, exchange, and decomposition could be desirable for ALD, the etching of the same metals would require careful consideration of the etching mechanisms at the atomic and molecular level. Given that the mechanisms of ALE can be very complex, the key concepts and approaches will be described here for thermal dry etching processing, which would allow for eliminating the role of solvents and for distinguishing thermodynamic and kinetic regimes of etching. The mechanistic investigation of thermal dry etching of cobalt will be the primary target of this work. This process will be used to illustrate the limitations of the single-reagent etching by analyzing the reaction of 1,1,1,5,5,5-hexafluoro-2,4-pentanedione (hexafluoroacetylacetone, hfacH) or 2,4-pentanedione (acetylacetone, acacH)) with a clean cobalt surface. Then the effects of surface oxidation and chlorination will be explored as a means of kinetically controlled process. Finally, a number of potential effects of the mechanisms of dry etching on the morphology of the surfaces produced and, specifically, on the "smoothing" effect of dry etching will be discussed.

Electronic Materials and Photonics Division
Room A214 - Session EM+AP+MS+NS+TF-ThM

Advanced Processes for Interconnects and Devices

Moderators: Andy Antonelli, Nanometrics, Bryan Wiggins, Intel Corporation

8:00am **EM+AP+MS+NS+TF-ThM1 High-density Plasma for Soft Etching of Noble Metals**, ***Gerhard Franz****, V. Sushkov,* Munich University of Applied Sciences, Germany*; W. Oberhausen, R. Meyer,* Technische Universität München, Germany

During our research to define a contact which can be serve as thin hard mask in III/V semiconductor processing, we focused on the Bell contact which consists of Ti/Pt(Mo)/Au and chlorine-based plasmas generated by electron cyclotron resonance. For platinum, we identified PF_3 as main component which acts comparable to CO [1]. This fact triggered our search for suited etchants for gold and copper. For Au, the best ambient is a mixture of CH_4, Cl_2, and O_2 which is stabilized by Ar [2]. This mixture generates residual-free etching of metal films which are clearly free of "fencing" and "hear's ears."

The etching process has been established up to thicknesses of half a micron which is the typical thickness of metal films on the p-side of laser devices. With the aid of optical emission spectroscopy, the generation of CO could be proven [3]. This reagent seems to be the main component for real etching without residual fencing.

[1] G. Franz, R. Kachel, and St. Sotier, Mat. Sci. Semicond. Proc. **5**, 45 (2002)

[2] G. Franz, R. Meyer, and M.-C. Amann, Plasma Sci. Technol. **19**, 125503 (2017)

[3] G. Franz, W. Oberhausen, R. Meyer, and M.-C. Amann, AIP Advances **8**, 075026 (2018)

8:20am **EM+AP+MS+NS+TF-ThM2 Crystalline InP Growth and Device Fabrication Directly on Amorphous Dielectrics at Temperatures below 400°C for Future 3D Integrated Circuits**, ***Debarghya Sarkar****, Y. Xu, S. Weng, R. Kapadia,* University of Southern California

A fundamental requirement to realize 3D integrated circuits is the ability to integrate single crystal semiconductor devices on the back-end of functional layers within a thermal budget of ~400 °C. Present state-of-the-art methods involve wafer bonding or epitaxial growth and transfer, since directly growing on amorphous materials by traditional epitaxial growth processes like MOCVD and MBE would give polycrystalline films with submicron-scale grains. To that end, a newly introduced and actively developing growth method called Templated Liquid Phase (TLP) has demonstrated the ability to achieve single crystal compound semiconductor mesas of areal dimension ~ 10um diameter on diverse amorphous substrates. While previous demonstrations of TLP growth were at temperatures around 500-600 °C, in this presentation we would discuss some of the recent material characteristics and device results achieved and insights obtained, for crystalline InP mesas grown on amorphous dielectrics at temperatures below 400 °C. InP nucleation and growth was obtained for temperatures 360 °C down to 200 °C. Morphological variations of the grown crystals observed under different growth conditions (temperature, pressure, precursor flux) and strategies to obtain compact macro-defect free crystal growth would be presented. Contrary to general expectation of poor optoelectronic quality at these lower temperatures, the room temperature steady-state photoluminescence shows peak position and full width at half maximum comparable to that of commercial InP wafer. External quantum efficiency is within an order of magnitude of single crystal commercial wafer at optimal growth conditions. Back-gated phototransistor was fabricated using low temperature InP grown directly on the amorphous gate oxide, and with all processing steps below the thermal budget of 400 °C. A typical device showed reasonable ON-OFF ratio of about 3 orders of magnitude, with peak responsivity of 20 A/W at V_{gs}=3.2V and V_{ds}=2.1V under an irradiance of 4 mW/cm^2 of broadband light. In summary, this technology could potentially open up a viable avenue to realize 3D integrated circuits by enabling integration of high performance electronic and optoelectronic devices on the back-end of functional layers within the acceptable thermal budget of 400^0C.

8:40am **EM+AP+MS+NS+TF-ThM3 The Role and Requirements of Selective Deposition in Advanced Patterning**, ***Charles Wallace,*** Intel Corporation **INVITED**

The edge placement error (EPE) margin on features patterned at tight pitches presents a difficult integrated challenge. Area selective deposition, chemically selective etches and the design of thin films for selectivity have risen to the top priorities in advanced patterning. The EPE control requirement creates a complex interaction between many integrated modules such as thin film deposition, etch (wet and dry), chemical-mechanical polish and lithography. The introduction of EUV lithography into the semiconductor patterning process has enabled some simplification of process architecture; however, has not decreased EPE margin enough to keep up with the pitch scaling requirements. Chemical selectivity is the most effective way to avoid EPE-caused failures on devices which lead to poor yield. Some of the limits to achieving selective growth solutions include development of self-assembled monolayers (SAMs), selective ALD/CVD growth and the metrology required to prove success. The development of manufacturable deposition chambers by the industry is a key requirement in order to adequately test the capability of these new process options.

9:20am **EM+AP+MS+NS+TF-ThM5 Graphene-Template Assisted Selective Epitaxy (G-TASE) of Group IV Semiconductors**, ***M. Arslan Shehzad****, A. T. Mohabir, M.A. Filler,* Georgia Institute of Technology

As conventional 2-D transistor scaling approaches its limits, 3-D architectures promise to increase the number of devices and reduce interconnect congestion. A process able to monolithically integrate single-crystalline group IV materials into the back-end-of-line (BEOL) may enable such designs. Here, we demonstrate the graphene-template assisted selective epitaxy (G-TASE) of single-crystal Ge on amorphous substrates at temperatures as low as 250 ˚C. This work represents a significant step forward for TASE methods, which have been largely limited to III-V and II-VI materials, bulk crystal templates, as well as higher temperatures. We specifically grow Ge nanostructures on graphene-on-oxide at the bottom of nanometer-scale oxide trenches by leveraging differences in group IV atom sticking probability between graphene and oxide surfaces. Raman mapping confirms the single crystallinity of as-grown Ge crystals. Time-dependent studies show a linear increase in Ge crystal height even after emerging from the oxide trench, indicating Ge atoms preferentially adsorb to the top facet under our growth conditions. Our studies also reveal that G-TASE is sensitive to the plasma process used to expose graphene in the oxide trenches. This work extends TASE to a new, technologically-relevant materials system and provides fundamental insight into the underlying physicochemistry.

KEY WORDS: silicon, germanium, epitaxy, graphene, selective deposition

9:40am **EM+AP+MS+NS+TF-ThM6 Resistivity and Surface Scattering Specularity at (0001) Ru/dielectric Interfaces**, *S.S. Ezzat,* University of Central Florida*; P.D. Mani,* View Dynamic Glass, Inc.*; A. Khaniya, W.E. Kaden,* University of Central Florida*; D. Gall,* Rensselaer Polytechnic Institute*; K. Barmak,* Columbia University*; **Kevin Coffey**,* University of Central Florida

In this work we report the variation of resistivity with film thickness and with changes in surface characteristics for ex-situ annealed single crystal (0001) Ru thin films grown on c-axis sapphire single crystal substrates. The room temperature deposition of SiO_2 on the Ru surface increased the resistivity of the annealed films and is interpreted as an increase in diffuse scattering of the upper surface from a primarily specular previous condition in the context of the Fuchs-Sondheimer model of surface scattering. The characterization of the films and upper Ru surface by low energy electron diffraction (prior to SiO_2 deposition), x-ray reflectivity, x-ray diffraction, and sheet resistance measurements is reported. The film resistivity and specularity of the Ru/SiO_2 interface is observed to reversibly transition between high resistivity (low specularity) and low resistivity (high specularity) states.

11:00am **EM+AP+MS+NS+TF-ThM10 Electrochemical Atomic Layer Deposition and Etching of Metals for Atomically-Precise Fabrication of Semiconductor Interconnects**, *Y. Gong, K. Venkatraman, **Rohan Akolkar**,* Case Western Reserve University **INVITED**

Moore's law drives continued device miniaturization in nano-electronics circuits. As critical dimensions are approaching the single nanometer length scale, the semiconductor industry is seeking novel technologies for precisely tailoring materials and structures at the atomic scale. While vapor-phase, plasma-assisted techniques of atomic layer deposition (ALD) and etching (ALE) are capable of providing nano-scale control over metal deposition and etching, these processes may not provide the requisite atomic-scale precision. Additionally, ALD precursors are unstable and often expensive. Thus, alternative solution-phase electrochemical processes are being developed in our laboratory. In our electrochemical ALD (e-ALD) approach, a sacrificial monolayer of zinc is first deposited on the noble substrate via underpotential deposition (UPD). The zinc adlayer then

undergoes spontaneous surface-limited redox replacement (SLRR) by the desired metal such as Cu or Co. Sequential UPD and SLRR steps enable fabrication of multi-layered deposits in a layer-by-layer fashion. An analogous approach for electrochemical ALE (e-ALE) is also being developed. In electrochemical ALE of Cu, surface-limited sulfidization of Cu forms a cuprous sulfide (Cu_2S) monolayer. The sulfidized Cu monolayer is then selectively removed through spontaneous complexation of the Cu^{+1} in a chloride-containing etchant medium. The sequence can be repeated to etch bulk metal films one atomic layer at a time. This talk will highlight numerous advantages and fundamental characteristics of e-ALD and e-ALE processes and describe opportunities for integrating them in wafer-scale metallization applications.

12:00pm **EM+AP+MS+NS+TF-ThM13 Wafer-Scale Fabrication of Carbon-Based Electronic Devices***, **Zhigang Xiao**, J. Kimbrough, J. Cooper, K. Hartage, Q. Yuan,* Alabama A&M University

In this research, we report the wafer-scale fabrication of carbon nanotube or graphene-based electronic device such as field-effect transistors (FETs). Carbon nanotube-based devices were fabricated with the alternating electric field-directed dielectrophoresis (DEP) method, and the graphene-based devices were fabricated with the carbon films grown with plasma-enhanced atomic layer deposition (PEALD) or e-beam evaporation. Semiconducting carbon nanotubes were dispersed ultrasonically in solutions, and were deposited and aligned onto a pair of gold electrodes in the fabrication of carbon nanotube-based electronic devices using the dielectrophoresis method. The DEP-aligned tubes were further fabricated into carbon nanotube field-transistors (CNTFETs) and CNTFET-based electronic devices such as CNT-based inverters and ring oscillators using the microfabrication techniques. The fabricated devices were imaged using the scanning electron microscope (SEM) and high-resolution transmission electron microscope (HRTEM), and the electrical properties were measured from the fabricated devices using the semiconductor analyzer. The semiconducting CNTs achieved higher yield in the device fabrication, and the fabricated devices demonstrated excellent electrical properties.

Thin Films Division
Room A122-123 - Session TF+EM+NS+SS-ThM
Thin Films for Energy Harvesting and Conversion

Moderators: Siamak Nejati, University of Nebraska-Lincoln, Xinwei Wang, Shenzhen Graduate School, Peking University

8:00am **TF+EM+NS+SS-ThM1 Redesigning Batteries into Efficient Energy Harvesters and Sensors for Wearable Applications***, **Cary Pint**,* Vanderbilt University **INVITED**

Here I will discuss the research efforts of my team demonstrating how active materials utilized in batteries can be reconfigured into an electrochemical framework to harvest, rather than store, energy. This new functionality of battery materials arises from the fundamental coupling between mechanical stresses and electrochemistry that my group has demonstrated while investigating the "strain-engineering" of battery materials. By exploiting this coupling in a symmetric cell device configuration, we are able to construct devices that convert mechanical energy to electrical energy by mechanical modulation of the electrochemical reaction potential. I will discuss the development of this device platform from proof-of-concept device fabrication using 2D materials to our most recent demonstration of textile-integrated biocompatible fibers integrated into fabrics for harvesting/sensing of human motion. Most notably, I will discuss how the sluggish diffusion kinetics of ions between two electrodes – whereas a challenge for emerging battery applications, enables these devices to measure a continuous response from the whole broad range of frequencies associated with human motion. This allows these wearable harvesters to provide real-time sensing data that can be directly correlated with dynamic human motion models. This new approach leverages the efficient nature of electrochemistry, the wide range of materials selection and chemistries relevant for batteries, and without any of the safety concerns of batteries due to the symmetric electrode configuration.

8:40am **TF+EM+NS+SS-ThM3 Engineering Effective Back Contact Barrier by interfacial $MoSe_2$ defect states for CZTSe: nanolayer Ge solar cells.***, **Sanghyun Lee**,* Indiana State University

The steadily emerging $Cu_2ZnSnSSe_4$ (CZTSSe) devices are alternative thin film solar cells with abundant elements in earth's crust for the past several years. Despite several advantagessuch as high absorption coefficient (>10^4 cm^{-1}) and a tunable direct band gap energy (1 to 1.4 eV), the improvement and understanding have been stagnant in the past several years. Recently, CZTSe: nanolayer Ge solar cells have shown significantly improved pseudo-mono grain toward the depth direction.

Due to the improvement and the similarity between CZTSe and Cu(In,Ga)Se_2 (CIGS) thin film solar cells, the CZTSe/ Molybdenum (Mo) back contact interface was often misinterpreted by expecting the similar back contact property to CIGS. However, unlike the stable CISe ($CuInSe_2$)/Mo interface, the CZTSe/Mo interface is thermodynamically unstable due to the higher oxidation states of Sn. Although the presence of an interfacial $MoSe_2$ layer at Mo/absorber is always confirmed, properties of the back contact-interface such as structure and electrical behaviors are convoluted.

Following our empirical results about the back contact barrier of CZTSe: nanolayer Ge devices, we perform analytical and numerical modeling to explain the back contact improvement theoretically. The device modeling are carried out with the simulator, developed at Indiana State University. The tool is run in MATLAB environment, connected to other external tools (Sentaurus TCAD). Based on our result, defects in $MoSe_2$ interfacial layer dominate the back contact property of CZTSe: nanolayer Ge devices by increasing of the effective back contact barrier, which consists of two different back contact barriers, thereby increasing series resistance as well. The reduction of $MoSe_2$ defect concentration from 1×10^{17} to 1×10^{15} cm^{-3} decreases the effective barrier height by 51 meV, which results in approximately 34 % decrease in the series resistance (See supporting data). Conversely, as the defect concentration increases, the benefit from the back contact barrier lowering by the valence bands offset between $MoSe_2$ and CZTSe absorber is reduced and essentially eliminated. However, the back contact barrier between $MoSe_2$ and Mo metal contact remains the same even with increased $MoSe_2$ defect concentration. Incorporating thin Ge nanolayer at the interface between the absorber and $MoSe_2$ positively influences and possibly reduces the defect states, lowering the effective barrier. The exponential fitting of the effective barrier and series resistance agrees well with the experimental results. The improvement of the back contact barrier for CZTSe: nanolayer Ge devices is calculated as 23.8 meV than CZTSe without nanolayer Ge devices.

9:00am **TF+EM+NS+SS-ThM4 Development of Low-Cost, Crack-Tolerant Metallization Using Screen Printing for Increased Durability of Silicon Solar Cell Modules***, O.K. Abudayyeh,* Osazda Energy*; A. Chavez,* University of New Mexico*; J. Chavez,* Osazda Energy*; **Sang M. Han**,* University of New Mexico*; F. Zimbardi, B. Rounsaville, V. Upadhyaya, A. Rohatgi,* Georgia Institute of Technology*; B. McDanold, T. Silverman,* National Renewable Energy Laboratory

One of the ways to reduce the cost of solar electricity to 3¢/kWh, thus reaching parity with fossil-fuel-based generation, is to reduce the degradation rate of solar modules and extend their lifetime well beyond 30 years. The extended module lifetime in turn can positively influence the financial model and the bankability of utility-scale PV projects. Today, the highest-risk-priority solar module degradation mechanism is what is known as hot spots, often induced by cell cracks. In order to address this degradation mechanism, we make use of low-cost, multi-walled carbon nanotubes embedded in commercial screen-printable silver pastes, also known as metal matrix composites. When the carbon nanotubes are properly functionalized and appropriately incorporated into commercial silver pastes, the resulting metal contacts on solar cells, after screen-printing and firing, show exceptional fracture toughness. These composite metal contacts possess increased ductility, electrical gap-bridging capability up to 50 µm, and "self-healing" to regain electrical continuity even after cycles of complete electrical failure under extreme strain [1]. Accelerated thermal cycling tests on mini-modules constructed from aluminum back surface field (Al-BSF) cells show a slower degradation rate for the cells integrated with the composite grid fingers and busbars for the front surface metallization compared to the cells with conventional metallization.

[1] O. K. Abudayyeh, A. Chavez, J. Chavez, S. M. Han, F. Zimbardi, B. Rounsaville, V. Upadhyaya, A. Rohatgi, B. McDanold, T. J. Silverman, and N. Bosco, in "Low-Cost Advanced Metallization to Reduce Cell-Crack-Induced Degradation for Increased Module Reliability," 2019 NREL PV Reliability Workshop, Lakewood, CO, 2019.

9:20am **TF+EM+NS+SS-ThM5 Fabrication of Optical Test Structures for Enhanced Absorption in Thin Multi-junction Solar Cells**, ***Erin Cleveland***, *N.A. Kotulak, S. Tomasulo, P. Jenkins,* U.S. Naval Research Laboratory*; A. Mellor, P. Pearce,* Imperial College London, UK*; N.J. Ekins-Daukes,* University of New South Wales, Australia*; M.K. Yakes,* U.S. Naval Research Laboratory

In space applications, a key figure of merit is conversion efficiency at end-of-life, which combines both beginning–of-life efficiency with degradation due to radiation exposure on orbit. In currently used InGaP/GaAs/Ge triple junctions, the GaAs middle cell has the most pronounced degradation, which limits the total current generation at the end-of-life. Recently, we demonstrated that as the thickness of the GaAs cell decreases, the tolerance to radiation damage increases. [1] However, because the cell absorbs less light as the thickness of the active region is reduced, the beginning-of-life performance suffers as compared to optically thick cells. To realize the benefits of both structures, light trapping architectures may be used to increase absorption within the cell while still maintaining the increased radiation tolerance of the thinner geometry.

Designing a wavelength selective light trapping structure positioned interstitially between two of the subcells of a multi-junction device is a new challenge which prohibits many of the well-known light trapping techniques. Recently, we have proposed a structure which combines a distributed Bragg reflector (DBR) with a textured diffraction grating. [2] Such a structure would provide substantial absorption of light in the middle subcell of a multi-junction device, while still allowing enough low-energy light to pass through the structure so the bottom cell remains well current matched with the other junctions. This structure is proposed to have over an order of magnitude increase in overall radiation tolerance while maintaining comparable beginning of life performance to the current technology.

In this presentation, we present a first experimental demonstration of this structure. The design combines a diffraction grating fabricated via nanosphere natural lithography [3], a low-index transparent spacer layer, and a DBR, which synergistically traps light inside the targeted subcell. This presentation will highlight processing techniques and challenges associated with fabricating a textured ultra-thin solar cell, while illustrating the effectiveness of integrating light trapping structures within an ultra-thin solar cell as an effort towards realizing high efficiency ultra-thin photovoltaic devices.

[1] L. C. Hirst, *et.al*, "Intrinsic radiation tolerance of ultra-thin GaAs solar cells", *APL*, 109 (2016)

[2] A. Mellor, N.P. Hylton, S.A. Maier, N. Ekins-Daukes, "Interstitial light-trapping design for multi-junction solar cells", *Solar Energy Materials & Solar Cells*, 159, (2017)

[3] H.W. Deckman and J.H. Dunsmuir, "Natural lithography", *Applied Physics Letters*, 41(4) (1982)

9:40am **TF+EM+NS+SS-ThM6 Phosphorus as a *p*-Dopant in Pyrite FeS_2, a Potential Low-cost earth-abundant Thin Film Solar Absorber**, ***Bryan Voigt*** [1], *W. Moore, D. Ray, M. Manno,* University of Minnesota, Minneapolis*; J.D. Jeremiason,* Gustavus Adolphus College*; L. Gagliardi, E.S. Aydil, C. Leighton,* University of Minnesota, Minneapolis

Pyrite FeS_2 has long been considered an ideal absorber material for low-cost and sustainable thin film solar cells because it is composed of earth-abundant, non-toxic, inexpensive elements, has a suitable band gap (0.95 eV), and absorbs light so strongly that a 100-nm-thick film absorbs >90 % of photons with energies above the band gap. Lack of doping control, however, has presented a barrier to realization of the *p-n* pyrite homojunction, *i.e.*, the simplest route to a pyrite solar cell. *Heterojunction* pyrite solar cells have proven to have disappointingly low efficiencies (~3%), surface conduction and leaky surface inversion layers being implicated as the culprit. While mitigation of pyrite surface conduction remains a challenge, doping has begun to yield to understanding, renewing optimism for a *p-n* pyrite homojunction solar cell. In particular, we have shown that rigorously phase-pure pyrite single crystals and thin films are exclusively *n*-type, due to a common dopant. Most recently, we have identified sulfur vacancies as this unintentional *n*-dopant, enabling robust control over *n*-doping levels in single crystals grown by chemical vapor transport (CVT). Progressing towards a *p-n* pyrite homojunction, here we demonstrate effective *p*-type doping in crystals by introducing phosphorus in the vapor phase during CVT growth. Increasing the phosphorus concentration from <0.1 ppm to 30 ppm evolves electronic conduction from *n*-type to *p*-type, with a clear and reproducible majority carrier inversion for concentrations >10 ppm. Typical transport properties of phosphorus-doped, *p*-type pyrite crystals include a hole thermal activation energy, room temperature resistivity, hole density, and mobility of ~170 meV, 3 Ω cm, 2×10^{18} cm^{-3}, and 1 cm^2 $V^{-1}s^{-1}$, respectively. Density functional theory calculations confirm that phosphorus substituted on the S site is an acceptor, predicting a defect level at 200 meV above the valence band maximum, in good agreement with experiment. With both *n*- and *p*-type doping control achieved, attempts at *p-n* pyrite homojunction solar cells become possible.

This work was supported by the customers of Xcel Energy through a grant from the Renewables Development Fund and in part by the National Science Foundation through the University of Minnesota MRSEC under DMR-1420013.

11:00am **TF+EM+NS+SS-ThM10 Relaxor-ferroelectric Thin Films for Energy Harvesting from Low-grade Waste-heat**, ***Amrit Sharma***, *B. Xiao, S.K. Pradhan, M.J. Bahoura,* Norfolk State University

The need for efficient energy utilization is driving research into ways to harvest waste-heat which is ubiquitous, abundant and free. Thermal harvesting is a promising method for capturing freely available heat and converting it to a more usable form, such as electrical energy. Thermal harvesting for low power electronic devices using ferroelectric materials is one of the emerging areas of research because they possess spontaneous polarization and exhibit excellent piezoelectric as well as excellent pyroelectric coefficients. These materials are unique as they only sense time-dependent temperature change to generate electric power. We have grown lead-free $BaZr_{0.2}Ti_{0.8}O_3$ (BZT)/ $Ba_{0.7}Ca_{0.3}TiO_3$ (BCT) multilayer heterostructures and studied the structural, dielectric, ferroelectric, pyroelectric and energy density characteristics. The BZT/BCT multilayer epitaxial heterostructures were grown on SrRuO (SRO) buffered SrTiO (STO) single crystal substrate by optimized pulsed laser deposition technique. The large angle x-ray scans showed only diffraction peaks from the substrate and pseudocubic reflections (00*l*) from the multilayer heterostructure, confirming that these films are phase pure and epitaxial in nature. The atomic force microscopy (AFM) studies indicate that the surface roughness is low and that film growth is of high quality. The ferroelectric phase transitions have been probed above room temperature with relaxor behavior. The polarization versus electric field (P-E) measurement exhibits well-saturated hysteresis loop with maximum and remnant polarization of 138 and 64 μC/cm^2, respectively. Solid-state, thin-film devices, that convert low-grade heat into electrical energy, are demonstrated using pyroelectric Ericsson cycles, and their performance is optimized by independently enhancing pyroelectric coefficient and suppressing dielectric permittivity in compositionally graded heterostructures. Our findings suggest that pyroelectric devices may be competitive with thermoelectric devices for low-grade thermal harvesting.

11:20am **TF+EM+NS+SS-ThM11 Thermal Treatment Effects on the Thermoelectric Devices from Sn/Sn+SnO_2 Thin Films**, ***Satilmis Budak***, *E. McGhee, Z. Xiao, E. Barnes, R. Norwood,* Alabama A&M University

Approximately two-thirds of energy is lost as waste heat; the direct harvest of this waste heat using thermoelectric (TE) materials has attracted worldwide interest. TE materials can convert waste heat from industrial processes, furnaces, and engine exhaust streams into useful electricity by the Seebeck effect. The energy conversion efficiency is shown by the dimensionless figure of merit, ZT, and $ZT=S^2\sigma T/K$, where S is the Seebeck coefficient, σ is the electrical conductivity, K is the total thermal conductivity, and T is the absolute temperature. The numerator $S^2\sigma$ defines the power factor (PF), which primarily relates to the electric properties [1]. When operating as an energy-generating device, the TE device is termed a thermoelectric generator (TEG). The source of thermal energy manifests itself as a temperature difference across the TEG. When operating in a cooling or heating mode the TE device is termed a thermoelectric cooler (TEC). Similarly, the TE device produces heating or cooling that takes the form a heat flux which then induces a temperature difference across the TEC. TE devices are solid-state mechanisms that are capable of producing these three effects without any intermediary fluids or processes. For power generation applications TE devices are used in automobiles as exhaust gas waste heat recovery devices where thermal energy is scavenged along the exhaust line of a vehicle and converted into useful electricity [2]. The TE devices from 50 alternating layers of Sn/Sn+SnO_2 thin films were prepared using DC/RF Magnetron Sputtering. They were heat treated at different temperatures to form nanostructures to increase the Seebeck coefficients and electrical conductivity and decrease thermal conductivity. Seebeck

[1] **TFD James Harper Award Finalist**

coefficient, van der Pauw resistivity, and thermal conductivity were used for the characterization. SEM/EDS was used to characterize the surface morphology of the films.

[1] Hongchao Wang, Wenbin Su, Jian Liu, Chunlei Wang, "Recent development of n-type perovskite thermoelectrics", J Materiomics 2 (2016) 225-236

[2] Chetan Jangonda, Ketan Patil, Avinash Kinikar, Raviraj Bhokare, M.D.Gavali, "Review of Various Application of Thermoelectric Module", International Journal of Innovative Research in Science, Engineering and Technology Vol. 5, Issue 3, (March 2016), 3393-3400.

Acknowledgement

Research was sponsored by NSF with grant numbers NSF-HBCU-RISE-1546965, NSF-EPSCOR-R-II-3-EPS-1158862, NSF-MRI-1337616, DOD with grant numbers W911 NF-08-1-0425, and W911NF-12-1-0063, U.S. Department of Energy National Nuclear Security Administration (DOE-NNSA) with grant numbers DE-NA0001896 and DE-NA0002687.

11:40am **TF+EM+NS+SS-ThM12 Thermoelectric Properties of Efficient Thermoelectric Devices from Sb/Sb+SnO_2 Thin Films***, **Eshirdanya McGhee**, S. Budak, Z. Xiao, N. Caver, B. McNeal,* Alabama A&M University

The thermoelectric (TE) concept could be seen as a perfect solution for recovering waste heat from engine exhaust and converts in to electric energy. TE generators are all solid-state devices that convert heat into electricity. Unlike traditional dynamic heat engines, TE generators contain no moving parts and are completely silent. Such generators have been used reliably for over 30 years of maintenance-free operation in deep space probes such as the Voyager missions of NASA. TE systems can be easily designed to operate with small heat sources and small temperature differences [1]. An ideal TE material behaves like an electron crystal and phonon glass, allowing a large temperature gradient across it while conducting electricity efficiently to generate a TE voltage. Significant progress in the TE performance of materials has been made by exploring ultra low thermal conductivity at high temperature and reducing thermal conductivity by nano-structuring, as well as by resonant doping and energy-dependent scattering of electrons [2]. The figure of merit ZT describes material performance. ZT depends on the thermoelectric material properties of Seebeck coefficient S, electrical conductivity σ, and thermal conductivity K, and ZT=S2σT/K where T is the temperature of the material [3]. TE devices from 50 alternating layers of Sb/Sb+SnO_2 thin films were prepared by DC/RF Magnetron Sputtering. TE devices were annealed at different temperatures to form nano-structures to increase the Seebeck coefficients and electrical conductivity and decrease thermal conductivity. For the characterization, Seebeck coefficient, van der Pauw resistivity, and thermal conductivity were used. The surface morphology was characterized using SEM/EDS.

[1] Krishna Purohit, Sheetal Kumar Jain, Dr. P M Meena, Khushaboo Singh, Manish Dadhich,

"Review Paper on Optimizations of Thermoelectric System", International Journal of Innovative Research in Engineering & Management (IJIREM), ISSN: 2350-0557, Volume-3, Issue-4, (July-2016), 259-263.

[2] Kedar Hippalgaonkar, Ying Wang, Yu Ye, Diana Y. Qiu, Hanyu Zhu, Yuan Wang, Joel Moore, Steven G. Louie, and Xiang Zhang, "High thermoelectric power factor in two-dimensional crystals of MoS_2", PHYSICAL REVIEW B 95, 115407 (2017) 1-9.

[3] Saniya LeBlanc, Sustainable Materials and Technologies 1–2 (2014) 26–35.

Acknowledgement

Research was sponsored by NSF with grant numbers NSF-HBCU-RISE-1546965, NSF-EPSCOR-R-II-3-EPS-1158862, NSF-MRI-1337616, DOD with grant numbers W911 NF-08-1-0425, and W911NF-12-1-0063, U.S. Department of Energy National Nuclear Security Administration (DOE-NNSA) with grant numbers DE-NA0001896 and DE-NA0002687.

12:00pm **TF+EM+NS+SS-ThM13 3D Printed Triboelectric Nanogenerator***, I. Fattah, E. Utterback, **Naga Srinivas Korivi**, V. Rangari,* Tuskegee University

We report on the development of polymer nanocomposite layers made by 3D printing. The nanocomposite is composed of polydimethylsiloxane (PDMS), barium titanate nanoparticles, and multi-walled carbon nanotubes. Flexible layers of this composite have been 3D printed using a commercial 3D printer, and function as triboelectric energy generators. To the best of our knowledge, this is the first report of a PDMS based triboelectric nanogenerator fabricated by 3D printing. The nanogenerators have been evaluated in contact and separation mode and produce a maximum of 2.6 Volts under pressure from a human finger.

The fabrication procedure involves sonicating barium titanate ($BaTiO_3$, Skyspring Nanomaterials) and multi walled carbon nanotubes (MWCNT, Skyspring Nanomaterials) together in ethyl alcohol. This is followed by removing the excess ethyl alcohol, and manually grinding the nanoparticle powder to break any clusters. This is followed by mechanically blending liquid PDMS pre-polymer and its curing agent (~10:1 ratio by weight) with the nanoparticle powder in one beaker. Finally, the blend is filled into a dual plastic syringe, which is loaded onto an extrusion printing head of a commercial 3D printer (Hydra 16A, Hyrel LLC, USA). The printer reads a software file that defines the pattern or shape to be printed and dispenses the material from the syringe accordingly onto a base plate. For printing this composite, the base plate temperature was maintained between 75 – 90 °C, to allow curing within a few minutes. Once cured, the solid composite layers (270 µm thickness) can be peeled off the base plate.

The 3D printed PDMS-BaTiO3-MWCNT layers have been evaluated as triboelectric energy generation. In one embodiment, the 3D printed functions as the negatively charged layer in a contact-separation scheme. A polyimide sheet is used as positively charged layer. Carbon tapes are used as current collectors on both positive and negative charged layers. When these two layers are brought in contact with some pressure applied by a human finger, and then released, characteristic negative and positive voltage spikes are respectively observed. Peak voltages as high as 2.6 Volts have been obtained with the present 3D printed PDMS-BaTiO3-MWCNT layers. These observations indicate the applicability of this 3D printed composite in triboelectric energy generation.

Acknowledgments: This research was supported by the National Science Foundation grant #1827690.

Plasma Science and Technology Division
Room B130 - Session PS+2D+EM+SS+TF-ThA
Plasma-Enhanced Atomic Layer Etching

Moderators: Steven Vitale, MIT Lincoln Laboratory, Mingmei Wang, TEL Technology Center, America, LLC

2:20pm **PS+2D+EM+SS+TF-ThA1 Atomic Layer Etch: Real World Utilization of an Idealized Solution**, ***Peter Biolsi,*** TEL Technology Center, America, LLC **INVITED**

Atomic Layer Etch: Real World Utilization of an Idealized Solution

Critical dimensions (CD) continue to shrink driven by the quest for cheaper, faster and less power-consuming devices. If simple shrink was not enough, all of the back end, middle and front end of line (BEOL, MOL and MOL) also have introduced structural complexity and stringent topographic dimension, material property integrity and fundamental integration yield requirements. Atomic layer etching (ALE) has gained favor as an approach to extract more control over the fabrication of small CD complex topographic structures, atomic later etching. The idea is that alternating steps of self-limiting processes (e.g., passivation layer formation) and desorption (e.g., the removal of a passivation layer) mitigate aspect ratio dependence effects that lead to the aforementioned problems. The problem is that not all passivation processes are self-limiting. For the etching of dielectric materials, a self-limiting precursor step is not available as etch processes relies on cyclic process (fluorocarbon deposition and ion bombardment steps). Fluorocarbon based processes are not self-limiting rendering them quasi-atomic layer etch. Without special consideration, quasi-ALE has the same problems that continuous processes possess with additional burden of throughput.

Even though ALE can be difficult to be utilized in real-word scenarios, the learning from ALE finds its use in many etch applications. An etch chamber which can provide wide range of radical to ion flux ratios and precise ion energy control (using pulsing techniques) is suitable for ALE or utilizing ALE learnings. Currently, new ALE techniques based on surface modification by ions (Hydrogen plasma treatment of Silicon Nitride) followed by removal of modified layer by F radicals (High pressure NF3 or SF6 plasma) or surface modification by NH3/HF (to create a quasi-self-limiting diffusion barrier layer) followed by removal of modified layer by thermal means, are employed to etch critical layers where requirements are stringent. New frontier of etch technology will be the ability to achieve area selective etch without compromising etch rate of the process. Examples of such activities will be presented in this presentation.

3:00pm **PS+2D+EM+SS+TF-ThA3 Mechanism of SiN Etching Rate Fluctuation in Atomic Layer Etching**, ***Akiko Hirata****, M. Fukasawa, K. Kugimiya, K. Nagaoka,* Sony Semiconductor Solutions Corporation, Japan; *K. Karahashi, S. Hamaguchi,* Osaka University, Japan

Atomic layer etching (ALE) enables atomic-precision control of the surface reaction and low damage etching of the underlying layer for device fabrication. In this study, we investigated SiN ALE with process optimization of the surface adsorption and desorption steps, and we clarified the rate fluctuation mechanism.

A dual frequency CCP reactor (60 MHz/2 MHz) was used in this study. A SiN (50 nm) was deposited on the Si substrate by LPCVD. One etching cycle consisted of two steps. CH_3F/Ar plasma was applied to deposit the hydrofluorocarbon (HFC) polymer as the adsorption step. Then, Ar plasma was used in the desorption step. The thicknesses of SiN and the HFC polymer were measured by spectroscopic ellipsometry. The chemical bonding was analyzed by XPS.

A 1.2-nm-thick HFC polymer was deposited on SiN as the adsorption step. Next, we investigated the desorption step by using Ar plasma. The etched amount for 1 cycle was 0.58 nm. However, we found the etch-stop of SiN after 10 cycles of ALE, owing to the deposition (>6 nm) of a protective film on the surface. The etch-stop could be caused by sputtering of the Si upper electrode and/or re-deposition of the HFC film. To investigate the etch rate fluctuation, the SiN surface after ALE was analyzed. C-C and C-N bonds were detected after 1 cycle, and C-C bonds increased after 10 cycles. It was clear that the excess HFC polymer deposition suppressed the ALE reactions. Ar^+ ion bombardment during the desorption step selectively eliminated the H and F in the HFC polymer, because the bonding energies of C-H and C-F were low. As the bonding energies of C-C (6.4 eV) and C-N (7.8 eV) are relatively high, these bonds remained after the desorption step. We speculated that excess C-rich polymer deposition after ALE started from the residual C-C bond. Residual Si-C bond is also possible reason, since the MD simulation revealed that the formation of Si-C bond was promoted in the fluorocarbon layer during SiO_2 ALE. [1] These results clearly showed that the initial adsorption kinetics of HFC polymer was strongly affected by the residual carbon on the SiN surface. To suppress the C-rich polymer deposition, we studied stable SiN ALE using the desorption step of Ar/O plasma (0.36 nm/cycle) and the two-step sequential desorption step of Ar and O plasma (0.6 nm/cycle). Although the effect of O adsorption in SiO ALE has been studied previously,[2] few studies have been reported for the case of SiN. Because the surface condition is able to fluctuate with the number of cycles, precise surface control is strongly required to achieve stable ALE.

[1] S. Hamaguchi et al., 2018 AVS, PS-FrM6. [2]T. Tsutsumi et al., JVST A 35 (2017) 01A103.

3:20pm **PS+2D+EM+SS+TF-ThA4 Effect of Polymerization on Ar+ Bombardment Modification of SiO_2 and Si_3N_4 Substrates: Molecular Dynamics Simulation Study**, ***Hojin Kim****, Y. Shi, Y.-H. Tsai, D. Zhang, Y. Han,* TEL Technology Center, America, LLC; *K. Taniguchi,* TEL Miyagi Limited, Japan; *S. Morikita,* TEL Miyagi Limited; *M. Wang, A. Mosden, A. Metz, P.E. Biolsi,* TEL Technology Center, America, LLC

To understand the selective removal of silicon oxide (SiO_2) against silicon nitride (Si_3N_4) with gaseous reactants for advanced etch process, we have studied the surface modification of both SiO_2 and Si_3N_4 substrates with Ar+ bombardment by using molecular dynamics (MD) simulation. The substrate samples was prepared with and without carbon (C) and hydrogen (H) polymerization to investigate the effect of polymerization on surface modification. C and H atoms were deposited with low ion energy not to disrupt the surface much. After preparation of substrate, Ar+ bombardment with various ion energy (IE) were performed. We obtained a damage depth with a wigner-seitz defect analysis as a function of IE and compared the cases with and without polymerization to check the role of the added polymer layer on surface modification. In pristine Si_3N_4 and SiO_2 case, at IE=25eV, both substrates starts to show the damage with penetration of Ar+ and follows with an exponential raise as the IE increases. Damage depth at Si_3N_4 is deeper than that at SiO_2. In polymerization, simulations show that H is more deposited than C on Si_3N_4 while on SiO_2, C is more deposited than H. no silicon-hydrogen bonds appear on both substrates and in Si_3N_4, nitrogen-hydrogen bond is dominated while oxygen-carbon bond is popular in SiO_2. For damage analysis, in Si_3N_4 case, CH polymerization helps to lower about 30% in the damage depth with exponential behavior. However, SiO_2 case shows the opposite effect of CH polymerization in the damage depth. Formed polymer layer leads to increase the damage depth by comparing with pristine SiO_2 and helps more clear exponential behavior as a function of IE. Finally, analyzed results using XPS and/or SIMS from blanket SiO_2 and Si_3N_4 films etched in a Capacitively Coupled Plasma (CCP) chamber are compared with the MD simulation results.

4:00pm **PS+2D+EM+SS+TF-ThA6 Advanced Cyclic Plasma Etch Approaches for Metal Patterning: Synergy and Surface Modification Effects**, ***Nathan Marchack,*** IBM T.J. Watson Research Center; *K. Hernandez,* University of Texas at Dallas; *J. Innocent-Dolor, M.J.P. Hopstaken, S.U. Engelmann,* IBM T.J. Watson Research Center **INVITED**

Atomic layer etching or ALE is a burgeoning research area of plasma processing that offers critical advantages needed for future advancements in semiconductor devices, namely lower damage and enhanced selectivity, through its self-limited reaction cycles separated by purge steps.[1] ALE processes offer a significantly higher degree of tunability over traditional continuous-wave (CW) plasma etching, due to the fact that parameters such as gas flows, pressure, and bias power can be adjusted on a step-specific basis rather than as a global setting for the length of the process.

Our previous work investigated the effect of varying the purge step times in a quasi-ALE process using alternating Cl_2/H_2 exposures on the etched profiles of titanium and tantalum nitride.[2] Titanium and tantalum-based conductive films have been previously evaluated as gate materials for CMOS devices but more recently have been incorporated as top electrodes for novel technologies such as magnetoresistive RAM (MRAM) and hard masks for carbon electrodes utilized in biological sensing. As the trend of downscaling device size continues, the ability to pattern these films at tight pitches with minimal redeposition becomes highly important.

Sub-surface modification of films such as Si_3N_4 and indium-doped tin oxide (ITO) by low atomic weight (LAW) ions such as H^+ has been discussed in literature as facilitating self-limited etch behavior.[3,4] We present new

data exploring the incorporation of LAW species into cyclic etch processes, namely penetration depth into these metal nitride films and their role in surface oxide formation, the latter of which can contribute to novel pitch multiplication schemes.[5] SIMS measurements reveal that the depth of penetration of H^+ for TaN films can be >40 nm and can occur through a native oxide layer that inhibits etching by Cl species. Pressure variation is a significant factor in tuning this effect, which can potentially modify the etch resistance of these films and enable novel integration schemes.

[1] K. J. Kanarik, T. Lill, E. A. Hudson, S. Sriraman, S. Tan, J. Marks, V. Vahedi, R. A. Gottscho, J. Vac. Sci. Technol. A. 2015, 33, 020802.

[2] N. Marchack, J. M. Papalia, S. U. Engelmann, E. A. Joseph, J. Vac. Sci. Technol. A. 2017, 35, 05C314.

[3] S. D. Sherpa, A. Ranjan, J. Vac. Sci. Technol. A. 2017, 35, 01A102.

[4] A. Hirata, M. Fukasawa, K. Nagahata, H. Li, K. Karahashi, S. Hamaguchi, T. Tatsumi, Jpn. J. Appl. Phys. 2018, 57, 06JB02.

[5] N. Marchack, K. Hernandez, B. Walusiak, J-l. Innocent-Dolor, S. U. Engelmann, Plasma Process Polym. 2019, e1900008.

4:40pm **PS+2D+EM+SS+TF-ThA8 Surface Modification and Stability of Plasma-assisted Atomic-layer Etching (ALE) of Si based Materials; Analysis by Molecular Dynamics (MD) Simulation***, **Satoshi Hamaguchi**, M. Isobe, E.J.C. Tinacba, S. Shigeno, Y. Okada, T. Ito, K. Karahashi,* Osaka University, Japan

A plasma-assisted atomic-layer etching (ALE) process typically consists of alternating application of chemically reactive species (adsorption step) and Ar ion bombardment with low bias energy (desorption step) to the surface to be etched. In the adsorption step, a modified layer is formed on the material surface and, in the desorption step, the modified layer is removed with the original material underneath being intact. In this presentation, using the results of MD simulation of ALE for Si, SiO2, and SiN, together with experimental observations, physical mechanisms of the formation and removal of surface modified layers in typical ALE processes will be discussed.

Our molecular dynamics (MD) simulation of SiO2 ALE by fluorocarbon adsorption and Ar+ ion bombardment shows that preferential sputtering of oxygen takes place by Ar+ ion bombardment and a Si rich layer mixed with fluorine and carbon atoms is formed on the SiO2 surface. Ideally this modified layer should be removed completely in the subsequent desorption step, but in general it is not. In such a layer, the atomic number ratio of Si to O can be as high as unity and carbon provided in the subsequent adsorption step tends be deposited rather than removing O atoms from the surface by forming CO molecules. Therefore as the ALE cycles proceed, the adsorbed fluorocarbon layer thickens and eventually an etch stop may occur. With fine tuning of incident Ar+ ion energy, an etch stop may be avoided but the process window to achieve both continuous ALE cycles (by sufficiently high Ar+ ion energy) and ideal self-limit in each cycle (by sufficiently low Ar+ ion energy) may still be small or even nonexistent. The incompleteness of the modified surface removal in each ALE cycle seems universal phenomena for plasma-assisted ALE for most materials. For other plasma-assisted ALE processes that we examined by MD simulation, the surface modified layer formed during the adsorption step could not be removed completely by low-energy Ar+ ion bombardment, either. Indeed low-energy Ar+ ion bombardment contributes to the formation of a deeper modified layer by pushing down adsorbed species into the bulk, rather than simply removing it.

5:00pm **PS+2D+EM+SS+TF-ThA9 Innovative Future Etch Technology by Atomic-order Control***, **Yoshihide Kihara**, T. Katsunuma, S. Kumakura, T. Hisamatsu, M. Honda,* Tokyo Electron Miyagi Ltd., Japan **INVITED**

In recent years, with the progress of device miniaturization and increased challenges in the scale of integration of semiconductor devices, ultra-high selectivity and atomic layer-level critical dimension (CD) control techniques are required in the fabrication processes.

In the conventional etching, using a fluorocarbon (FC) gas, the high selectivity is obtained by taking advantage of the difference of the FC protective film thickness due to the difference of materials.[1] However, adopting the conventional approach to cutting-edge pattern structure becomes difficult due to the excessive FC film clogging the micro slit facet. To meet the highly complex requirements, alternative process was developed by using ion modification and chemical dry removal.[2] We have made several improvements on this new approach and applied it to SiN and SiC etching. The improved new approach achieves ultra-high selectivity without FC protective film and we also confirmed this process has the characteristics of a self-limiting reaction based on ion depth profile as well as ALE.

In the patterning processes, lower pattern densities have a larger CD shrinking due to micro-loading. Hence, we developed the new process flow that combines atomic layer deposition (ALD) technique and etching. With this method, we achieved CD shrinking at atomic-layer level precision for various patterns, without causing CD loading.[3]

Moreover, Quasi-ALE can etch the pattern while maintaining the mask CD for different pattern density. This is because Quasi-ALE precisely controls the surface reaction by controlling the radical flux and ion flux independently.[3] Also, it was necessary to control oval CD size between X and Y respectively. We found that X-Y CD control can be easily performed by changing the balance of FC adsorption and Ar desorption in Quasi-ALE. However, there are concerns about mask selectivity and ion damage in this approach. To solve these problems, we introduce the Advanced Quasi-ALE technique which combines mask protection together with Quasi-ALE. The Advanced Quasi-ALE achieves wider X-Y CD control margin.

On the other hand, as aspect ratio is increased in the memory fabrication process, the occurrence of bowing profile is a serious problem. To address the issue, the new improvement technique has been developed that combines the concept of ALD and etching. With this method, we are able to etch profile more vertically in high A/R feature.

Reference

[1] M. Matsui et al., J. Vac. Sci. Technol. A 19 1282 (2001)

[2] N. Posseme et al., Applied Physics Letters105 051605 (2014)

[3] M. Honda et al., J. Phys. D: Appl. Phys., Vol.50, No.23 (2017)

Thin Films Division
Room A124-125 - Session TF+AS+EL+PS+RA-ThA
Characterization of Thin Film Processes and Properties

Moderators: Richard Vanfleet, Brigham Young University, Virginia Wheeler, U.S. Naval Research Laboratory

2:20pm **TF+AS+EL+PS+RA-ThA1 Phase Separation in III-V Semiconductor Thin Films***, **Mark Twigg**, N.A. Mahadik, N.A. Kotulak, S. Tomasulo, M.K. Yakes,* U.S. Naval Research Laboratory **INVITED**

Phase separation in III-V semiconductor alloys remains a problem that limits the performance of electronic materials. As the first stage in a comprehensive program addressing this issue, we have begun investigating an alloy system in which only the group III elements differ: InGaAs. Lattice-matched InGaAs alloy films were deposited at three temperatures (400, 450, and 500C) by molecular beam epitaxy on a (001) InP substrate.

According to kinetic instability theory, the critical temperature for spinodal phase separation in InGaAs is 814C, a temperature well above the growth temperatures used in this study [1,2]. Dark-field (DF) cross-sectional transmission electron microscopy (XTEM), using the composition sensitive g=002 reflection, was used to determine the amplitude of composition modulations averaged over the thickness of the XTEM sample. The amplitude of composition modulation was found to decrease with increasing growth temperature, yielding values of 0.6, 0.4, and 0.3 atomic percent for the growth temperatures 400, 450, and 500C, respectively, a trend in accord with kinetic instability theory. X-ray reflectivity and 2-dimensional small angle x-ray measurements also indicate that the 400C growth shows significantly greater phase separation than the 450 and 500C growths. Atom probe tomography indicates that the amplitude of composition modulation for the 400C growth is approximately 1 atomic percent, a value that compares favorably with the 0.6 atomic percent measured by DF XTEM.

The range of wavelengths for lateral composition modulation is found to extend from approximately 3 to 30 nm. According to the literature, such wavelengths have been found to depend on growth temperature for a number of III-V semiconductor alloys, in agreement with predictions based on surface diffusion. Measurements of the composition modulation wavelength as a function of temperature have been performed by analyzing DF XTEM images recorded using the g=220 diffraction vector, from XTEM samples with the glue line along the rapidly-diffusing [110] direction. Fast Fourier Transform (FFT) power spectra recorded from each image allowed the dominant composition modulation wavelengths to be determined. Analyzing these wavelengths as a function of temperature yields the same activation energy (0.55 eV) as that found in surface diffusion measurements for In adatoms on the (001) InGaAs surface [3];

thereby confirming the role of surface diffusion in phase separation driven composition modulations.

[1] F. Glas, Phys. Rev.B, 62, 7393 (2000).

[2] I. P. Ipatova, V. G. Malyshkin, and V. A. Shchukin, J. Appl. Phys. 7198 (1993).

[3] Stevens et al., J. Appl. Phys. 121, 195302 (2017).

3:00pm **TF+AS+EL+PS+RA-ThA3 In-Situ Spectroscopic Monitoring of Methylamine-Induced Hybrid Perovskite Phase Transitions***, **Jonathan Meyers**[1], L.Y. Serafin, J.F. Cahoon,* University of North Carolina at Chapel Hill

Lead halide perovskites have shown remarkable promise for use in thin film optoelectronic devices such as photodetectors, light-emitting diodes, and solar cells. Methods for casting thin films of perovskite have been extensively studied, and great improvements have been made in an effort to improve device efficiency and stability. A few reports have suggested some benefits to processing or post-processing techniques in a methylamine (MA) atmosphere, including healing grain boundary defects to create pinhole free films with grains on the order of tens of microns and improving crystallinity. The process can be observed spectroscopically as the MA induces a reversible phase change which bleaches the dark perovskite film. In this work, we perform the MA-treatment in a vacuum reactor while monitoring in-situ the UV-visible spectral response correlated with temperature and MA partial pressure. Clear evidence is found for the existence of a solid intermediate phase in transitioning from $MAPbI_3$(s) to $MAPbI_3*x$MA(l) and back again. We construct a phase diagram and demonstrate that the critical partial pressure of the phase transition changes from 10 to 500 torr between 25 and 120 °C. By tuning the kinetics of film crystallization, compact films with domains up to 80 µm can be produced.

4:00pm **TF+AS+EL+PS+RA-ThA6 Obtaining Smooth Surfaces and Measuring Surface Roughness***, **Steven M. George,*** University of Colorado at Boulder **INVITED**

Smooth surfaces are important in many areas including friction, adhesion, optics and film growth. Smooth surfaces can be obtained from rough surfaces using chemical mechanical polishing (CMP). Rough surfaces can also be smoothed using atomic layer deposition (ALD) if the conformal ALD film thickness is comparable with the lateral length scale of the roughness. In addition, rough surfaces can be smoothed using isotropic thermal atomic layer etching (ALE) if the ALE etch depth is comparable with the width of the surface asperities. Quantifying the degree of surface roughness after CMP, ALD or ALE is challenging. Surface roughness can be obtained using atomic force microscope (AFM) or x-ray reflectivity (XRR) measurements. However, the AFM and XRR techniques do not always agree. Some of the inconsistencies are attributed to the different lateral length scales for the AFM and XRR measurements. Using both AFM and XRR to characterize surface roughness is recommended for reliable measurements. In addition, XRR measurements for surface roughness should include both specular and diffuse off-specular scattering.

4:40pm **TF+AS+EL+PS+RA-ThA8 Characterizing Ultra-thin Layer Growth and Area Selective Deposition using High Resolution Low Energy Ion Scattering (LEIS)***, **Thomas Grehl,*** IONTOF GmbH, Germany*; P. Brüner,* ION-TOF GmbH, Germany*; V. Pesce, B. Pelissier, R. Gassilloud, C. Vallée,* Laboratoire des Technologies de la Microélectronique (LTM), France

When depositing ultra thin films of only very few nm of thickness, the characterization of the early stages of film growth is crucial for the quality of the film. For example, the initial thickness distribution before layer closure, created by the nucleation mechanism, will often remain after the film is complete. To analyze these early stages of growth requires very surface sensitive analytical techniques with good detection limits.

Specifically for area selective deposition, the demand for characterization increases even further. The deposition processes get more complex, involving atomic layer or plasma etching to remove nucleation on blocked areas. This also requires means of characterization, determining the effects of etching steps on the film being created, possible contamination and the level of success of the blocking.

One technique specifically suited for this application is Low Energy Ion Scattering (LEIS). By scattering noble gas ions from the surface of the sample, the mass of the atoms in the outer atomic layer is determined non-destructively. Due to specific charge exchange processes, the peaks in the scattering spectrum correspond only to the outer atomic layer, making LEIS the most surface sensitive technique to determine the elemental composition of a surface.

In addition, information from deeper layers is available in two ways: First of all, features in the spectrum contain information about the first few nm of the sample – especially for heavier elements, the in-depth distribution can be determined non-destructively. For more complex systems or light elements, sputter depth profiling can be applied as well.

In this presentation, we will illustrate the main features of LEIS on ALD films. The main part will be on an area selective deposition (ASD) process for Ta_2O_5 films on TiN or Si. Here, plasma-enhanced ALD (PE-ALD) and various plasma or ALE like etching processes, all using fluorine-containing compounds, are used to develop a super-cycle scheme for ASD. We show the effect of the different etching methods and use sputter depth profiling to determine the distribution of F – a light element not accessible to non-destructive depth profiling in LEIS. An important result is the distribution of F close to the surface, in the bulk of the film, or at the interface.

Besides this, some further sample systems will be used to highlight the use of LEIS for ultra-thin film characterization.

5:00pm **TF+AS+EL+PS+RA-ThA9 Real-Time Monitoring of Aluminum Oxidation Through Wide Band Gap MgF_2 Layers for Protection of Space Mirrors***, B.I. Johnson, T.G. Avval, G. Hodges, K. Membreno, D.D. Allred, **Matthew Linford,*** Brigham Young University

Because of its extraordinary and broad reflectivity, aluminum is the only logical candidate for advanced space mirrors that operate deep into the UV. However, aluminum oxidizes rapidly in the air, and even a small amount of oxide (as little as a nanometer) can have a noticeable, detrimental impact on its reflectivity at short wavelengths. Thin films of wide band gap materials like MgF_2 have previously been used to protect aluminum surfaces. Here we report the first real-time, spectroscopic ellipsometry (SE) study of aluminum oxidation as a function of MgF_2 over layer thickness, which ranged from 0 – 6 nm. SE data analysis was performed vis-à-vis a multilayer optical model that included a thick silicon nitride layer. The optical constants for evaporated aluminum were initially determined using a multi-sample analysis (MSA) of SE data from MgF_2 protected and bare Al surfaces. Two models were then considered for analyzing the real-time data obtained from Al/MgF_2 stacks. The first used the optical constants of aluminum obtained in the MSA with two adjustable parameters: the thicknesses of the aluminum and aluminum oxide layers. The thicknesses obtained from this model showed the expected trends (increasing Al_2O_3 layer thickness and decreasing Al layer thickness with time), but some of the Al_2O_3 thicknesses were unphysical (negative). Because the optical constants of very thin metals films depend strongly on their structures and deposition conditions, a second, more advanced model was employed that fit the optical constants for Al, and also the Al and Al_2O_3 thicknesses, for each data set. In particular, the Al and Al_2O_3 thicknesses and optical constants of Al were determined in an MSA for each of 50 evenly spaced analyses in each four-hour dynamic run performed. The resulting optical constants for Al were then fixed for that sample and the thicknesses of the Al and Al_2O_3 layers were determined. While the first and second models yielded similar Al and Al_2O_3 thickness vs. time trends, the film thicknesses obtained in this manner were more physically reasonable. Thicker MgF_2 layers slow the oxidation rate of aluminum. The results from this work should prove useful in protecting space mirrors prior to launch. Detailed surface/material analysis by X-ray photoelectron spectroscopy will also be shown, as well as more advanced SE modeling.

5:20pm **TF+AS+EL+PS+RA-ThA10 Visualization of Ultrafast Charge Motion in Thin Films via THz Emission Spectroscopy***, **Aaron Lindenberg,*** Stanford University **INVITED**

We describe a method for probing ultrafast time-dependent currents in thin films and heterostructures by recording the associated emitted electromagnetic fields. This detection scheme offers direct sensitivity to the flow of charges at the atomic-scale and enables a real-time probe for investigating ultrafast charge transfer processes at molecular interfaces. Applied to transition metal dichalcogenide heterostructures having a staggered (Type-II) band alignment, we observe a burst of electromagnetic radiation at terahertz frequencies following above gap excitation. The emitted electric field transients encode information about the charge transfer within the heterostructure. The polarity of the emitted field reflects the direction of the charge transfer and the polarity is reversed as the order of the bilayer within the heterostructure is altered. We find that the charge transfer proceeds at an ultrafast rate (~100 fs) indicating a remarkable efficiency for the charge separation across these atomic-scale bilayers.

[1] **National Student Award Finalist**

We will also describe initial experiments and coupled theoretical efforts probing charge separation and ultrafast photovoltaic responses in multiferroic BFO periodic domain structures. We show that charge separation occurs dominantly at the domain walls and provide a quantitative estimate of the efficiency of this process.

Thin Films Division
Room A122-123 - Session TF+SS-ThA
Metal Halide Perovskites, Other Organic/Inorganic Hybrid Thin Films

Moderators: Mark Losego, Georgia Institute of Technology, Greg Szulczewski, University of Alabama

2:20pm **TF+SS-ThA1 Tailoring Electrode-electrolyte Interfaces in Lithium-ion Batteries using Molecularly Engineered Functional Polymers***, **Laisuo Su,*** Carnegie Mellon University*; J. Weaver,* National Institute of Standards and Technology (NIST)*; M. Groenenboom,* National Institute of Sandards and Technology (NIST)*; B.R. Jayan,* Carnegie Mellon University **INVITED**

The performance and stability of lithium ion batteries (LIBs) depend on charge transfer and reactions at electrode-electrolyte interfaces (EEI), making interfaces design a key issue. Here we molecularly engineer this interface using conformal, functional polymer nanolayers via a novel vapor-based deposition technique. We demonstrate that poly(3,4-ethylenedioxythiophene) (PEDOT) nanolayer doubles the capacities of $LiCoO_2$ at high rates and extends its 4.5 V cycling life by 260%. The improved rate performance is enabled by high diffusion coefficient of Li^+ in PEDOT measured from neutron depth profiling. Such behavior is further understood by density functional theory (DFT) simulation. The extended cycling stability comes from strong interactions between PEDOT and Co atoms, as suggested from X-ray photoelectron spectroscopy and DFT simulations. Additionally, in-situ synchrotron X-ray diffraction reveals that PEDOT uniformizes current distribution and improves $LiCoO_2$ structural stability during cycling tests. This work adds understanding and provides guidelines for designing the EEI for advanced LIBs.

3:00pm **TF+SS-ThA3 Chemoselective Adsorption of Alkyne-functionalized Cyclooctynes for the Formation of Si/organic Interfaces***, C. Laenger,* ***Julian Heep,*** Justus-Liebig-University, Giessen, Germany*; P. Nikodemiak, T. Bohamud,* Philipps-University, Marburg, Germany*; P. Kirsten,* Justus-Liebig-University, Giessen, Germany*; U. Hoefer, U. Koert,* Philipps-University, Marburg, Germany*; M. Duerr,* Justus-Liebig-University, Giessen, Germany

Controlled organic functionalization of the Si(001) surface may play an important role in the efforts towards further miniaturization of silicon based electronic devices. The first step of such an organic functionalization in terms of organic molecular layer deposition on Si(001) would be the chemoselective adsorption of bifunctional molecules on silicon: whereas one functionality binds to the surface, the other stays intact for the attachment of further layers. This task, however, is complicated by the high reactivity of the dangling bonds with respect to almost all organic functional groups. As a consequence, bifunctional organic molecules typically react via both functional groups on the silicon surface. We solved this problem using cyclooctyne as the main building block of our strategy. The strained triple bond of cyclooctyne reacts via a direct reaction channel, in contrast to most other organic functional groups, which react on Si(001) via a metastable intermediate. This makes the latter ones effectively unreactive in competition with the direct pathway of cyclooctyne's strained triple bond [1].

In this work, we focus on the preparation of a functionalized organic layer on Si(001) using an alkyne-functionalized cyclooctyne, i.e., ethynyl-cyclopropyl-cyclooctyne (ECCO). If the ECCO molecule binds chemoselectively to the silicon substrate via cyclooctyne's strained triple bond, the terminal, linear triple bond of the ECCO molecule can be employed for the attachment of the second layer of molecules, e.g., via alkyne-azide coupling. We first show that the linear triple bond follows an indirect reaction pathway via a weakly bound intermediate. XPS and STM results then clearly indicate that ECCO adsorbs selectively on Si(001) via a [2+2] cycloaddition of cyclooctyne's strained triple bond. No indication for a reaction via the ethynyl group was detected. This chemoselectivity was observed for all coverages, starting from the isolated molecules up to saturation coverage of one monolayer [2]. The ECCO molecules can thus form an organic functionalization of the Si(001) surface which can be used for controlled attachment of further molecular layers.

[1] Reutzel, et al., J. Phys. Chem. C **120** 26284 (2016).

[2] C. Länger, et al., J. Phys.: Condens. Matter **31** 034001 (2019).

3:20pm **TF+SS-ThA4 Durability of Property Changes in Polyester Fabrics Infused with Inorganics via Vapor Phase Infiltration***, **Kira Pyronneau**, E.K. McGuinness, M.D. Losego,* Georgia Institute of Technology

Vapor Phase Infiltration (VPI) is a processing method for transforming polymers into organic-inorganic hybrid materials. During VPI, a polymer is exposed to vapor-phase metalorganic precursors that sorb, diffuse, and react within the bulk of the polymer to create new hybrid materials. VPI has been shown to modify properties such as the mechanical strength of spider silk, the thermal and UV degradation resistance of Kevlar, and the fluorescence of polyester. This study aims to better understand how VPI can change textile properties for industrial applications and the durability of these changes. To this end, polyester fabrics were treated with trimethylaluminum (TMA) and co-reacted with water in a custom-built vacuum chamber. The temperature of the treatment process was varied from 60˚C to 140˚C to establish a relationship between processing temperature, physiochemical structure, and material properties. Using thermogravimetric analysis (TGA), these infiltrated fabrics were found to have inorganic loadings between 5 and 8 weight percent, with a maximum inorganic loading at 100 °C (Figure 1). These results are consistent with our current understanding of precursor / polymer sorption thermodynamics and indicate that processing temperature can be used to control the loading of inorganics through both the diffusion rate and the sorption equilibrium. To examine the durability of this inorganic loading, wash fastness testing at 100˚C for 90 minutes followed by TGA and SEM/EDX was used to determine the effects of high temperature wash cycles. These tests demonstrated that the inorganic loading remains even after intense laundering (Figure 2). To further characterize the durability of VPI treatment, known changes due to the VPI process were compared before and after washing. In particular, mechanical properties, fluorescence, and thermal degradation behavior were investigated. This talk will explore the wash-fastness of VPI treatments of polyester at different processing temperatures and the retention of enhanced properties relevant to the textile industry.

4:00pm **TF+SS-ThA6 Materials Synthesis and Device Fabrication for Novel Inorganic Perovskites***, **Mingzhen Liu**,* UESTC, China **INVITED**

In recent years, organic lead halide perovskite materials have attracted much attention due to their outstanding optoelectric properties and low manufacturing cost. To improve the stability of perovskite solar cells, inorganic $CsPbI_3$ perovskite has been demonstrated as promising material for solar cells owing to the superb photoelectronic property and composition stability. However, the low stability of perovskite phase $CsPbI_3$ (α-phase) with an appropriate band gap under ambient environment hinders its practical application.

Here, we investigate new ways of synthesizing inorganic perovskite materials and optimizing the device stability through dimensional engineering. we tailor the three-dimension $CsPbI_3$ perovskite into quasi-two-dimensional $Cs_xPEA_{1-x}PbI_3$ perovskite, where an optimal $Cs_xPEA_{1-x}PbI_3$ film remains stable in α phase up to 250℃Moreover, we further present an in-depth investigation of the so-called stable 'α-$CsPbI_3$,' especially the starting material hydrogen lead trihalide ($HPbI_3$, also known as $PbI_2{\cdot}x$HI) that is usually used for synthesizing α-$CsPbI_3$. We notice that the "mythical" $HPbI_3$, the often-assumed reaction product of HI and PbI_2, does not actually exist. Instead, adding acid to DMF is known to generate a weak base dimethylamine (DMA) through hydrolysis, and with the presence of PbI_2 the actual final product is believed to be a compound of $DMAPbI_3$. Our findings offer new insights into producing inorganic perovskite materials, and lead to further understanding in perovskite materials for solar cells with improved efficiency and stability.

4:40pm **TF+SS-ThA8 Carrier-Gas Assisted Vapor Deposition of Metal Halide Perovskite Thin Films***, **Catherine Clark**,* University of Minnesota*; E.S. Aydil,* New York University*; R.J. Holmes,* University of Minnesota

Hybrid organic-inorganic halide perovskites have emerged as an important class of optoelectronic materials with potential applications in photovoltaics and light emitting devices. One of the challenges in forming thin films of halide perovskites is controlling stoichiometry and morphology. We have designed and built a carrier-gas assisted vapor deposition (CGAVD) system capable of depositing halide perovskite thin films (*e.g.,* $CH_3NH_3SnI_xBr_{3-x}$) with independent control over their stoichiometry and morphology. In our CGAVD system, an inert carrier gas (N_2) transports sublimed material vapors through a hot-walled chamber to a cooled substrate where they selectively condense and/or react. By separately controlling the precursor sublimation rate, *via* source

temperature, and the transport rate to the substrate, *via* carrier gas flow rate, we realize fine control of species flux at the substrate and successfully co-deposit materials with very different vapor pressures (*e.g.* CH_3NH_3Br,$SnBr_2$). Four additional independent parameters (dilution gas flow, chamber pressure, gas temperature, and substrate temperature) can be varied to access a wide range of deposition conditions and film morphologies with controlled stoichiometry. To navigate the vast parameter space of CGAVD, we use an experimentally validated transport and reaction model, which informs the deposition parameter selections. We find that repeatable and spatially uniform deposition requires operating in a regime where solid source material is at equilibrium with its vapor and convective transport determines the flux of species arriving at the substrate. Importantly, we find that films grown using CGAVD have a stoichiometric "self-correcting" and robust operation window, wherein excess precursor flux during co-deposition is rejected from the film and a phase-pure perovskite film results. This is practically advantageous as it relaxes the need for balancing precursor fluxes exactly during co-deposition. We demonstrate the growth of $CH_3NH_3SnI_xBr_{3-x}$ thin films with a wide range of stoichiometries and morphologies. Specifically, by tuning the source material temperature (140 °C – 290 °C), the carrier gas flow rate (2 sccm – 100 sccm), the substrate temperature (8 °C – 70 °C), and the chamber pressure (350 mTorr – 10 Torr), we realize corresponding changes in grain orientation and grain size from <100 nm to over 1 µm. CGAVD is a promising approach to deposition of other halide perovskites and can potentially enable the growth of previously inaccessible morphologies and multi-layer perovskite films.

5:00pm **TF+SS-ThA9 Synthesis and Optical Properties of Organo-halide 2D Perovskites***, **Misook Min**, A.B. Kaul,* University of North Texas

Organic-inorganic halide perovskite materials have attracted interest in recent years due to their excellent optoelectronic properties, such as high absorption coefficient, tunable band gap, small exciton binding energy. These advantages combined with the extremely low fabrication coat make this kind material suitable as a light absorber for solar cells, light emitting diodes, field-effect transistors and photo-detectors [1]. Hybrid organic-inorganic perovskite described by the formula ABX_3 (A = organic ammonium cation, B = inorganic compounds, X = halide anion). Specifically, the iodide and bromide versions of $CH_3NH_3PbX_3$ have led to a breakthrough in various research field. We report the scalable synthesis and properties of the 2D series of lead iodide $(CH_3(CH_2)_3NH_3)_2(CH_3NH_3)_{n-1}Pb_nI_{3n+1}$($n$ = 2, 3, and 4) perovskites [2]. The 2D $(CH_3(CH_2)_3NH_3)_2(CH_3NH_3)_{n-1}Pb_nI_{3n+1}$ were synthesized and materials characterization was conducted using atomic force microscopy (AFM), X-ray diffraction (XRD), and Photoluminescence (PL) spectroscopy. The crystal structure and surface morphology for n = 2, 3, and 4 perovskites was validated using XRD and AFM, and the peak optical absorption was consistent with the composition-tunable bandgap for these formulations occurring at ~ 2.18 eV, 2.06 eV, and 2.03 eV. Our results show that hybrid organic-inorganic perovskites can be easily and efficiently prepared. Also, the hybrid organic-inorganic perovskites define a promising class of stable and efficient light absorbing materials for photo-detectors and other applications.

5:20pm **TF+SS-ThA10 Encapsulation of Perovskite Nanocrystal Solids using Metal Oxides - A Closer Look into Optical Properties***, **Riya Bose**, Y. Zheng, T. Guo, Y. Garstein, A.V. Malko,* University of Texas at Dallas

The performance (i.e., light harvesting, optical gain or emission outputs) of many optoelectronics devices (i.e., lasers, photovoltaics (PVs), light emitting diodes (LEDs), etc.) critically depends on the ability to deposit solution processed nanocrystals (NCs) into well-organized, close-packed solids with high photoluminescence quantum yields (PL QYs) and the long term stability of NC films. However, irrespective of the high quality of NCs or the passivation techniques used in solution, the deposition of NC multilayers as well as the exposure to the environment during solid state device fabrication often require or lead to changes in the NCs chemical environment, such as exchange/loss of ligands, which eventually lead to formation of trap states that decrease the PL QYs of NCs and are often detrimental to device performances. An attractive approach to protect the NCs' integrity is the use of atomic layer deposition (ALD) in which self-limiting surface reactions of the precursors allows conformal growth of the metal oxide layer with precise thickness control to encapsulate NCs. This process, though prevents the deterioration of NCs, is observed to decrease their PLQY significantly. To mitigate this issue, we recently developed an alternate gas phase deposition technique where a pulsed co-deposition of both metal and oxidant precursors at room temperature (RT) (reminiscent of chemical vapor deposition, CVD) is able to deposit uniform metal oxide (AlO_x) films, originating from gas-phase reactions in the immediate vicinity of the NC layer. Unlike conventional ALD, this method is observed to preserve the optical properties, e.g., PLQY and lifetime of metal chalcogenide NCs film. With this new approach, we investigate the encapsulation of hybrid metal halide perovskite NCs, which have been at the forefront of recent optoelectronic materials research due to their high absorption coefficients, high charge carrier mobilities, balanced ambipolar transport properties, and easy solution processability. However, in spite of the exceptional upsurge in the lab scale device efficiency of perovskites in a remarkably short time frame, the practical application of the same in real world is restricted by their inherent instability. AlO_x deposition on perovskite nanocrystals with our modified approach not only retains the optical properties of the NCs, but also improves them, even at a single particle level, which paves the way for unique optoelectronic opportunities.

5:40pm **TF+SS-ThA11 Self-Limited Surface Reaction between Trimethyl Aluminum and Formamidinium Lead Iodide Perovskite***, **Qing Peng**, X. Yu, H. Yan,* University of Alabama

Surface site-limited reaction is critical to modifying hybrid halide perovskites without destroying their bulk properties. However, no surface site-limited reaction on hybrid halide perovskites has been demonstrated and confirmed. Herein, we report one surface-site limited reaction on FA lead iodide with tri-methyl aluminum. The strong coordination between organic cations $FA^+$and trimethyl aluminum, a very strong Lewis acid, is found to be the key for this self-limited reaction behavior. Our results provide a model system to understand the effect of surface species on surface reaction behavior on hybrid halide perovskites.

Thin Films Division
Room Union Station B - Session TF-ThP
Thin Films Poster Session

TF-ThP1 Oxygen Partial Pressure Dependence of Structural and Photoluminescence Properties in Eu^{3+} doped Tantalum based Double-perovskite Thin Film, ***Jung Hyun Jeong**, J.H. Oh, B.C. Choi, J.H. Kim, S.Y. Seo,* Pukyong National University, Republic of Korea*; K. Jang,* Changwon National University, Republic of Korea

In this study, we investigated the structural and photoluminescence properties of Eu^{3+} doped $SrLaMgTaO_6$ (SLMTOE) double-perovskite thin films depending on the oxygen partial pressure. The X-ray diffraction patterns were examined to determine the growth behaviors of the SLMTOE films on the $SrTiO_3$ (100) substrates. In the oxygen partial pressure range of 10-200 mTorr, the SLMTOE thin films were aligned with the $SrTiO_3$ (001) substrate. The SLMTOE films grown at 100 mTorr have a low crystallinity but emitted the strongest red light corresponding to $^5D_0$-$^7F_2$ transition (Eu^{3+}). Based on this sample, the behavior of PL intensity was different at low oxygen partial pressure (10-100 mTorr) and high oxygen partial pressure (100-200 mTorr). To figure out the different PL intensity behavior, we performed the x-ray photoelectron spectroscopy (XPS). Our XPS result implies that the enhancement of PL intensity at low partial pressures is associated with defects in the thin film lattice, and the weakening of PL intensity at high partial pressures is due to the change in the ratio of Eu^{3+} to Eu^{2+} by the self-reduction process.

TF-ThP2 Influence of the Crystal Structure on Photoluminescence Properties of Dy^{3+} and Pr^{3+} Doped Rare-earth Oxyorthosilicates (R_2SiO_5) (R = La, Gd, Y) Thin Film Phosphors, *S.N. Ogugua, H.C. Swart,* University of the Free State, South Africa*; **O. Martin Ntwaeaborwa**,* University of the Witwatersrand, South Africa

Phosphors have many technological uses in applications such as solid-state lighting, optical laser, data storage, medicine, quantity control, scintillation, advertising, solar cells, theft prevention, etc. We have prepared a series of praseodymium (Pr^{3+}) and dysprosium (Dy^{3+}) doped mixed rare-earths oxyorthosilicate phosphors with a general formula R_2SiO_5 hosts (R = La, Gd or Y) using the solution combustion method. By varying the molar ratio of La to Y and Gd to Y, we modified the unit cells and the crystal field strengths of the host lattices. This modification of the crystal field of the host lattice can lead to the shifting of the emission wavelengths, increase of the rate of radiative transitions, and minimization of energy loss by non-radiative transitions. We evaluated the crystal structure and photoluminescence properties of Pr^{3+}/Dy^{3+} doped R_2SiO_5 (R = La, Gd or Y) in powder and laser ablation deposited thin film forms. We varied several deposition parameters including partial pressure of gas (O_2 and Ar), type of laser pulse, and substrate temperature using the 1064 nm Nd:YAG solid state laser. The effects of varying the La to Y/Gd ratios on the field strengths of the host lattices and the influence of the various deposition conditions on the emission colour and photoluminescent intensities will be discussed.

TF-ThP4 Fabrication of IrO_2/Pt Composite Films by Pulsed-dc Magnetron Sputtering and Plasma-enhanced Atomic Layer Deposition, ***Chao-Te Lee**, Y.-H. Yu, W.-H. Cho,* Taiwan Instrument Research Institute, Taiwan*; W.-C. Chen,* Taiwan Instrument Research Institute, Taiwan, Taiwan, Republic of China*; H.-P. Chen,* Taiwan Instrument Research Institute, Taiwan

The IrO_2/Pt films were prepared on Si substrate by pulsed-dc magnetron sputtering and plasma-enhanced atomic layer deposition (PEALD), respectively. The IrO_2 film was prepared from a high purity Ir target and deposited on Si substrate at room temperature with various working pressure, gas ratio (Ar/O_2 ratio) and pulse frequencies (10~100 kHz) by a pulsed-dc magnetron sputtering. Effects of process parameters on the film composition, microstructure, surface roughness, and electrical properties were investigated by field emission scanning electron microscopy with energy dispersive X-ray spectroscopy (FESEM-EDX), X-ray diffraction (XRD), high resolution transmission electron microscopy (HRTEM), atomic force microscopy (AFM), and cyclic voltammetry (CV) measurement, respectively. The nanoblade structure of the IrO_2 film was prepared at a working pressure was 20×10^{-3} Torr, and Ar/O_2 rate was 10. The Pt film was prepared on the nanoblade structure of IrO_2 film by PEALD. Effects of plasma power, and thickness on the microstructure, and electrical properties of the IrO_2/Pt films were investigated. The research goal is to obtain high charge delivery capacity (CDC) of the film. It is expected that the high quality IrO_2/Pt film can be explicated in biomedical technology.

TF-ThP5 The Effect of Deposition Parameters on the Optical and Electrical Properties of MoO_3/Ag/Mo/ MoO_3 Films by Reactive rf Magnetron Sputtering, *C.-T. Lee,* Taiwan Instrument Research Institute, Taiwan*; **Wei-Chun Chen**,* Taiwan Instrument Research Institute, Taiwan, Taiwan, Republic of China*; H.-P. Chen,* Taiwan Instrument Research Institute, Taiwan*; C.-C. Jaing,* Minghsin University of Science and Technology, Japan

Stacked MoO_3/Ag/Mo/MoO_3 (MAMM) films were deposited on glass substrate as ITO-free and electrochromic applications. The effects of the thickness of Mo layer on the electrical and optical properties of the MAMM films were examined by the four-point probe system and a spectrophotometer. The resistivity of MAMM films was decreased with increasing the thickness of Mo layer. The resistivity of the films were 5000 and $3X10^{-5}$ Ω/cm when the thickness of Mo layer was 1 and 2 nm, respectability. It was found that the ITO-free MAMM film as the Mo layer is over 2 nm. The luminous transmittance of MAMM films was decreased with increased the thickness of Mo layer. After the optical simulated, and prepared the electrochromic MAMM films, the MAMM films for hot-mirror and electrocromic applications was also investigated.

TF-ThP6 Effect of Sintering Conditions on Characteristic of $BaFe_2(PO_4)_2$ and Ceramic Target Production for Thin Films, ***Jung Hwan Kim**, B.S. Jung, J.H. Jeong, S.Y. Seo,* Pukyong National University, Republic of Korea*; K. Jang,* Changwon National University, Republic of Korea

Inorganic compounds composed of low-dimensional ferromagnets exhibit fascinating properties and provide a rich opportunity to investigate the ferromagnetic states, phase transitions, magnetic transitions and magnetization phases. Among them, $BaFe_2(PO_4)_2$ (BFPO), which is a two-dimensional ferromagnetic material, has a special structural and magnetic structure at low temperature. Anomalous distortion at about 150K causes a structural phase transition from rhombohedral(R) to triclinic(P). However, further cooling results in a magnetic phase transition from paramagnetic to ferromagnetic at about 80K, and at the same time, it returns to the original rhombohedral(P →R). The change of structural phase transition and the change of band gap in the sintering process of BFPO. This study could be a preliminary study on the fabrication of ceramic targets for thin film deposition of BFPO.

TF-ThP7 Development of Thin Film of Ferric Hydroxide Dispersed in Polymer Matrix Doped with Ethylenediamine, *S.H. Fernandes, **Leandro Tiago Manera**, H.J. Ceragioli,* UNICAMP, Brazil

The present work presents the development of a thin film based on ferric hydroxide ($Fe(OH)_3$) dispersed in a polymer matrix of polyvinyl acetate (PVA) containing ethylenediamine (H_2N-$(CH_2)_2$-NH_2) to form a membrane phosphate in solution. Ferric hydroxide was obtained from the stoichiometric reaction of iron ($FeCl_3$) perchloride with ammonium hydroxide (NH_4OH), and after washing, filtration and drying the $Fe(OH)_3$ was diluted with ethyl alcohol to add to ethylenediamine doped PVA. The thin film for the formation of the membrane was obtained by the spin-coating method. For the selectivity tests, the membrane was applied in a semiconductor insulating electrolyte (EIS) device to be used as hydrogen phosphate sensor. The EIS device is formed by the selective membrane deposited on a structure composed of a thin layer of silicon oxide on the silicon substrate, and a gold-plated tungsten micro tip as the reference electrode. The thin film composing the selective membrane was characterized structurally by elliptiometry, Raman spectroscopy, X-ray diffraction, and atomic force microscopy (AFM). In order to evaluate the selectivity of the thin film of the membrane, the electrical characterization of the EIS device was carried out, obtaining the voltage capacitance curves for the pH variation and for the variation of the hydrogen phosphate concentration in solution, which showed a result in the sensitivity of 143 mV/pH and sensibility in the measurement of the hydrogen phosphate concentration of 42 mV/mg/dL.

Keywords— ferric hydroxide; hydrogen phosphate; thin films; selective membrane

TF-ThP8 Dual-temperature Atomic Layer Deposition of HfO_2/Al_2O_3 on $In_{0.53}Ga_{0.47}As$, ***Changmin Lee**, S. Choi, Y. An, W. Lee, W. Oh, D. Eom, J. Lee, H. Kim,* Sungkyunkwan University, Republic of Korea

$In_{1-x}Ga_xAs$ has been considered to be one of the promising candidates for future n-channel metal-oxide-semiconductor field-effect transistors (MOSFETs) [1]. However, due to its poor interface quality with the high-*k* gate dielectrics (e.g., high interface state density, D_{it}), Al_2O_3 has been used preferably as an interface passivation layer under the HfO_2 gate dielectric

with a higher *k* value [2-5]. Most recently, Choi *et al*. [6] reported that low-temperature atomic layer deposition (ALD) of a HfO_2 (4 nm)/Al_2O_3 (1 nm) stacked structure at 100 °C was effective in reducing both D_{it} and leakage current density. However, because they used an identical ALD temperature for both HfO_2 and Al_2O_3 layers, the capacitance equivalent thickness (CET) of the HfO_2/Al_2O_3 gate dielectric stack was significantly increased [6].

In this presentation, we will introduce a dual-temperature ALD process for the HfO_2/Al_2O_3 stacked gate dielectric to decrease the CET values while maintaining low D_{it} and leakage current density values. While the ALD temperature for the Al_2O_3 passivation layer (~1 nm) on a n-type $In_{0.53}Ga_{0.47}As$ substrate was fixed at 100 °C, the following ALD temperature for the HfO_2 layer (~4 nm) was varied from 100 to 300 °C to decrease the CET values. After the fabrication of MOS capacitors with a stacked gate dielectric structure, the effects of the ALD temperature for the overlaid HfO_2 film on various electrical parameters and characteristics, such as CET, D_{it}, bulk trap density, and static/dynamic leakage currents, were studied.

[1] Shinichi Takagi, Rui Zhang, Junkyo Suh, Sang-Hyeon Kim, Masafumi Yokoyama, Koichi Nishi, and Mitsuru Takenaka, 2015, 545, 06FA01.

[2] A. O'Mahony, S. Monaghan, R. Chiodo, I.M. Povey, K. Cherkaoui, R. E. Nagle, É. O'Connor, R. D. Long, V. Djara, D. O'Connell, F. Crupi, M. E. Pemble, and P. K. Hurley, 2010, 33, 69.

[3] S. Monaghan, A. O'Mahony, K. Cherkaoui, É. O'Connor, I. M. Povey, M. G. Nolan, D. O'Connell, M. E. Pemble, P. K. Hurley, G. Provenzano, F. Crupi, and S. B. Newcomb, J. Vac. Sci. Techno. B, 2011, 29, 01A807.

[4] R. Suzuki, N. Taoka, M. Yokoyama, S. Lee, S. H. Kim, T. Hoshii, T. Yasuda, W. Jevasuwan, T. Maeda, O. Ichikawa, N. Fukuhara, M. Hata, M. Takenaka, and S. Takagi, Appl. Phys. Lett., 2012, 100, 132906.

[5] K. Ohsawa, S. Netsu, N. Kise, S. Noguchi, and Y. Miyamoto, Jpn. J. Appl. Phys., 2017, 56, 04CG05.

[6] S. Choi, J. Song, Y. An, C. Lee, and H. Kim, J. Korean Phys. Soc., 2018, 72, 283.

TF-ThP9 Conformal CVD of $Hf_{1-x}V_xB_2$ from Two Precursors: Control of Composition *x* in Deep Trenches*, **Kinsey Canova**, G.S. Girolami, J.R. Abelson,* University of Illinois at Urbana-Champaign

Fabrication of device interconnects in the high aspect ratio features of modern electronics requires highly conformal, electrically conductive films. HfB_2 is a metallic ceramic which can be deposited with excellent conformality at low temperatures using the single-source CVD precursor $Hf(BH_4)_4$; conformality is due to the kinetic saturation of growth rate at precursor pressures of a few mTorr. Here we report the conformal growth of $Hf_{1-x}V_xB_2$ alloys by adding a co-flow of the vanadium precursor $V[N(CH_3)_2]_4$. This alloy is of special interest for its reported superconducting transition near 7 K.

Alloy compositions previously investigated were limited to the solubility limit of ~ 4 % V in HfB_2. In our low-temperature process, however, metastable compositions with excess V can be obtained, and the film stoichiometry *x* is controlled by relative reaction rates of the two precursors. We report the compositional variation versus precursor flux, which is then used to develop a kinetic model of growth based on the adsorption and reaction rates for both precursors. This model is extended to estimate compositional variation vs. depth *z* in a deep trench and tested by coating macro-trenched substrates. We also report the electrical resistivity from ambient to cryogenic temperatures.

TF-ThP10 Catalyst-enhanced Chemical Vapor Deposition of Titanium-doped MgB_2 Thin Films*, **Xiaoqing Chu**, Y. Yang, C. Caroff, G.S. Girolami, J.R. Abelson,* University of Illinois at Urbana-Champaign

We report a CVD process to deposit titanium-doped polycrystalline MgB_2 films at low temperatures (≤ 400 °C) using Mg $(DMADB)_2$, a highly volatile Mg precursor. The low growth temperature assures that the film does not lose Mg by evaporation, which occurs above 400 °C. When used alone, however, this precursor requires higher temperatures in order to react (it is slightly too stable chemically). We show that CVD proceeds at temperatures as low as 300 °C upon addition of the analogous Ti precursor, $Ti(DMADB)_2$. We identify $Ti(DMADB)_2$ as a catalyst because each Ti molecule drives the decomposition of up to 4 $Mg(DMADB)_2$ molecules. With a high precursor to catalyst pressure ratio, the films are stoichiometric (metal : boron = 1 : 2), and the concentration of oxygen, carbon, and nitrogen is each below the detection limit of ~ 1 at. %. For a film grown at 350 °C, the stoichiometry determined by RBS is $Mg_{0.82}Ti_{0.18}B_2$; it is well crystallized; and the room temperature resistivity is a few hundred μΩ·cm. Literature reports suggest the possibility of superconductivity at T = 10-33 K depending on the doping levels of Ti.

TF-ThP12 Kinetically Stabilized Growth of InN by MEPA-MOCVD*, **G. Brendan Cross**, Z. Ahmad,* Georgia State University*; D. Seidlitz,* Technische Universität Berlin, Germany*; M. Vernon, A.Y. Kozhanov,* Georgia State University

We report on kinetically stabilized indium nitride grown on sapphire and gallium nitride, by migration enhanced plasma assisted metal organic chemical vapor deposition (MEPA-MOCVD). Deposition is studied over a range of temperatures, pressures, flows and plasma power, outside the range of indium nitride grown in conventional MOCVD. Raman and FTIR spectroscopy, XRD and atomic force microscopy are used to explore the crystalline quality, growth rate, and surface morphology change with these parameters.

TF-ThP13 Structure Characterization of PECVD a-SiCN:H Thin Films: Toward Machine Learning Algorithms for Modeling of Complex Disordered Solids*, **Sai Siva Kumar Pinnepalli**, C. Burkett,* University of Missouri-Kansas City*; J. Hwang,* Ohio State University*; O. Oyler, M.M. Paquette,* University of Missouri-Kansas City

Plasma-enhanced chemical vapor deposition (PECVD) is a routinely employed process in thin-film technologies. Despite its array of advantages and affordability, it suffers from the lack of systematic principles to define growth conditions for an intended output. A deeper understanding of plasma processes is necessary for rational design and strategic synthesis of robust materials spanning a broad spectrum of applications. The properties of these materials are highly dependent on structure; and the structure varies as a function of growth conditions. Interpreting or predicting the effects of PECVD process variables such as temperature, pressure, flow rate and plasma power density on structural features of thin-films is a formidable task. The traditional 'cook and quench' molecular dynamics approach is incapable of replicating the relatively longer time scales and non-thermodynamic nature of the actual experiment. An alternative approach entails advanced machine learning algorithms applied not to reproduce, but rather to map the process-structure-property correlations. However, this requires training data in the form of empirically determined chemical models obtained under known process conditions. Here, PECVD grown amorphous hydrogenated SiCN thin films obtained from structurally different molecular precursors are studied to compile such a data set due to their stability, scope for precursor synthesis, and compatibility with various characterization techniques: FT-IR, solid-state NMR, fluctuation electron microscopy (FEM), as well as X-ray and neutron diffraction. We present the effects of process parameters on a-SiCN:H thin films, extensive structure and property characterization, and propose chemical structure models.

TF-ThP14 Growth of Hafnium Oxide and Zirconium Oxide for the Fabrication of Electronic Devices Using Plasma-Enhanced Atomic Layer Deposition*, **Samuel Banks**, K. Bell, S. Chance III, B. Rodgers, Z. Xiao,* Alabama A&M University

Hafnium dioxide (HfO_2) and zirconium oxide (ZrO_2) have been used widely as the gate oxide in the fabrication of integrated circuits (ICs) because of their high dielectric constants. In this research, we report the growth of hafnium dioxide (HfO_2) and zirconium oxide (ZrO_2) thin film using plasma-enhanced atomic layer deposition (PEALD), and the fabrication of complementary metal-oxide semiconductor (CMOS) integrated circuits using the PEALD-grown HfO and ZrO thin films as the gate oxide. The PE-ALD-grown films were analyzed using high-resolution transmission electron microscopy (HRTEM) and energy dispersive X-ray spectroscopy (EDS). MOSFETs, CMOS inverters, and CMOS ring oscillator were fabricated, and the electrical properties of the fabricated devices were measured. The measurement results on the devices fabricated with the two films were compared.

TF-ThP15 Nanoscale Multilayered Thin-Film Thermoelectric Materials and Devices*, **Joevonte Kimbrough**, A. Glenn, A. Henderson, S. Budak, Z. Xiao,* Alabama A&M University

In this research, we report the growth of nanoscale multilayered thermoelectric thin films and fabrication of integrated thermoelectric devices for high-efficiency energy conversion and solid-state cooling. Nanoscale multilayered thin films such as Sb/Sb_2Te_3 and Te/Bi_2Te_3 thin films

were grown using the e-beam evaporation. Integrated thermoelectric devices were fabricated with the nanoscale multilayered thin films using the clean room-based microfabrication techniques such as UV lithography. X-ray diffraction and reflection and high-resolution tunneling electron micrograph (HR-TEM) were used to analyzed the e-beam-grown nanoscale multilayered thin films. SEM was used to image and analyze the fabricated devices. The thermoelectric characteristics of the fabricated devices were measured and analyzed.

TF-ThP18 Characterization of Fluorine-doped SiO_2 Films Deposited by Magnetron Sputtering, ***Bohuei Liao,*** Taiwan Instrument Research Institute*;* *C.-N. Hsiao,* Taiwan Instrument Research Institute, Taiwan, Republic of China

Fluorine-doped SiO_2 films were deposited by magnetron sputtering with a Si metal target at room temperature. In order to obtain better optical and mechanical properties, films were investigated under different ratios of O_2 to CF_4 gas. The optical properties, microstructure, surface roughness, and crystalline structure, of fluorine-doped SiO_2 films have been studied. The transmittance increased as increasing the CF_4 gas in the ultraviolet range. The refractive index decreased as increasing the CF_4 gas.

TF-ThP19 MOCVD Growth and Characterization of Wide Bandgap $ZnGeN_2$ Thin Films, ***Md Rezaul Karim,*** The Ohio State University*; B.H.D. Jayatunga,* Case Western Reserve University*; Z. Feng, M. Zhu, J. Hwang,* The Ohio State University*; K. Kash,* Case Western Reserve University*; H. Zhao,* The Ohio State University

$ZnGeN_2$ is a wide bandgap material having less than 0.1% lattice mismatch and similar bandgap as GaN [1]. Based on first principles calculations, the valence band maximum of $ZnGeN_2$ is ~1.4 eV above that of GaN at the heterointerface [2]. Such a staggered band alignment between two closely lattice-matched materials has promising applications for novel optoelectronic device designs, for example, high efficiency blue and green light emitting diodes [3]. However, the thin film synthesis of $ZnGeN_2$ is still at an early stage, in contrast to the mature GaN.

Here, we study the growth of $ZnGeN_2$ thin films using metalorganic chemical vapor deposition (MOCVD) and characterization of the crystalline, optical, and electrical properties. Diethylzinc (DEZn), germane (GeH_4) and ammonia were used as the precursors for Zn, Ge and N, respectively, and GaN templates and sapphire were used as substrates. The Zn/Ge atomic ratios in $ZnGeN_2$ were determined from energy dispersive X-ray spectroscopy. They were found to decrease with increase in growth temperature (from 600 to 700 °C) but to increase with increase in pressure (from 300 to 500 Torr) and DEZn/GeH_4 molar flow rate ratio. The X-ray diffraction 2θ-ω spectra of the $ZnGeN_2$ films are consistent with orthorhombic (perfectly ordered cations) or distorted wurtzite (disordered cations) polymorphs. High resolution scanning transmission electron microscopy imaging was used to investigate the crystalline quality and crystalline structure of the films. The $ZnGeN_2$ films grown on c-sapphire and GaN substrates have planar surfaces from scanning electron micrographs while those on r-sapphire substrate have stepped surface morphologies. A broad peak at ~2.05 eV was observed from room temperature photoluminescence (PL) spectra and is was attributed to transitions involving deep level defects. The PL excitation spectra peaked around 3.4 eV, and is attributed to excitonic enhancement of the absorption near the band gap. The as-grown films were found to be n-type with 10^{18} -10^{19} cm^{-3} carrier concentrations and room temperature mobilities up to 17 $cm^2/V{\cdot}s$.

In summary, the studies from this work on the MOCVD growth of $ZnGeN_2$ thin films are a step towards the better understanding of this material and thus, towards the implementation of $ZnGeN_2$ for device applications.

Acknowledgements

The authors acknowledge funding support from the National Science Foundation (DMREF-1533957).

References

1. A. Punya, T. R. Paudel, and W. R. L. Lambrecht, Phys. Status Solidi C, 8, 2492 (2011).

2. A. P. Jaroenjittichai, S. Lyu, and W. R. L. Lambrecht, Phys. Rev. B., 96, 079907(E) (2017).

3. L. Han, K. Kash, and H. Zhao, J. Appl. Phys., 120, 103102 (2016).

TF-ThP20 Low Temperature Charging Dynamics of Ionic Liquid and Its Gating Effect on $FeSe_{0.5}Te_{0.5}$ Superconducting Films, ***Cheng Zhang,*** University of Tennessee Knoxville*; W. Zhao, S. Bi,* Huazhong University of Science and Technology, China*; C.M. Rouleau, J.D. Fowlkes,* Oak Ridge National Laboratory*; W.L. Boldman,* University of Tennessee Knoxville*; G. Gu, Q. Li,* Brookhaven National Laboratory*; G. Feng,* Huazhong University of Science and Technology*; P.D. Rack,* University of Tennessee Knoxville

Ionic liquids (ILs) have been investigated extensively due to its unique ability to form the electric double layer (EDL) which induces high electrical field. For certain materials low temperature IL charging is needed to limit the electrochemical etching. Here we report our investigation of the low temperature charging dynamics in two widely used ILs – DEME-TF_2N and C_4mim-TF_2N. Results show that the formation of the EDL at ~220 K requires several hours relative to milliseconds at room temperature, and an equivalent voltage V_e is introduced as a measure of the EDL formation during the biasing process. The experimental observation is supported by molecular dynamic simulation, which shows that the dynamics are logically a function of gate voltage, time and temperature. To demonstrate the importance of understanding the charging dynamics, a 140 nm thick $FeSe_{0.5}Te_{0.5}$ film was biased using the DEME IL, showing a tunable Tc between 18 and 35 K. Notably, this is the first observation of the tunability of the T_c in thick film $FeSe_{0.5}Te_{0.5}$ superconductors.

TF-ThP21 Design and Characterization of Nanomaterials using PREVAC's Research Platforms, ***Lukasz Walczak,*** PREVAC sp. z o.o., Poland

Magnetics, optoelectronics, energy storage and renewables, catalysis and nanoelectronics, semiconductors, new graphene-type materials and their surface are under intensive investigation of many research groups [1-3]. The wide variety of novel technologies and materials available, precise, well defined scientific problems or proprietary production recipes demand customized analysis and deposition systems.

Innovative and compact PREVAC surface analysis platform as part of multi-technique surface analysis system will be presented, in order to permit complete characterization of nanomaterials in the UHV and ambient pressure conditions. We will report some results from these systems.

Also we introduced PREVAC deposition platforms, based on well tested MBE system technology, offering a high quality and stable UHV performance. Compact construction allows the connection of different deposition sources at versatile configurations as well as the incorporation of RHEED, inventive alternative GIFAD [4] and other analysis techniques.

As the next deposition platform the sputtering systems for depositing metal and dielectric thin films on substrates at the different temperature will be shown. A range of magnetron sputtering sources, using RF, DC, or pulsed DC power, can be operated in the multimode by SYNTHESIUM software for producing thin films.

Finally we describe PREVAC's PLD systems. Typically it is used with a focused pulsed excimer laser to vaporize a small section of a solid target material in a vacuum chamber in order to produce thin-films. Standalone configuration or as part of a larger integrated research system, system is fully automated. The transfer system features a six position target manipulator which allows transfer of both target and substrate holders for simple and efficient operation.

References:

1. L. K. Preethi, et al., Sci. Rep. , 14314 (2017)

2. M. Weis, et al., Sci. Rep. **7**, 13782 (2017)

3. N. M. Freitag et al., Nature Nanotechn. **13**, 392-397 (2018)

4. A. Momeni et al. J. Phys. Chem. Lett., **9**, 908–913 (2018)

TF-ThP22 Deposition of the Porous Film on the Reactive Liquid Substrate via Metal-organic Precursors, ***Haoming Yan,*** *Q. Peng,* University of Alabama

Solid on liquid deposition (SOLID) has been achieved and reported for a few times. It has potential in many applications, such as gas sensors, optical lens, selective deposition and etc. SOLID can also take the advantages of the nature of the liquid substrate, like the atomically smooth surface and the naturally formed shape of the liquid. However, the materials that can be deposited onto the liquid substrate are very limited. The reported material that can be deposited on a liquid substrate is mainly poly-para-xylylene via CVD and metals via sputtering. There is no report of using a reactive liquid as a substrate for the solid film deposition. In this work, the metal oxide film can be deposited onto the liquid substrate using the metal-organic precursors and the liquid that can react with them. This method creates more possibilities of the materials that can be deposited

on the liquid substrate and potentially broaden the application of the SOLID.

TF-ThP24 The Evolution of Atomic Layer Processing as a Field: Atomic Layer Etching,and its Connections with Atomic Layer Deposition*, Elsa Alvaro,* Northwestern University*; A. Yanguas-Gil,* Argonne National Laboratory

Atomic layer processing, with its ability to manipulate materials with atomic layer precision, is becoming increasingly relevant for a wide range of applications. A counterpart to Atomic Layer Deposition (ALD), Atomic Layer Etching (ALE) allows controlled layer-by-layer removal of material by using self-limiting, sequential steps. This technique, which appeared in the 1990s, has garnered the interest of the semiconductor industry, where the ability to remove material selectively and in a self limiting way could help fabricate structures and devices at increasingly smaller dimensions. In this paper, we describe the trajectory of ALE, and its connection and overlap with ALD and other research fields. Using citation, network and text analysis methods, we have studied trends in topics, authors and publications. In addition, we have examined the overlap between ALD and ALE, using cocitations as a way of identifying papers that may draw from both fields. The ultimate goal is to understand not only the evolution of ALE, but whether ALD and ALE are effectively merging into a larger, atomic layer processing community.

TF-ThP25 Electrical Properties of In_2O_3 Thin-film Transistors under Vacuum and Inert Environments*, Keisuke Nakamura,* *K. Sasaki, Y. Shibata, K. Oe, S. Aikawa,* Kogakuin University, Japan

Indium oxide (In_2O_3)-based thin-film transistor (TFT) have attractive much attention because high field-effect mobility (> 10 cm^2/Vs) can be obtained even room temperature deposition. However, a high-temperature post-annealing is necessary for typical fabrication processes. This sacrifices the merit of In_2O_3-based TFTs that can be fabricated at low temperature. One reason for high-temperature treatment is that an In_2O_3 surface might be sensitive to ambient gases, thus, the electrical properties of the film is changed in various environmental conditions. In order to clarify such instability, we investigate the electrical properties of In_2O_3 TFT in ambient, vacuum and N_2 environments.

The In_2O_3 TFT was fabricated on a Si substrate with a thermally-grown oxide layer (SiO_2 thickness: 200 nm). Before deposition of In_2O_3 active channels, the substrate was ultrasonically cleaned in acetone and isopropyl alcohol, and was irradiated by an excimer lamp (wavelength: 172 nm) for 5 min to remove the organic residue. The In_2O_3 film was then deposited at room temperature by RF magnetron sputtering. The O_2/(Ar + O_2) ratio, RF power and total pressure during sputtering deposition were fixed at 25 %, 100 W and 0.24 Pa, respectively. The background pressure was below ~5 × 10^{-4} Pa. The thickness of the active channel formed through a stencil shadow mask was 20 nm by optimizing the deposition time. Source and drain electrodes (Cu: 100 nm) were then formed by an electron beam evaporation through a stencil shadow mask. The In_2O_3 TFT was characterized in a vacuum probe station with a semiconductor parameter analyzer (Agilent 4156A) at room temperature in the dark condition. The electrical measurement of the TFTs was performed in ambient at first, then the chamber was evacuated to ~4 × 10^{-2} Pa for vacuum measurement. A N_2 gas was subsequently introduced into the chamber to be N_2 environmental condition.

The In_2O_3 TFT properties were drastically changed between ambient and vacuum conditions. This might be caused by desorption of excess oxygen in the film. To investigate a measurement environmental sensitivity in In_2O_3 TFT, a sequential *I-V* measurement was performed. The result showed that the transfer characteristics between 1st and 2nd measurement is obviously different. The degradation of the sensitivity after the 2nd measurement might be due to N_2 molecule passivation. However, the sensitivity tended to slight recover with increasing the number of measurements. We will discuss the N_2 passivation effect, and the relationship between the sensitivity and number of measurements.

TF-ThP26 Toward Ultra-fast Switching Speed Electrochromic Supercapacitor*, Weimin Jiao,* *S.C. Wei, C.R. Chang, F. Yao,* University at Buffalo

As one of the most promising energy storage devices, supercapacitors have been widely adopted in different fields due to their high power density and long service life. However, with the rapid development of intelligent electronic products, there is an urgent need to construct multifunctional supercapacitors to broaden the range of applications. Integration of electrochromism into supercapacitors is one of the innovative approaches to achieve device multifunctionality. An electrochromic supercapacitor can change color reversibly in response to different applied voltages. The instant capacity of the devices can be simply recognized by naked eyes. Implementation of electrochromism to supercapacitors can also prevent device overcharging, leading to a longer device lifetime. Nevertheless, the performance of previously reported electrochromic supercapacitor devices suffers from a slow switch mechanism as well as a low power density, which highlights the need for the electrode structures optimization.

In this report,an electrochromic asymmetrical supercapacitor device (EASD) is developed, which successfully achieves the multifunctional combination of electrochromism and energy storage by adopting polyaniline and tungsten trioxide as the positive and negative electrodes, respectively. In order to improve the device performance, a facile electrochemical activation process is applied to the electrode. The optimized EASD shows a high volumetric energy density of 35.3 mWh/cm^3 at a high power density of 1.02 W/cm^3 with excellent cycling stability. More importantly, it exhibits a high coloration efficiency of 123.4 cm^2/C with an ultra-fast switching speed of 0.4 s / 1.4 s for colored / bleached states, which is one of the fastest switching devices reported so far. Such an EASD shows great potential in the applications of smart windows, smart electronics, and intelligent energy storage.

TF-ThP27 Growth and Structure of Cr-doped ZnO Thin Films*, Gabrielle Pasternak,* Washington and Jefferson College*; A. Gardill,* Lawrence University*; S.E. Chamberlin,* Washington and Jefferson College

There is a constant search for more efficient materials for use in electronics. Zinc Oxide (ZnO) is a well-known semiconductor used in numerous applications. However, the effects of doping ZnO with chromium (Cr) are less documented. Using spray pyrolysis – a robust and industrially relevant technique – an aqueous solution of Zn and Cr nitrates is sprayed onto a heated substrate to create thin films of polycrystalline $(Zn_{1-x}Cr_x)O$ with various Cr concentrations below x = 0.05.

X-ray diffraction (XRD) is used to verify the retention of ZnO's structure, confirming that Cr substitutes for Zn in the crystal lattice. XRD can also give detailed information about the crystal lattice parameters and crystallite size – both important in understanding the effectiveness of our growth process. Verifying with XRD that we have grown good crystalline material is the first step to increasing the understanding of $(Zn_{1-x}Cr_x)O$. We have also begun to investigate the optical and chemical properties of this material.

TF-ThP28 Developing an Approach to Improve the Beta-phase in Ferroelectric PVDF-HFP Thin Films*, Ashley S. Dale,* *A. Mosey, J. Soruco, R. Cheng,* Indiana University Purdue University Indianapolis

Improved fabrication of poly(vinylindene fluoride)-hexafluropropylene (PVDF-HFP) thin films is of particular interest due to the high electric coercivity found in the beta-phase structure of the thin film. For example, ongoing studies of ferroelectric-spin crossover coupling using x-ray spectroscopy imply the ferroelectric-spin coupling would benefit from a better ferroelectric response. Langmuir-Blodgett (LB) deposition and Langmuir-Schaffer (LS) deposition methods create a beta-phase dominant PVDF-HFP thin film when the deposition is followed by annealing. However, applications for PVDF-HFP thin films exist in organic spintronic devices where annealing is prohibited by other materials in the device heterostructure. We show that it is possible to obtain high-quality, beta-phase dominant PVDF-HFP thin films using a modified approach to LB deposition and without the use of annealing or additives. Samples implement a unique step design with a bottom electrode of copper and aluminum and a top electrode of gold or aluminum. This design allows a single thin film sample to be characterized using scanning electron microscopy, atomic force microscopy, X-ray diffraction, and electrical hysteresis measurements.

TF-ThP31 Size Dependent Strengthening in High Strength Nanotwinned Al/Ti Multilayers*, Yifan Zhang,* *S. Xue, Q. Li, J. Li, J. Ding, T.J. Niu, R.Z. Su, H. Wang, X. Zhang,* Purdue University

Here we report on the study of magnetron-sputtered highly textured Al/Ti multilayers with various layer thicknesses (h = 1 - 90 nm). The hardness of Al/Ti multilayers increases monotonically with decreasing layer thickness without softening and exceeds 7 GPa, making it one of the strongest light-weight multilayer systems reported to date. High resolution transmission electron microscopy (TEM) and X-ray diffraction pole figure analyses confirm the formation of high-density nanotwins and 9R phase in Al layers. The density of nanotwins and stacking faults scales inversely with individual layer thickness. In addition, there is an HCP-to-FCC phase transformation of Ti when h ≤ 4.5 nm. And the post-indentation TEM analysis reveals

deformation induced phase transformation in Ti layer. The high strength of Al/Ti multilayers primarily originates from incoherent interface, high-density twin boundaries, as well as stacking faults. Our findings have general implication for the design of high-strength and light-weight heterogeneous nanocomposite materials.

Plasma Science and Technology Division
Room B130 - Session PS+2D+SE+TF-FrM

Plasma Deposition and Plasma-Enhanced Atomic Layer Deposition

Moderators: David Boris, U.S. Naval Research Laboratory, Chenhui Qu, University of Michigan

8:20am **PS+2D+SE+TF-FrM1 Plasma-based Synthesis of 2D Materials for Devices on Flexible Substrates***, N.R. Glavin,* Air Force Research Laboratory*;* ***Christopher Muratore,*** Department of Chemical and Materials Engineering, University of Dayton **INVITED**

Synthesis of flexible two-dimensional electronic devices using low-cost, naturally abundant materials (e.g., MoS_2) directly onto inexpensive polymeric materials at economically viable scales enables use of their unique characteristics in grand challenge areas of energy, healthcare, and national security. Recently-proven approaches for low temperature, plasma-based 2D synthesis suitable for flexible substrates developed by the authors include growth of amorphous materials with subsequent photonic annealing to access crystalline domain sizes up to several microns. This approach has been demonstrated for synthesis of large area ultrathin monolithic layers as well as MoS_2/WS_2/BN multilayers with pristine interfaces, allowing interrogation of intrinsic properties of 2D materials and their heterostructures as they apply to diverse optoelectronic devices, with a current focus on molecular sensing. Advantages of plasma-based approaches will be discussed in terms of detailed kinetic studies of crystal formation and compositional evolution on the substrate surface. Correlations of structure, especially defect densities, to materials properties and device performance will be discussed in the context of diverse device applications including photodetectors and molecular sensors.

9:00am **PS+2D+SE+TF-FrM3 Homogeneous Ternary Oxides of Aluminum with Silicon, Molybdenum, and Niobium by Plasma Enhanced ALD by Sequential Precursor Pulses***,* ***Steven Vitale,*** MIT Lincoln Laboratory

Deposition of ternary oxide films by ALD is well known. In the vast majority of cases ternary films are deposited by sequential deposition of thin layers of the constituent binary oxides, such as Al_2O_3 / SiO_2. This nanolaminate approach allows for precise control of the global film stoichiometry and is a good solution for many applications, including optical coatings where the wavelength of light is much greater than the nanolaminate thickness thus the film appears quasi-uniform. The nanolaminate approach is less desirable for electronic applications which are sensitive to surface defect sites in the material which may acts as charge traps. For these applications a truly homogenous film which does not possess internal interface states is preferred. True homogenous ternary oxide growth by sequential precursor pulses before the oxidation step is much less well explored. In this work we grow homogeneous ternary oxides of $Al_xSi_yO_z$, $Al_xNb_yO_z$, $Al_xMo_yO_z$ by plasma enhanced ALD using sequential precursor pulses. The stoichiometry of the films is measured by XPS. Using this data we propose models of how the precursors interact with the surface under competitive adsorption. It is found that trimethyl aluminum (TMA) is so strongly adsorbed to the surface at unity surface coverage that ternary oxide growth is not possible if the surface is first exposed to TMA. However if the surface is exposed to the Si, Nb, or Mo precursor first, ternary oxide growth is achieved. The growth kinetics for the three films are markedly different, however, and we explain this through models of the adsorption energy of each precursor.

9:20am **PS+2D+SE+TF-FrM4 Piezoelectric Response of ZnO Thin Films Grown by Plasma-Enhanced Atomic Layer Deposition***,* ***Julian Pilz****, T. Abu Ali,* Graz University of Technology, Austria*; P. Schäffner, B. Stadlober,* Joanneum Research Forschungsgesellschaft mbH, Austria*; A.M. Coclite,* Graz University of Technology, Austria

ZnO is a direct band gap semiconductor with attractive piezoelectrical, optical, and electrical properties, particularly appealing for a variety of functional devices. Especially the utilization of piezoelectric properties of ZnO nanostructures for transforming mechanical to electrical energy has attracted much research interest. For most of these so called nanogenerators, solution based deposition methods have been applied to create the desired nanostructures, often lacking a precise control of the deposition parameters. Atomic layer deposition, on the other hand, allows conformal and uniform deposition on high aspect ratio structures with Å-level thickness control.

In this study, we investigate the piezoelectric response of ZnO thin films on flexible substrates as a starting point for piezoelectric nanostructures. The films are grown by plasma-enhanced atomic layer deposition (PE-ALD) to thicknesses below 100 nm by adapting diethylzinc and O_2-plasma as reactants. In comparison to thermal ALD (where diethylzinc and water are used as reactants), PE-ALD allows the deposition of films with higher resistivity, an important property to minimize the leakage of piezoelectric charges. Commercially available Polyethylenterephthalat (PET) coated with Indium Tin Oxide (ITO) serves as the flexible substrate and bottom electrode, respectively. The deposition of ZnO thin films is carried out at substrate temperatures between room temperature and 100 °C, as a change in preferential crystal orientation from (100) to (002) can be observed in this temperature range. The macroscopic piezoelectric characterization is performed in a home-built stamp station, in which a defined periodic force is exerted onto the samples and the generated piezoelectric charges are measured. Out of this, the longitudinal piezoelectric coefficient d_{33} can be obtained. Preliminary results show d_{33} coefficients > 7 pC/N, which is comparable to literature results. The piezoelectric characterization is made for the different samples to understand how the d_{33} coefficient changes for films deposited at different substrate temperatures and thus having different crystal orientation. Since the [002] is the polar axis in the ZnO wurtzite crystal structure, films with preferred orientation in this direction are therefore expected to show higher d_{33} coefficients.

The work lays the basis for developing functional piezoelectric generators and sensors in thin film form. However, the concepts can be easily transferred to depositions on lithographically defined templates in order to create nanostructured ZnO, which exhibits increased piezo response.

10:00am **PS+2D+SE+TF-FrM6 Plasma-enhanced Molecular Layer Deposition of Boron Carbide from Carboranes***,* ***Michelle M. Paquette****, R. Thapa, L. Dorsett, R. Bale, S. Malik, D. Bailey, A.N. Caruso,* University of Missouri-Kansas City*; J.D. Bielefeld, S.W. King,* Intel Corporation

Atomic layer deposition (ALD) research has exploded in this era of electronic miniaturization, smart materials, and nanomanufacturing. To live up to its potential, however, ALD must be adaptable to many types of materials growth. To extend the reach of this layer-by-layer deposition framework, researchers have begun to explore molecule based processes. Still relatively rare, existing molecular layer deposition (MLD) processes are limited and typically based on the condensation of "linear" 2D or "brush-type" organic polymer chains. To this end, icosahedral carborane ($C_2B_{10}H_{12}$) molecules provide an interesting target. Carboranes have been used in the plasma-enhanced chemical vapor deposition of boron carbide films for low-*k* interlayer dielectrics, neutron detection, and a variety of protective coatings. These are symmetric twelve-vertex molecules, known to form close-packed monolayers and to possess labile H atoms at each of the vertices capable of cross-linking in the presence of heat, plasma, or other energy source. As such, the carborane molecule is particularly intriguing as a novel MLD precursor for 3D growth, possessing unique symmetry, reactivity, and volatility properties not commonly encountered in traditional organic molecules. However, a challenge in developing a layer-by-layer process lies in achieving the selective coupling chemistry required, which in the case of molecular reagents requires typically exotic bis-functional derivatives. Herein we describe progress in developing a plasma-enhanced molecular layer deposition process based on carborane derivatives, where the plasma is exploited to create the surface functionalization necessary for selective coupling and to cross-link carborane layers. We investigate the deposition of several carborane derivatives on different functionalized surfaces with the application of various types of plasmas toward achieving controlled layer-by-layer growth of thin boron carbide films.

10:20am **PS+2D+SE+TF-FrM7 Gas Phase Kinetics Optimization Study for Scaling-up Atmospheric Pressure Plasma Enhanced Spatial ALD***,* ***Yves Creyghton,*** Holst Centre / TNO, The Netherlands, Netherlands

DBD plasma sources have been successfully integrated in spatial ALD equipment for low-temperature ALD (<120 °C) of metal-oxides. Applications involving (semi)conductive substrates require remote plasma operation. Radical losses during transport from remote plasma limit substrate speeds or demand excessive plasma flow rates. Proximity remote plasma sources were developed with sufficient radical flux even at low gas flow rates. The sources were demonstrated for ALD of InZnO for high mobility thin film transistors. Further optimization asks for deeper understanding of radical kinetics. In this contribution experimental and calculated data will be presented which allow insight in the radical gain and

loss processes. A reference temperature of 100 °C and gas flows in the range 2-10 slm (for a 4 cm wide source) were applied. Alumina depositions were carried out using TMA and 2% O_2-N_2 plasma gas. Deposited layers obtained for different relative height positions of the plasma source were analyzed. Growth per cycle (GPC) values indicate a strong decay of plasma reactivity for gaps > 0.5 mm. As O_3 --should not decay over such small distance, this indicates that the process is radical based. Surprisingly the GPC also shows a peak value at 0.1 mm (Fig. 1). O_3 and NO_x were measured in the plasma exhaust gas as a function of % O_2 (Fig. 2). The 1-2% O_2 for maximum NO appears to correspond with the optimal gas composition for both high GPC values and refractive index values close to 1.58 indicating high layer quality. This result suggests NO plays a role in downstream plasma radical formation. Further understanding of the role of plasma species such as N, metastable N_2(A) and NO has been obtained by modelling. Kinetic data sets for optimization of O_3 production have been implemented in a CFD model for the transport of plasma species from the remote plasma. For the analysis of modelling results, the reaction volume has been divided in 3 parts (1) the plasma ionization zone itself, (2) the flow dominated plasma source aperture and (3) the diffusional transport dominated surface reaction zone. The dominating reactions for gain and loss of O radicals differ much between zones (Fig. 3). As the main O radical formation in zone (2) is due to metastable excited N_2(A), in zone (3) reactions between N radicals and NO are the main source of O radical generation. In both zones, the main O radical loss process is due to generation of O_3. The experimentally validated model has been used for finding improved plasma process settings (source geometry, frequency, flow) allowing the further optimization of high-throughput plasma enhanced spatial ALD of metal oxides.

10:40am **PS+2D+SE+TF-FrM8 Taking Plasma ALD to the Next Level: From Fundamental Understanding to Selective 3D Processing**, *T.F. Faraz, K. Arts,* Eindhoven University of Technology, The Netherlands, Netherlands; *L. Martini, R. Engeln, H.C.M. Knoops,* Eindhoven University of Technology, The Netherlands; ***Erwin Kessels***, Eindhoven University of Technology, The Netherlands, Netherlands **INVITED**

Current trends in semiconductor device manufacturing impose extremely stringent requirements on nanoscale processing techniques, both in terms of accurately controlling material properties and in terms of precisely controlling nanometer dimensions. Plasma-based processing remains key in next-generation device manufacturing with plasma-enhanced atomic layer deposition (PE-ALD or plasma ALD) being a method that has obtained a very prominent position in obtaining ultrathin films with atomic scale precision [1]. In this contribution the state-of-the-art of PE-ALD will be presented including latest insights into reaction mechanisms as well as some developments in plasma ALD equipment and emerging applications. Aspects such as the role of (energetic) ions, conformality in high aspect ratio structures, and selective processing will be discussed [2].

[1] H.C.M. Knoops, T. Faraz, K. Arts, and W.M.M. Kessels, J. Vac. Sci. Technol. A 37, 030902 (2019)

[2] T. Faraz, K. Arts, S. Karwal, H.C.M. Knoops, and W.M.M. Kessels, Plasma Sources Sci. Technol. 28, 024002 (2019).

11:20am **PS+2D+SE+TF-FrM10 Computational Investigation of Plasma Enhanced ALD of SiO_2**, *C. Qu,* University of Michigan; *P. Agarwal, Y. Sakiyama, A. LaVoie,* Lam Research Corporation; ***Mark J. Kushner***, University of Michigan

Plasma enhanced atomic layer deposition (PE- ALD) of dielectric films typically consists of two steps – precursor deposition and oxidation. For example, in a SiO_2 PE-ALD process, the Si-containing precursor is often deposited in the feature without use of plasma while the oxidation step is performed by an oxygen containing plasma. In principle, the surface kinetics of both steps are self-terminating. Although the plasma step is performed using gas pressures of several to 10 Torr, in addition to O-atoms the fluxes onto the wafer contain energetic particles in the form of ions, photons, hot-neutrals and excited states. When performing PE-ALD in high aspect ratio (HAR) features, transport of these species into the feature determine the quality of the deposition. Optimizing the PE-ALD depends on control of these fluxes.

In this work, results from a computational investigation of reactor and feature scale processes in idealized PE-ALD of SiO_2 will be discussed. Reactor scale simulations of a capacitively coupled plasma sustained in Ar/O_2 mixtures were performed using the Hybrid Plasma Equipment Model (HPEM); and provided fluxes and energy distributions of radicals, ions, excited states and photons onto the wafer. Feature scale simulations were performed with the Monte Carlo Feature Profile Model (MCFPM). The idealized ALD process consists of a non-plasma first step using an Si-R (R indicates organic) precursor. The second step uses fluxes from the Ar/O_2 plasma to remove the organic and oxidize the Si site. The base-case features are moderate to high aspect ratio (AR = 7-20) vias and trenches. The metrics to evaluate the process are surface coverage of Si, O, R, stoichiometry, defect density, surface roughness and deposition rate.

In self-terminating processes, many of these metrics should scale with pt, where p is the probability of reaction and t is the step length. For example, a given surface coverage of Si-R or Si-O should depend on first order on pt. However, as deposition proceeds and a feature fills, the effective AR increases. When coupled with conductance limited transport into the feature, with increasing AR the value of pt to produce a given surface coverage increases. As the deposition proceeds and AR increases, stoichiometry and defect density begins to have a dependence on height inside the feature, as surfaces deep in the feature receive less exposure to the reactive fluxes. The consequences of ion- and photon-induced damages will also be discussed.

* Work supported by LAM Research Corp. and the DOE Office of Fusion Energy Science.

11:40am **PS+2D+SE+TF-FrM11 Analyzing Self-limiting Surface Reaction Mechanisms of Metal Alkyl Precursors and Nitrogen Plasma Species: Real-time In-situ Ellipsometric Monitoring of III-nitride Plasma-ALD Processes**, ***Ali Okyay***, OkyayTech Inc., Turkey; *A. Mohammad, D. Shukla, S. Ilhom,* University of Connecticut; *B. Johs,* Film Sense LLC; *B.G. Willis, N. Biyikli,* University of Connecticut

ALD-grown films are vastly characterized via ex-situ measurements to quantify various material properties. However, gaining insight into the saturating surface reactions and growth mechanisms is only possible with real-time in-situ process monitoring of individual ALD cycles. While several in-situ measurement techniques have been employed in ALD research, in-situ ellipsometry stands out as one of the best options for real-time monitoring surface reactions. The promising potential of in-situ spectroscopic ellipsometry has already been demonstrated for a number of materials grown by remote plasma-ALD. Here, we verify that cost-effective multi-wavelength ellipsometer (MWE) can also be used effectively for real-time in-situ analysis of plasma-ALD growth cycles. We demonstrate for the first time that real-time dynamic in-situ MWE measurements convey not only accurate film deposition rate, but as well resolve single chemisorption, ligand removal, and nitrogen incorporation events with remarkable clarity. Moreover, forcing the limits for fitting the acquired in-situ MWE data, we were able to track the evolution of the optical constants of III-nitride films along the ALD cycles which indeed showed thickness-dependent behavior.

Our main motivation behind this study was twofold: (i) Analyze and compare the self-limiting growth characteristics of binary III-nitride (AlN, GaN, and InN) thin films via real-time in-situ ellipsometry and to gain insight into the ALD surface reaction mechanisms including chemical adsorption, ligand removal, and nitrogen incorporation steps. (ii) Performance evaluation of our custom designed ALD reactor featuring improved hollow-cathode plasma source by comparing our results with previous plasma-ALD grown III-nitrides.

Despite using the conventional alkyl metal precursors (trimethyaluminum, trimethyl/ethylgallium, trimethylindium) utilized also widely in MOCVD epitaxial growth, their solid-gas surface interactions with nitrogen plasma species shows notable differences, particularly with respect to substrate temperature, plasma power, plasma exposure time, and plasma gas composition. In terms of substrate temperature, AlN exhibited crystallinity at lower temperatures when compared to GaN and InN. Even at 100 °C, AlN showed crystalline behavior whereas GaN displayed amorphous character up to 200 °C. While $Ar/N_2/H_2$ composition is optimal for AlN, N_2/H_2 and Ar/N_2 mixtures proved to be better for GaN and InN. InN experiments revealed that the inclusion of H_2 gas led to mixed phase growth with substantial c-In_2O_3 phase. The possible surface reaction mechanisms that lead to these different growth behaviors will be discussed in detail.

12:00pm **PS+2D+SE+TF-FrM12 Tribological Properties of Plasma Enhanced Atomic Layer Deposition TiMoN with Substrate Bias**, ***Mark Sowa,*** Veeco ALD; *A.C. Kozen,* University of Maryland; *N.C. Strandwitz, T.F. Babuska, B.A. Krick,* Lehigh University

In our previous study, we demonstrated a tertiary plasma enhanced atomic layer deposited transition metal nitride (TiVN) with exceptional wear rates and friction coefficients. We have extended that work with an investigation of another tertiary transition metal nitride system, $Ti_xMo_yN_z$. For films deposited at 250°C and 300W on a Veeco CNT G2 Fiji PEALD system, we have demonstrated how the ratio of TiN:MoN cycles (1:0, 2:1, 1:1, 1:2, 0:1)

provides linear control of the Ti:Mo in the resulting film. Through application of an 13.56MHz RF substrate bias (0-188V) during the plasma step, ion bombardment energy of the substrate can be varied, providing a means for tweaking the films physical and chemical characteristics which in turn are shown to impact the resulting film's tribological properties. As PEALD metal nitrides have broader interest than wear layers and to gain insights on the interrelationships of the mechanical properties, the processing details, and other film properties, we also report on the resulting film composition/impurities, density, crystallinity, optical properties, resistivity, and morphology.

Thin Films Division
Room A216 - Session TF-FrM
Theory and Characterization of Thin Film Properties

Moderators: Angel Yanguas-Gil, Argonne National Laboratory, Gerben van Straaten, Eindhoven University of Technology, The Netherlands

8:20am **TF-FrM1 Incorporation Mechanisms and Electronic Properties of Impurities in Wide-Band-Gap Semiconductors***, **John (Jack) Lyons,** S.C. Erwin,* U.S. Naval Research Laboratory **INVITED**

The management of unwanted impurities as well as the controlled introduction of dopant species continue to be challenges in wide-band-gap (WBG) semiconductors such as AlN and Ga_2O_3. In these materials, contaminants such as carbon often incorporate during growth and subsequently act as trapping centers, which can have a detrimental impact on device performance. Moreover, establishing hole conductivity through the introduction of acceptor impurities has proven to be especially difficult in these compounds. In this talk, I will discuss the use of first-principles calculations to understand the incorporation and electronic properties of impurities in WBG semiconductors.

In many growth techniques carbon-containing precursors, such as trimethylaluminum (TMA) for AlN, are often employed. These precursors are thought to be a major source of carbon contamination during growth. Focusing on atomic-layer deposition, we have developed a model to elucidate the decomposition of TMA at the AlN surface, and subsequent incorporation of carbon into the AlN film during growth. We find that the use of H-containing plasma is crucial for scrubbing methyl species from the surface. However, the plasma also leads to atomic carbon, which opens a channel for trapping carbon impurities into the film. In light of this dual role, we propose a solution for minimizing carbon contamination into AlN.

Quantitative determination of the electrical role of particular impurity species present within WBG semiconductors has long been a challenge for theoretical calculations. However, using hybrid density functional theory we are now able to accurately predict the role of impurities such as carbon. We find that carbon acts predominantly as a deep acceptor trap in AlN, as it does for GaN. In contrast, carbon is found to act as a donor species in WBG oxides such as Ga_2O_3. Other potential acceptor dopants, such as magnesium, are also found to act as deep acceptors, due to their propensity to trap localized holes. In fact, no acceptors are found to be effective *p*-type dopants in either Ga_2O_3 or AlN. However, acceptor dopants are still found to be useful for producing semi-insulating material.

9:00am **TF-FrM3 Review and Demonstration of Feature Scale Simulations***, **Paul Moroz,*** TEL Technology Center, America, LLC

Feature-scale simulations (FSS) represent an important tool for modeling of etching, deposition, and implantation processes routinely applied during semiconductor materials processing and device fabrication. Traditionally, FSS uses a combination of Monte Carlo methods with special algorithms for modeling gaseous and solid (in volume and at the surface) species, as well as algorithms for advancing feature profiles and materials composition as a result of reactive interactions of incoming species with solid materials. The mentioned FSS approach, at least at present time, seems to be the only feasible approach to simulate materials processing at the feature-scale level ranging from tens of nanometers to tens of micrometers, while applications of such advanced methods as quantum chemistry or molecular dynamics are still too expensive computationally in spite of highly efficient code parallelization to run on multi-processor computers. Phenomenological description of reactions (chemical and physical) represents a weakness of FSS, as it is very difficult to implement proper sets of reactions valid at different conditions. Here, we discuss an approach used in the FPS3D code [1-5], for simulation of etching, deposition, and implantation with the present focus given to simulation of ALD/CVD processes. Examples include such difficult topics as HAR etching, as well as CVD and ALD. For ALD examples we consider silicon nitride deposition [5] for different chemistries, some of them allowing deposition of a single monolayer per cycle, while others allowing only a fraction of a monolayer to be deposited per cycle.

References:

[1] P. Moroz, IEEE Trans. on Plasma Science, 39 2804 (2011).

[2] P. Moroz, D. J. Moroz, ECS Transactions, 50 61 (2013).

[3] P. Moroz, D. J. Moroz, J. Physics: CS 550 012030 (2014).

[4] P. Moroz, 15th Int. Conf. on Atomic Layer Deposition, Portland, OR (2015).

[5] P. Moroz, D. J. Moroz, Japan. J. Appl. Phys. **56**, 06HE07 (2017).

9:20am **TF-FrM4 Process Optimization in Atomic Layer Deposition Using Machine Learning***, A. Yanguas-Gil, S. Letourneau, A.U. Mane, **Noah Paulson,** A.N. Lancaster, J.W. Elam,* Argonne National Laboratory

Process development and process optimization are ubiquitous, resource-intensive tasks in thin film research and development. The goal of these activities is to find the set of process parameters (e.g. temperature, pressure, and flow) that maximize film quality at minimal cost. Typically, this is accomplished by coating a substrate (e.g. a silicon wafer) under a given set of conditions, measuring the film properties ex situ, and adjusting the conditions to improve the film quality. This activity can consume significant time and resources, especially if an additional goal is to achieve uniform films across a large substrate. Process development can be accelerated and economized using in situ measurements. For instance, quartz crystal microbalance (QCM) measurements can be employed to monitor film thickness in real time as the deposition conditions are varied. However, this still requires the careful attention of a skilled operator to make informed choices based on experience and intuition. An alternative strategy is to use machine learning (ML) to analyze the QCM data and adjust the growth conditions based on an algorithm. To explore this possibility, we used ML to optimize the atomic layer deposition (ALD) of Al_2O_3 with trimethyl aluminum (TMA) and H_2O in a viscous-flow tubular reactor using in situ QCM measurements. We initially developed the ML code using simulated QCM data generated by a 1-D model of ALD transport and reaction. This allowed us to tailor the algorithm to ensure saturation of the TMA and H_2O ALD reactions and to converge efficiently on the optimal dose and purge times. An additional benefit of these simulations was that we could explore the effects of non-ideal behavior such as a CVD component to the surface reactions and strong interaction between the reaction products and the surface. Next, we interfaced the ML code to our ALD system and allowed the algorithm to optimize the TMA and H_2O timings. We observed rapid convergence, as predicted by our simulations, and found that the ML algorithm was capable of adapting to large variations in the initial conditions such as the precursor partial pressures and the carrier gas flow rate. We are now building an array of QCM sensors to measure the thickness simultaneously at 10 locations along our flow tube, and we hope to report on ML opimization of thickness and uniformity using this array.

9:40am **TF-FrM5 Electroless Deposition of Cobalt Metal on a Palladium Layer on an Amine-modified Surface***, A. Ng, **Anthony Muscat,*** University of Arizona

Solution-deposited palladium on amine-terminated self-assembled monolayers (SAMs) is a well-characterized catalyst and adhesion layer combination for solution-based electroless metallization of dielectric films. A reducing agent is typically added to the deposition bath or a sensitizer such as tin is co-deposited producing relatively thick Pd layers. Thinner Pd deposits would enable barrier seed layers for filling < 10 nm wide gaps in patterned dielectric films with metal. In this work, we eliminated the reducing agent from the deposition bath and worked at pH < 2 to deposit monomeric Pd(2+) species and show that the amine groups terminating the SAM reduce Pd(2+) to Pd(0). The amount of Pd deposited depended on the coverage of the two types of amines on the SAM. The adsorption of $PdCl_4^{2-}$ ions in solution on protonated amine groups ($–NH_3^+$) is well known. Our data suggest that the nonprotonated amine groups ($–NH_2$), which coexist with $–NH_3^+$, chemically reduce the Pd(2+) ion to Pd metal by oxidizing to the amine radical cation ($–NH_2^{\bullet +}$). Pd bonds to and covers the $–NH_2^{\bullet +}$groups in the process depositing around a monolayer of Pd from solution on the SAM-covered silicon oxide surface. The Pd layer served as a catalyst for solution deposition of cobalt films on the surface using a reducing agent under oxygen-free conditions. The cobalt deposited initially as islands that grew together into a closed film with good adhesion.

10:00am **TF-FrM6 The Origins of Condensation-Driven Degradation of Hydrophobic Thin Films**, ***Jingcheng Ma***, *N.M. Miljkovic,* University of Illinois at Urbana-Champaign

Dropwise condensation of steam on metallic surfaces coated with thin (~ 1µm) functional hydrophobic films has the potential to achieve remarkable heat transfer coefficients approaching ~100 kW/m^{2}K. However, the long-term durability of these thin films has limited the application of functional coatings for the past century. Although degradation due to steam condensation has been qualitatively described as 'blistering', no satisfactory insight exists capable of answering two key questions: what is the mechanism of water vapor mass transfer, and what is the driving force for film delamination. Hence, scientists have been forced to abandon rational thin film development in favor of ad-hoc trial-and-error approaches. Here, we demonstrate that pinholes on hydrophobic coatings are the source of blisters so commonly seen during degradation. By creating shape-controlled pinhole-blister structures in thin deposited films, we show that blisters form in a spatially-controlled order during water vapor condensation from the ambient. The shape, initiation, and growth of the blisters was systematically investigated. Our experiments demonstrate that water vapor is mainly transferred to the blister through spatially-random pinholes which exist in the film after deposition, and the driving force for film delamination is capillary force. Based on the new insights developed here, we propose a non-dimensional pressure to determine the threshold when blistering will be initiated by a pinhole, or when discrete droplets grow up and above pinholes. To the best of our knowledge, our work represents the first quantitative description of blistering initiation. The techniques and insights presented here will inform future work on polymeric thin films to enable their rational and durable design for a variety of applications.

10:20am **TF-FrM7 Structural and Electrical Properties of Sputtered HEA Thin Films of CrFeCoNiCu and their Oxidation Studies**, ***Jeyanthinath Mayandi,*** SMN, Department of Physics,University of Oslo, Norway*; M. Stange, E. Sagvolden, M.F. Sunding, Ø. Dahl,* SINTEF Materials and Chemistry, Norway*; M. Schrade,* SINTEF, Materials and Chemistry, Norway*; J. Deuermeier, E.Fortunato. Fortunato,* Universidade Nova de Lisboa, Portugal*; O.M.Løvvik. Løvvik, S. Diplas,* SINTEF Materials and Chemistry, Norway and University of Oslo, Norway*; P.A. Carvalho,* SINTEF Materials and Chemistry, Norway and Universidade de Lisboa, Portugal*; T.G. Finstad,* SMN, Department of Physics, University of Oslo, Norway

High-entropy alloys (HEAs) represent a class of materials that is intensively investigated for a range of possible applications. They generally show a high degree of phase stability by the high entropy while the structure is a random atom position disorder unlike other alloys which can influence physical properties differently than regular alloys. In general, there are few studies on oxidation of HEA and studies on adding oxygen during the fabrication of HEA. In this study we have sputtered thin films of CrFeCoNiCu onto insulating and optically transparent substrates in order to measure structural, electrical and optical functional properties. We have varied the oxygen pressure in the sputtering environment as well as oxidizing the samples at elevated temperatures after deposition. Optical and electrical characterization was performed on films sputter deposited on fused quartz wafers. The films were characterized by TEM, XRD and XPS. The films with no intentional oxygen had an FCC structure with a texture showing strong (111) preferred orientation as seen by XRD. TEM analysis showed columnar morphology with twins parallel to (111) planes. Samples sputtered under high oxygen content showed a simple NaCl structure(FeO). The samples were annealed in air and O_2 ambient in the temperature range of 300 to 500 °C. This caused an oxide layer growing on top of the FCC structure. XPS was utilized to find the atomic compositions and chemical stated of the elements. Hall measurements and Seebeck measurements were performed on the as prepared and oxidized films from 10 K to 600K. For the FCC structure the resistivity was a factor 10^4 higher than the elemental metals while can be satisfactory described by electron phonon scattering by the Bloch-Grüneisen description and the low temperature negative temperature effect by the Kondo effect. The sign of the Hall coefficient was positive while the Seebeck coefficient was negative, indicating the Fermi surface containing pockets of electrons and holes and an energy dependent scattering time. A detailed comparison of the as prepared and the oxidized thin films will be discussed in terms of the structural chemical and electrical properties of the grown films. In addition the electric properties will be discussed in terms of a model considering electronic structure and scattering.

10:40am **TF-FrM8 Observation of Topological Hall and Curie Temperature above Room Temperature in Strain-engineered FeGe Thin Films**, ***Adam Hauser***, *S. Budhathoki, K. Law, S. Ranjit, A. Sapkota,* The University of Alabama*; A. Thind, R. Mishra,* Washington University in St. Louis*; D. Heiman,* Northeastern University*; M.E. Jamer,* United States Naval Acadamy*; A. Borisevich,* Oak Ridge National Laboratory*; T. Mewes,* The University of Alabama*; J. Gallagher,* U.S. Naval Research Laboratory

The need to control and manipulate magnetic spin in nonvolatile memory applications drives exploration of new magnetic materials with non-uniformly ordered magnetic phases. Of particular interest are materials with inversion asymmetry, most commonly found in non-centrosymmetric space groups. Our group has successfully grown epitaxial B20 FeGe films with 4% tensile strain on a Ge(111) substrate by Sputter Beam Epitaxy, an off-axis magnetron sputtering technique in which beam-shaping, shutter control, and QCM-guided flux control of off-axis, direct-current (DC) magnetron sputter sources are employed upon high-purity elemental Fe and Ge targets in ultra-high vacuum. QCM control is modified to relative atomic ratios, and film compositions are confirmed by energy dispersive x-ray spectroscopy (EDS) and Rutherford Backscattering (RBS). X-ray diffractometry has confirmed that the films are single-crystal and phase pure, with near-substrate-limited rocking curve (FWHM 0.07º) and strong Keissig fringes in x-ray reflectometry. We find no evidence of strain relaxation up to 110nm, and off-axis XRD and HAADF STEM confirm the B20 phase necessary for the Skyrmionic phase. A strain-enhanced T_C = 350K by SQUID magnetometry and a clear Topological Hall effect (THE) signature observed at 330K suggest potential for Skyrmionic behavior at or above room temperature in a single layer thin film. Direct observation is required for confirmation of a Skyrmion lattice phase.

11:00am **TF-FrM9 Infrared Absorption Oscillator Strength Factors in SiNx Thin Films**, ***Sara DiGregorio***, *S. Habermehl,* Sandia National Laboratories

The oscillator strength factor of the Si-N asymmetric stretch mode of SiN films was studied for films of varying composition and thickness. Thin films were deposited by low pressure chemical vapor deposition at 850°C from mixtures of dichlorosilane and ammonia. The oscillator strength factor for each film was determined from Fourier Transform infrared spectroscopy and ellipsometric measurements. We found that the oscillator strength factor systematically decreases with increasing silicon volume fraction from2.10x10 cm to 1.44x10 cm for compositions ranging from 0% to 25% volume fraction amorphous silicon. We believe this trend is related to charge transfer induced structural changes in the basal SiN_x tetrahedron as the volume fraction of amorphous silicon increases. For stoichiometric silicon nitride the oscillator strength factor was found to be $2.01x10^{19}$ ± $7.25x10^{17}$ cm^{-2}, which is consistent with a reported value of $2.07x10^{19}$ cm^{-2} and a theoretical value of $1.99x10^{19}$ cm^{-2} . Additionally, in the composition range investigated, we found that the oscillator strength values agree favorably with trends observed in films deposited by plasma enhanced chemical vapor deposition. This work was selected as the best graduate student presentation at the 2019 NMAVS symposium (Albuquerque-June2019).

11:20am **TF-FrM10 Computer Aided Molecular Design of novel precursor materials for Atomic Layer Deposition**, ***Mina Shahmohammadi,*** University of Illinois at Chicago*; R. Mukherjee,* Vishwamitra Research Institute*; C.G. Takoudis,* University of Illinois at Chicago*; U.M. Diwekar,* Vishwamitra Research Institute

Atomic Layer Deposition (ALD) is a vapor phase technique to deposit thin films of various metals and metal oxides on a substrate. Due to sequential and self-limiting reactions, conformal and pinhole-free thin films can be produced which have widespread applications. In this process, a precursor, which is often a metal surrounded by organic functional groups, chemisorbs on the substrate and part of the molecule subsequently desorbs from the surface after completion of the reaction. Precursor chemisorption on the substrate leads to a self-limiting process and it eventually results in films with desired thickness at the Ångström length scale. To design and conduct an ALD experiment, the precursor(s) should be chosen based on the ALD conditions (i.e., bubbler and reactor temperatures, pressure, gas flow, etc.) and likely applications of the final film. It is practically impossible to carry out a huge number of ALD experiments using numerous precursors and deposition conditions in order to find the optimum one depending on the applications of interest. In addition, only existing precursors can be tested experimentally. This study focuses on developing a computational tool for the design of novel precursor materials with enhanced properties for the ALD of metal oxides and metals.

Computer-Aided Molecular Design (CAMD) is a methodology where materials with optimal desired properties are generated from the combination of functional groups. This approach is the reverse of Group Contribution Method (GCM) in which the thermodynamic properties of a compound are estimated from the structural and functional groups comprising the molecule. For CAMD, we need the properties of the functional groups. In our previous work, we have redeveloped a new GCM for ALD effectively to predict the growth rate curve using Adsorbate Solid Solution Theory (ASST). In this work, novel precursor molecules for ALD are generated using properties of the functional groups. In order to do that, we will be using a combinatorial optimization method called Efficient Ant Colony Optimization (EACO). This is the first time CAMD is being applied to design precursor materials for ALD. In the future, novel designed precursors will be synthesized and their properties will be tested experimentally using a Kurt J. Lesker ALD150LE^{TM} system. Characterization of the deposited films with designed precursors will validate the proposed simulation technique and help us to optimize materials in the best possible way.

11:40am **TF-FrM11 The Use of Molecular Oxygen for a Low Cost and Low Temperature ALD of Amorphous Titania***, **Harshdeep S. Bhatia**, C.G. Takoudis,* University of Illinois at Chicago

The interest in Titania films has been increasing in the past few decades. This interest can be attributed to the various applications of ultrathin films of Titanium dioxide. The thin film deposition of amorphous titania can be done at a low temperature using tetrakis(dimethylamido) titanium (TDMAT) along with ozone and oxygen; growth rates have only been reported at temperatures greater than 150 °C. For titania use with organic substrates, it is important that the reaction is performed at low temperatures to prevent denaturation and degradation. The use of Ozone has also been reported to cause degradation in some elastomeric polymers. Along with the high cost of manufacturing a high concentration of ozone, Oxygen could be considered as a replacement for Ozone. In this study, growth temperatures at or below 150 °C were used to uniformly deposit amorphous titania using TDMAT and oxygen using a highly sophisticated pulse gas source (c/o Kurt J Lesker Co.) ensuring a constant pressure of gas is pulsed into the reactor which is believed to be the contributing factor in the success of this reaction. The as-deposited films were characterized using Spectroscopic Ellipsometry (SE) and X-ray Photoelectron Spectroscopy (XPS). Applications of this reaction could lead to low temperature deposition of titanium oxide on organic substrates for the use in biomedical implants, as a protective coating, and as a seed layer to deposit other conductive metals on organic substrates. One of the interesting phenomena observed using SE was the appearance of a very small but non-zero extinction coefficient in the visible range. This extinction coefficient was similar to the urbach tail absorption usually observed in the UV range. This could also point towards slight absorption of visible light by the deposited Titania films which opens new avenues for research in photocatalytic activity of Titania films within the visible light spectrum.

12:00pm **TF-FrM12 Ultra-High Purity Process Capability for High-Performance Atomic layer Deposition***, **Noel O'Toole**, G.B. Rayner, Jr.,* Kurt J. Lesker Company*; N.A. Strnad,* General Technical Services, LLC*; D.M. Potrepka,* U.S. Army Research Laboratory

Ultra-high purity (UHP) process capability is motivated by the need to produce superior, high-quality thin films and interfaces by atomic layer deposition (ALD) techniques. In particular, UHP equipment design reduces background impurity levels, including oxygen, to limit incorporation during film growth. Creating and maintaining a UHP process environment are also essential for ALD process reproducibility. This presentation will address the potential sources of background contamination, as well as system design requirements to obtain a controlled UHP process environment. Results will be presented that demonstrate the effectiveness of this technology to obtain high-quality titanium nitride thin films by plasma-enhanced ALD (PEALD) techniques.

Author Index

Bold page numbers indicate presenter

— A —
Abdulagatov, A.I.: AP+PS+TF-ThM10, **50**
Abelson, J.R.: TF+2D+AP+EL+SS-MoA5, 15; TF-ThP10, 61; TF-ThP9, 61
Abu Ali, T.: PS+2D+SE+TF-FrM4, 65
Abudayyeh, O.K.: TF+EM+NS+SS-ThM4, 52
Abugri, J.B.: TF+EM+MI+MN+OX+PS-MoM6, 3
Acosta, A.: TF+EM+MI+MN+OX+PS-MoM3, 3
Adamsen, K.C.: OX+EM+HC+MI+NS+SS+TF-TuA10, 27
Agarwal, P.: PS+2D+SE+TF-FrM10, 66
Agarwal, S.: AP+2D+EM+PS+TF-MoM10, **2**; AP+2D+EM+PS+TF-MoM2, 1; AP+2D+EM+PS+TF-MoM8, 2
Ager, J.W.: EM+2D+NS+TF-WeA9, 44
Aggarwal, N.: TF+EM+MI-TuM3, **21**
Ahmad, Z.: TF-ThP12, 61
Ahsan, R.: EM+2D+AS+MI+MN+NS+TF-WeM10, **38**; EM+2D+NS+TF-WeA8, 44
Aikawa, S.: TF-ThP25, 63
Akaishi, A.: 2D+AP+EM+MI+MN+NS+PS+TF-MoA9, 9
Akay, S.: TL+AS+SS+TF-TuA7, 32
Akolkar, R.: EM+AP+MS+NS+TF-ThM10, **51**
Akyildiz, H.I.: TF-TuA8, **31**
Alema, F.: TF+EM-WeA2, **47**
Aleman, A.: TF+PS-TuA2, 28
Allen, N.E.: EL+AS+EM+TF-WeM5, **35**
Allerman, A.A.: EM+OX+TF-TuA12, 27
Allred, D.D.: TF+AS+EL+PS+RA-ThA9, 57
Al-Quaiti, F.: TF+PS-TuA12, 29
Alvarez, D.: TF+AP-TuM3, **19**
Alvaro, E.: TF-ThP24, **63**
An, Y.: TF-ThP8, 60
Ando, T.: OX+EM+HC+MI+NS+SS+TF-TuA3, 27
Angel, D.: AP+EL+MS+PS+SS+TF-TuA12, 25
Antonelli, G.A.: AP+EL+MS+PS+SS+TF-TuA7, **24**
Archenti, A.: TF+SE-MoA9, 18
Arias, P.: TF+PS-TuA2, 28
Armstrong, A.M.: EM+OX+TF-TuA12, 27
Arora, P.: PS+AS+EM+SS+TF-MoA6, **14**
Arts, K.: PS+2D+SE+TF-FrM8, 66; PS+AS+EM+SS+TF-MoA10, **14**
Artyushkova, K.: RA+AS+CA+PS+TF-WeM11, 39
Aso, R.: TL+AS+SS+TF-TuA3, 32
Avila, J.R.: TF+AP-TuM4, **19**; TF+EM-WeA10, 48
Avval, T.G.: TF+AP-TuM13, **21**; TF+AS+EL+PS+RA-ThA9, 57
Aydil, E.S.: TF+EM+NS+SS-ThM6, 53; TF+SS-ThA8, 58
— B —
Baba, K.: TF1-WeM5, **40**
Babuska, T.F.: PS+2D+SE+TF-FrM12, 66
Baca, A.G.: EM+OX+TF-TuA12, 27
Baer, D.R.: RA+AS+CA+PS+TF-WeM10, 39
Bahceci, S.: TL+AS+SS+TF-TuA7, 32
Bahoura, M.J.: TF+EM+NS+SS-ThM10, 53
Bailey, C.: EM+PS+TF-MoA9, 13
Bailey, D.: PS+2D+SE+TF-FrM6, 65
Bailey-Crandell, R.: 2D+AP+EM+MI+MN+NS+PS+TF-MoA5, 8
Bakkers, E.P.A.M.: TF+EM+MI-TuM10, 22
Balasubramanyam, S.: 2D+AP+EM+MI+NS+PS+TF-MoA5, **10**
Baldo, M.: EM+PS+TF-MoA2, 12
Bale, R.: PS+2D+SE+TF-FrM6, 65
Balke, N.: TF+EM+MI+MN+OX+PS-MoM10, 4
Ballard, J.: EM+2D+AS+MI+MN+NS+TF-WeM4, 37; TF-MoM5, 5
Banerjee, S.: EM+PS+TF-MoA10, **13**
Bangasi, G.: TF1-WeM5, 40
Banks, S.: TF-ThP14, **61**
Barmak, K.: EM+AP+MS+NS+TF-ThM6, 51
Barnes, E.: TF+EM+NS+SS-ThM11, 53
Basaldua, I.: TF+EM+MI-TuM6, 22
Basher, A.H.: AP+PS+TF-ThM5, **49**
Basker, V.: TF+EM+MI-TuM11, 22
Bassiri-Gharb, N.: TF+EM+MI+MN+OX+PS-MoM8, **4**
Baumgartner, Y.: TF+EM+MI-TuM1, 21
Beach, G.S.D.: TF+EM+MI+MN+OX+PS-MoM5, 3
Beckmann, K.: TF-TuA11, 31
belahcen, S.: AP+EL+MS+PS+SS+TF-TuA9, 24
Bell, K.: TF-ThP14, 61
Belyansky, M.: TF+EM+MI-TuM11, 22
Ben Sedrine, N.: EM+OX+TF-TuA9, 26
Bent, S.F.: TF1-WeM11, 41
Berghuis, W.J.H.: TF+EM+MI-TuM10, **22**
Bergsman, D.S.: TF-TuA12, **31**
Bernard, M.: TF+EM-WeA7, 47
Bertoni, M.: EM+2D+NS+TF-WeA1, **44**
Bhatia, H.S.: TF-FrM11, **69**
Bi, S.: TF-ThP20, 62
Bielefeld, J.D.: PS+2D+SE+TF-FrM6, 65
Bignardi, L.: 2D+AP+EM+MI+MN+NS+PS+TF-MoA3, 8
Bilgilisoy, E.: AP+BI+PS+TF-WeM13, 34
Binek, C.: OX+EM+HC+MI+NS+SS+TF-TuA1, 27
Biolsi, P.E.: PS+2D+EM+SS+TF-ThA1, **55**; PS+2D+EM+SS+TF-ThA4, 55
Bittrich, E.: EL+AS+EM+TF-WeM11, **36**
Biyikli, N.: EM+OX+TF-TuA8, **26**; PS+2D+SE+TF-FrM11, 66
Bohamud, T.: TF+SS-ThA3, 58
Bol, A.A.: 2D+AP+EM+MI+NS+PS+TF-MoA5, 10
Boldman, W.L.: TF-ThP20, 62
Bonvalot, M.: AP+EL+MS+PS+SS+TF-TuA9, 24
Borchers, J.: TF+EM+MI+MN+OX+PS-MoM3, 3
Boreman, G.D.: EL+AS+EM+TF-WeM13, 36
Borisevich, A.: TF-FrM8, 68
Borman, T.: TF+SE-MoA5, **17**
Boscher, N.D.: TF1-WeM5, 40
Bose, R.: TF+SS-ThA10, **59**
Bourgeois, G.: TF+EM-WeA7, **47**
Bournel, F.: TF+2D+AP+EL+SS-MoA8, 16
Brehm, J.: TF+EM+MI+MN+OX+PS-MoM10, 4
Brena, B.: TF+2D+AP+EL+SS-MoA8, 16
Brenning, N.: TF+SE-MoA1, 17
Brillson, L.J.: EM+2D+AS+MI+MN+NS+TF-WeM2, 37; EM+2D+AS+MI+MN+NS+TF-WeM4, 37; EM+OX+TF-TuA7, 25; TF-MoM5, 5
Bruner, P.: AP+EL+MS+PS+SS+TF-TuA9, 24
Brüner, P.: TF+AS+EL+PS+RA-ThA8, 57
Bsiesy, A.: AP+EL+MS+PS+SS+TF-TuA9, 24
Bu, H.: TF+EM+MI-TuM11, 22
Budak, S.: TF+EM+NS+SS-ThM11, **53**; TF+EM+NS+SS-ThM12, 54; TF-ThP15, 61
Budhathoki, S.: TF+EM+MI+MN+OX+PS-MoM6, **3**; TF-FrM8, 68
Buechler, K.: EM+2D+NS+TF-WeA3, **44**
Burkett, C.: TF-ThP13, 61
Burkins, P.: TF+EM+MI-TuM6, 22
Burzynski, K.M.: TF-TuA4, **30**
— C —
Cada, M.: TF+SE-MoA1, 17
Cady, N.C.: TF-TuA11, 31
Cahoon, J.F.: TF+AS+EL+PS+RA-ThA3, 57
Cai, H.: 2D+AP+EM+MI+NS+PS+TF-MoA3, 10
Caldwell, J.D.: TF+EM-WeA10, 48
Canova, K.: TF-ThP9, **61**
Canulescu, S.: 2D+AP+EM+MI+NS+PS+TF-MoA3, 10
Carman, G.P.: TF+EM+MI+MN+OX+PS-MoM3, 3
Caroff, C.: TF-ThP10, 61
Caruso, A.N.: PS+2D+SE+TF-FrM6, 65
Carvalho, P.A.: TF-FrM7, 68
Carver, A.G.: TF+PS-TuA9, 29
Carver, V.: TF+AP-TuM13, 21
Cavanagh, A.S.: TF+AP-TuM5, 19
Caver, N.: TF+EM+NS+SS-ThM12, 54
Ceragioli, H.J.: TF-ThP7, 60
Chae, H.U.: EM+2D+AS+MI+MN+NS+TF-WeM10, 38; EM+2D+NS+TF-WeA8, **44**
Chamberlin, S.E.: TF-ThP27, 63
Chance III, S.: TF-ThP14, 61
Chang, C.R.: TF-ThP26, 63
Chang, J.P.: AP+BI+PS+TF-WeM12, 34; PS+AS+EM+SS+TF-MoA3, **13**; TF+EM+MI+MN+OX+PS-MoM3, 3; TF-MoM4, 5
Chang, Y.H.: TF+AP-TuM6, 20
Chaudhary, S.: TF+2D+AP+EL+SS-MoA8, 16
Chavez, A.: TF+EM+NS+SS-ThM4, 52
Chavez, J.: TF+EM+NS+SS-ThM4, 52
Chen, E.: AP+BI+PS+TF-WeM12, 34
Chen, H.-P.: TF-ThP4, 60; TF-ThP5, 60
Chen, L.H.: AP+PS+TF-ThM4, **49**
Chen, M.: EM+PS+TF-MoA9, 13
Chen, P.Y.: TF+PS-TuA12, **29**
Chen, S.: TF+EM-WeA11, 48
Chen, W.-C.: TF-ThP4, 60; TF-ThP5, **60**
Chen, X.: SE+AS+TF-WeA4, 45
Chen, XG.: EM+PS+TF-MoA6, 12
Cheng, R.: TF-ThP28, 63
Chiang, S.: EM+2D+AS+MI+MN+NS+TF-WeM12, **38**
Cho, W.-H.: TF-ThP4, 60
Choi, B.C.: TF-ThP1, 60
Choi, C.: AP+BI+PS+TF-WeM12, 34
Choi, S.: TF-ThP8, 60
Chong, D.: RA+AS+CA+PS+TF-WeM1, **39**
Christopher, R.: EM+PS+TF-MoA8, 12
Chu, J.P.: SE+AS+TF-WeA3, **45**
Chu, X.: TF-ThP10, **61**
Chuang, H.-J.: 2D+AP+EM+MI+NS+PS+TF-MoA2, 10
Chung, P.: EM+OX+TF-TuA11, 26
Churikova, A.: TF+EM+MI+MN+OX+PS-MoM5, 3
Clark, B.D.: TF+EM+MI+MN+OX+PS-MoM6, 3
Clark, C.P.: TF+SS-ThA8, **58**
Clark, R.D.: TF-TuA11, 31
Cleveland, E.: TF+EM+NS+SS-ThM5, **53**
Cobas, E.D.: 2D+AP+EM+MI+NS+PS+TF-MoA2, 10
Coclite, A.M.: PS+2D+SE+TF-FrM4, 65; TF1-WeM3, 40
Coffey, K.R.: EM+AP+MS+NS+TF-ThM6, **51**
Cola, B.A.: EM+2D+AS+MI+MN+NS+TF-WeM1, 37
Collazo, R.: TF+SE-MoA8, 18
Collette, R.: TF+EM+MI-TuM4, **22**
Colon, A.: EM+OX+TF-TuA12, 27
Conley, Jr., J.F.: TF+EM+MI-TuM12, 23
Consiglio, S.: TF-TuA11, 31
Convertino, C.: TF+EM+MI-TuM1, 21
Cooper, J.: EM+AP+MS+NS+TF-ThM13, 52
Copeland, C.R.: EM+2D+AS+MI+MN+NS+TF-WeM13, 38
Crabtree, G.W.: RA+AS+CA+PS+TF-WeM5, **39**

Author Index

Creatore, M.: TF-MoM11, 6
Creyghton, Y.L.M.: PS+2D+SE+TF-FrM7, **65**
Cross, G.B.: TF-ThP12, **61**
Cunniff, A.: OX+EM+HC+MI+NS+SS+TF-TuA12, 28
Currie, M.: TF+EM-WeA10, 48
Cyrille, M.C.: TF+EM-WeA7, 47
— D —
D'Acunto, G.: TF+2D+AP+EL+SS-MoA8, 16
Dahl, Ø.: TF-FrM7, 68
Dale, A.S.: TF-ThP28, **63**
Darling, S.B.: TL+AS+SS+TF-TuA1, **32**
Das, K.: EM+OX+TF-TuA11, 26
Dasari, K.: EL+AS+EM+TF-WeM2, 35
David, S.: AP+EL+MS+PS+SS+TF-TuA9, 24
Davis, R.C.: EL+AS+EM+TF-WeM5, 35; TF-TuA10, 31
Deckers, R.: TF-MoM11, 6
Demarest, J.: TF+EM+MI-TuM11, 22
Demkov, A.A.: TF+EM+MI-TuM5, 22; TF+PS-TuA12, 29
Deshpande, A.: TF+PS-TuA2, 28
Desport, J.: TF1-WeM5, 40
Deuermeier, J.: TF-FrM7, 68
Dhall, A.: SE+AS+TF-WeA10, 46
Dickmann, M.: AP+BI+PS+TF-WeM1, 33
Diebold, A.C.: EL+AS+EM+TF-WeM3, **35**; EM+2D+AS+MI+MN+NS+TF-WeM3, 37; TF-TuA11, 31
DiGregorio, S.: TF-FrM9, **68**
Dijkstra, A.: TF+EM+MI-TuM10, 22
Diler, S.: TF-TuA8, 31
Ding, J.: TF-ThP31, 63
Diplas, S.: TF-FrM7, 68
DiStasio, Jr., R.A.: AP+2D+EM+PS+TF-MoM9, 2
Diwekar, U.M.: TF-FrM10, 68
Dixson, R.G.: EM+2D+AS+MI+MN+NS+TF-WeM13, 38
Dodson, B.D.: TF-TuA10, **31**
Dong, C.: TF+EM+MI+MN+OX+PS-MoM3, 3
Donnelly, V.M.: PS+AS+EM+SS+TF-MoA5, 14; PS+AS+EM+SS+TF-MoA6, 14
Dorsett, L.: PS+2D+SE+TF-FrM6, 65
Douglas, E.A.: EM+OX+TF-TuA12, **27**
Dowben, P.A.: OX+EM+HC+MI+NS+SS+TF-TuA1, **27**
Du, D.: TF+EM+MI+MN+OX+PS-MoM11, 4
Du, L.: PS+AS+EM+SS+TF-MoA5, 14
Du, Y.: OX+EM+HC+MI+NS+SS+TF-TuA7, **27**
Duerr, M.: TF+SS-ThA3, 58
Dunn, B.: TF-MoM4, 5
Durfee, C.: TF+EM+MI-TuM11, 22
Duscher, G.: 2D+AP+EM+MI+NS+PS+TF-MoA3, 10
Dutta, S.: EM+PS+TF-MoA2, 12
Dzara, M.J.: RA+AS+CA+PS+TF-WeM11, 39
— E —
Ebdah, M.: EL+AS+EM+TF-WeM2, 35
Economou, D.J.: PS+AS+EM+SS+TF-MoA5, 14
Eddy, C.R.: TF+2D+AP+EL+SS-MoA6, 15
Eddy, Jr., C.R.: EM+OX+TF-TuA4, **25**; TF+AP-TuM6, 20
Edmondson, B.I.: TF+EM+MI-TuM5, 22
Egger, W.: AP+BI+PS+TF-WeM1, 33
Ehiasarian, A.P.: TF+SE-MoA6, **17**
Eichhorn, K.-J.: EL+AS+EM+TF-WeM11, 36
Ekerdt, J.G.: TF+EM+MI-TuM5, **22**; TF+PS-TuA12, 29
Ekins-Daukes, N.J.: TF+EM+NS+SS-ThM5, 53
El Assad, D.: TF1-WeM5, 40
Elam, J.W.: AP+EL+MS+PS+SS+TF-TuA3, **24**; TF-FrM4, 67
Eliseev, E.: TF+EM+MI+MN+OX+PS-MoM10, 4
Elliott, L.C.C.: EM+2D+AS+MI+MN+NS+TF-WeM13, 38
Ellis, C.T.: TF+EM-WeA10, 48
Emdadi, L.: 2D+AP+EM+MI+MN+NS+PS+TF-MoA8, **9**
Engelmann, S.U.: OX+EM+HC+MI+NS+SS+TF-TuA3, **27**; PS+2D+EM+SS+TF-ThA6, 55
Engeln, R.: PS+2D+SE+TF-FrM8, 66
English, C.: EM+PS+TF-MoA9, 13
Engstrom, J.R.: 2D+AP+EM+MI+NS+PS+TF-MoA11, **11**; AP+2D+EM+PS+TF-MoM9, 2
Eom, D.: TF-ThP8, 60
Eres, G.: 2D+AP+EM+MI+NS+PS+TF-MoA3, 10
Erwin, S.C.: TF-FrM1, 67
Esat, B.: TL+AS+SS+TF-TuA7, **32**
Ezzat, S.S.: EM+AP+MS+NS+TF-ThM6, 51
— F —
Fadaly, E.M.T.: TF+EM+MI-TuM10, 22
Fairbrother, D.: AP+BI+PS+TF-WeM13, 34
Faraz, T.F.: PS+2D+SE+TF-FrM8, 66
Fattah, I.: TF+EM+NS+SS-ThM13, 54
Favela, E.: EM+OX+TF-TuA11, 26
Feigelson, B.N.: 2D+AP+EM+MI+NS+PS+TF-MoA6, 10
Feng, G.: TF-ThP20, 62
Feng, Z.: TF-ThP19, 62
Ferguson, I.: EM+OX+TF-TuA9, **26**
Ferguson, S.: TF1-WeM4, **40**
Fernandes, S.H.: TF-ThP7, 60
Ferri, K.: TF+SE-MoA8, **18**
Feygelson, B.: TF+2D+AP+EL+SS-MoA3, 15
Fields, S.: EM+PS+TF-MoA8, 12
Filler, M.A.: EM+2D+AS+MI+MN+NS+TF-WeM1, **37**; EM+AP+MS+NS+TF-ThM5, 51
Fink, K.: AP+PS+TF-ThM5, 49
Finstad, T.G.: EL+AS+EM+TF-WeM1, **35**; TF-FrM7, 68
Fischer, A.: AP+PS+TF-ThM3, **49**
Fitzell, K.: TF+EM+MI+MN+OX+PS-MoM3, **3**
Fong, C.Y.: EM+2D+AS+MI+MN+NS+TF-WeM12, 38
fontelaye, c.: TF-TuA7, 30
Fortunato, E.Fortunato.: TF-FrM7, 68
Fowlkes, J.D.: TF-ThP20, 62
Frache, G.: TF1-WeM5, 40
Franz, G.: EM+AP+MS+NS+TF-ThM1, **51**
Fredriksson, H.O.A.: TF-MoM11, 6
Frijters, C.: TF-TuA3, 30
Fujisaki, S.: AP+PS+TF-ThM1, 49
Fukasawa, M.: PS+2D+EM+SS+TF-ThA3, 55
Fukatsu, S.: EL+AS+EM+TF-WeM10, **36**
— G —
Gagliardi, L.: TF+EM+NS+SS-ThM6, 53
Galazka, Z.: EM+OX+TF-TuA11, 26
Gall, D.: EM+AP+MS+NS+TF-ThM6, 51
Gallagher, J.: TF-FrM8, 68
Gallant, B.M.: TL+AS+SS+TF-TuA8, **32**
Gao, H.: EM+2D+AS+MI+MN+NS+TF-WeM2, **37**
Gardill, A.: TF-ThP27, 63
Garrione, J.: TF+EM-WeA7, 47
Garstein, Y.: TF+SS-ThA10, 59
Gassilloud, R.: AP+EL+MS+PS+SS+TF-TuA9, 24; TF+AS+EL+PS+RA-ThA8, 57
Gasvoda, R.J.: AP+2D+EM+PS+TF-MoM2, **1**
Geohegan, D.: 2D+AP+EM+MI+NS+PS+TF-MoA3, **10**
George, A.: 2D+AP+EM+MI+NS+PS+TF-MoA9, 11
George, S.M.: AP+PS+TF-ThM10, 50; AP+PS+TF-ThM11, 50; AP+PS+TF-ThM6, 50; TF+AP-TuM12, 20; TF+AP-TuM5, 19; TF+AS+EL+PS+RA-ThA6, **57**
Getachew, B.A.: TF-TuA12, 31
Ghalichechian, N.: TF+EM-WeA11, 48
Ghods, A.: EM+OX+TF-TuA9, 26
Ghosh, S.: SE+AS+TF-WeA4, **45**
Giles, A.J.: TF+EM-WeA10, 48
Girolami, G.S.: TF+2D+AP+EL+SS-MoA5, 15; TF-ThP10, 61; TF-ThP9, 61
Glavin, N.R.: PS+2D+SE+TF-FrM1, 65; TF-TuA4, 30
Gleason, K.K.: TF1-WeM1, **40**; TF1-WeM13, 42
Glenn, A.: TF-ThP15, 61
Gong, Y.: EM+AP+MS+NS+TF-ThM10, 51
Goorsky, M.S.: TF+PS-TuA2, 28
Gopman, D.: TF+EM+MI+MN+OX+PS-MoM3, 3
Goswami, L.: TF+EM+MI-TuM3, 21
Goto, T.: PS+AS+EM+SS+TF-MoA2, **13**
Gougousi, T.: TF+EM+MI-TuM6, **22**
Gowda, R.G.: EM+2D+AS+MI+MN+NS+TF-WeM3, **37**
Granados, M.: TF-TuA7, 30
Greczynski, G.: SE+AS+TF-WeA7, **45**
Greenberg, B.: TF+2D+AP+EL+SS-MoA3, **15**
Greene, J.E.: SE+AS+TF-WeA7, 45
Greer, J.: TF+EM+MI+MN+OX+PS-MoM5, 3
Gregorczyk, K.: TF1-WeM6, 41; TF-MoM6, 5
Grehl, T.: AP+EL+MS+PS+SS+TF-TuA9, 24; TF+AS+EL+PS+RA-ThA8, **57**
Groenenboom, M.: TF+SS-ThA1, 58
Grossman, J.C.: TF-TuA12, 31
Grundmann, M.: EM+2D+AS+MI+MN+NS+TF-WeM2, 37
Grzeskowiak, J.: TF+AP-TuM6, 20
Gu, G.: TF-ThP20, 62
Gu, Y.: 2D+AP+EM+MI+NS+PS+TF-MoA3, 10
Gudmundsson, J.T.: TF+SE-MoA1, **17**
Guo, D.: TF+EM+MI-TuM11, 22
Guo, T.: TF+SS-ThA10, 59
Gupta, G.: TF+EM+MI-TuM3, 21
Gupta, S.: TF+EM+MI+MN+OX+PS-MoM6, 3
Gurudayal, G.: EM+2D+NS+TF-WeA9, **44**
Gustafson, M.E.: EM+2D+AS+MI+MN+NS+TF-WeM1, 37
— H —
Haastrup, M.J.: 2D+AP+EM+MI+MN+NS+PS+TF-MoA6, **9**
Habermehl, S.: TF-FrM9, 68
Hadamek, T.: TF+PS-TuA12, 29
Hajihoseini, H.: TF+SE-MoA1, 17
Hamada, I.: AP+PS+TF-ThM5, 49
Hamaguchi, S.: AP+BI+PS+TF-WeM3, 33; AP+BI+PS+TF-WeM4, 33; AP+PS+TF-ThM5, 49; PS+2D+EM+SS+TF-ThA3, 55; PS+2D+EM+SS+TF-ThA8, **56**
Han, S.E.: EM+2D+NS+TF-WeA11, 45
Han, S.M.: EM+2D+NS+TF-WeA11, 45; TF+EM+NS+SS-ThM4, **52**
Han, Y.: PS+2D+EM+SS+TF-ThA4, 55
Hanbicki, A.T.: 2D+AP+EM+MI+NS+PS+TF-MoA2, 10
Hao, Y.: EM+PS+TF-MoA6, 12
Hartage, K.: EM+AP+MS+NS+TF-ThM13, 52
Haseman, M.: EM+2D+AS+MI+MN+NS+TF-WeM2, 37; EM+OX+TF-TuA7, **25**
Hashemi Astaneh, S.: SE+AS+TF-WeA9, **46**
Hassani, E.: TF+EM+MI-TuM13, 23
Hauser, A.J.: TF+EM+MI+MN+OX+PS-MoM6, 3; TF-FrM8, **68**
Hausmann, D.M.: AP+2D+EM+PS+TF-MoM4, 1; AP+2D+EM+PS+TF-MoM8, 2
Haverkort, J.E.M.: TF+EM+MI-TuM10, 22
Hayden, J.: TF+EM+MI+MN+OX+PS-MoM4, **3**
Hazra, J.H.: TF-TuA11, 31
Head, A.R.: TF+2D+AP+EL+SS-MoA8, 16
Heckman, E.M.: TF-TuA4, 30

Heep, J.: TF+SS-ThA3, **58**
Heezen, H.: TF-TuA3, **30**
Heiman, D.: TF-FrM8, 68
Heinze, K.: TF1-WeM5, 40
Henderson, A.: TF-ThP15, 61
Heng, C.L.: EL+AS+EM+TF-WeM1, 35
Hernandez, K.: PS+2D+EM+SS+TF-ThA6, 55
Hilfiker, J.N.: AP+EL+MS+PS+SS+TF-TuA1, **24**
Hirata, A.: PS+2D+EM+SS+TF-ThA3, **55**
Hirsch, E.: PS+AS+EM+SS+TF-MoA5, **14**
Hisamatsu, T.: PS+2D+EM+SS+TF-ThA9, 56
Hodges, G.: TF+AP-TuM13, 21; TF+AS+EL+PS+RA-ThA9, 57
Hoefer, U.: TF+SS-ThA3, 58
Hoenk, M.E.: TF+PS-TuA9, 29
Hofmann, T.: EL+AS+EM+TF-WeM13, 36; EL+AS+EM+TF-WeM6, 36
Hogan, C.J.: SE+AS+TF-WeA4, 45
Hojo, K.: TF+PS-TuA2, 28
Holden, K.E.K.: TF+EM+MI-TuM12, **23**
Holmes, R.J.: TF+SS-ThA8, 58
Holtz, M.: TF+EM+MI+MN+OX+PS-MoM1, **2**
Honda, M.: PS+2D+EM+SS+TF-ThA9, 56
Hong, X.: EM+PS+TF-MoA6, **12**
Hopstaken, M.J.P.: PS+2D+EM+SS+TF-ThA6, 55
Hossain, M.D.: TF+SE-MoA5, 17
Hovsepian, P.Eh.: TF+SE-MoA6, 17
Hrebik, J.: TF+SE-MoA11, **18**
Hsiao, C.-N.: TF-ThP18, 62
Hubbard, L.: EM+OX+TF-TuA1, 25
Hubicka, Z.: TF+SE-MoA1, 17
Hübner, U.: 2D+AP+EM+MI+NS+PS+TF-MoA9, 11
Hudson, E.A.: AP+2D+EM+PS+TF-MoM2, 1
Hugenschmidt, C.: AP+BI+PS+TF-WeM1, 33
Huhtinen, H.: OX+EM+HC+MI+NS+SS+TF-TuA11, 28
Hultman, L.: SE+AS+TF-WeA7, 45
Hwang, J.: TF+EM-WeA1, 46; TF-ThP13, 61; TF-ThP19, 62
Hyvärinen, T.: TF2-WeM13, 43
— I —
Ideno, Y.: TF+AP-TuM11, 20
Ihlefeld, J.: EM+PS+TF-MoA8, 12
Ilhom, S.: EM+OX+TF-TuA8, 26; PS+2D+SE+TF-FrM11, 66
Ilic, B.R.: EM+2D+AS+MI+MN+NS+TF-WeM13, 38
Inbanathan, F.P.N.: EL+AS+EM+TF-WeM2, **35**
Inbar, H.S.: TF+AP-TuM6, 20
Innocent-Dolor, J.: PS+2D+EM+SS+TF-ThA6, 55
Ishibashi, S.: AP+BI+PS+TF-WeM1, 33
Isobe, M.: AP+BI+PS+TF-WeM4, 33; AP+PS+TF-ThM5, 49; PS+2D+EM+SS+TF-ThA8, 56
Ito, T.: AP+BI+PS+TF-WeM3, 33; AP+PS+TF-ThM5, 49; PS+2D+EM+SS+TF-ThA8, 56
Izawa, M.: AP+PS+TF-ThM1, 49
— J —
Jadwisienczak, W.M.: EL+AS+EM+TF-WeM2, 35
Jaffal, M.: AP+EL+MS+PS+SS+TF-TuA9, 24
Jaing, C.-C.: TF-ThP5, 60
Jamer, M.E.: TF+EM+MI+MN+OX+PS-MoM3, 3; TF-FrM8, 68
Jang, K.: TF-ThP1, 60; TF-ThP6, 60
Jarry, A.: EM+2D+AS+MI+MN+NS+TF-WeM4, 37; TF-MoM5, **5**; TF-MoM6, 5
Jaszewski, S.: EM+PS+TF-MoA8, 12
Jayan, B.R.: TF+SS-ThA1, 58
Jayatunga, B.H.D.: TF+EM-WeA1, **46**; TF-ThP19, 62
Jayatunga, D.: EM+OX+TF-TuA7, 25
Jean-Jacques, J.-J.: TF+2D+AP+EL+SS-MoA8, 16
Jenkins, P.: TF+EM+NS+SS-ThM5, 53
Jeong, J.H.: TF-ThP1, **60**; TF-ThP6, 60
Jeremiason, J.D.: TF+EM+NS+SS-ThM6, 53
Jesse, S.: TF+EM+MI+MN+OX+PS-MoM10, 4
Jewell, A.D.: TF+PS-TuA9, **29**
Jiang, K.: EM+OX+TF-TuA11, 26
Jiang, L.: TF+EM+MI-TuM11, 22
Jiang, Z.T.: TF+SE-MoA10, 18
Jiao, W.M.: TF-ThP26, **63**
Johnson, A.M.: TF+EM+MI-TuM6, 22
Johnson, B.I.: TF+AS+EL+PS+RA-ThA9, 57
Johnson, N.S.: AP+PS+TF-ThM11, **50**
Johnson, S.D.: TF+2D+AP+EL+SS-MoA6, 15
Johs, B.: PS+2D+SE+TF-FrM11, 66
Jones, J.: 2D+AP+EM+MI+NS+PS+TF-MoA10, 11
Jonker, B.T.: 2D+AP+EM+MI+NS+PS+TF-MoA2, 10
Jung, B.S.: TF-ThP6, 60
Jungjohann, K.: TF-MoM4, 5
— K —
Kaden, W.E.: EM+AP+MS+NS+TF-ThM6, 51; TF+PS-TuA10, 29
Kaiser, D.: 2D+AP+EM+MI+NS+PS+TF-MoA9, 11
Kalanyan, B.: TF+2D+AP+EL+SS-MoA10, 16
Kalinin, S.V.: TF+EM+MI+MN+OX+PS-MoM10, 4
Kallio, P.: TF2-WeM13, 43
Kamiuchi, N.: TL+AS+SS+TF-TuA3, 32
Kanasaki, J.: EL+AS+EM+TF-WeM10, 36
Kapadia, R.: EM+2D+AS+MI+MN+NS+TF-WeM10, 38; EM+2D+NS+TF-WeA8, 44; EM+AP+MS+NS+TF-ThM2, 51; EM+PS+TF-MoA1, 11
Kaplar, R.J.: EM+OX+TF-TuA12, 27
Kara, A.: TF+PS-TuA10, 29
Karahashi, K.: AP+BI+PS+TF-WeM3, **33**; AP+BI+PS+TF-WeM4, 33; AP+PS+TF-ThM5, 49; PS+2D+EM+SS+TF-ThA3, 55; PS+2D+EM+SS+TF-ThA8, 56
Karim, M.R.: TF-ThP19, **62**
Karim, R.: EM+OX+TF-TuA7, 25
Kash, K.: EM+OX+TF-TuA7, 25; TF+EM-WeA1, 46; TF-ThP19, 62
Katiyar, R.S.: EL+AS+EM+TF-WeM2, 35
Kato, T.: AP+PS+TF-ThM4, 49; TF+AP-TuM11, **20**
Katsunuma, T.: PS+2D+EM+SS+TF-ThA9, 56
Kaul, A.B.: TF+SS-ThA9, 59
Kaviani, S.: TF1-WeM12, **42**
Kawakami, R.: 2D+AP+EM+MI+MN+NS+PS+TF-MoA5, 8
Kawamura, K.: AP+PS+TF-ThM1, 49
Kawasaki, J.: TF+EM+MI+MN+OX+PS-MoM11, **4**
Kelber, J.A.: 2D+AP+EM+MI+NS+PS+TF-MoA10, 11
Keller, N.: AP+EL+MS+PS+SS+TF-TuA7, 24
Kessels, W.M.M.: 2D+AP+EM+MI+NS+PS+TF-MoA5, 10; AP+2D+EM+PS+TF-MoM4, 1; PS+2D+SE+TF-FrM8, **66**; PS+AS+EM+SS+TF-MoA10, 14; TF+EM+MI-TuM10, 22; TF-MoM11, 6
Khan, A.: EM+PS+TF-MoA3, 12
Khanal, M.P.: TF+EM+MI-TuM13, 23
Khaniya, A.: EM+AP+MS+NS+TF-ThM6, 51; TF+PS-TuA10, **29**
Khoury, J.: AP+BI+PS+TF-WeM10, 34
Kihara, Y.: PS+2D+EM+SS+TF-ThA9, **56**
Kim, H.: PS+2D+EM+SS+TF-ThA4, **55**; TF-ThP8, 60
Kim, J.: 2D+AP+EM+MI+MN+NS+PS+TF-MoA10, **9**
Kim, J.H.: TF-ThP1, 60; TF-ThP6, **60**
Kim, M.J.: TF+EM+MI-TuM5, 22; TF+PS-TuA12, 29
Kimbrough, J.: EM+AP+MS+NS+TF-ThM13, 52; TF-ThP15, **61**
King, S.W.: PS+2D+SE+TF-FrM6, 65
Kirby, B.: TF+EM+MI+MN+OX+PS-MoM3, 3
Kirsten, P.: TF+SS-ThA3, 58
Kishi, Y.: PS+AS+EM+SS+TF-MoA2, 13
Klein, B.A.: EM+OX+TF-TuA12, 27
Klump, A.: TF+SE-MoA8, 18
Knoops, H.C.M.: PS+2D+SE+TF-FrM8, 66; PS+AS+EM+SS+TF-MoA10, 14
Knudsen, J.: TF+2D+AP+EL+SS-MoA8, 16
Kobayashi, H.: AP+PS+TF-ThM1, 49
Kocherga, M.: EL+AS+EM+TF-WeM13, 36
Kodambaka, S.: TF+PS-TuA2, 28
Koert, U.: TF+SS-ThA3, 58
Komninou, P.: TF+EM+MI+MN+OX+PS-MoM6, 3
Korde, M.: EM+2D+AS+MI+MN+NS+TF-WeM3, 37
Korivi, N.S.: TF+EM+NS+SS-ThM13, **54**
Koschine, T.: AP+BI+PS+TF-WeM1, 33
Kotulak, N.A.: TF+AS+EL+PS+RA-ThA1, 56; TF+EM+NS+SS-ThM5, 53
Kozak, D.: EM+2D+AS+MI+MN+NS+TF-WeM13, 38
Kozen, A.C.: PS+2D+SE+TF-FrM12, 66
Kozhanov, A.Y.: EM+OX+TF-TuA1, 25; TF-ThP12, 61
Krick, B.A.: PS+2D+SE+TF-FrM12, 66
Krishna, S.: TF+EM+MI-TuM3, 21
Kropp, J.A.: TF+EM+MI-TuM6, 22
Krstic, M.: AP+PS+TF-ThM5, 49
Kugimiya, K.: PS+2D+EM+SS+TF-ThA3, 55
Kuis, R.: TF+EM+MI-TuM6, 22
Kumakura, S.: PS+2D+EM+SS+TF-ThA9, 56
Kumar, P.: EL+AS+EM+TF-WeM2, 35
Kushner, M.J.: PS+2D+SE+TF-FrM10, **66**
Kwon, S.: TF+EM+MI-TuM5, 22; TF+PS-TuA12, 29
— L —
Lacovig, P.: 2D+AP+EM+MI+MN+NS+PS+TF-MoA3, 8
Laenger, C.: TF+SS-ThA3, 58
Lalk, R.: TF+EM-WeA1, 46
Lancaster, A.N.: TF-FrM4, 67
Lao, K.U.: AP+2D+EM+PS+TF-MoM9, 2
Larciprete, R.: 2D+AP+EM+MI+MN+NS+PS+TF-MoA3, **8**
Lata, M.: EL+AS+EM+TF-WeM13, 36; EL+AS+EM+TF-WeM6, **36**
Lau, J.: TF-MoM4, 5
Lauritsen, J.V.: 2D+AP+EM+MI+MN+NS+PS+TF-MoA6, 9; OX+EM+HC+MI+NS+SS+TF-TuA10, 27
LaVoie, A.: 2D+AP+EM+MI+NS+PS+TF-MoA10, 11; PS+2D+SE+TF-FrM10, 66
Law, K.: TF-FrM8, 68
Law, S.: TF2-WeM10, **42**; TF2-WeM12, 42
Lee, C.: TF-ThP8, **60**
Lee, C.-T.: TF-ThP4, **60**; TF-ThP5, 60
Lee, H.: TF+EM+MI-TuM13, 23
Lee, I.: 2D+AP+EM+MI+MN+NS+PS+TF-MoA8, 9
Lee, J.: TF-ThP8, 60
Lee, S.: TF+EM+NS+SS-ThM3, **52**
Lee, S.B.: TF1-WeM6, 41
Lee, S.H.: EM+2D+NS+TF-WeA11, **45**
Lee, W.: TF-ThP8, 60
Lee, Y.: AP+PS+TF-ThM11, 50
Lei, M.K.: TF+SE-MoA10, 18

Author Index

Leighton, C.: TF+EM+NS+SS-ThM6, 53
Lekkala, J.: TF2-WeM13, 43
Lemaire, P.C.: AP+2D+EM+PS+TF-MoM8, 2
Leng, C.Z.: TF1-WeM10, 41
Letourneau, S.: TF-FrM4, 67
Leusink, G.J.: TF-TuA11, 31
Levichkova, M.: EL+AS+EM+TF-WeM11, 36
Li, C.: SE+AS+TF-WeA4, 45
Li, J.: TF+EM+MI-TuM11, 22; TF-ThP31, 63
Li, Q.: TF-ThP20, 62; TF-ThP31, 63
Li, Y.: EL+AS+EM+TF-WeM13, **36**; EL+AS+EM+TF-WeM6, 36
Li, Y.G.: TF+SE-MoA10, **18**
Liang, L.: 2D+AP+EM+MI+NS+PS+TF-MoA3, 10
Liao, B.H.: TF-ThP18, **62**
Liao, K.-T.: EM+2D+AS+MI+MN+NS+TF-WeM13, 38
Liao, M.E.: TF+PS-TuA2, 28
Liau, D.: TF1-WeM6, **41**
Liddle, J.A.: EM+2D+AS+MI+MN+NS+TF-WeM13, 38
Lill, T.B.: AP+PS+TF-ThM3, 49
Lin, E.: TF+EM+MI-TuM5, 22
Lin, K.-Y.: PS+AS+EM+SS+TF-MoA11, 14
Lin, Q.: EM+2D+NS+TF-WeA8, 44
Lin, T.: EM+OX+TF-TuA11, 26
Lin, Y-C.: 2D+AP+EM+MI+NS+PS+TF-MoA3, 10
Lindenberg, A.: TF+AS+EL+PS+RA-ThA10, **57**
Linford, M.R.: EL+AS+EM+TF-WeM5, 35; TF+AP-TuM13, 21; TF+AS+EL+PS+RA-ThA9, **57**; TF+SE-MoA2, 17
Liu, C.: 2D+AP+EM+MI+NS+PS+TF-MoA3, 10
Liu, H.: TF+AP-TuM10, 20
Liu, L.: EM+PS+TF-MoA2, 12
Liu, M.: TF+SS-ThA6, **58**
Liu, Y.: OX+EM+HC+MI+NS+SS+TF-TuA12, 28
Lizzit, D.: 2D+AP+EM+MI+MN+NS+PS+TF-MoA3, 8
Lizzit, S.: 2D+AP+EM+MI+MN+NS+PS+TF-MoA3, 8
Loch, D.A.: TF+SE-MoA6, 17
Loeffler, D.: TF-MoM8, **6**
Looker, Q.: TF+PS-TuA9, 29
Losego, M.D.: TF+PS-TuA11, **29**; TF+SS-ThA4, 58; TF1-WeM10, 41
Løvvik, O.M.Løvvik.: TF-FrM7, 68
Lu, M.C.: EM+2D+NS+TF-WeA7, **44**
Ludwig, K.F.: EM+OX+TF-TuA4, 25; TF+2D+AP+EL+SS-MoA6, 15
Lundin, D.: TF+SE-MoA1, 17
Luo, YK.: 2D+AP+EM+MI+MN+NS+PS+TF-MoA5, **8**
Lust, M.: TF+EM-WeA11, **48**
Lyalin, I.: 2D+AP+EM+MI+MN+NS+PS+TF-MoA5, 8
Lyle, L.A.M.: EM+OX+TF-TuA11, **26**
Lyons, J.: TF-FrM1, **67**
— M —
Ma, J.M.: TF-FrM6, **68**
MacIsaac, C.: TF1-WeM11, 41
Mackus, A.J.M.: 2D+AP+EM+MI+NS+PS+TF-MoA5, 10; AP+2D+EM+PS+TF-MoM4, **1**
Madison, A.C.: EM+2D+AS+MI+MN+NS+TF-WeM13, 38
Mahadik, N.A.: TF+AS+EL+PS+RA-ThA1, 56
Mahoney, L.: 2D+AP+EM+MI+MN+NS+PS+TF-MoA8, 9
Mahuli, N.: TF+AP-TuM12, **20**
Maindron, T.: TF-TuA7, **30**
Major, G.: TF+SE-MoA2, **17**
Maksymovych, P.: TF+EM+MI+MN+OX+PS-MoM10, **4**
Malik, S.: PS+2D+SE+TF-FrM6, 65
Malko, A.V.: TF+SS-ThA10, 59
Mameli, A.: AP+2D+EM+PS+TF-MoM3, 1
Mammen, M.: 2D+AP+EM+MI+MN+NS+PS+TF-MoA6, 9
Mane, A.U.: TF-FrM4, 67
Manera, L.T.: TF-ThP7, **60**
Mani, P.D.: EM+AP+MS+NS+TF-ThM6, 51
Manno, M.: TF+EM+NS+SS-ThM6, 53
Marchack, N.P.: PS+2D+EM+SS+TF-ThA6, **55**
Maria, J.-P.: TF+EM+MI+MN+OX+PS-MoM4, 3; TF+SE-MoA3, **17**; TF+SE-MoA5, 17; TF+SE-MoA8, 18
Martinazzo, R.: 2D+AP+EM+MI+MN+NS+PS+TF-MoA3, 8
Martini, L.: PS+2D+SE+TF-FrM8, 66
Maslar, J.E.: TF+2D+AP+EL+SS-MoA10, 16
Matos-Abiague, A.: 2D+AP+EM+MI+MN+NS+PS+TF-MoA5, 8
Matsuda, S.: AP+BI+PS+TF-WeM13, 34
Matsukuma, M.: TF+AP-TuM11, 20
Matsuyama, H.: 2D+AP+EM+MI+MN+NS+PS+TF-MoA9, 9
Mauthe, S.: TF+EM+MI-TuM1, 21
Mauze, A.: TF+EM-WeA2, 47
Mayandi, J.: TF-FrM7, **68**
McClellan, C.: EM+PS+TF-MoA9, **13**
McCreary, K.M.: 2D+AP+EM+MI+NS+PS+TF-MoA2, **10**
McDanold, B.: TF+EM+NS+SS-ThM4, 52
McDonnell, S.: EM+PS+TF-MoA8, 12
McElwee-White, L.: AP+BI+PS+TF-WeM13, 34; TF+AP-TuM1, **19**; TF+AP-TuM10, 20
McGhee, E.: TF+EM+NS+SS-ThM11, 53; TF+EM+NS+SS-ThM12, **54**
McGuinness, E.K.: TF+SS-ThA4, 58; TF1-WeM10, **41**
McGuire, M.A.: TF+EM+MI+MN+OX+PS-MoM10, 4
McLamb, M.J.: EL+AS+EM+TF-WeM13, 36; EL+AS+EM+TF-WeM6, 36
McNeal, B.: TF+EM+NS+SS-ThM12, 54
Meeker, M.A.: TF+EM-WeA10, 48
Mellor, A.: TF+EM+NS+SS-ThM5, 53
Melton, O.: AP+EL+MS+PS+SS+TF-TuA12, 25
Membreno, K.: TF+AS+EL+PS+RA-ThA9, 57
Meriläinen, E.: TF2-WeM13, 43
Merkx, M.J.M.: 2D+AP+EM+MI+NS+PS+TF-MoA5, 10; AP+2D+EM+PS+TF-MoM4, 1
Metz, A.: PS+2D+EM+SS+TF-ThA4, 55
Mewes, T.: TF-FrM8, 68
Meyer, R.: EM+AP+MS+NS+TF-ThM1, 51
Meyers, J.K.: TF+AS+EL+PS+RA-ThA3, **57**
Mikkelsen, A.: TF+2D+AP+EL+SS-MoA8, 16
Miljkovic, N.M.: TF-FrM6, 68
Min, M.: TF+SS-ThA9, **59**
Mishra, R.: TF-FrM8, 68
Mohammad, A.: EM+OX+TF-TuA8, 26; PS+2D+SE+TF-FrM11, 66
Momchilov, A.: TL+AS+SS+TF-TuA7, 32
Moody, D.: EM+OX+TF-TuA11, 26
Moore, W.: TF+EM+NS+SS-ThM6, 53
Morikawa, Y.: AP+PS+TF-ThM5, 49
Morikita, S.: PS+2D+EM+SS+TF-ThA4, 55
Moroz, P.: TF-FrM3, **67**
Morozovska, A.N.: TF+EM+MI+MN+OX+PS-MoM10, 4
Mosden, A.: PS+2D+EM+SS+TF-ThA4, 55
Moselund, K.E.: TF+EM+MI-TuM1, **21**
Mosey, A.: TF-ThP28, 63
Mueller, K.T.: RA+AS+CA+PS+TF-WeM12, 39
Mukherjee, R.: TF-FrM10, 68
Mukhopadhyay, P.: TF+EM-WeA2, 47
Mukundan, V.: EM+2D+AS+MI+MN+NS+TF-WeM3, 37; TF-TuA11, **31**
Munoz-Rojas, D.: TF-TuA7, 30
Mupparapu, R.: 2D+AP+EM+MI+NS+PS+TF-MoA9, 11
Muralter, F.: TF1-WeM3, **40**
Muratore, C.: PS+2D+SE+TF-FrM1, **65**; TF-TuA4, 30
Murdzek, J.A.: AP+PS+TF-ThM6, **50**
Murugesan, V.: RA+AS+CA+PS+TF-WeM12, **39**
Muscat, A.J.: TF-FrM5, **67**
Myung, J.-H.: EM+2D+AS+MI+MN+NS+TF-WeM13, 38
Mzezewa, R.: TF2-WeM13, 43
— N —
Nabatame, T.: AP+BI+PS+TF-WeM1, 33
Naczas, S.: TF+EM+MI-TuM11, 22
Nagaoka, K.: PS+2D+EM+SS+TF-ThA3, 55
Nakahata, K.: AP+PS+TF-ThM4, 49
Nakamura, H.: TF+AP-TuM11, 20
Nakamura, J.N.: 2D+AP+EM+MI+MN+NS+PS+TF-MoA9, **9**
Nakamura, K.: TF-ThP25, **63**
Nam, C.Y.: TF+EM+MI-TuM13, 23
Nam, S.: PS+AS+EM+SS+TF-MoA6, 14
Narayanan, V.: OX+EM+HC+MI+NS+SS+TF-TuA3, 27
Narkilahti, S.: TF2-WeM13, 43
Navarro, G.: TF+EM-WeA7, 47
Nejati, S.: TF1-WeM12, 42
Nepal, N.: EM+OX+TF-TuA4, 25; TF+2D+AP+EL+SS-MoA6, 15; TF+AP-TuM4, 19
Neumann, C.: 2D+AP+EM+MI+NS+PS+TF-MoA9, 11
Neumayer, S.: TF+EM+MI+MN+OX+PS-MoM10, 4
Neupane, M.: 2D+AP+EM+MI+MN+NS+PS+TF-MoA5, 8
Newburger, M.: 2D+AP+EM+MI+MN+NS+PS+TF-MoA5, 8
Newhouse-Illige, T.: TF+EM+MI+MN+OX+PS-MoM5, 3
Ng, A.: TF-FrM5, 67
Nguyen, T.: PS+AS+EM+SS+TF-MoA6, 14
Nguyen, V.: 2D+AP+EM+MI+MN+NS+PS+TF-MoA4, **8**
Ni, Z.: TF+AP-TuM11, 20
Nicolescu, C.M.: TF+SE-MoA9, 18
Nikodemiak, P.: TF+SS-ThA3, 58
Nikzad, S.: TF+PS-TuA9, 29
Niu, T.J.: TF-ThP31, 63
Nolot, E.: TF+EM-WeA7, 47
Nonglaton, G.: TF-TuA7, 30
Norwood, R.: TF+EM+NS+SS-ThM11, 53
Nowak, E.: TF+EM-WeA7, 47
Ntwaeaborwa, O.M.: TF-ThP2, **60**
Nuwayhid, B.: TF-MoM6, **5**
Nyakiti, L.O.: 2D+AP+EM+MI+NS+PS+TF-MoA6, 10
— O —
O'Toole, N.: TF-FrM12, **69**
Oberhausen, W.: EM+AP+MS+NS+TF-ThM1, 51
Oe, K.: TF-ThP25, 63
Oehrlein, G.S.: PS+AS+EM+SS+TF-MoA11, 14; PS+AS+EM+SS+TF-MoA8, **14**
Ogugua, S.N.: TF-ThP2, 60
Oh, J.H.: TF-ThP1, 60
Oh, T.S.: TF+EM+MI-TuM13, 23
Oh, W.: TF-ThP8, 60
Ohanaka, O.: TF+EM-WeA1, 46
Ohta, T.: EM+2D+AS+MI+MN+NS+TF-WeM11, 38
Okada, Y.: PS+2D+EM+SS+TF-ThA8, 56
Okyay, A.K.: PS+2D+SE+TF-FrM11, **66**
Olson, B.: SE+AS+TF-WeA4, 45

Opila, R.L.: AP+EL+MS+PS+SS+TF-TuA12, 25
Orvis, T.: OX+EM+HC+MI+NS+SS+TF-TuA12, **28**
Osinsky, A.: TF+EM-WeA2, 47
O'Toole, N.: AP+BI+PS+TF-WeM6, 34
Oyler, O.: TF-ThP13, 61
— P —
Paik, H.: TF+EM+MI+MN+OX+PS-MoM11, 4
Palai, R.: OX+EM+HC+MI+NS+SS+TF-TuA11, **28**
Palmstrøm, C.J.: TF+AP-TuM6, 20
Pana, A.: TF+EM+MI-TuM11, 22
Pantelides, S.: TF+EM+MI+MN+OX+PS-MoM10, 4
Paquette, M.M.: PS+2D+SE+TF-FrM6, **65**; TF-ThP13, 61
Park, M.: TF+EM+MI-TuM13, 23
Park, S.: EL+AS+EM+TF-WeM13, 36; EL+AS+EM+TF-WeM6, 36
Parsons, G.N.: AP+2D+EM+PS+TF-MoM5, **1**
Pasquale, F.: 2D+AP+EM+MI+NS+PS+TF-MoA10, 11
Pasternak, G.: TF-ThP27, **63**
Paulson, N.H.: TF-FrM4, **67**
Pearce, P.: TF+EM+NS+SS-ThM5, 53
Pelissier, B.: AP+EL+MS+PS+SS+TF-TuA9, 24; TF+AS+EL+PS+RA-ThA8, 57
Peng, Q.: TF+SS-ThA11, **59**; TF-ThP22, 62
Pennachio, D.J.: TF+AP-TuM6, 20
Perrotta, A.: TF1-WeM3, 40
Pesce, V.: AP+EL+MS+PS+SS+TF-TuA9, 24; TF+AS+EL+PS+RA-ThA8, 57
Petrie, R.J.: TF+PS-TuA11, 29
Petrov, I.: SE+AS+TF-WeA7, 45
Phok, B.: AP+BI+PS+TF-WeM10, 34
Piercy, B.D.: TF+PS-TuA11, 29
Pilli, A.: 2D+AP+EM+MI+NS+PS+TF-MoA10, **11**
Pilz, J.: PS+2D+SE+TF-FrM4, **65**
Pinnepalli, S.S.K.: TF-ThP13, **61**
Pint, C.: TF+EM+NS+SS-ThM1, **52**
Pintar, A.: EM+2D+AS+MI+MN+NS+TF-WeM13, 38
Poodt, P.: AP+2D+EM+PS+TF-MoM3, **1**; TF-TuA3, 30
Pookpanratana, S.: EM+2D+AS+MI+MN+NS+TF-WeM11, **38**
Pop, E.: EM+PS+TF-MoA9, 13
Popp, A.: EM+OX+TF-TuA11, 26
Porter, L.M.: EM+OX+TF-TuA11, 26
Posadas, A.: TF+PS-TuA12, 29
Posseme, N.: AP+EL+MS+PS+SS+TF-TuA9, 24
Potrepka, D.M.: AP+BI+PS+TF-WeM6, 34; TF-FrM12, 69
Pradhan, S.K.: TF+EM+NS+SS-ThM10, 53
Pranda, A.: PS+AS+EM+SS+TF-MoA11, **14**
Pribil, G.K.: AP+EL+MS+PS+SS+TF-TuA1, 24
Pronin, N.: EM+2D+AS+MI+MN+NS+TF-WeM4, 37; TF-MoM5, 5
Pulskamp, J.S.: AP+BI+PS+TF-WeM6, 34
Puretzky, A.A.: 2D+AP+EM+MI+NS+PS+TF-MoA3, 10
Puurunen, R.L.: AP+EL+MS+PS+SS+TF-TuA10, **24**; PS+AS+EM+SS+TF-MoA10, 14
Pylypenko, S.: RA+AS+CA+PS+TF-WeM11, **39**
Pyronneau, K.: TF+SS-ThA4, **58**
— Q —
Qi, Y.: TF+EM+MI-TuM12, 23
Qu, C.: PS+2D+SE+TF-FrM10, 66
Qu, Y.Z.: TF+SE-MoA10, 18
— R —
Raadu, M.A.: TF+SE-MoA1, 17
Rack, P.D.: 2D+AP+EM+MI+NS+PS+TF-MoA3, 10; TF+EM+MI-TuM4, 22; TF-ThP20, 62
Rahman, T.S.: EM+2D+AS+MI+MN+NS+TF-WeM12, 38
Ramdin, D.: EM+OX+TF-TuA7, 25
Ramesh, P.: SE+AS+TF-WeA10, 46
Ramos, C.: TF+AP-TuM3, 19
Rangari, V.: TF+EM+NS+SS-ThM13, 54
Ranjit, S.: TF-FrM8, 68
Rashid, M.M.: TF+SE-MoA9, **18**
Ravichandran, J.: OX+EM+HC+MI+NS+SS+TF-TuA12, 28
Ray, D.: TF+EM+NS+SS-ThM6, 53
Rayner, G.B.: AP+BI+PS+TF-WeM6, 34
Rayner, Jr., G.B.: TF-FrM12, 69
Rehman, F.: TF+2D+AP+EL+SS-MoA8, 16
Rementer, C.R.: TF+EM+MI+MN+OX+PS-MoM3, 3
Reza, M.D.: TF+EM-WeA1, 46
Rezaeifar, F.R.: EM+2D+AS+MI+MN+NS+TF-WeM10, 38
Robey, S.W.: EM+2D+AS+MI+MN+NS+TF-WeM11, 38
Robinson, Z.R.: TF+2D+AP+EL+SS-MoA6, 15; TF+AP-TuM6, 20
Rochet, F.: TF+2D+AP+EL+SS-MoA8, 16
Rodgers, B.: TF-ThP14, 61
Rodríguez-Fernández, J.: 2D+AP+EM+MI+MN+NS+PS+TF-MoA6, 9
Rohatgi, A.: TF+EM+NS+SS-ThM4, 52
Roozeboom, F.: AP+2D+EM+PS+TF-MoM3, 1
Rosenberg, S.G.: EM+OX+TF-TuA4, 25; TF+2D+AP+EL+SS-MoA6, 15; TF+AP-TuM6, **20**
Rosenberger, M.R.: 2D+AP+EM+MI+NS+PS+TF-MoA2, 10
Rosowski, F.: TF-MoM8, 6
Ross, C.: EM+PS+TF-MoA2, 12
Rouleau, C.M.: 2D+AP+EM+MI+NS+PS+TF-MoA3, 10; TF-ThP20, 62
Rounsaville, B.: TF+EM+NS+SS-ThM4, 52
Routzahn, A.: AP+PS+TF-ThM3, 49
Rubloff, G.W.: EM+2D+AS+MI+MN+NS+TF-WeM4, 37; TF1-WeM6, 41; TF-MoM5, 5; TF-MoM6, 5
Runnerstrom, E.: TF+SE-MoA8, 18
Ryynänen, T.: TF2-WeM13, **43**
— S —
Saare, H.: AP+2D+EM+PS+TF-MoM5, 1
Sabbione, C.: TF+EM-WeA7, 47
Sagvolden, E.: TF-FrM7, 68
Sajid, M.: TF+PS-TuA10, 29
Sakamoto, T.: EL+AS+EM+TF-WeM10, 36
Sakiyama, Y.: PS+2D+SE+TF-FrM10, 66
Salazar, B.G.: TF+AP-TuM10, **20**
Sales, M.G.: EM+PS+TF-MoA8, **12**
Sanchez, M.O.: TF+PS-TuA9, 29
Sánchez-de-Armas, R.: TF+2D+AP+EL+SS-MoA8, 16
Sandoval, T.E.: AP+2D+EM+PS+TF-MoM4, 1
Sang, X.: AP+BI+PS+TF-WeM12, **34**
Sapkota, A.: TF-FrM8, 68
Saravade, V.G.: EM+OX+TF-TuA9, 26
Sarkar, D.: EM+AP+MS+NS+TF-ThM2, **51**
Sarwar, S.: TF+EM+MI-TuM13, 23
Sasaki, K.: TF-ThP25, 63
Schäffner, P.: PS+2D+SE+TF-FrM4, 65
Schlom, D.G.: TF+EM+MI+MN+OX+PS-MoM1, 2
Schmedake, T.A.: EL+AS+EM+TF-WeM13, 36
Schmid, H.: TF+EM+MI-TuM1, 21
Schnadt, J.: TF+2D+AP+EL+SS-MoA8, **16**
Schneider, D.J.: TF+EM+MI+MN+OX+PS-MoM3, 3
Schoenfeld, W.: TF+EM-WeA2, 47
Schrade, M.: TF-FrM7, 68
Schubert, M.: EL+AS+EM+TF-WeM11, 36
Schwartz, J.: TF+EM+MI+MN+OX+PS-MoM4, 3
Scipioni, L.: TF+EM+MI+MN+OX+PS-MoM5, **3**
Scurti, F.: TF+EM+MI+MN+OX+PS-MoM4, 3
Seidlitz, D.: TF-ThP12, 61
Seo, S.Y.: TF-ThP1, 60; TF-ThP6, 60
Serafin, L.Y.: TF+AS+EL+PS+RA-ThA3, 57
Serizawa, Y.: TF+AP-TuM11, 20
Shah, D.S.: EL+AS+EM+TF-WeM5, 35
Shahmohammadi, M.: TF-FrM10, **68**
Shamsi, Z.: TF+AP-TuM3, 19
Shankwitz, J.: TF-TuA9, 31
Sharma, A.: TF+EM+NS+SS-ThM10, **53**
Sharma, K.: AP+2D+EM+PS+TF-MoM8, 2
Shashkov, D.: AP+BI+PS+TF-WeM10, **34**
Shayesteh, P.: TF+2D+AP+EL+SS-MoA8, 16
Shehzad, M.A.: EM+AP+MS+NS+TF-ThM5, **51**
Sheil, R.: TF-MoM4, **5**
Shepard, A.: TF+EM+MI+MN+OX+PS-MoM5, 3
Shi, J.: TF1-WeM11, **41**
Shi, Y.: PS+2D+EM+SS+TF-ThA4, 55
Shiba, Y.: PS+AS+EM+SS+TF-MoA2, 13
Shibata, Y.: TF-ThP25, 63
Shigeno, S.: PS+2D+EM+SS+TF-ThA8, 56
Shinoda, K.: AP+PS+TF-ThM1, 49
Sholl, D.: RA+AS+CA+PS+TF-WeM3, **39**
Shuai, G.: TF+SE-MoA9, 18
Shukla, D.: EM+OX+TF-TuA8, 26; PS+2D+SE+TF-FrM11, 66
Shukla, N.: EM+PS+TF-MoA8, 12
Si, M.: EM+PS+TF-MoA5, **12**
Siddiqui, S.: EM+PS+TF-MoA2, **12**; TF+EM+MI-TuM11, 22
Silverman, T.: TF+EM+NS+SS-ThM4, 52
Simmonds, P.J.: TF+PS-TuA3, **28**
Sinanan, D.: TF-TuA9, 31
Sitar, Z.: EM+OX+TF-TuA1, 25; TF+SE-MoA8, 18
Smeltink, J.: TF-TuA3, 30
Smithe, K.: EM+PS+TF-MoA9, 13
Sobell, Z.: TF+AP-TuM5, **19**
Sohr, P.: TF2-WeM12, **42**
Song, S.K.: AP+2D+EM+PS+TF-MoM5, 1
Song, Y.: TF+EM+MI-TuM11, **22**
Sood, A.: EM+PS+TF-MoA9, 13
Soruco, J.: TF-ThP28, 63
Sousa, N.: TF+EM+MI-TuM1, 21
Sowa, M.J.: PS+2D+SE+TF-FrM12, **66**
Speck, J.S.: TF+EM-WeA2, 47; TF+EM-WeA3, **47**
Speed, D.: TF-TuA9, 31
Sperling, B.A.: TF+2D+AP+EL+SS-MoA10, **16**
Spiegelman, J.: TF+AP-TuM3, 19
Sridhara, K.: 2D+AP+EM+MI+NS+PS+TF-MoA6, **10**
Stadlober, B.: PS+2D+SE+TF-FrM4, 65
Stange, M.: TF-FrM7, 68
Staude, I.: 2D+AP+EM+MI+NS+PS+TF-MoA9, 11
Staudinger, P.: TF+EM+MI-TuM1, 21
Stavis, S.M.: EM+2D+AS+MI+MN+NS+TF-WeM13, **38**
Stephenson, C.A.: EM+OX+TF-TuA12, 27
Stewart, D.: TF-MoM5, 5
Stiff-Roberts, A.D.: TF1-WeM4, 40
Strandwitz, N.C.: PS+2D+SE+TF-FrM12, 66
Strasser, A.: 2D+AP+EM+MI+NS+PS+TF-MoA3, 10
Strnad, N.A.: AP+BI+PS+TF-WeM6, **34**; TF-FrM12, 69
Strohbeen, P.: TF+EM+MI+MN+OX+PS-MoM11, 4
Strohmayer, M.: SE+AS+TF-WeA10, **46**

Author Index

Stuckert, E.P.: TF+EM+MI-TuM11, 22
Su, L: TF+SS-ThA1, **58**
Su, R.Z.: TF-ThP31, 63
Su, W.Y.: EL+AS+EM+TF-WeM1, 35
Subramanian, A.: TF+EM+MI-TuM13, 23
Sugawa, S.: PS+AS+EM+SS+TF-MoA2, 13
Suh, T.: 2D+AP+EM+MI+NS+PS+TF-MoA11, 11; AP+2D+EM+PS+TF-MoM9, **2**
Sukotjo, C.: SE+AS+TF-WeA9, 46
Sumiya, M.: AP+BI+PS+TF-WeM1, 33
Sun, N.: TF+EM+MI+MN+OX+PS-MoM3, 3
Sun, X.: TF-MoM10, 6
Sunding, M.F.: TF-FrM7, 68
Surendran, M.: OX+EM+HC+MI+NS+SS+TF-TuA12, 28
Sushkov, V.: EM+AP+MS+NS+TF-ThM1, 51
Susner, M.A.: TF+EM+MI+MN+OX+PS-MoM10, 4
Swart, H.C.: TF-ThP2, 60
Szulczewski, G.J.: TF-TuA9, **31**
— T —
T. Mohabir, A.: EM+AP+MS+NS+TF-ThM5, 51
Takeda, S.: TL+AS+SS+TF-TuA3, **32**
Takeya, K.: AP+PS+TF-ThM4, 49
Takoudis, C.G.: SE+AS+TF-WeA9, 46; TF-FrM10, 68; TF-FrM11, 69
Tamaoka, T.: TL+AS+SS+TF-TuA3, 32
Tanaka, K.: TF+PS-TuA2, **28**
Tang, A.: EM+PS+TF-MoA2, 12
Tang, Z.: 2D+AP+EM+MI+NS+PS+TF-MoA9, 11
Taniguchi, K.: PS+2D+EM+SS+TF-ThA4, 55
Tao, J.: EM+PS+TF-MoA1, **11**
Tapily, K.: TF-TuA11, 31
Tavakoli, E.: TF1-WeM12, 42
Taylor, H.: 2D+AP+EM+MI+MN+NS+PS+TF-MoA4, 8
Tenhaeff, W.E.: TF-MoM1, **4**
Teplyakov, A.V.: AP+PS+TF-ThM12, **50**
Teramoto, A.: PS+AS+EM+SS+TF-MoA2, 13
Tervo, E.J.: EM+2D+AS+MI+MN+NS+TF-WeM1, 37
Thapa, R.: PS+2D+SE+TF-FrM6, 65
Thind, A.: TF-FrM8, 68
Thorman, R.: AP+BI+PS+TF-WeM13, **34**
Tierney, B.D.: TF+PS-TuA9, 29
Timm, R.: TF+2D+AP+EL+SS-MoA8, 16
Tinacba, E.J.C.: AP+BI+PS+TF-WeM4, **33**; PS+2D+EM+SS+TF-ThA8, 56
Tischler, J.G.: TF+EM-WeA10, 48
Tiwari, P.: TF+EM+MI-TuM1, 21
Tokranova, N.: SE+AS+TF-WeA10, 46
Tomasulo, S.: TF+AS+EL+PS+RA-ThA1, 56; TF+EM+NS+SS-ThM5, 53; TF2-WeM12, 42
Tomkowski, R.: TF+SE-MoA9, 18
Tortai, J-H.: AP+EL+MS+PS+SS+TF-TuA9, 24
Toyoda, N.: AP+BI+PS+TF-WeM5, **33**
Tran, D.: 2D+AP+EM+MI+MN+NS+PS+TF-MoA8, 9
Trioni, M.I.: 2D+AP+EM+MI+MN+NS+PS+TF-MoA3, 8
Triyoso, D.H.: TF-TuA11, 31
Troian, A.: TF+2D+AP+EL+SS-MoA8, 16
Tronic, T.: AP+BI+PS+TF-WeM12, 34
Tsai, Y.-H.: PS+2D+EM+SS+TF-ThA4, 55
Tsyshevskiy, R.: TF+2D+AP+EL+SS-MoA8, 16
Turchanin, A.: 2D+AP+EM+MI+NS+PS+TF-MoA9, **11**
Twigg, M.E.: TF+AS+EL+PS+RA-ThA1, **56**
— U —
Uedono, A.: AP+BI+PS+TF-WeM1, **33**; AP+EL+MS+PS+SS+TF-TuA9, 24
Uematsu, K.: AP+BI+PS+TF-WeM5, 33
Uhlmann, P.: EL+AS+EM+TF-WeM11, 36
Unaldi, S.: TF+SE-MoA1, 17
Upadhyaya, V.: TF+EM+NS+SS-ThM4, 52
Uprety, S.: TF+EM+MI-TuM13, **23**
Urpelainen, S.: TF+2D+AP+EL+SS-MoA8, 16
Ushirozako, M.: 2D+AP+EM+MI+MN+NS+PS+TF-MoA9, 9
Utriainen, M.: PS+AS+EM+SS+TF-MoA10, 14
Utterback, E.: TF+EM+NS+SS-ThM13, 54
— V —
Vallee, C.: AP+EL+MS+PS+SS+TF-TuA9, **24**
Vallée, C.: TF+AS+EL+PS+RA-ThA8, 57
van der Zande, A.M.: 2D+AP+EM+MI+MN+NS+PS+TF-MoA1, **8**
van Ommen, J.R.: TF+2D+AP+EL+SS-MoA1, **15**
van Straaten, G.: TF-MoM11, **6**
VanDerslice, J.: AP+EL+MS+PS+SS+TF-TuA1, 24
Vanfleet, R.R.: EL+AS+EM+TF-WeM5, 35; TF-TuA10, 31
Vaziri, S.: EM+PS+TF-MoA9, 13
Venkatraman, K.: EM+AP+MS+NS+TF-ThM10, 51
Ventrice, Jr., C.A.: SE+AS+TF-WeA10, 46; TF+AP-TuM6, 20
Verheijen, M.A.: TF+EM+MI-TuM10, 22
Vernon, M.: TF-ThP12, 61
Vico Trivino, N.: TF+EM+MI-TuM1, 21
Visscher, P.B.: TF+EM+MI+MN+OX+PS-MoM6, 3
Vitale, S.A.: PS+2D+SE+TF-FrM3, **65**
Voigt, B.: TF+EM+NS+SS-ThM6, **53**
von Wenckstern, H.: EM+2D+AS+MI+MN+NS+TF-WeM2, 37
Vos, M.F.J.: TF-MoM11, 6
Voyles, P.: TF+EM+MI+MN+OX+PS-MoM11, 4
— W —
Wagner, G.: EM+OX+TF-TuA11, 26
Walczak, L.: TF-ThP21, **62**
Walker, A.V.: TF+AP-TuM10, 20
Walker, M.: EM+2D+AS+MI+MN+NS+TF-WeM4, **37**; TF-MoM5, 5
Wallace, C.H.: EM+AP+MS+NS+TF-ThM3, **51**
Wallas, J.M.: TF+AP-TuM12, 20
Walzer, K.: EL+AS+EM+TF-WeM11, 36
Wang, C.: RA+AS+CA+PS+TF-WeM10, **39**
Wang, H.: TF-MoM3, **5**; TF-ThP31, 63
Wang, K.: 2D+AP+EM+MI+NS+PS+TF-MoA3, 10
Wang, M.: PS+2D+EM+SS+TF-ThA4, 55
Wang, S.: AP+2D+EM+PS+TF-MoM2, 1
Wang, T.: EL+AS+EM+TF-WeM1, 35
Wang, X.: TF+2D+AP+EL+SS-MoA11, **16**; TF1-WeM13, **42**
Wang, Y.: TF+EM+MI+MN+OX+PS-MoM3, 3; TF+PS-TuA2, 28
Wang, Z.: AP+EL+MS+PS+SS+TF-TuA12, **25**; EM+PS+TF-MoA3, **12**
Weaver, J.: TF+SS-ThA1, 58
Wei, D.: TF2-WeM12, 42
Wei, S.C.: TF-ThP26, 63
Wendt, S.: OX+EM+HC+MI+NS+SS+TF-TuA10, 27
Weng, S.: EM+AP+MS+NS+TF-ThM2, 51
Wenzel, W.: AP+PS+TF-ThM5, 49
Weststrate, K.-J.: TF-MoM11, 6
Wheeler, V.D.: TF+AP-TuM4, 19; TF+EM-WeA10, **48**
Williams, J.D.: TF-TuA1, **30**
Willis, B.G.: PS+2D+SE+TF-FrM11, 66
Winter, A.: 2D+AP+EM+MI+NS+PS+TF-MoA9, 11
Wollmershauser, J.A.: 2D+AP+EM+MI+NS+PS+TF-MoA6, 10; TF+2D+AP+EL+SS-MoA3, 15
Woods, V.: EM+OX+TF-TuA1, **25**
Woodward, J.M.: EM+OX+TF-TuA4, 25; TF+2D+AP+EL+SS-MoA6, **15**; TF+AP-TuM6, 20
Wormington, M.: EM+2D+AS+MI+MN+NS+TF-WeM3, 37
Wu, Y.: TF+EM+MI-TuM4, 22
— X —
Xiang, W.: EL+AS+EM+TF-WeM1, 35
Xiao, B.: TF+EM+NS+SS-ThM10, 53
Xiao, K.: 2D+AP+EM+MI+NS+PS+TF-MoA3, 10
Xiao, Z.: EM+AP+MS+NS+TF-ThM13, **52**; TF+EM+NS+SS-ThM11, 53; TF+EM+NS+SS-ThM12, 54; TF-ThP14, 61; TF-ThP15, 61
Xie, R.K.: EM+2D+AS+MI+MN+NS+TF-WeM12, 38
Xing, H.Z.: EM+2D+AS+MI+MN+NS+TF-WeM12, 38
Xu, T.: OX+EM+HC+MI+NS+SS+TF-TuA10, **27**
Xu, W.: AP+2D+EM+PS+TF-MoM8, **2**
Xu, X.: OX+EM+HC+MI+NS+SS+TF-TuA1, 27
Xu, Y.: EM+AP+MS+NS+TF-ThM2, 51
Xue, S.: TF-ThP31, 63
— Y —
Yakes, M.K.: TF+AS+EL+PS+RA-ThA1, 56; TF+EM+NS+SS-ThM5, 53; TF2-WeM12, 42
Yalisove, R.: 2D+AP+EM+MI+NS+PS+TF-MoA11, 11
Yalon, E.: EM+PS+TF-MoA9, 13
Yamaguchi, Y.: AP+PS+TF-ThM1, **49**
Yan, H.: TF+SS-ThA11, 59; TF-ThP22, **62**
Yang, Y.: AP+2D+EM+PS+TF-MoM9, 2; TF-ThP10, 61
Yanguas-Gil, A.: TF+EM-WeA9, **47**; TF-FrM4, 67; TF-ThP24, 63
Yao, F.: TF-ThP26, 63
Yao, Z.: TF+EM+MI+MN+OX+PS-MoM3, 3
Yasutake, Y.: EL+AS+EM+TF-WeM10, 36
Ye, P.: EM+PS+TF-MoA5, 12
Yin, P.G.: EL+AS+EM+TF-WeM1, 35
Yngman, S.: TF+2D+AP+EL+SS-MoA8, 16
Yoo, J.: TF-MoM4, 5
Yoon, M.: 2D+AP+EM+MI+NS+PS+TF-MoA3, 10
Yoshida, H.: TL+AS+SS+TF-TuA3, 32
Young, E.C.: TF+AP-TuM6, 20
Yu, X.: TF+SS-ThA11, 59
Yu, Y.: 2D+AP+EM+MI+NS+PS+TF-MoA3, 10
Yu, Y.-H.: TF-ThP4, 60
Yuan, B.: AP+EL+MS+PS+SS+TF-TuA12, 25
Yuan, Q.: EM+AP+MS+NS+TF-ThM13, 52
— Z —
Zaccarine, S.F.: RA+AS+CA+PS+TF-WeM11, 39
Zaid, H.: TF+PS-TuA2, 28
Zeng, L.: TF1-WeM11, 41
Zhang, B.: TF1-WeM4, 40
Zhang, C.: TF+EM+MI+MN+OX+PS-MoM11, 4; TF-ThP20, **62**
Zhang, D.: PS+2D+EM+SS+TF-ThA4, 55
Zhang, L.: EM+PS+TF-MoA6, 12
Zhang, W.: 2D+AP+EM+MI+NS+PS+TF-MoA3, 10
Zhang, X.: TF+EM+MI-TuM13, 23; TF-ThP31, 63
Zhang, Y.: TF+EM-WeA2, 47; TF-ThP31, **63**
Zhang, Z.: AP+2D+EM+PS+TF-MoM2, 1; TF+2D+AP+EL+SS-MoA5, **15**
Zhang, Z.M.: EM+2D+AS+MI+MN+NS+TF-WeM1, 37
Zhao, H.: EM+OX+TF-TuA7, 25; TF+EM-WeA1, 46; TF-ThP19, 62
Zhao, W.: TF-ThP20, 62
Zhao, Y.: TF-MoM10, **6**

Author Index

Zheng, Y.: TF+SS-ThA10, 59
Zhou, C.: EM+OX+TF-TuA9, 26
Zhou, T.: 2D+AP+EM+MI+MN+NS+PS+TF-MoA5, 8
Zhu, M.: TF+EM-WeA1, 46; TF-ThP19, 62
Zimbardi, F.: TF+EM+NS+SS-ThM4, 52
Zutic, I.: 2D+AP+EM+MI+MN+NS+PS+TF-MoA5, 8